Shear Design of Straight and Haunched Concrete Beams without Stirrups

Vom Promotionsausschuss der
Technischen Universität Hamburg-Harburg
zur Erlangung des akademischen Grades

Doktor-Ingenieur (Dr.-Ing.)

genehmigte Dissertation

von
Vu Hong Nghiep

aus
Haiduong, Vietnam

2011

1. Gutachter: Prof. Dr.-Ing. Günter A. Rombach

2. Gutachter: Prof. Dr.-Ing. Dipl.-Wirtsch.-Ing. Oliver Fischer

Tag der mündlichen Prüfung: 14.10.2011

Schriftenreihe des Instituts für Massivbau der TUHH

Heft 7

Vu Hong Nghiep

Shear Design of Straight and Haunched Concrete Beams without Stirrups

Shaker Verlag

Aachen 2011

Acknowledgments

First of all, I would like to express my deep gratitude to my supervisor, Professor Dr.-Ing. G. Rombach, for his guidance in the past four years. I would also thank my second dissertation reviewer, Professor Dr.-Ing. O. Fischer from the department of concrete structures at the TU München, for his valuable comments and suggestions. I also thank all members of the Institute of Concrete Structures of the Hamburg University (TUHH), especially testing staff, for all the valuable helps during my stay in Hamburg.

My thankfulness is also given to Mrs. Greta Gottwald who shows me the hospitality of the German people during my time in Germany.

The author appreciates the Vietnamese Government for the scholarship through Project 322 organized by the Vietnamese Ministry of Education as well as DAAD for the useful grant in the last four years.

Finally, I like to dedicate this work to my parents and all members of my Vu family in Vietnam. Their endless support was a great encouragement to me to finish this work.

Thank you so much.

Vorwort

Die Querkrafttragfähigkeit sowie die Querkraftbemessung von Stahlbetonbauteilen *ohne* Bügelbewehrung sind trotz langjährigen Forschungsaktivitäten und mehr als 2000 Versuchen weltweit bislang noch nicht zufriedenstellend geklärt. Da derzeit noch kein mechanisches, allgemein anerkanntes Modell existiert, basieren fast alle Bemessungsverfahren auf empirischen Ansätzen. Dies hat zu zahlreichen Modellen geführt, welche sich erheblich sowohl was die relevanten Einflussfaktoren als auch die Ergebnisse betrifft unterscheiden. Dieser Zustand ist auch für die Baupraxis nicht zufriedenstellend. Bei gevouteten Stahlbetonträgern, kommt noch der Einfluss eines geneigten Druckgurtes hinzu, welcher bislang weder experimentell noch mechanisch geklärt ist.

Herr Nghiep untersucht in seiner Forschungsarbeit die Querkrafttragfähigkeit von Stahlbetonbalken *ohne* Bügelbewehrung. Schwerpunktmäßig widmet er sich *gevouteten Trägern*. Nach einer eingehenden Literaturrecherche führt er Versuche an 2×9 Stahlbetonbalken mit Voutenneigungen von 0^o bis 10^o und Schubschlankheiten von a/d = 3 und 5 durch. Hierbei zeigte sich, dass die Einfeldbalken mit konstanter Höhe im Allgemeinen im Bereich der Feldmitte versagten, während sich der kritische Schubriss bei gevouteten Trägern in der Nähe des Auflagers, d.h. im Bereich minimaler Querschnittshöhe, bildete. Letzteres steht im Gegensatz zu der derzeitigen Bemessungspraxis.

In Versuchen lassen sich nur wenige Parameter studieren und nur punktuell Werte messen. Daher studiert Herr Nghiep das Tragverhalten der Versuchsbalken mittels stofflich nichtlinearer Finite-Elemente-Berechnungen. Die FE-Simulationen liefern sehr gute Ergebnisse, sowohl was das Last-Verformungsverhalten als auch die Ausbreitung und den Verlauf der Biege- und Schubrisse betreffen. Aus den rechnerisch ermittelten Spannungsverläufen im gerissen Zustand folgert Herr Nghiep, dass signifikante Schubspannungen sowohl in der Druck- als auch in der ungerissenen Zugzone auftreten. Weiterhin ergeben die Berechnungen, dass die Schubspannung in der gerissenen Betonzugzone über die Trägerhöhe keineswegs konstant ist, wie von manchen Rechenansätzen angenommen. Die Rissreibung sowie die Dübelwirkung der Längsbewehrung haben nach seinen numerischen Untersuchungen einen vernachlässigbar kleinen Anteil am Querkraftabtrag.

Aufbauend auf den experimentellen Untersuchungen und den FE-Berechnungen entwickelt Herr Nghiep zwei einfache Rechenmodelle zur Bestimmung der Querkrafttragfähigkeit $V_{Rd,ct}$ von Stahlbetonbalken mit konstantem und veränderlichem Querschnitt. Statistische Untersuchungen seines Modelles anhand von ca. 900 Versuchswerten zeigen, dass es trotz seiner Einfachheit sehr gute Ergebnisse liefert.

Zusammenfassend lässt sich festhalten, dass die durchgeführten Versuche sowie die komplexen numerischen Untersuchungen von Herrn Nghiep wichtige neue Erkenntnisse zum Tragverhalten von Stahlbetonbalken ohne Querkraftbewehrung mit konstantem oder veränderlichem Querschnitt ergeben haben. Es sind jedoch noch weitere Untersuchungen notwendig, um das Tragverhalten von Stahlbetonbalken besser zu verstehen und ein mechanisch begründetes Rechenmodell zu entwickeln.

Hamburg, 2010 Prof. Dr.-Ing. G. A. Rombach

Abstract

In spite of very long research activities with the first tests conducted by Mörsch in the 1920th, the design for shear of concrete members without transverse reinforcement is still not cleared. This may be demonstrated in the fact that most shear design procedures are not based on mechanical models but on empirical equations which show very big uncertainties. Thus very high safety factors have to be used. The problem of shear design exists primarily for slabs. In Germany numerous old concrete bridges show a lack of safety in transverse direction since the year 2001, when a new DIN-code was introduced. Furthermore the shear design principle of haunched concrete structures, as for example, cantilever slab of bridges, is hardly cleared, up to now.

This research work aims to improve the understanding of the shear behaviour, to identify the significant shear resistance mechanisms and finally to develop new shear design models for practical use which is valid for straight and haunched concrete beams without stirrups.

The essential, partially very different approaches known from the literature are analysed first and their accuracies are checked by a comparison with the test values from a shear database. Considerable differences appear between the arithmetic results and the test values.

To study the behaviour of concrete members under high shear loads an extensive test program with 18 reinforced concrete beams without web reinforcement of different shear slenderness and inclination of compression chord was conducted. These experiments focused on haunched beams. It appears that the existing approaches describe the influence of an inclined compression chord on the shear capacity only in an insufficient manner. In some cases the design according to the DIN- or EC-Code results in unsafe values.

To get a better understanding of the load-bearing mechanisms all tests are simulated by means of non-linear Finite Elements analysis with the programme ABAQUS. Very good agreement appears between the test results and those of FE-analysis including the load-deflection curves, the load bearing capacity and the crack patterns. Thus the developed numerical model can simulate the behaviour of reinforced concrete beams up to the ultimate limit state. The FE-analysis demonstrates that the shear forces are transferred in uncracked compression zone mainly. Therefore crack friction and dowel action plays no significant role on shear bearing capacity at the ultimate limit state. As a result of the FE-analysis and the test program, a shear resistance action of uncracked concrete part in the tension zone is firstly introduced to be one of the two main shear bearing actions of concrete structures without stirrups.

Based on the theoretical and experimental investigations an easy analytic model is developed for the estimation of the shear capacity of straight and haunched reinforced concrete beams without stirrups. It shows more accurate results than the known approaches.

Kurzfassung

Trotz langjähriger Forschungsaktivitäten, die ersten Versuche führte Mörsch 1920 durch, ist die Querkraftbemessung von Stahlbetonbalken ohne Querkraftbewehrung bislang unzureichend geklärt. Dies zeigt sich unter anderem darin, dass die meisten Bemessungsverfahren nicht auf einem mechanischen Modell sondern auf empirisch entwickelten Gleichungen basieren, welche sehr große Streuungen und damit sehr hohe Sicherheitsfaktoren aufweisen. Das Problem der Querkraftbemessung besteht vor allem bei Platten. So weisen zahlreiche Massivbrücken in Deutschland nach der seit dem Jahre 2001 gültigen Norm rechnerisch eine zu geringe Tragfähigkeit in Querrichtung auf. Weiterhin ist die Querkraftbemessung von gevouteten Trägern, wie Sie beispielsweise bei Fahrbahnplatten von Brücken auftreten, bislang kaum geklärt.

Diese Forschungsarbeit soll zu einem besseren Verständnis des Querkrafttragverhaltens von Stahlbetonbalken ohne Bügelbewehrung beitragen. Hierzu werden zunächst die wesentlichen aus der Literatur bekannten, teilweise sehr unterschiedlichen Rechenmodelle analysiert und deren Genauigkeit durch einen Vergleich mit den Versuchswerten aus einer Schubdatenbank bestimmt. Es zeigen sich erhebliche Streuungen zwischen den Rechen- und den Versuchsergebnissen.

Zum Studium des Tragverhaltens wurden umfangreiche Versuche mit insgesamt 18 Stahlbetonbalken ohne Bügelbewehrung unterschiedlicher Schubschlankheit durchgeführt. Hierbei lag der Schwerpunkt bei gevouteten Trägern. Es zeigt sich, dass die bestehenden Ansätze den Einfluss eines geneigten Druckgurtes auf die Querkrafttragfähigkeit nur unzureichend beschreiben. Teilweise ergeben sich auf der unsicheren Seite liegende Rechenwerte.

Zu einem genaueren Studium der Beanspruchungen und der Tragmechanismen werden die Versuche mittels stofflich nichtlinearer Finite Elemente Berechnungen mit dem Programm ABAQUS simuliert. Es zeigen sich sehr gute Übereinstimmungen zwischen Versuch und FE-Analyse. Dies trifft sowohl bei den Kraft-Weg-Verläufen, bei den Traglasten als auch bei den Rissbildern zu. Das entwickelte numerische Modell gibt somit das Verhalten von Stahlbetonbalken im Gebrauchs- und Grenzzustand zutreffend wieder. Die FE-Berechnungen zeigen, dass die Querkräfte im Wesentlichen in der ungerissen Druckzone übertragen werden und somit die Rissreibung im Grenzzustand der Tragfähigkeit keine wesentliche Rolle spielt. Die numerischen und experimentellen Untersuchungen haben weiterhin ergeben, dass die ungerissene Betonzugzone einen wesentlichen Anteil der Querkraft aufnimmt.

Basierend auf den theoretischen und experimentellen Untersuchungen wird ein einfaches analytisches Modell zur Berechnung der Querkrafttragfähigkeit von geraden und gevouteten Stahlbetonbalken ohne Bügelbewehrung entwickelt, was erheblich genauere Werte als die bekannten Ansätze liefert.

Table of Contents

1 Introduction

1.1 Problem Statement

Intense research had been conducted in the last decades regarding the shear design of reinforced or prestressed concrete members. Nevertheless a generally accepted shear design model is still not available particularly for reinforced concrete (RC) members without transverse reinforcements (or stirrups) which can often be found in practice, like retaining walls, tunnels or bridge slabs. Different codes, such as German code DIN 1045-01 (2001), Swiss code SN 262 (2003), ACI 318-05 (2005) or Canadian Standard CSA (2004) introduce different shear design formulae. Even if these shear strength equations have been derived from either empirical approach or theoretical backgrounds, they show a big scatter of safety level as presented in figure 1.1.

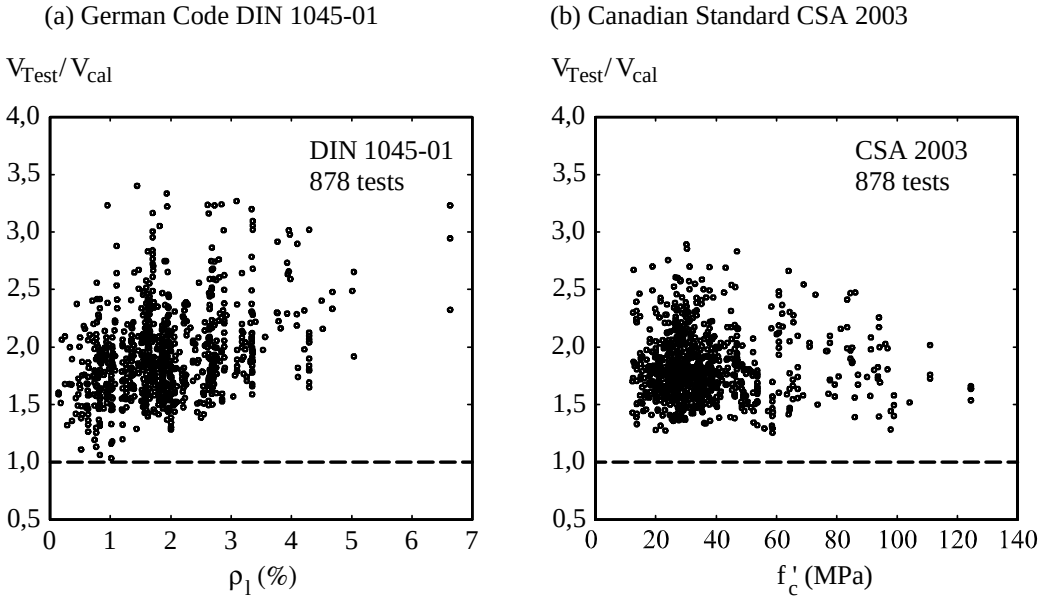

Figure 1.1– Safety level of DIN 1045-01 versus longitudinal reinforcement ratio ρ_l (left) and safety level of Canadian standard CSA 2003 versus concrete strength f'_c (right)

The shear design concept for concrete structures without transverse reinforcements proposed in the Eurocode *[EC2 (2003), 6.2.2]* and the German Code *[DIN 1045-01 (2001), 10.3.3]* reduces considerably the shear bearing capacity of these members with regard to the older codes *[Rombach et al. (2005)]*. As a result, most concrete bridge decks in Germany require shear reinforcements while that was not the case in the last 50 years. This raises the question whether all of formerly designed concrete bridge decks have safety deficits or whether the shear design model in the new Eurocode and DIN 1045-01 is too conservative. For concrete

bridge decks, the arrangement of shear reinforcements or increasing the depth of slab as an alternative cause construction difficulties and increase time-consumption and cost.

The shear design model for concrete members without transverse reinforcement in DIN 1045-01 adopted an empirical expression from the CEB-FIP Model Code 90 with a little adjustment of the safety factor 0,10 instead of 0,15 *[Reineck (1996), Hegger et al. (1999)]*. The value of 0,1 was suggested for safety reason after evaluation of 282 reliable tests out of 604 shear tests on reinforced concrete members without axial force. Now a new shear database of 1849 test results of RC beams with and without stirrups has been published *[Collins et al. (2008)]*. Thus it is necessary to evaluate the shear strength formula with updated shear database in order to have more sufficient assessments on its efficiency and safeness. Besides, the empirical approach should be also substituted by a more rational mechanical model. Usually, an empirical approach will require a relatively large number of tests in order to cover adequately all relevant cases in practical construction. For concrete structures, even just for members without stirrups, it seems to be impossible to consider all relevant parameters due to a wide variety of geometrical features as well as material proportions and especially diverse testing circumstances. In fact, there are many unreliable test results out of the new shear database *[Collins et al. (2008)]*. For that reason, a shear design model should be derived from a theoretically mechanical background and the shear database should play a role as a means of verification.

The varied–depth (or haunched) concrete structures without stirrups are very popular in practice for example in bridge deck slabs. It is surprised to know that there is not any practical code except the German code DIN 1045-01 (10.3.2) to give detailed instructions for the design of these structures *[DIN 1045-01(2001)]*. However, the shear resistance principle which combines an empirical expression and constituents of other forces is questionable. The existence of V_{cc}, a so-called vertical shear resistance component due to inclination of the concrete compression chord is not confirmed. In most cases V_{cc} reduces the design shear force V_{Ed} or increases the shear resistance V_{Rd} in other words. For that reason, it is implied that the shear bearing capacity of haunched structures is usually larger than that of straight depth ones even though the haunched structures apparently have less amount of composed materials. This remarkable fact encourages me to study more about the basis of this approach. It is also surprising that there have been very little researches conducted on this topic which cannot give reasonable explanations for the existence of V_{cc}.

1.2 Objectives of the Thesis

The main goals of this research are:

1) to clarify the shear resistance mechanisms of concrete beams without stirrups

2) to find out differences of shear behaviour between straight depth beams and haunched reinforced concrete beams without stirrups,
3) to propose rational and simple models to calculate shear capacity of straight and haunched concrete members and finally,
4) to evaluate the safety level of the German code DIN 1045-01 and other practical codes in comparison with the proposed models.

The objectives will be processed by mechanical analysis and by experiments.

1.3 Structure of the Thesis

The thesis consists of six chapters and six appendices.

Chapter 1- Introduction- gives an overview of the research, the objectives and the structure of the thesis.

Chapter 2- State of the Art- summarizes some results of existing researches on the shear behaviour of concrete members without stirrups. Some typical shear design models and practical shear design provisions including DIN 1045-01, ACI 318-02, CSA 2003, SN 262… will be presented and discussed as well. Some guidelines for shear design of variable-depth RC structures are also introduced in details in this Chapter.

Based on the above intense study, an experimental program had been planned and accomplished. Chapter 3- Experimental Program- describes in detail the experimental investigations of 18 test beams including geometrical features, material properties, used instrumentations, testing procedure and test results.

In Chapter 4- Nonlinear FEM Analysis- all the test beams will be modelled and analyzed with the Finite Element software ABAQUS. The outcomes of the Nonlinear FEM analysis include the ultimate load bearing capacity, load deflection curves, maximum deformation, formation and propagation of cracks as well as redistribution of stresses during loading of test beams…

Based on the achieved results of the test program and Non-FEM analysis, significant shear resistance mechanisms of straight and haunched concrete beams without stirrups will be identified. The differences of the two types of beams under loading in test program and Non-FEM analysis will be examined and described as well. Based on these load bearing mechanisms, two shear strength models for straight depth concrete member and varied depth concrete member will be developed. The two shear strength models and their design formations will be verified with the updated shear database as well as be compared with other shear

strength models and design equations in some practical codes. All of these will be presented in the Chapter 5- New Model Proposals- of the thesis.

Finally, Chapter 6- Conclusions and Recommendations – summarizes the main results of the conducted research work and gives recommendations for further research.

2 State of the Art

2.1 Introduction

This section presents a brief background of shear behaviours and approaches for shear design of concrete members without stirrups. The study of shear behaviour has recognized some dominant shear resistance mechanisms in concrete and some main factors such as concrete strength, reinforcement ratio ρ_l ...which influence most on shear bearing capacity of concrete members. These understandings play a key role in developing most of the shear design models later.

There have been many shear design models proposed from many different theories or methods. In the following, some typical shear design models will be presented and classified into two main approaches, mechanical models which are based mainly on conceptual backgrounds and empirical models which are based mainly on shear databases. The description of these models is quite complex and wordy. Therefore only main concepts, shear resistance mechanisms and major influencing factors of the presented models will be highlighted.

The shear design models provided in practical codes including German Code DIN 1045-1, ACI Code 318–05, Canadian Standard A23.3 and Swiss Code SN262 are mentioned in the following. Besides, some rare researches and design instructions of two codes ACI 318-05 and DIN 1045-01 for concrete haunched beams are also summarized. This will demonstrate the need of further researches in this field to get a better understanding on shear behaviours and more accurate design models of these common concrete structures.

Finally, the conclusions will summarize some general outcomes of the existing researches on shear of concrete members without transverse reinforcements. From these backgrounds, the purposes of further research will be proposed accompanied with the research methodology suggested for solving the existing design problems.

2.2 Shear Behaviours of Concrete Members without Stirrups

Studying of shear behaviour of concrete members is to find out shear transfer mechanisms and shear bearing capacity up to failure of concrete structures. For common structures, the behaviours are dominated not only by shear forces alone but also by shear forces in conjunction with bending moments and axial forces. If any point in a member is considered, according to theory of elasticity, its plane stress state can be described either by three stress com-

ponents σ_x, σ_y, τ_{xy} or by two principal stresses including principal tensile stress σ_2 and principal compressive stress σ_1. If shear stresses τ_{xy} exist, the direction of the principal tensile stress is inclined to the neutral axis of the structure (Figure 2.1).

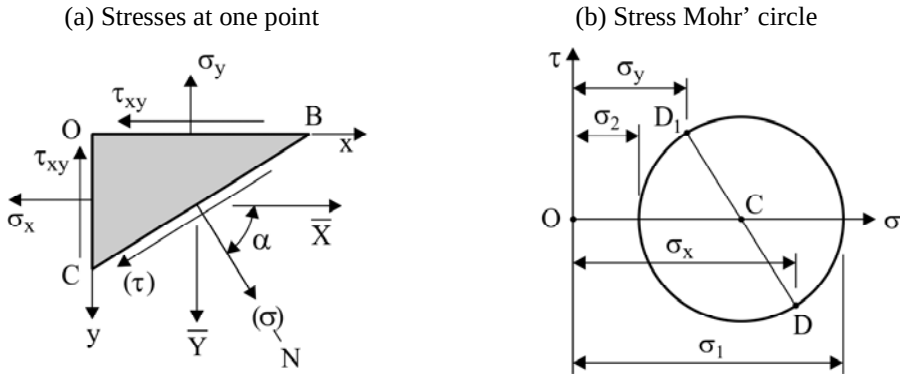

Figure 2.1– Plane stress state of one point and stress Mohr' circle *[Timoshenko et al. (1951)]*

When the principal tensile stress at any point reaches the tensile strength of concrete, a crack will occur and open normal to the direction of the principal tensile stress or parallel with the direction of the principal compressive stress. Therefore, concrete members subjected to shear forces at ultimate load always have inclined cracks named diagonal cracks or shear cracks. Inclined cracks can be initiated in the web of beams where is proved to be the highest shear stress region and named web shear cracks. Inclined cracks developed from former flexural cracks are called flexure–shear cracks (Figure 2.2).

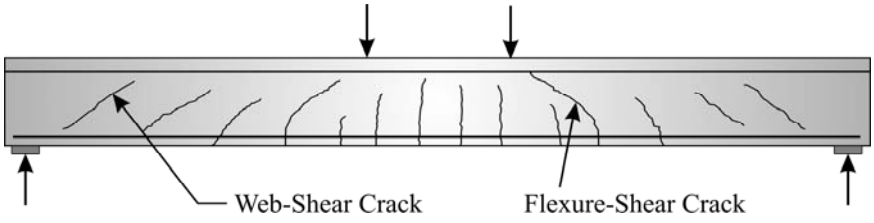

Figure 2.2– Types of inclined cracks *[NCHRP Report 549 (2005)]*

The type of failure caused by these cracks, usually in a very brittle and abrupt way, is called diagonal failure or shear failure. Normally, there are five different modes of failure caused by diagonal cracks depending on the dimensions, geometries, type of loading, amount of longitudinal reinforcement and structural properties of concrete members (Fig. 2.3) as follows: (1) Diagonal tension failure (2) Shear compression failure (3) Shear tension failure (4) Web crushing failure and (5) Arch rib failure *[Pillai et al. (2003)]*.

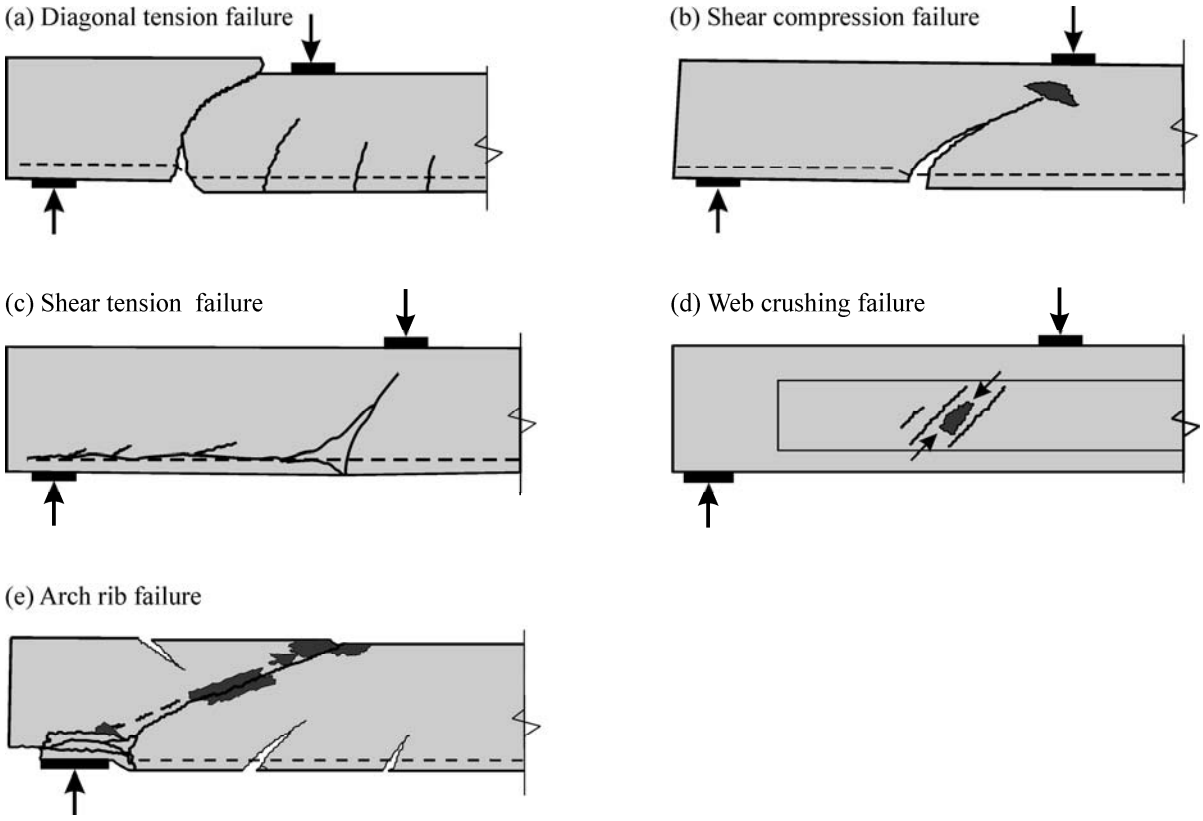

Figure 2.3– Modes of shear failure of concrete beams *[Pillai et al. (2003)]*.

Diagonal tension failure usually occurs in concrete members with low amount of stirrups and longitudinal reinforcement. Diagonal cracks may initiate from former flexural cracks and propagate rapidly over the whole cross section of the member until collapse (Fig. 2.3.a). For concrete members with low amount of web reinforcement but adequate longitudinal reinforcement ratio to form a compression zone, shear cracks may easily initiate from former flexural cracks but do not pass through the compression zone. The failure of structure is caused by the crushing of the concrete in compression zone above the tip of the shear crack and named shear compression failure (Fig. 2.3.b). In cases that the longitudinal reinforcement loses the bond with concrete due to inadequate anchorage of the longitudinal bars or concrete cover, cracks tend to develop along the main bars until they combine with a flexural shear crack to cause shear tension failure as in the figure 2.3.c. Web crushing failure seems to be only identified in I-beams due to slender web thickness while arch rib failure usually occurs in deep beams or short span beams in which the direct force transfer from the loading location to the bearings is dominant (Fig. 2.3.d and 2.3.e). In fact, some normal modes of failure can totally be as a combination of two or more above modes of failure, for example, shear tension failure and shear compression failure.

2.2.1 Shear Transfer Mechanisms

How shear is transferred and which parts of concrete structures carry shear still seem to be a challenge to the research community due to the complicated physical mechanisms that do not follow to any conventional mechanical theory. Though some basic actions of shear resistance in concrete structures are recognized including: (1) shear resistance of the uncracked compression concrete zone, (2) friction of contact surfaces between cracks (or aggregate interlock), (3) dowel action of longitudinal reinforcements, (4) crack–bridging tension forces existing in closed cracks (residual tensile stress in concrete) and (5) arch action *[ASCE-ACI Committee 445 (1998), p.1395]* as presented in figure 2.4. Nevertheless, the level of importance of each corresponding action of shear resistance is still a controversy.

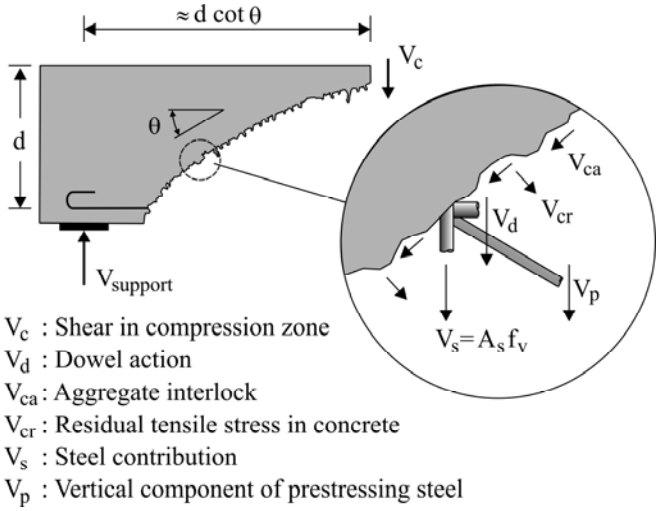

Figure 2.4– Mechanism of shear resistance *[NCHRP Report 549 (2005)]*

The uncracked concrete compression zone: As showed in the figure 2.3(a) and the figure 2.3(b), the concrete compression zone plays an important role in guiding and limiting the development of inclined cracks. It is apparent that shear cracks are responsible for the failure of concrete members in shear and the failure occurs only if the critical shear crack passes through the compression zone or the compressive strength of concrete is exceeded. Therefore, the depth of the compression zone will determine the load bearing capacity of a member. The larger the depth of the compression zone, the higher the shear carrying capacity. However, the level of significance of concrete compression zone in carrying shear is still a controversy. Many authors, for example Bresler et al. (1958), Zwoyer et al. (1954), stated that it is the uncracked zone, an effective area in resisting normal stresses, to carry the whole of shear in concrete members while others, for example Reineck (1991), believed that the concrete compression zone can carry not more than 30% of the total shear force. Recently, many authors, such as Zararis et al. (2001), Zink (2000), Tureyen et al. (2003), Park et al. (2006), Choi et al. (2007), only considered the failure mechanisms of compression zone to estimate the shear strength of concrete members.

Friction between contact surfaces of cracks: The roughness of the crack surfaces acts as interlocks to prevent the slip between contact surfaces. Some called the mechanism “aggregate interlock” depending on the width of cracks and the aggregate size. The shear resistance increases as the width of cracks decreases and the aggregate size increases. According to Reineck (1991), the shear force is mainly transferred by this mechanism (accompanied with dowel action). In contrast, Zararis et al. (2001) stated that because the uncracked concrete zone exists above the tip of the critical inclined crack, it acts as a buffer to prevent any slip along crack interfaces and hence, there are no contribution of aggregate interlock and dowel action at all.

Dowel action of longitudinal reinforcements: When the critical shear crack develops and gradually increase the width of the former flexural cracks, main longitudinal bars will act as dowels to resist shear. The shear resistance depends closely on vertical displacements of the critical shear crack and most on effective width of concrete beams as well as concrete tensile strength. Watstein et al. (1958) conducted tests with 9 rectangular beams without stirrups and concluded that the shear carried by longitudinal reinforcement is in range of 0,38 to 0,74 of the total shear at loads ranging from 0,42 to 0,46 of the maximum. After that the dowel action would decrease as the width of the shear crack increases and would reach zero at failure. Acharya et al. (1965) concluded on the results of 20 tests with rectangular beams without stirrups that dowel action not only carries shear but also plays a key role in deciding which type of failure, flexure failure or shear failure, will happen.

Crack–bridging tension forces existing in closed cracks: Experimental investigations by Gopalaratnam et al. (1985) came to a conclusion that cracked concrete does resist tension. Hence, small pieces of concrete crossing cracks can carry shear as long as the crack width does not exceed a certain limit value. The larger the crack width, the less significant the shear capacity of cracked pieces of concrete. Nevertheless, Bažant (1997) theoretically verified that the crack–bridge tensile stresses are insignificant and should be neglected as their magnitude is much lower than the shear capacity of the compression zone of concrete.

Arch Action: Theoretically the shear resistance of concrete members can be divided into two separate modes: beam action and arch action. The critical state before shear failure shows a change of depth of uncracked concrete compression zone from the position of load application to support or a change of inner lever arm in other words. That means arch action may play a more important role that beam action does at the critical state. Strut-and-tie models suggested by Ritter (1899), Mörsch (1920), Drucker (1961), Nielsen (1978), Marti (1985), Schlaich et al. (1987) are used in case of arch action. Kim et al. (1999) introduced a shear strength equation that combines beam action and arch action based on analytical models and experimental data.

2.2.2 Significant Factors for Shear Bearing Capacity

Analytical and experimental studies have revealed that the shear bearing capacity of concrete members is controlled by following dominant parameters: (1) concrete strength f'_c (or f_{ck}), (2) size effect d, (3) longitudinal reinforcement ratio ρ_l, (4) shear span to depth ratio a/d and (5) axial force *[ASCE-ACI Committee 445 (1998)]*. However, the significance of each parameter to the shear bearing capacity of concrete members is still under debate. The importance of these factors and some opinions of their contribution to shear strength of concrete members can be summarized as follows:

Concrete strength: Normally, concrete members with higher concrete strength will have higher load bearing capacity or more shear strength in other words. Because the concrete strength is represented by concrete compressive strength and concrete tensile strength, the use of each type of strength will imply the failure mechanism of structure. As it is assumed that cracks in concrete are caused by principal tensile stresses, the concrete tensile strength will have more decisive influence on shear carrying capacity of concrete structures. This hypothesis has been widely agreed by many researchers and especially has governed almost all design codes. In these codes, concrete tensile strength is usually described as a term of concrete compressive strength to the power of a third or a half for convenience such as $f_{ck}^{1/3}$ in DIN 1045-01 or $f'^{1/2}_c$ in ACI 318-05.

However, as presented in the figure 2.3, the modes of shear failure are quite different and complex. As a result, the influence of concrete tensile strength on the shear strength of a structure may not be the same for different failure modes. The inconsistent test results from different authors also partly confirmed the conclusion. Ferguson et al. (1953) conducted tests on 24 T–beams without stirrups and reported that the diagonal tensile strength increases very slowly as f'_c increases. Moody et al. (1955) carried out tests with 136 rectangular beams (101 beams without stirrups) and concluded that the nominal shear stress increases as concrete strength increases and becomes independent if the concrete strength exceeds 34,5 MPa (5000psi). Kani (1966), based on the test results of 132 beams without shear reinforcements, stated “that the shear strength of rectangular, reinforced concrete beams does not depend on concrete strength within the entire range of f'_c = 17,2–34,5MPa (2500 to 5000psi) and ρ_l = 0,50 to 2,80 % “.

Size effect: Kani (1967), by four series of test beams without stirrups having different depths of 15^2, 30^5, 61^0, 121^9cm (6, 12, 24, 48 in), identical ratio of longitudinal reinforcement and concrete strength, confirmed that the shear strength will decrease as the depth of beam increases. The tests conducted by Shioya et al. (1989) with beams having depths ranging from 10 to 305 cm (4 to 120 in) also gave the same conclusion. To explain this phenomenon, Reineck (1991) and Collins et al. (1986) supposed that the crack width at failure is propor-

tional to the depth of beam. Since a wide crack width will reduce the shear transfer capability due to friction and aggregate interlock, the higher the beam depth the lower the shear stress transfer capacity. Bažant (1997) also suggested a theory of fracture energy release to explain the size effect in terms of energy from the fracture mechanics viewpoints.

Longitudinal reinforcement: Kani (1966), by 133 rectangular test beams without stirrups, concluded that the influence of longitudinal reinforcement ratio on shear strength is considerable as shown in figure 2.5. It was already proved that the percentage of longitudinal reinforcement ρ_l governs the height of the compression zone and tensile strain of concrete (or crack width). The increase of ρ_l will enlarge the height of compression zone as well as lessen the width of cracks and, as a result, raises the shear strength of structures. This has been widely accepted by research the community and that's why the longitudinal reinforcement ratio appears in shear strength formulae of most all of practical design codes.

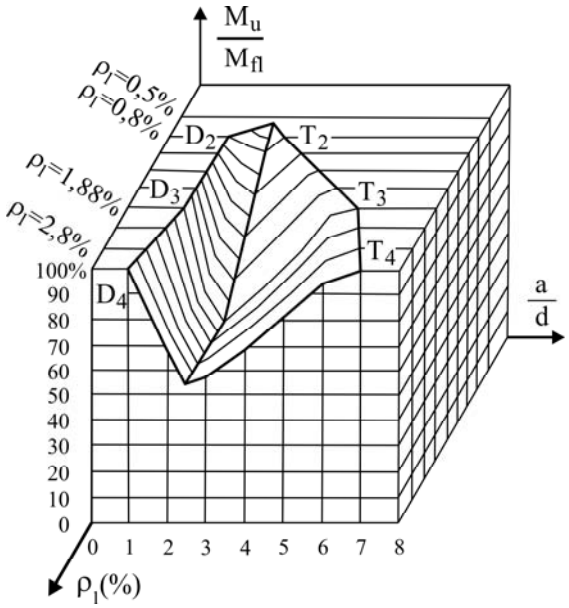

Figure 2.5– Relative beam strength $M_{ultimate}$ /$M_{flexure}$, versus *a/d* and ρ_l *[Kani (1966)]*

Shear span to depth ratio a/d: The influence of *a*/*d* on shear strength was early recognized by Talbot, Turneaure and Maurer *[Ferguson et al. (1953), p.673]*. Clark and later Ferguson et al. (1953) showed that for the same beam, the shear stress at failure changes by 225 % if the value of *a*/*d* varies from 2,35 to 1,17 *[Kani (1964)]*. Kani (1966) conducted 11 series of 133 test beams without stirrups and with the *a*/*d* range of 1,0 to 6,5. By considering M_u, the maximum bending moment at failure as an indicator of diagonal failure, Kani presented graphs of M_u/M_{fl} versus *a*/*d* and introduced the term "valley of diagonal failure" as shown in the figure 2.5. These graphs showed a trend that the beam strength M_u reached the full flexural strength M_{fl} at $a/d = 1$ and reduced to 51% of M_{fl} as the value of *a*/*d* increased to 2,5. As *a*/*d* continued to increase, the beam strength M_u, nevertheless, increased astonishingly to

reach the full flexural strength M_{fl} at $a/d = 6,5$. The flexural failure occurred in the vicinity of $a/d = 1,0$ and $a/d = 6,5$ while the diagonal failure was found at the remaining values of a/d. To explain the influence of the slenderness ratio, some authors considered a/d in relation with moment as $a/d = M/V{\cdot}d$ and hence, implied the role of moment on shear bearing capacity of concrete members. In agreement with this approach, many authors such as Collins et al. (1996), Muttoni et al. (2008)…included this factor in their strength models. The a/d ratio can be seen in most codes for example ACI 318-05 (eq. 2), CSA 2003, SN 262 while it is neglected in CEP–FIB Model Code, DIN 1045–01 and Eurocode 2.

Axial force: It is widely accepted that axial tension force reduces the shear strength of concrete members and that axial compression force due to applied normal loads or prestressing increases the shear strength of concrete members. Since axial tension force reduces the height of the concrete compression zone as well as widens the crack width, it reduces the shear resistance of compression zone and the shear interface transfer. By contrast, axial compression force increases the height of concrete compression zone as well as narrows the crack width and so, it raises the shear resistance of the two above mechanisms and the shear bearing capacity of concrete structures in general.

Other factors: Kim et al. (1991) considered other effects such as the confined horizontal cracking, preformed cracks, released horizontal cracking and unbonded reinforcement. However, these factors have been proved to have insignificant roles on shear bearing capacity of concrete members.

In conclusion, theoretical analysis and experimental investigations have identified generally accepted shear transfer mechanisms as follows: (1) shear resistance of the uncracked concrete compression zone, (2) friction of contact surfaces between cracks (aggregate interlock), (3) dowel action of longitudinal reinforcements, (4) crack-bridging tension forces existing in closed cracks (residual tensile stress in concrete) and (5) arch action. Based on one or more of the above mentioned mechanisms, many shear models to estimate the shear strength of reinforced concrete members had been suggested. These models originated from this approach can be called as mechanical models.

Another approach, based mainly on significant factors such as material properties of concrete (E_c, f'_c or f_{ck}, f_{ct}) and steel (E_s, f_s) combined with structural dimensions (b, d, a/d) as well as boundary conditions (load type, axial force…) to formulate and later calibrated with test database, has introduced many shear strength formulae as well. The models originated from this approach can be called as semi-empirical or purely empirical models. Almost all of shear design models of practical codes surprisingly are in this later group. Typical shear strength models of the two approaches and practical codes will be presented in the next sections.

2.3 Mechanical Models

It is interesting to know that some mechanical models for shear design (for example truss model, variable-angle truss model, compression field theory) did not acknowledge the shear resistance of concrete beams without stirrups though some tests totally did confirm the contradistinction. One rational model to explain failures which are not of flexural type was early developed by Kani (1964) (Fig. 2.6). He used the term “diagonal failure” to name these failures and also suggested two internal shear carrying mechanisms of concrete beams: (a) a comb-like structure and (b) a tied arch. Kani introduced analytical expressions for both mechanisms. From these models and tests, Kani strongly confirmed the influence of *a*/*d* ratio on shear resistance and diagonal failure mechanism of concrete beams. For small *a*/*d* ratios, the concrete beams tend to form a tied arch to resist shear while comb-like structure will prefer to occur for larger *a*/*d* ratios. In the comb-like model or tooth model, the concrete teeth were assumed to be cantilevers fixed in the compression zone and loaded by forces transferred from longitudinal reinforcements. The shear bearing capacity of beams was expressed in term of bending capacity of these teeth.

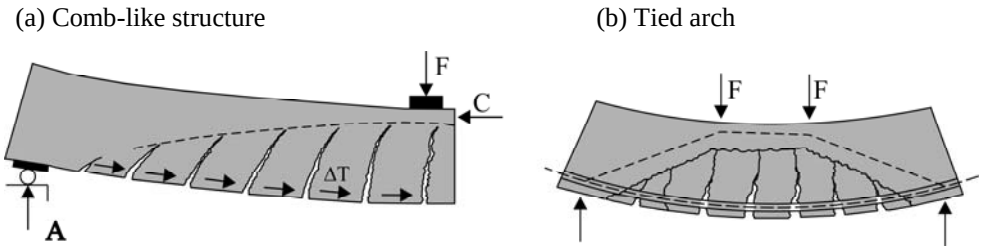

Figure 2.6– Kani’ models *[Kani (1964)]*

Some other authors, such as Fenwick et al. (1968) or Taylor (1972, 1974) *[Reineck (1996)]*, later showed that the teeths of comb-like model could not bend freely due to the influences of the friction between crack surfaces and the dowel action of longitudinal reinforcement. To consider these mechanisms, tooth model were further developed by Fenwick and Paulay, Taylor, Hamadi and later by Reineck *[NCHRP Report 549 (2005)]*. Generally, these approaches were characterized by modelling of discrete cracks with different assumptions for inclination and spacing of the cracks. In the “truss model with crack friction” suggested by Reineck (1990), the cracks were assumed to be inclined at $\beta_{cr} = 60°$ with a spacing of 70 % of the flexural crack height (Fig. 2.7). In addition, Reineck also assumed that the depth of the compression zone is almost constant along shear span and that shear failure would occur somewhere at the middle of shear span of a beam (Fig. 2.7). The distribution of the friction stresses along the cracked surfaces was also simplified to define the states of stresses in the web of a member (Fig. 2.8). Finally, an explicit formula for the ultimate shear strength of concrete beams was proposed as follows:

$$V_{Rm} = \frac{b_{eff} \cdot d \cdot 0,4 f_{ct} + V_d}{1 + 0,16 \frac{f_{ct}}{f_c} \cdot \lambda \cdot \left(\frac{a}{d} - 1 \right)} \tag{2.1}$$

Where:

$\lambda = \frac{f_c}{E_s \cdot \rho_l} \cdot \frac{d}{w}$	f_c in MPa; d in m and w = 0, 9 mm
$f_{ct} = 0,246 f_c^{2/3}$	axial tensile strength in MPa
$f_c = 0,95 f'_c$	uniaxial compressive strength of concrete for short-time loading in MPa
$V_d = \frac{6}{f_c^{1/3}} \cdot b_{eff} \cdot d_s \cdot f_{ct}$	V_d in MN; d_s and b_{eff} in m; f_c and f_{ct} in MPa (dowel effect)
$b_{eff} = b - \sum d_s$	effective width of section
d_s	diameter of main longitudinal bar.

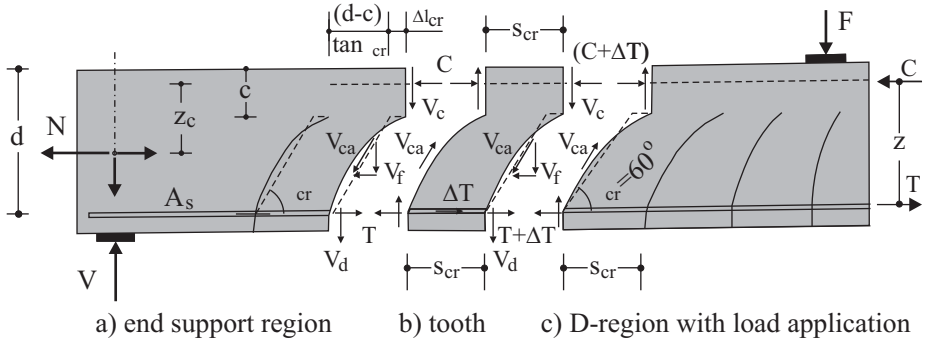

Figure 2.7– Reinforced concrete member with tooth-element and its forces in B-regions *[Reineck (1991)]*

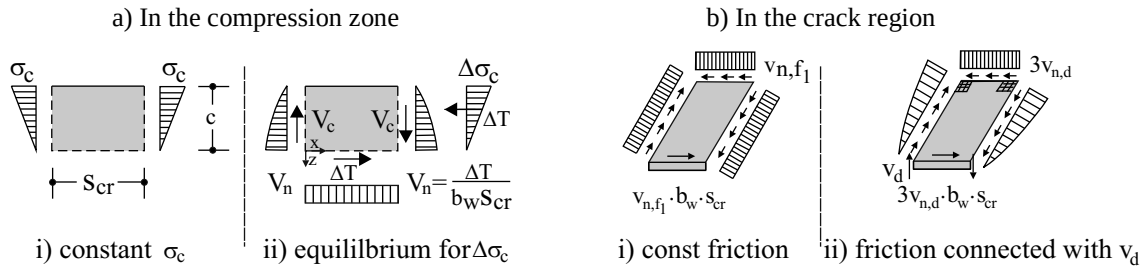

Figure 2.8– Stress distribution of Reineck's model in the compression zone and in the cracked region *[Reineck (1991)]*

In Reineck's model, shear forces are mainly transferred in the tension zone by the friction along the cracked surfaces (or aggregate interlock) and the dowel action of the longitudinal reinforcements while the compression zone only carries at most a maximum of about 30% of the total shear force *[Reineck (1991)]*. In contrast, many authors believe that it is the compression zone which carries most shear force and not the cracked tension zone. Furthermore, the assumption that the height of the compression zone is almost constant in the shear span will be appropriate only for beams with relatively large ratio *a*/*d*. In addition, the assumption

that shear failure occurs somewhere at the middle of shear span of a beam is also not realistic because the stress fields in a beam usually tends to focus on the load position and the support which play a role as two inclined poles. As a result, the inclined shear failure crack will mostly propagate either to the load position or to the support or to both of them as showed in many tests. It will be verified by the test program in the next chapter that the "truss model with crack friction" suggested by Reineck do not predict well the shear capacity of the short test beams ($a/d \approx 3$). This model also shows bad correlation to test data which will be presented in the Chapter 5- New Model Proposals.

Zararis et al. (2001) proposed a totally different shear failure mechanism in reinforced concrete slender beams without web reinforcements. These authors stated that it is the type of splitting of concrete responsible for the diagonal shear failure of beams under concentrated load. They showed that the critical diagonal shear crack (leading to collapse) typically involves two crack branches which are formed at different time and are due to different causes (Fig. 2.9).

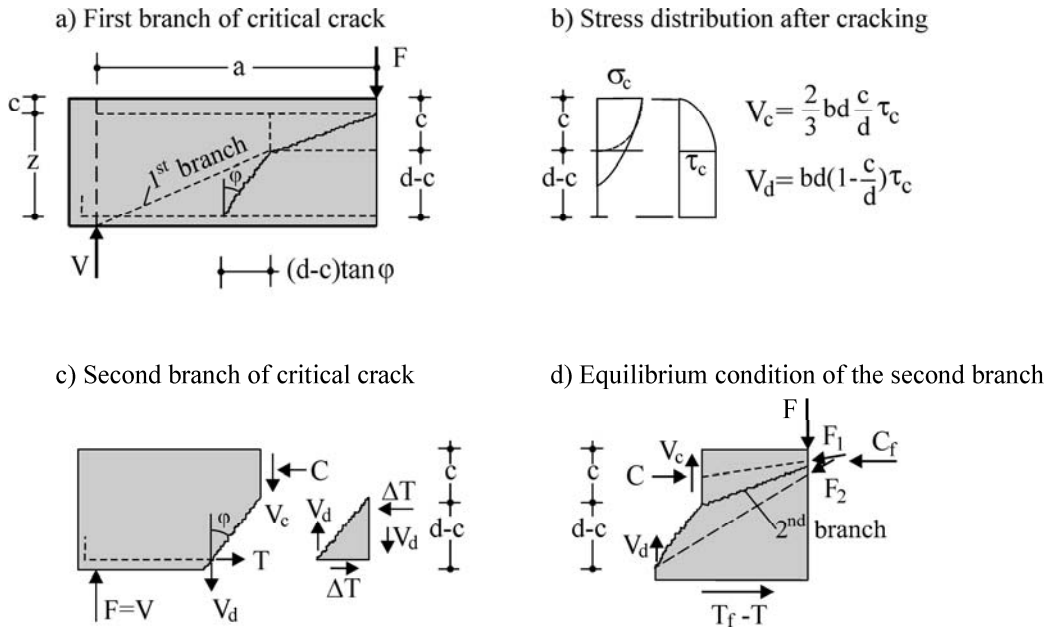

Figure 2.9– Mechanical model of Zararis et al. (2001) under the equilibrium condition of forces *[Zararis et al. (2001)]*

The failure is caused by the formation of the second branch of the critical crack, which initiates from the tip of the first branch and propagates, abruptly or gradually, toward the position of load application crossing the compression zone (Fig. 2.10a). Based on the theories of elasticity, plasticity and force equilibrium conditions (Fig. 2.10b), the shear strength equation at failure of slender beams without stirrups was proposed as follows:

$$V_{Rm} = \left(1,2 - 0,2\frac{a}{d}\cdot d\right)\cdot\frac{c}{d}\cdot f_{ct}\cdot b_w\cdot d \qquad (2.2)$$

Where: $f_{ct} = 0,30\left(f_c'\right)^{2/3}$ the splitting tensile strength of concrete in MPa.

$1,2 - 0,2\frac{a}{d}\cdot d \geq 0,65$ an expression to consider the size effect of beams.

$$\frac{c}{d} = \sqrt{-600\frac{\rho_l}{f_c'}\cdot\frac{c}{d} + 600\frac{\rho_l}{f_c'}}$$

(a) Distribution of normal stresses (b) Splitting of concrete in circular disk

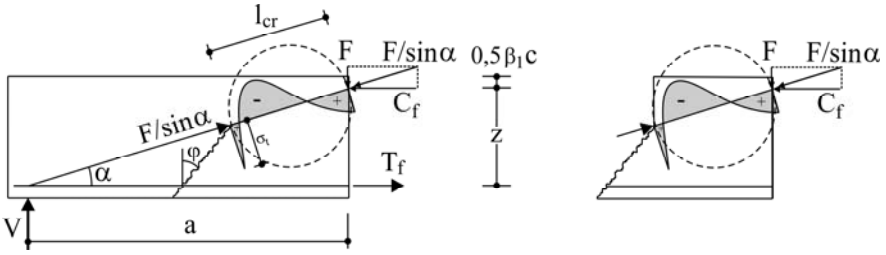

Figure 2.10– Distribution of normal stresses along the second branch of critical crack and splitting of concrete in circular disk *[Zararis et al. (2001)]*

It is noted from the above formula that the shear strength of beams at failure, as the product of the neutral axis depth *c* to the effective depth *d* ratio times the splitting tensile strength of concrete f_{ct}, is purely carried only by the uncracked concrete compression zone under the arch action and there is no dowel action and aggregate interlock (or friction between cracks) since the compression zone essentially acts as a buffer preventing any meaningful contribution of shear slip along the crack interface as other authors explained. The purely mechanical model is found to predict very well the ultimate shear forces of extensive test series of slender beams with various strengths of concrete, steel ratios, shear span to depth (*a*/*d*) ratios, and geometrical features which will be presented in the chapter 5-New Model Proposals.

Also considering the main role of the uncracked compression zone in resisting shear, Zink (2000) suggested another model to predict the shear strength of beams without stirrups. Basing on the Hillerborg's fracture mechanics model, the author showed a different distribution of shear stress at a cracked cross section in which the shear stress, after reaching the maximum value at the tip of the critical diagonal crack, will gradually reduce to zero along a certain length on the crack (Fig. 2.11).

The shear strength of concrete beams without stirrups includes the principal shear resistance force V_0 of the compression zone multiplied with the factors $k(a/d)$ and $k(l_{ch}/d)$ to consider the influences of slenderness and size effect of beams as follows:

$$V_{Rm} = V_0 \cdot k\left(a/d\right) \cdot k\left(l_{ch}/d\right) \tag{2.3}$$

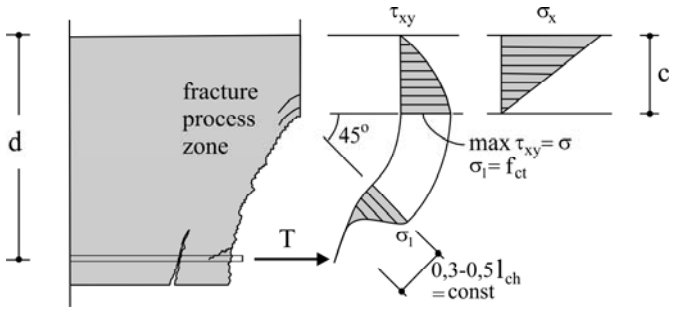

Figure 2.11–Stress distribution at cracked section *[Zink (2000)]*

These two factors were later determined by experimental data. The final shear capacity formula of concrete beams without stirrups was proposed by Zink (2000) as follows:

$$V_{Rm} = \frac{2}{3} f_{ct} \cdot \left(\frac{4d}{a}\right)^{1/4} \cdot \left(\frac{5l_{ch}}{d}\right)^{1/4} \cdot b \cdot c \tag{2.4}$$

Where: $V_0 = \int_0^c \int_0^b \tau_{xy}(y) \cdot dxdy = \frac{2}{3} f_{ct} \cdot b \cdot c$

$$c = \frac{2d}{1+\sqrt{1+\frac{2}{\rho_l \cdot \alpha_E}}} = \left[\sqrt{\left(\rho_l \cdot \alpha_E\right)^2 + 2\rho_l \cdot \alpha_E} - \rho_l \cdot \alpha_E\right] \cdot d \approx 0,78 \cdot \sqrt[3]{\rho_l \cdot \alpha_E} \cdot d$$

$$\rho_l = \frac{A_{sl}}{b_w \cdot d} \quad \text{and} \quad \alpha_E = \frac{E_s}{E_c}$$

f_{ct} is the axial tensile strength $f_{ct} = 2,12 \ln\left(1+\frac{f_c'}{10\ MPa}\right)$

$k\left(a/d\right) = \left(4d/a\right)^{1/4}$

$k\left(l_{ch}/d\right) = \left(5l_{ch}/d\right)^{1/4}$

l_{ch} is the characteristic length according to Hillerborg $l_{ch} = \frac{E_c \cdot G_f}{f_{ct}^2}$ and G_f is the fracture energy of concrete: $G_f = 0,307\, f_{ct} \cdot 100$ if $f_c' \leq 80$MPa and $G_f = 143$ if $f_c' > 80$MPa.

Having the same opinion about the key role of the uncracked concrete compression zone, Tureyen et al. (2003) believed that it is the stress state in this region that initiates the shear failure of concrete beams (Fig. 2.12). The distributions of normal stress and shear stress at crack position and between cracks are assumed as shown in figure 2.13.

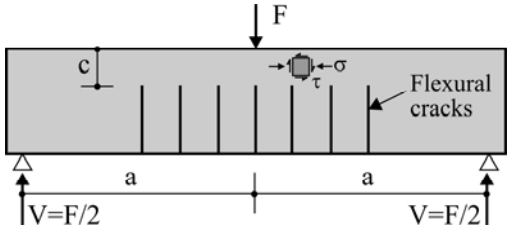

Figure 2.12– Simplified model before shear failure *[Tureyen et al. (2003)]*

a) Stress distribution at crack (b) Stress distribution between cracks

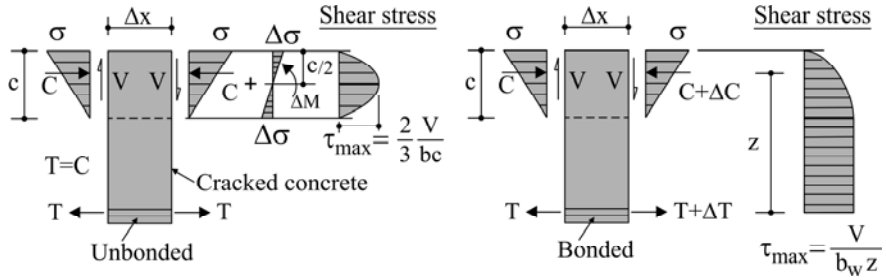

Figure 2.13– Stress distribution at crack and between cracks *[Tureyen et al. (2003)]*

With the assumption that failure occurs when the principal tensile stress reaches the tensile strength of the concrete f_{ct}, the shear strength equation was proposed as follows:

$$V_{Rm} = \frac{2}{3} b \cdot c \cdot \sqrt{\left(6\sqrt{f_c'}\right)^2 + 6\sqrt{f_c'} \cdot \frac{\sigma}{2}} \qquad (2.5)$$

Where: The concrete tensile strength f_{ct} was assumed and σ is the flexural stress at the extreme compression fibre.

After consideration of large experimental data, Tureyen proposed the following simple conservative shear strength equation::

$$V_{Rm} = 0,4152\sqrt{f_c'} \cdot b \cdot c \qquad (2.6)$$

Where: $c = \left[\sqrt{2\rho_l \cdot \alpha_E + \left(\rho_l \cdot \alpha_E\right)^2} - \rho_l \cdot \alpha_E\right] \cdot d$ depth of uncracked concrete compression zone.

The proposed model was found to predict well the shear strength of 370 test specimens from 25 different investigations. It was also suggested to use for concrete beams with fiber-reinforced polymer (FRP) bars.

Park et al. (2006) proposed a strain-based shear strength model for slender beams without web reinforcements based on the same assumption that the shear resistance of a slender beam is provided mainly by the uncracked compression zone of concrete. The distribution and interaction between the stress components was considered to evaluate the shear strengths of beams (Fig. 2.14). Based on the material failure criteria of concrete, failure controlled by

compression and failure controlled by tension (Fig. 2.15), the shear capacity was defined as a function of the flexural deflection (or strain) as presented in eq. (2.7):

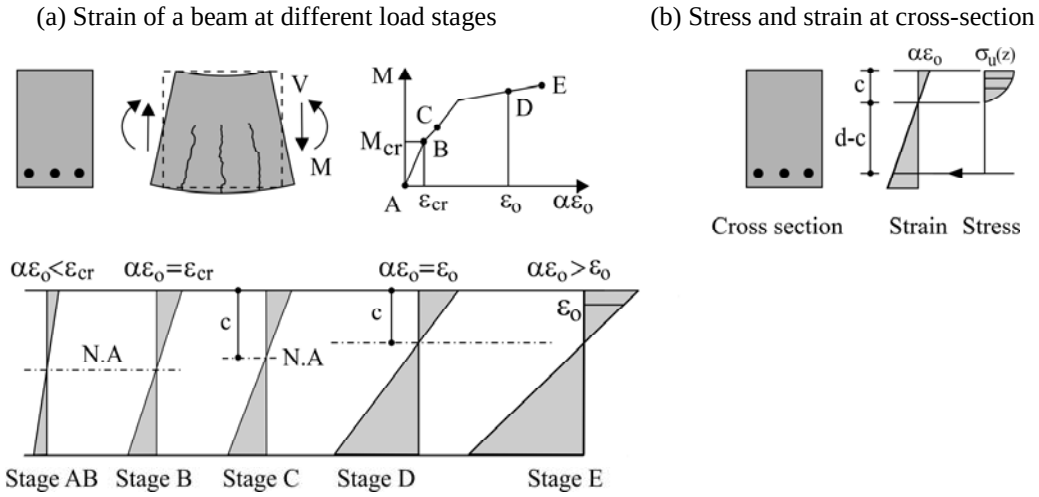

Figure 2.14– Strain of a beam at different load stages and stress and strain at cross-section *[Park et al. (2006)]*

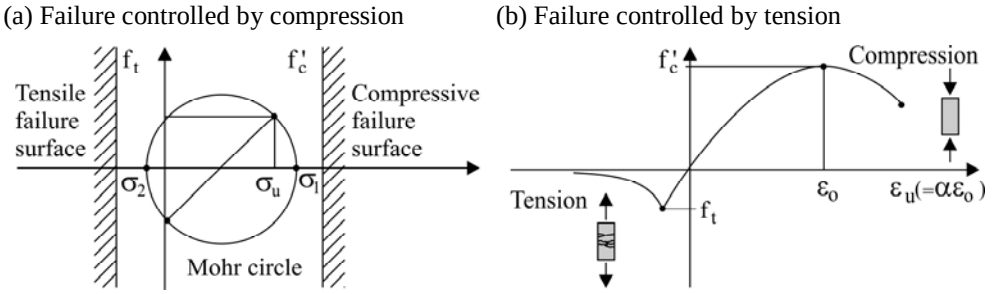

Figure 2.15– Condition for failure controlled by compression and by tension *[Park et al. (2006)]*

$$V_{Rm} = \frac{\left(\alpha_a - \alpha_a^2/3\right)\cdot c_a \cdot f_c' \cdot z}{a \cdot d} \cdot b \cdot d \qquad (2.7)$$

Where: z is the length of moment arm at the loading point is defined as follows:

$$z = \left(d - \frac{(1/3)\alpha_a - (1/12)\alpha_a^2}{\alpha_a - (1/13)\alpha_a^2} \cdot c_a \right)$$

c_a is the height of the compression zone at the loading point

α_a is the compressive normal strain factor at extreme compression fiber of the cross section at the loading point.

To avoid an iterative calculation, the above formula later was simplified conservatively as follows:

$$V_{Rm} = \lambda_s \cdot \sqrt{f_t \cdot (f_t + \bar{\sigma}_{ct})} \cdot b \cdot (c_{x1} - c_c) + \sqrt{f_c' \cdot (f_c' - \bar{\sigma}_{cc})} \cdot b \cdot c_c \qquad (2.8)$$

Where: $\lambda_s = 1{,}2 - 0{,}2(a/d) \cdot d \geq 0{,}65$

$f_t = 0{,}292\sqrt{f_c'}$

$\bar{\sigma}_{ct} = \dfrac{[f_r \cdot h^2/(6x_0) + 0{,}05\sqrt{f_c'} \cdot d] \cdot [x_0 + h - c_{x1}]}{c_{x1} \cdot [d - c_{x1}/3]}$

$f_r = 0{,}625\sqrt{f_c'}$

$x_0 = 0{,}22(a - 0.5d)$ *for* $a/d \leq 2{,}3$

$x_0 = 0{,}6a - d$ *for* $2{,}3 \leq a/d \leq 5$

$x_0 = a - 3d$ *for* $a/d > 5$

$$c_{x1} = c(\alpha_{x1}\varepsilon_0) = \frac{-\varepsilon_0 \cdot E_s \cdot d \cdot \rho_l}{(2 - 2/3 \cdot \alpha_a) \cdot f_c'} + \frac{\sqrt{[\varepsilon_0 \cdot E_s \cdot d \cdot \rho_l]^2 + (2 - 2/3\alpha_a) \cdot f_c' \cdot \varepsilon_0 \cdot E_s \cdot d^2 \cdot 2\rho_l}}{(2 - 2/3\alpha_a) \cdot f_c'}$$

$c_c = (1 - 0{,}43a/d) \cdot c_{x1} \geq 0$

$\bar{\sigma}_{cc} = \dfrac{c_{x1} \cdot (d - c_{x1}/3)}{c_{x1} \cdot 0{,}9d} \cdot \dfrac{a}{x_0 + h - c_{x1}} \cdot \bar{\sigma}_{ct} \leq 0{,}85 \cdot f_c'$

ε_o and α_a can be assumed in calculation.

Although this model requires a complicated calculation procedure, it predicts the shear strength in very good agreement with many existing experimental results. This proves that the models based on the failure mechanism of the compression zone are a very good approach to predict the shear strength of reinforced concrete beams without stirrups.

Derived from the lower bound theorem of plasticity, some simple strut-and-tie models were suggested by Drucker (1961), Nielsen (1978) and Marti (1985) *[ASCE-ACI Committee 445 (1998)]* to determine the shear capacity of deep concrete beams without stirrups. This approach was developed from the assumption that significant shear is transferred directly to the support by arch action, and so, less redistribution of internal stresses is involved after cracking. In these models, the concrete tensile strength is neglected and loads are carried by a single inclined strut. If the longitudinal reinforcement is anchored well behind the support, two failure mechanisms can occur: (1) failure of concrete in biaxial compression over the support or under the load; or (2) yielding of the longitudinal reinforcement.

Marti (1985) introduced other basic tools including nodes, fans, arches, and bands for more complex patterns of the flow of forces (Fig. 2.16). However, the simple strut-and-tie approach has been considered to result in an unsafe solution and should be used with caution for slender beams without stirrups *[ASCE-ACI Committee 445 (1998)]*.

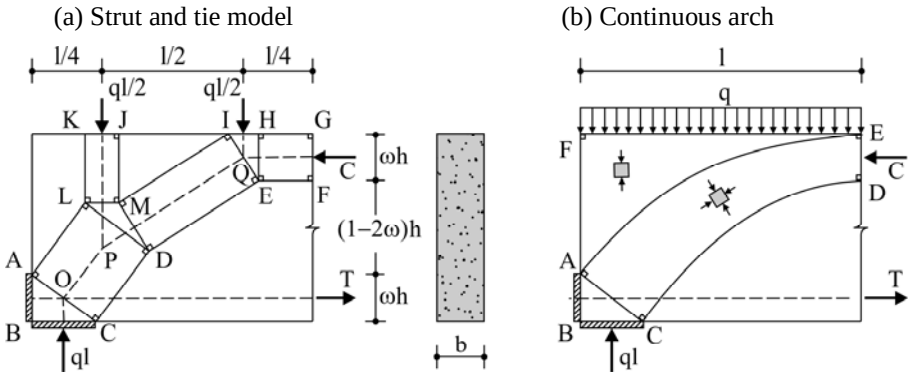

Figure 2.16– Arch action in strut and tie model and continuous arch *[Marti (1985)]*

In an attempt to generalize the strut-and-tie model to shear failure of slender beams, some authors suggested truss models with concrete ties to care for the role of tensile stresses in such members. Marti (1980) extended the plasticity approach by using a Mohr-Coulomb yield criterion for concrete that includes tensile stresses *[ASCE-ACI Committee 445 (1998)]*. Schlaich et al. (1987) also suggested a refined strut-and-tie model which includes concrete tension ties *[ASCE-ACI Committee 445 (1998)]*. Al-Nahlawi et al. (1992) proposed another truss model with concrete compression struts inclined at either 45° or 35° and concrete tension ties perpendicular to the struts (Fig. 2.17).

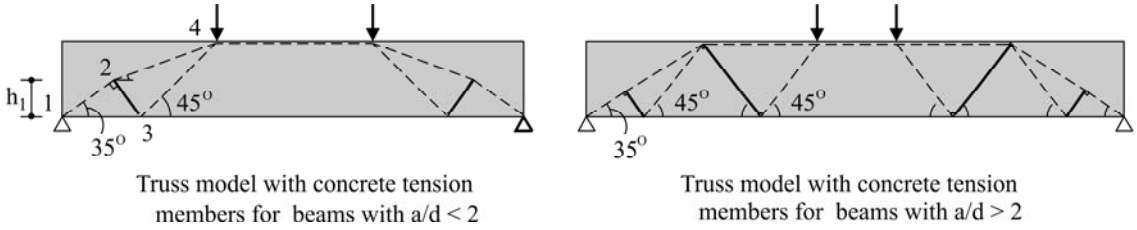

Figure 2.17– Refined strut-and-tie models *[Al Nahlawi et al. (1992)]*

The accuracy of the truss models with concrete ties and strut-and-tie models in general depends on the material strength properties (concrete, steel) and the assumed inclinations of struts and ties which were believed to be different for concrete beams with different concrete strengths and various shear span to depth ratios *a/d*. As a result, these approaches cannot capture the shear failure of slender members without stirrups which showed different shear failure mechanisms from those assumed in the truss models.

Vecchio and Collins (1986) introduced the Modified Compression Field Theory (MCFT) as a further development of the Compression Field Theory formerly suggested by Collins and Mitchell (1974) *[ASCE-ACI Committee 445 (1998)]*. Different from the Compression Field Theory, the Modified Compression Field Theory cares for influences of tensile stresses in post-cracked concrete; and as a result, this model can be implemented to determine the shear capacity of concrete beams without stirrups.

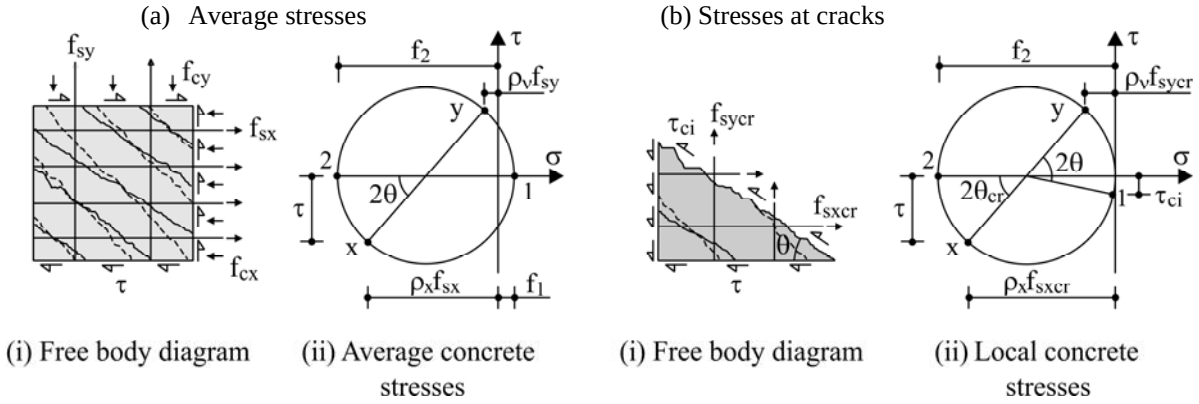

Figure 2.18–Equilibrium conditions of MCFT *[ASCE-ACI Committee 445 (1998)]*

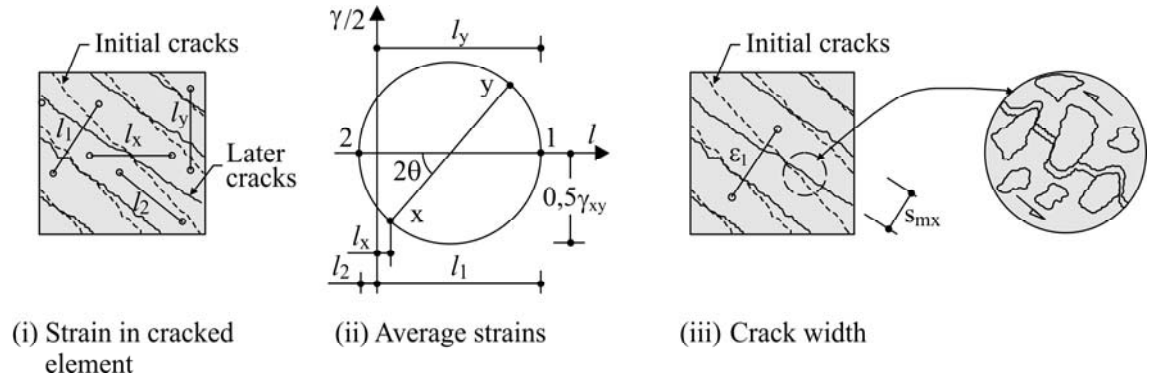

Figure 2.19–Compatibility conditions of MCFT *[ASCE-ACI Committee 445 (1998)]*

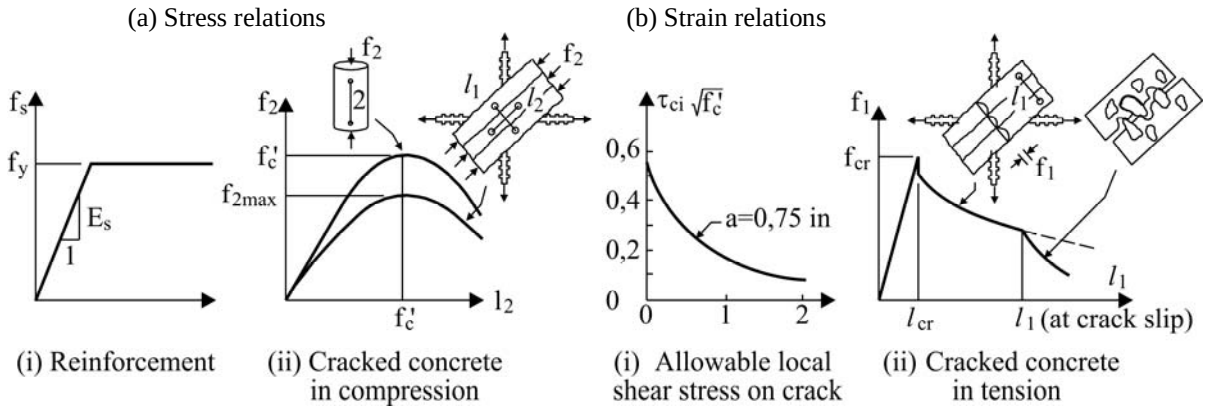

Figure 2.20– Stress and strain relations of MCFT *[ASCE-ACI Committee 445 (1998)]*

The MCFT, essentially a fully rotating, smeared crack model, describes the behaviours of cracked reinforced concrete under equilibrium conditions, compatibility conditions, and stress-strain relationships which were formulated in terms of average stresses and average strains (Figs 2.18, 2.19 and 2.20). In the MCFT formulation, cracked reinforced concrete was treated as an orthotropic material noticeably different from plain uncracked concrete with new constitutive relations of compression softening and tension stiffening derived from a comprehensive series of panel element tests. The MCFT may be the most conceptual and

sophisticated model among others for shear design of concrete structures. However, it was also recognized by tests that the MCFT underestimates shear strength and stiffness of panels containing heavy amounts of reinforcement in both directions (Fig. 2.21.a) but overestimates shear strength and stiffness of uniaxially reinforced panels or panels containing very light reinforcement in the transverse direction (Fig. 2.21.b) *[Vecchio (2000)]*.

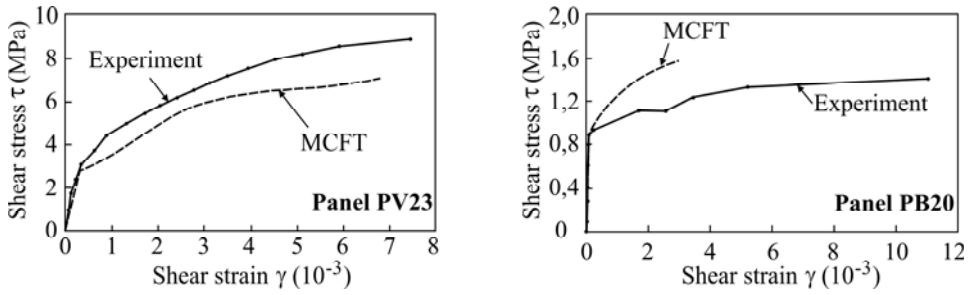

Figure 2.21−Shear stress-strain diagram of panel test PV 23 and panel test PB20 *[Vecchio (2000)]*

Tests also showed that the original simplifying assumption of MCFT which states the directions of the average principal strain remained coincident with the directions of the average principal stresses in the concrete was strictly not the case. Additionally, the crack shear check is a quite difficult procedure in the implementation of the MCFT. To overcome the above disadvantages, Vecchio (2000) suggested a Disturbed Stress Field Model which is a hybrid formulation between a fully rotating crack model and a fixed crack model. This new model fundamentally was established on the concepts of the Modified Compression Field Theory with two advancements including a new approach to the reorientation of concrete stress and strain fields and an improved treatment of shear stresses on crack surfaces. These two advancements theoretically were believed to help the Disturbed Stress Field Model produces a better result with a simpler calculating procedure than the MCFT does. However, this model was only introduced at the fundamentally theoretical level, and so it requires to be further developed for practical applications.

Other models to estimate the shear strength of concrete members without stirrups are based on fracture mechanics. From the typical shear failure of concrete beams, mostly caused by the propagation of a single critical diagonal crack, fracture mechanics approaches assumed that there was a peak tensile stress at the tip of this diagonal crack and a reduced tensile stress (softening) in the cracked zone. Some models of this approach explained the existence of size effect and suggested various size-effect laws for shear failure of concrete beams. Using the cohesive crack concept, Gustafsson et al. (1988) introduced the fictitious crack model and proposed a size effect law with the form $k/d^{1/4}$ (k is a constant of proportionality) after studying the influence of the size, the steel ratio, and the shear span-to-depth ratio (Fig. 2.22).

Jenq et al. (1989) proposed a two-parameter nonlinear fracture mechanics model. The ultimate shear capacity is assumed to be an algebraic summation of the contributions from concrete and reinforcement *[So et al. (1993)]*. The concrete contribution is formulated from the fracture mechanics model while the steel contribution is calculated by considering the average ultimate bond stress (Fig. 2.23). So et al. (1993) improved the Jenq et al's model by taking into account the bond–slip relationship, the dowel action, the aggregate interlock, and shear span to effective depth ratio *a*/*d*. This So et al.'s model predicts the shear capacity of slender beams quite accurately comparing with test results; but it adopted a lot of empirical formulae in the other hand.

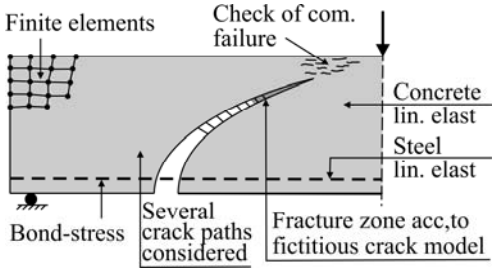

Figure 2.22– Fictitious crack model *[Gustafsson et al. (1988)]*

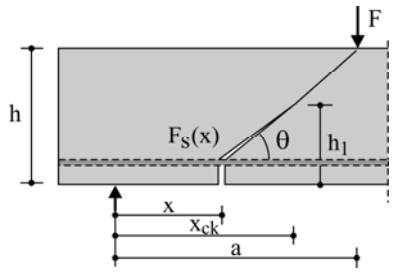

Figure 2.23– The model of Jenq et al. *[Jenq et al. (1989)]*

Bažant et al. developed a set of phenomenological equations from the combination of the arch action and beam action with various size effect's law in terms of fracture mechanics. Since all constant parameters of the final shear strength equations were calibrated with test database, these models should be classified as semi–empirical models and will be presented later in the next section.

The assumptions that flexural-shear failure is triggered by the propagation of a splitting crack at the level of the longitudinal reinforcement and that the ultimate shear load is reached when the splitting crack starts to propagate, Gastebled et al. (2001) proposed another analytical model to estimate the shear failure loads of the concrete beams without stirrups (Fig. 2.24). Derived from the fracture energy approach with a principle that the unit extra work produced by the extra moment to the unit rotation at the tip of diagonal shear crack is equal to the fracture energy necessary to extend the unit unbonded length of longitudinal reinforcement, the shear strength equation, resulted from this model, considered the size effect, shear span to effective depth ratio, longitudinal reinforcement ratio, elastic modulus of steel and concrete strength as follows:

$$V_{Rm} = \frac{1{,}109}{\sqrt{h}} \cdot \left(\frac{h}{a}\right)^{1/3} \cdot \left(1-\sqrt{\rho_l}\right)^{2/3} \cdot \rho_l^{1/6} \cdot \left(f_c'\right)^{0{,}35} \cdot \sqrt{E_s} \cdot b \cdot h \qquad (2.9)$$

This model adopted a semi-empirical formula proposed by Kim et al. (1991) from only 14 experimental results to predict the position of diagonal crack and the empirical Mode I fracture energy equation in the CEB-FIP Model Code 1990. However, the above shear strength

formula was found to have a good agreement with the purely empirical equation for shear design of CEB-FIP Model Code 1990. This outcome encouraged Reinhardt et al. in pursuing the fracture mechanics approach to improve the Gastebled et al.'s model. Basing on Mode II fracture tests, Xu et al. (2005) proposed a modified Gastebled et al.'s formula in which the Mode II fracture energy was used to replace the former empirical Mode I fracture energy as follows:

$$V_{Rm} = \frac{1,09}{\gamma_m \cdot \sqrt{h}} \cdot \left(\frac{h}{a}\right)^{1/3} \cdot \left(1 - \sqrt{\rho_l}\right)^{2/3} \cdot \rho_l^{1/6} \cdot K_{IIc} \cdot b \cdot h \qquad \text{(N, mm, N/mm}^{3/2}\text{ units)} \qquad (2.10)$$

Where: γ_m = 1,35 is the safety factor and K_{IIc} is the Mode II fracture toughness.

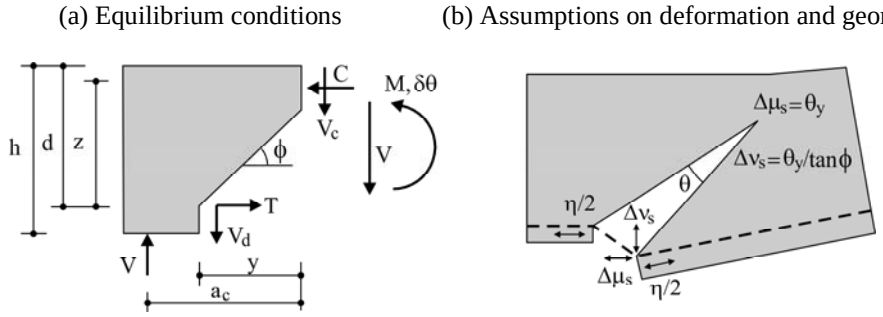

Figure 2.24– Equilibrium conditions and assumptions on deformation and geometry relation of crack of the model by Gastebled et al. (2001) *[Gastebled et al. (2001)]*.

This model actually implies the shear problem of concrete beams without stirrups in terms of another problem of fracture mechanics because it was found to be difficult to determine the Mode II fracture toughness or the Mode II fracture energy by both theoretical analyses and experimental investigations.

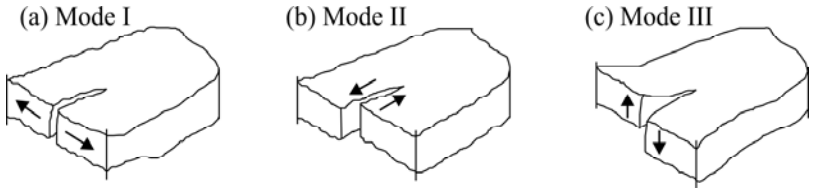

Figure 2.25– Three different cracking modes include Mode I – opening mode; Mode II – shearing mode and Mode III – tearing mode *[Xu et al. (2005)]*

In recent years a significant progress in modelling of concrete and reinforced concrete materials has been achieved and adopted in some commercial finite element method (FEM) software packages. The FEM-based approach, as a result, has rapidly been considered as a promising method to detect the real shear failure mechanisms of concrete beams without stirrups that seem still a challenge for theoretical and empirical analyses. Due to its specific characteristics, this approach will be discussed into details in the Chapter 4 (Nonlinear Finite Element Analysis).

2.4 Empirical Models

Empirical approach to formulate a strength model for shear design of concrete members without stirrups was early adopted by many authors, for example Moody et al. (1954, 1955), Morrow et al. (1957), Bresler et al. (1963), Mathey et al. (1963), Krefeld et al. (1966). Zsutty (1968), by using regression analysis of the shear data of 86 reinforced concrete slender beams without stirrups, introduced an empirical expression for the ultimate shear strength of simple, rectangular, slender (*a/d > 2,5*) beams without stirrups under concentrated load as in the following equations :

$$V_{Rm} = 2,21\left(f_c' \cdot \rho_l \cdot \frac{d}{a} \right)^{1/3} \cdot b \cdot d \qquad (2.11)$$

$$V_{Rm} = \left(2,5\frac{d}{a} \right) \cdot 2,2\left(f_c' \cdot \rho_l \cdot \frac{d}{a} \right)^{1/3} \cdot b \cdot d \qquad \text{for } a/d \le 2,5 \qquad (2.12)$$

It can be concluded from the formulae that the shear strength of slender beams depends on three parameters named as compressive concrete strength f'_c, longitudinal reinforcement ratio ρ_l and shear span to depth ratio a/d. However, it is quite interesting to note that these three main parameters have the same influence on the shear strength of beams. In addition, the formulae neglect the size effect that has a strong influence on shear strength as verified later.

Okamura et al. (1980) and Niwa et al. (1986, 1988), by using the weakest link assumption according to Weibull's statistical theory, proposed a different formula for shear strength of beams as follows *[Gastebled et al. (2001)]*:

$$V_{Rm} = 200\frac{\left(100\rho_l\right)^{1/3}}{d^{1/4}} \cdot \left(f_c' \right)^{1/3} \cdot \left(0,75 + \frac{1,4d}{a} \right) \cdot b \cdot d \qquad (V_{Rm} \text{ in kN}, f_c \text{ in MPa}, b, d \text{ in m}) \qquad (2.13)$$

The above formula has an identically exponential form of compressive concrete strength f'_c and percentage ratio of longitudinal reinforcement ρ_l as in Zsutty's function; but the shear span to depth ratio a/d is different and a new term $d^{0,25}$ is appended to consider size effect. This formula was later slightly modified and adopted in the Japanese code for shear design of concrete structures without stirrups.

Developed empirically from a large shear database, the formula in the CEB-FIP Model Code 1990 also owns the same dimensional form in relation of shear strength to compressive concrete strength f'_c and to longitudinal reinforcement ratio ρ_l as suggested by Zsutty (1968). The influence of shear span to depth ratio a/d and size effect d were judged in other forms different from those of Okamura et al.'s formula as follows:

$$V_{Rm} = 150\left(1+\sqrt{\frac{0,2}{d}}\right)\cdot\left(\frac{3d}{a}\right)^{1/3}\cdot\left(100\rho_l\right)^{1/3}\cdot\left(f_c'\right)^{1/3}\cdot b\cdot d \quad (V_{Rm} \text{ in kN, } f_c \text{ in MPa, } b, d \text{ in m}) \quad (2.14)$$

This formula later was slightly modified and adopted in Eurocode 2 and German code DIN 1045-01 for shear design of concrete structures without stirrups.

The ACI-ASCE Shear Committee (1962), after studying the large amount of available experimental results, introduced an empirical expression for the ultimate shear strength. That expression first appeared in the ACI 318 Code (1963) and is still present in ACI 318-05 (2005) as follows (V_{Rm} in kN, f_c in MPa, b, d in m):

$$V_{Rd} = \left(0,16\sqrt{f_c'}+17\rho_l\cdot\frac{V\cdot d}{M}\right)\cdot 10^3 b\cdot d \;\le 290\sqrt{f_c'}\cdot b\cdot d \quad \text{and } V_u\cdot d/M_u \le 1 \quad (2.15)$$

Accompanied with the above expression is another more simplified but more popular expression as follows:

$$V_{Rd} = 170\sqrt{f_c'}\cdot b\cdot d \quad (V_{Rm} \text{ in kN, } f_c \text{ in MPa, } b, d \text{ in m}) \quad (2.16)$$

It is noted from the two expressions in ACI 318 Code that compressive concrete strength f'_c and longitudinal reinforcement ratio ρ_l do not have the same influence on the shear strength as in other codes. In addition, the later expression in ACI 318 Code implies that shear will be mainly carried by concrete. It is also seen that the two expressions of ACI 318 Code noticeably did not take into account the size effect of concrete structures. That makes it become unsafe for design of relative large structures as many authors have mentioned *[Angelakos et al. (2001)]*.

Muttoni (2003) assumed that the arch action is the unique mechanism responsible for shear resistance of concrete beams as a result of the development of diagonal critical shear crack. The shear strength of members without stirrups was proposed to be correlated to the square root of the concrete compressive strength. Some parameters governing the arching action such as the critical shear crack width w and the maximum aggregate size a_g were considered as in the following equation:

$$V_{Rm} = \sqrt{f_c'}\cdot f\left(w, a_g\right)\cdot b\cdot d \quad (2.17)$$

To determine the value of the critical shear crack width w, the author assumed two hypotheses that (1.) the shear strength is checked at the critical section depending on the load configuration with a control depth *0,6d* from the extreme compression fiber (Fig. 2.26) and (2.) the critical crack width w is proportional to the product of the longitudinal strain in the control depth ε times the effective depth of beam d.

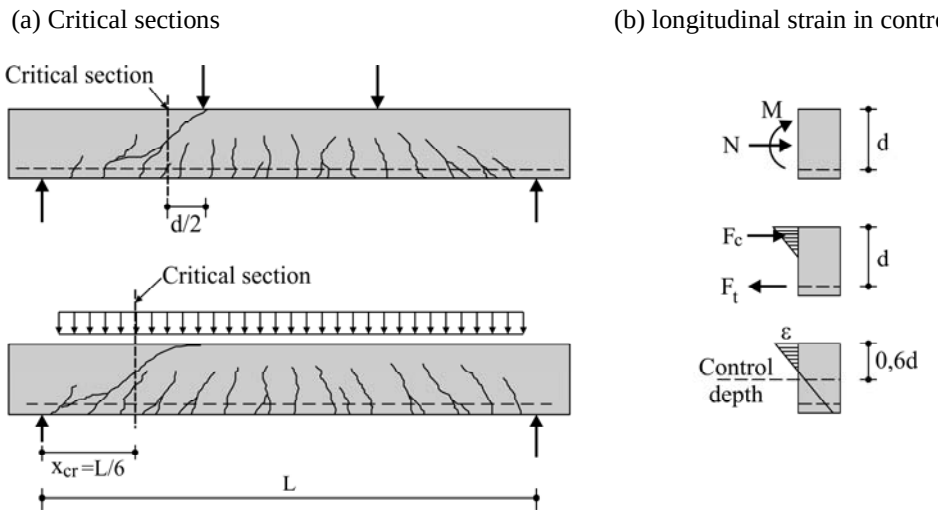

Figure 2.26– Critical section for point loading and distributed loading and determination of longitudinal strain in control depth using internal forces *N* and *M* of the critical shear crack model *[Muttoni (2003)]*.

Based on the systematic evaluation of 253 shear tests, the semi-empirical equation for shear strength of members without stirrups was expressed by the following formula:

$$V_{Rm} = \frac{\tau_c}{0,9 + 2,3\varepsilon_t \cdot d \cdot k_{dg}} \cdot b \cdot d \qquad (2.18)$$

Where:

$\tau_c = 0,3\sqrt{f_c'}$ with f'_c in MPa

$\varepsilon_t = \frac{M}{d \cdot \rho_l \cdot E_s \cdot (d - c/3)} \cdot \frac{0,6d - c}{d - c}$ is the strain in the control depth

$c = d \cdot \rho_l \cdot \frac{E_s}{E_c} \cdot \left(\sqrt{1 + \frac{2E_c}{\rho_l E_s}} - 1 \right)$ is the depth of the compression zone

$k_{dg} = \frac{48}{a_g + 16}$ includes the influence of the maximum aggregate size a_g [mm].

The above formula predicts quite well the critical shear strength of many tests. It is adopted in the Swiss Code SIA 262 (SIA 2003b) under a more simplified expression.

Basing on the model suggested by Muttoni (2003), Latte (2009) proposed another similar model for shear strength of concrete structures without stirrups as follows:

$$V_{Rm} = \frac{b_w \cdot d \cdot f_{ct}}{0,23 + 121\varepsilon_t \cdot k_{dg}} \cdot \frac{1}{\sqrt{1 + 55d \cdot f_{ct}^{0,25}}} \qquad (2.19)$$

Where:

$f_{ct} = 2{,}12 \ln\left(1 + \frac{f_c}{10}\right)$ concrete tensile strength according to Remmel (1994) [MPa]

$\varepsilon_t = \frac{\frac{M_{Ed}}{d - c/3} + V_{Ed}}{b_w \cdot d \cdot \rho_l \cdot E_s}$ strain in the axis of longitudinal reinforcement in the control section

$c = d \cdot \rho_l \cdot \frac{E_s}{E_c} \cdot \left(\sqrt{1 + \frac{2E_c}{\rho_l E_s}} - 1\right)$ depth of the compression zone

$k_{dg} = \frac{3}{\left(3 + a_g\right)^{0,25}}$ includes the influence of the maximum aggregate size a_g [mm].

d effective depth of section [m]

Bentz (2005) proposed a fractional equation with two independent parameters A2 and B2 and later calculated them to fit best with experimental data of 124 tests. The normalized shear stress at failure is expressed as follows:

$$\tau_u = \sqrt[0,333]{\rho_l} \cdot \frac{240}{1000 + s_e} \cdot \sqrt{f_c'} \quad \text{with} \quad s_e = 0{,}9d \cdot \frac{35}{a_g + 16} \tag{2.20}$$

and a more simplified form proposed for practice:

$$\tau_u = \frac{200}{1000 + s_e} \cdot \sqrt{f_c'} \quad \text{with} \quad s_e = 0{,}9d \cdot \frac{35}{a_g + 16} \tag{2.21}$$

According to the above formulae, longitudinal reinforcement ratio ρ_l does not have the same influence on the shear strength as large as compressive concrete strength f'_c does. The shear strength of concrete structures depends not only on the size effect but also aggregate size a_g in concrete mixture. In addition, it is also interesting to recognize the similar form of the above formulae with those suggested by Muttoni (2003).

In another attempt to achieve a more reasonable equation that captures the shear failure mechanism of beams, some authors firstly based on phenomenological study approach to set up mechanical models and later calibrated them with available experimental data to produce so-called semi-empirical formulae for shear strength of concrete beams without stirrups. One of such models is that based on the fundamental relationship between shear and the rate of change of bending moment along a beam. As a result, a shear strength equation that combines beam action and arch action is developed with some unknown parameters. Bažant et al. (1984) followed such procedure and introduced a nominal shear stress expression at failure with 5 unknown coefficients. The shear stress formula later was multiplied with a function,

proposed by Bažant from nonlinear fracture mechanics, to consider the size effect. These 6 unknown parameters of the final equation were later calibrated by statistical analysis of 296 test results. The mean ultimate nominal shear strength formula was suggested as follows:

$$V_{Rm} = \frac{\rho_l^{1/3}}{\sqrt{1+d/(25a_g)}}\left[0{,}833\sqrt{f_c'} + 207\sqrt{\rho_l/(a/d)^5}\right]\cdot b\cdot d \qquad (2.22)$$

Bažant et al. (2005, 2007) lately introduced another formula for shear strength of concrete members without stirrups by least-square optimum fitting of the ACI-445F shear database consisting of 398 data points. The key variation of this formula compared with others of Bažant et al. was that the general approximated mathematical form of the size effect's law was purely calibrated by experimental data *[Bažant et al. (2005)]*.

$$V_{Rm} = 0{,}083\mu\cdot\rho_l^{3/8}\cdot(1+d/a)\cdot\sqrt{\frac{f_c'}{1+d/d_o}}\cdot b\cdot d \qquad (2.23)$$

Where:

$$d_0 = 0{,}9201\cdot \mathrm{k}\cdot (f_c')^{-2/3}$$

$$k = 754\sqrt{a_g}$$

μ =13,3 for best fit and μ =10 for design

Bažant has been considered to be one of the first authors who treated size effect in view of nonlinear fracture mechanics and suggested some various size effect's laws. However, these size effect's laws, partly or purely empirical, have still not yet come to any convincing conclusion of size effect on shear strength of concrete structures because they have been derived from a quite limited database.

Similarly Kim et al. (1999) also developed another shear strength equation that combines beam action and arch action but with only two unknown parameters. After calibration with experimental data of 551 tests in the range of *a/d* = 0,98÷9,74, f'_c = 6,1÷109 MPa, and ρ_l = 0,001÷0,066, an ultimate shear strength equation was proposed as follows:

$$V_{Rm} = 0{,}2\left(1-\sqrt{\rho_l}\right)\cdot\left(\frac{d}{a}\right)^r\cdot\left[(f_c')^{0{,}5} + 1020\rho_l^{0{,}9}\cdot\left(\frac{d}{a}\right)^{0{,}6}\right]\cdot b\cdot d \qquad (2.24)$$

with $r = (d/a)^{0{,}6}\cdot\rho_l^{-0{,}1} \le 1$

Although the above equation was based on a rational analysis, it is considered to be quite complicated while it still does not take into account the size effect of concrete structures yet.

Kim et al. (1996) assumed that shear force in a cracked section was resisted by three main shear resistance mechanisms: the compression zone, interlocking action of aggregates and dowel action. Later they combined their model with a modified Bažant's size effect's law to develop a shear capacity equation with 6 unknown parameters. After determining these unknown parameters by experimental data, an equation was proposed for the mean nominal shear strength of reinforced concrete beams as follows:

$$V_{Rm} = 3{,}5 \cdot \left(f_c' \right)^{1/3} \cdot \rho_l^{3/8} \cdot \left(0{,}4 + d/a \right) \cdot \lambda(d) \cdot b \cdot d \qquad (2.25)$$

with $\lambda(d) = \frac{1}{\sqrt{1 + 0{,}008d}} + 0{,}18$

Another simplified equation was also suggested for practical design:

$$V_{Rm} = 15{,}5 \cdot \left(f_c' \right)^{1/3} \cdot \rho_l^{3/8} \cdot \left(0{,}4 + d/a \right) \cdot \left(d^{-0{,}5} + 0{,}07 \right) \cdot b \cdot d \quad \text{for } d \geq 250 \text{ mm} \qquad (2.26)$$

2.5 Code Provisions

This section gives a short overview about shear design provisions for concrete members without stirrups in codes of practice including German Code DIN 1045-01 (2001), ACI 318-05 (2005), Canadian Standard A23.3 (2004) and Swiss Code SN 262 (2003). Actually these proposals just are modified and simplified forms of the before-mentioned mechanical or empirical models.

2.5.1 German Code DIN 1045-1 (2001)

Published in 2001, the German code DIN 1045-01 (2001) uses the empirical formula of the CEB-FIP Model Code 1990 for shear design after neglecting the influence of shear span to depth ratio $(3d/a)^{1/3}$ and using a new safety factor 0,1 instead of 0,15. The design value for the shear resistance V_{Rd} of members without stirrups is given by:

$$V_{Rd} = \left[0{,}10k \cdot \eta_1 \cdot (100\rho_l \cdot f_{ck})^{1/3} - 0{,}12\sigma_{cd} \right] \cdot b_w \cdot d \qquad (2.27)$$

Where :

$\eta_1 = 1$ for normal concrete

$k = 1 + \sqrt{\frac{200}{d}} \leq 2$ factor for size effect with d in mm

$\rho_l = \frac{A_s}{b_w \cdot d} \leq 0{,}02$ longitudinal reinforcement ratio

f_{ck} characteristic cylinder concrete strength ($f_{ck} \leq 100$ MPa)

$\sigma_{cd} = N_{Ed}/(b_w \cdot d)$ axial stress

N_{Ed} design value of the axial force in the cross-section due to loading or prestressing ($N_{Ed} < 0$ for compression)

2.5.2 ACI Code 318-05

The ACI Code 318-05 published in 2005 still uses the expressions proposed by the ACI-ASCE Shear Committee (1962) as follows:

$$V_{Rd} = \left(0{,}16\sqrt{f_c'} + 17\rho_l \cdot \frac{V_{Ed} \cdot d}{M_{Ed}} \right) \cdot 10^3 b \cdot d \le 290\sqrt{f_c'} \cdot b \cdot d \quad \text{and } V_{Ed} \cdot d / M_{Ed} \le 1 \qquad (2.28)$$

and its simplified form:

$$V_{Rd} = 170\sqrt{f_c'} \cdot b \cdot d \qquad (2.29)$$

2.5.3 CSA A23.3 (2004)

The Canadian Standards CSA A23.3 published in 2004 adopted the Modified Compression Field Theory. The angle of the diagonal compression field θ is taken to $\theta = 30°$. The nominal strength for members without stirrups is defined by:

$$V_{Rd} = \frac{0{,}4}{(1+1500\varepsilon_x)} \cdot \frac{1300}{(1000 + s_{xe})} \cdot \sqrt{f_c'} \cdot b_w \cdot 0{,}9d \le 0{,}25 \cdot f_c' \cdot b_w \cdot 0{,}9d \qquad (2.30)$$

The longitudinal strain for members without prestressing, ε_x, is computed at mid-depth of the cross section by:

$$\varepsilon_x = \frac{M_{Ed} / 0{,}9d + 0{,}5N_{Ed} + V_{Ed}}{2E_s \cdot A_s} \qquad (2.31)$$

If ε_x is negative, it is taken as either zero or recalculated by changing the denominator of the above formula such that the equation becomes:

$$\varepsilon_x = \frac{M_{Ed} / 0{,}9d + 0{,}5N_{Ed} + V_{Ed}}{2(E_s \cdot A_s + E_c \cdot A_{ct})}$$

However ε_x shall not be taken as less than $0{,}2 \times 10^{-3}$. The equivalent crack spacing parameter, s_{xe} , is calculated as:

$$s_{xe} = \frac{31{,}5d}{16 + a_g} \le 0{,}765d$$

2.5.4 Swiss Code SN 262

The Swiss Concrete Structures Code SIA 262 published in 2003 utilized the semi-empirical formula suggested by Muttoni with little changes of constant factors and using the characteristic value of the concrete compressive strength f_{ck}. The shear strength of members without shear reinforcements is expressed as follows:

$$\tau_{Rd} = \frac{V_{Rd,ct}}{b_w \cdot d} = \frac{\tau_{cd}}{1,0 + 2,5\varepsilon \cdot d \cdot k_{dg}} \tag{2.32}$$

Where:

$\tau_{cd} = \frac{0,3}{\gamma_c}\sqrt{f_{ck}} = 0,2\sqrt{f_{ck}}$ design value of shear strength

$\varepsilon = \varepsilon_s \cdot \frac{0,6d - c}{d - c} \approx 0,41\varepsilon_s = 0,41\frac{f_{sd}}{E_s} \cdot \frac{m_{Ed}}{m_{Rd}}$

$f_{sd} = f_s / 1,15$ design strength of steel at yielding

$k_{dg} = 48 / (a_g + 16)$

m_{Ed} : the acting design moment

m_{Rd} : the yielding moment.

$\gamma_c = 1,5$: design safety factor

2.6 Shear Strength of Haunched Beams

The reinforced concrete haunched structures or varied-depth concrete members are often used in concrete bridges, such as bridge piers, frames in buildings or bridge slabs. These structures are supposed not only to be more economic but also to have a better load bearing capacity than that of similar straight depth ones. Despite of the popularity of these members, there have just been a small number of investigations about their behaviours under shear. Most codes do not offer any instruction for design of these structures at all except the German DIN code and the ACI code.

In section 11.1.1.2 of ACI 318–05, the term “effects of inclined flexural compression” is used to explain the different stress distribution of haunched beams compared with that of straight-depth beams. This stress distribution results in a shear resistance force as a vertical component of the inclined flexural stresses. These statements are found to be too cursory to apply simply in design of varied-depth concrete members.

In the other hand, the German code DIN 1045-01 explains the shear resistance mechanism of haunched beams and provides detailed design guides in the clause 10.3.2 (4). The shear design formula for haunched beams is introduced as follows:

$$V_{Ed} = V_{Ed0} - V_{ccd} - V_{td} - V_{pd} \le V_{Rd}^{\alpha} \tag{2.33}$$

Where:

V_{Ed0} : Shear force due to dead loads and live loads,

V_{ccd} : Design shear resistance due to inclination of compression chord of beam,

V_{td} : Design shear resistance component of inclined longitudinal tension reinforcements,

V_{pd} : Design shear resistance component of prestressed force,

V_{Rd}^{α} : Design value of shear bearing capacity of haunched beams at design section.

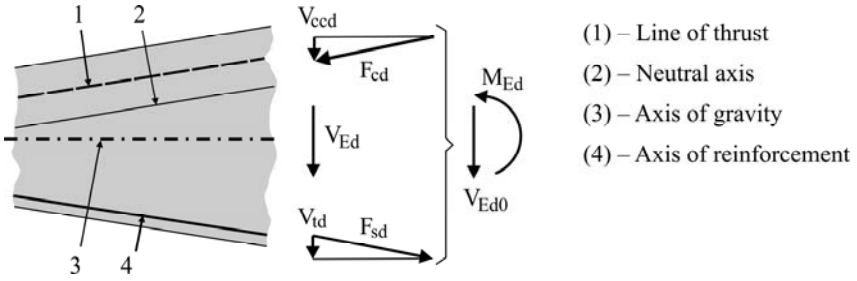

Figure 2.27–Shear resistance components of the varied-depth concrete members *[DIN 1045-01(2001)]*

In members without prestressing and horizontal longitudinal tension reinforcement, where the values of V_{pd} and V_{td} are equal zero, the shear design formula becomes:

$$V_{Ed} = V_{Ed0} - V_{ccd} \le V_{Rd}^{\alpha}$$

or in other form:

$$V_{Ed0} \le V_{Rd}^{\alpha} + V_{ccd}$$

The value of V_{ccd} is defined as follows:

$$V_{ccd} = \frac{M_{Ed}}{z} \cdot \tan\alpha \approx \frac{M_{Ed}}{0,9d} \cdot \tan\alpha \tag{2.34}$$

For other codes which do not mention the shear design of varied-depth concrete members, these structures are usually divided into many intervals with average depths to preserve the similar stiffness of the original structures. This technique may be acceptable for flexural design but it is found to be not accurate for shear design because the shear failure is typically caused by a diagonal crack which has been proved to be influenced by the geometrical features of structures.

The first author who conducted tests with haunched concrete beams was Mörsch in the year 1922 *[Mörsch (1922)]*. The design of test beams is presented in figure 2.28.

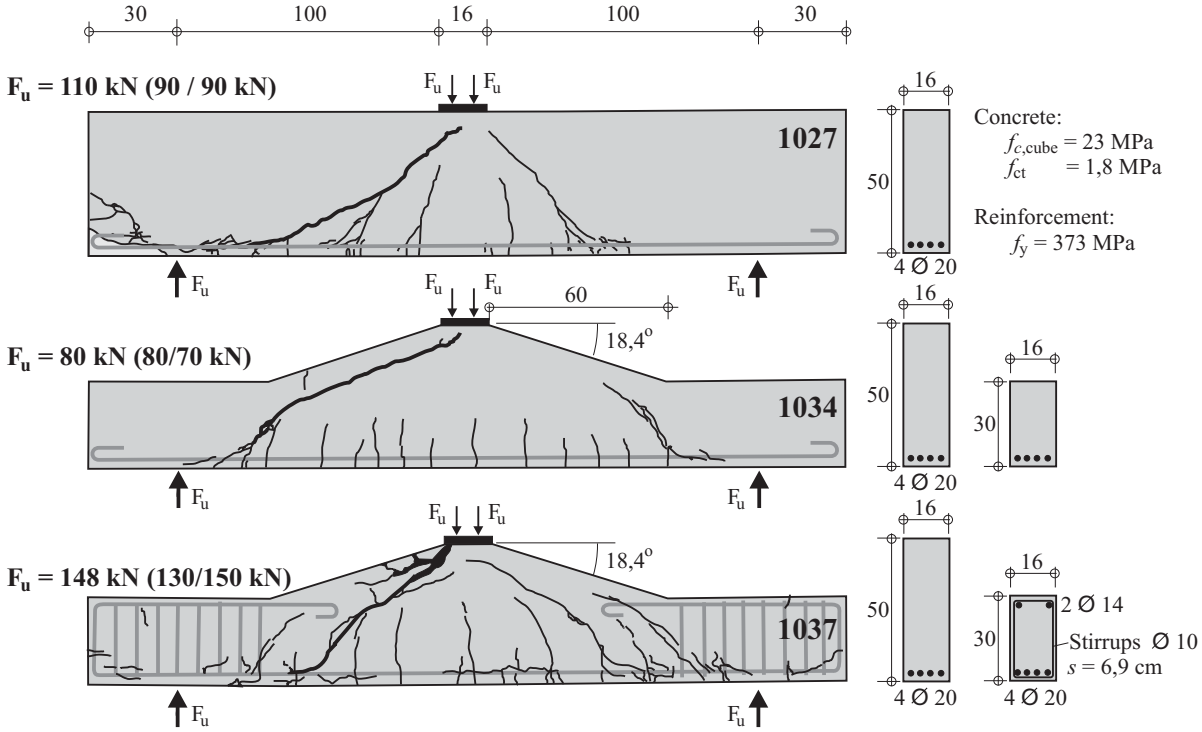

Figure 2.28– Tests beams used by Mörsch *[Mörsch (1922)]*

The test results showed that the load-carrying capacity of the haunched beam No. 1034 ($\alpha = 18{,}4^{o}$) without stirrups was 20 % less than that of the beam No. 1027 with constant depth. The beam No. 1037 with stirrups in the support area shows a considerably bigger load bearing capacity than the beam No. 1034 without stirrups (Fig. 2.28) does. It is noted that plain rebars were placed to reinforce the test beams instead of ribbed ones used today. However, the outcomes of these tests are very remarkable for later investigations.

Debaiky et al. (1982) continued to study the behaviours and strength of reinforced concrete haunched beams in shear. After conducting 33 tests with reinforced concrete beams with different inclinations (Fig. 2.29), the authors concluded that (1) there was no appreciable change in the value of the load at which initial crack appeared and (2) the critical shear crack initiated at different positions for beams of different haunch inclinations. These authors also supposed that the nominal shear contribution of concrete was influenced by the haunch's inclination and can be estimated by the following expression:

$$V_{Rm}^{\alpha} = 0{,}1661\sqrt{f_c'}\cdot\left(1+1{,}7\tan\alpha\right)\cdot b\cdot d \qquad (2.35)$$

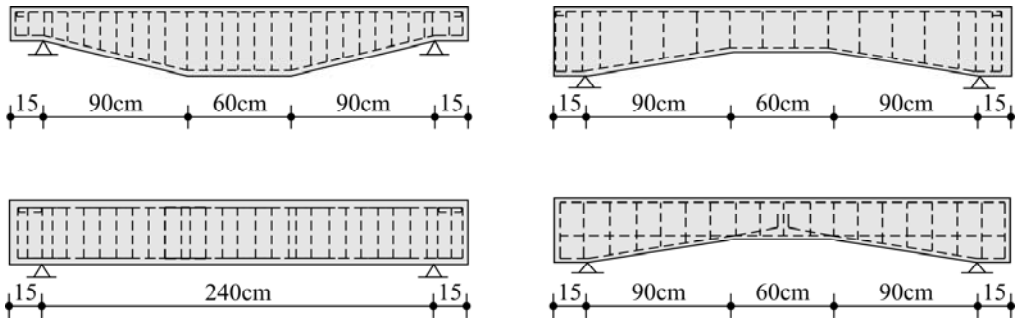

Figure 2.29–Test beams conducted by Debaiky et al. *[Debaiky et al. (1982)]*.

Since the above formula was formulated with the same form of ACI's equation, it can be concluded that the haunch's inclination increased the shear bearing capacity by the expression *(1+1,7tanα)*. It is also noted that all these 33 test beams had stirrups and were set–up in order that the haunched side of beam was under tension while the straight side was under compression. This set–up is found quite unusual because most haunched structures have been designed in the way that the haunched side will be the compression zone in practice.

MacLeod et al. (1994) proposed a formula for estimating the shear strength of reinforced concrete haunched beams without shear reinforcement. Basically, this method was based on the equation proposed in the German Code DIN 1045-01 with a new assumption on the section at which shear strength should be calculated. As a result, a factor *F'* was included to offer a new equation for shear strength of reinforced concrete haunched beams without stirrups as follows:

$$V_{Rm}^{\alpha} = V_{pc} + \frac{M_{Ed}}{d_{cr}} \cdot F' \cdot \tan\alpha \qquad (2.36)$$

Where: V_{pc} : concrete shear strength of parallel–side beam with effective depth d_0 according to clause 3.4.5.3 of the BS 8110 as followed:

$$V_{pc} = \nu_c \cdot b \cdot d_{cr}$$

$$\nu_c = \left(\frac{0,79}{1,25}\right)\left(\frac{f_{cu}}{25}\right)^{0,33}\left(\frac{100A_s}{b \cdot d_{cr}}\right)^{0,33}\left(\frac{400}{d_{cr}}\right)^{0,25}$$

f_{cu} is the cubic compressive strength of concrete

M_{Ed} is the bending moment at the critical section of depth d_{cr}

$$M_{Ed} = \nu_c \cdot b \cdot d_{cr} \cdot C_h$$

$$F' = 0,27\left(1+\tan\alpha\right)^{10}$$

The critical section was defined as in the Fig. 2.30

The effective depth at the critical section: $d_{cr} = d_0 + \left(C_h - S\right) \cdot \tan\alpha$

$$C_h = d_0 + \frac{d_0 \cdot \left(1+\tan\alpha\right) - S \cdot \tan\alpha}{0,68 - \tan\alpha} \approx 2,7d_0$$

Six tests with haunched beams which have slope angles in the range of 5° to 10 ° were also conducted by these authors to verify the proposed formula (Fig. 2.30). Though the proposed formula actually did not produce a good agreement with the test results, it is recognized that the set-up of these tests depicted the working circumstances of reinforced concrete haunched structures in practice as the haunched side is under compression.

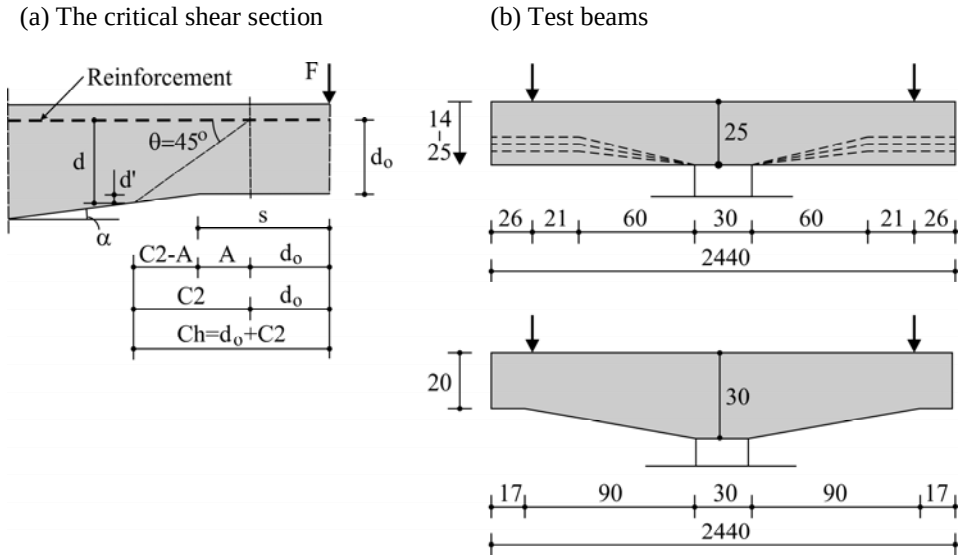

Figure 2.30– Critical shear section and test beams acc. to MacLeod et al. *[MacLeod et al. (1994)]*

2.7 Conclusions

This part gave a brief background of shear behaviours of concrete structures without stirrups. Five actions including (1) shear resistance of the uncracked compression concrete zone, (2) friction of contact surfaces between cracks (aggregate interlock), (3) dowel action of longitudinal reinforcements, (4) crack–bridging tension forces existing in closed cracks (residual tensile stress in concrete) and (5) arch action have been widely accepted as main shear resistance mechanisms in concrete structures without stirrups. In addition, some main factors such as concrete strength f'_c (or f_{ck}), percentage of longitudinal reinforcement ρ_l, *a/d* ratio, size effect *d*…have also believed to be significant factors influencing most on shear strength of these concrete members.

This part also presented about 13 typical shear strength models, which could be classified into mechanical approach and empirical approach, proposed by different authors. The shear design models of some main practical codes accompanied with some researches and tests about haunched concrete structures without stirrups were introduced as well.

The following conclusions can be taken:

There has been a general agreement on some main shear transfer mechanisms but the question of which mechanisms will contribute most to the shear resistance of concrete members without stirrups does not have a unique answer. As a result, there is still not a widely accepted shear strength model even though many mechanical models have been proposed up to now.

Similarly, different semi-empirical or purely empirical expressions show different influences of significant factors on the shear resistance strength of concrete members. Though some empirical formulae confirm a relatively good agreement with shear database, an unlimited number of testing is impossible to cover all structural cases in practice due to widely different geometries and material proportions as well as diverse testing conditions. Therefore, testing should be treated as a verifying means for a particular rational model.

Most of shear design models in practical codes are based on empirical approach. As a result, these models usually need to be checked and adjusted regularly for a while as well as to adopt relatively conservative factors for safety reasons.

There has been very little research on varied-depth concrete members and a lack of design instructions in practical codes in spite of their popularity. An adequate attention should be given to these structures in order to improve understandings of their behaviours as well as to offer more effective design instructions.

The above conclusions lead to a thought for this research that there may be a short understanding of shear transfer mechanisms in concrete. The widely accepted shear transfer mechanisms should be re-evaluated evidently and in quantities. Besides, there are also doubts about a certain unknown shear transfer mechanism. In order to detect load carrying mechanisms, nonlinear Finite Element Analysis (NFEM) is adopted to investigate the behaviours of concrete members under different loadings. An experimental program will be designed to survey structural behaviours under loading and to verify NFEM’s outcomes.

Based on these new shear resistance mechanisms, it is expected to introduce a new approach for shear strength models of the concrete members without stirrups. This model will be verified by updated shear database as well as compared with other models. This research focuses on both straight and varied-depth concrete beams without transverse reinforcements.

3 Experimental Program

The experimental program will be briefly presented in this section. Further details can be referred to Appendices A, B, C and D or research reports *[Rombach et al. (2009), (2011)]*.

3.1 Objectives

The experimental program was carried out

(1) to find out shear behaviours up to failure of concrete beams without stirrups with different inclinations of compression chord,
(2) to verify influences of the inclined angle of haunch to the shear resistance of concrete beams,
(3) to confirm effects of some main factors such as a/d ratio or longitudinal reinforcement ratio ρ_l on the shear resistance of test beams and finally
(4) to check the efficiency and safety level of 13 suggested shear strength models and shear design equations in practical codes for predicting the shear strength of straight and haunched concrete beams without stirrups.

3.2 Test Specimens

Test beams were designed to have similar geometries of most bridge deck's slab in practice and other shear tests which had been conducted before. In such structures, the relevant eccentric wheel load normally acts at a distance of about 1,5 m or more from the web and the effective depth is about at least 0,3 m at the critical flexural section. Therefore, the shear span to effective depth ratio of such concrete members correspond to $a/d = 5$. The minimum effective depths of beams at supports were chosen as d = 0,3 m, 0,2 m and 0,15 m. Consequently, inclined angles of such beams are approximately equal to 0°, 4° and 6° correspondingly (test beams 1L, 2L and 3L of figure 3.1).

In order to investigate effects of a/d ratio on shear bearing capacity of variable depth beams, another group of test beams with ratio $a/d = 3$ is designed. The "cantilever" length of these beams is equal to 0,9m. Therefore, inclined angles of beams will be α = 0°, 6,7° and 10° corresponding to effective depths of the beams at the supports of d = 0,3 m, 0,20 m and 0,15 m (beams 1K, 3K and 4K of figure 3.1). Another beam with an inclination of 4° is also added in this group to compare with the beam 2L that has the same inclined angle as well. The effective depth of this beam is 0,24 m at supports (beams 2K of Fig. 3.1). In order to evaluate the influence of moment on shear resistance of haunched beams, two test beams 4L

and 5L are designed with the identical features as 3K and 4K with the shear span to effective depth ratio $a/d = 5$ instead of $a/d = 3$. The region between the support and the end of the beam is reinforced by stirrups to increase the shear resistance strength of this region (beams 4L and 5L of Fig. 3.1). Accordingly, the experimental program will include 9 test beams with inclined angles varying from 0° to 10° in which 5 test beams have $a/d = 5$ and the others have $a/d = 3$ (Fig. 3.1). In order to improve the reliability of the test results and to avoid some risks while casting and testing, the test beams are fabricated in double and thus the final total number of test beams is 18. The shop drawing of test beams is shown in figure 3.1.

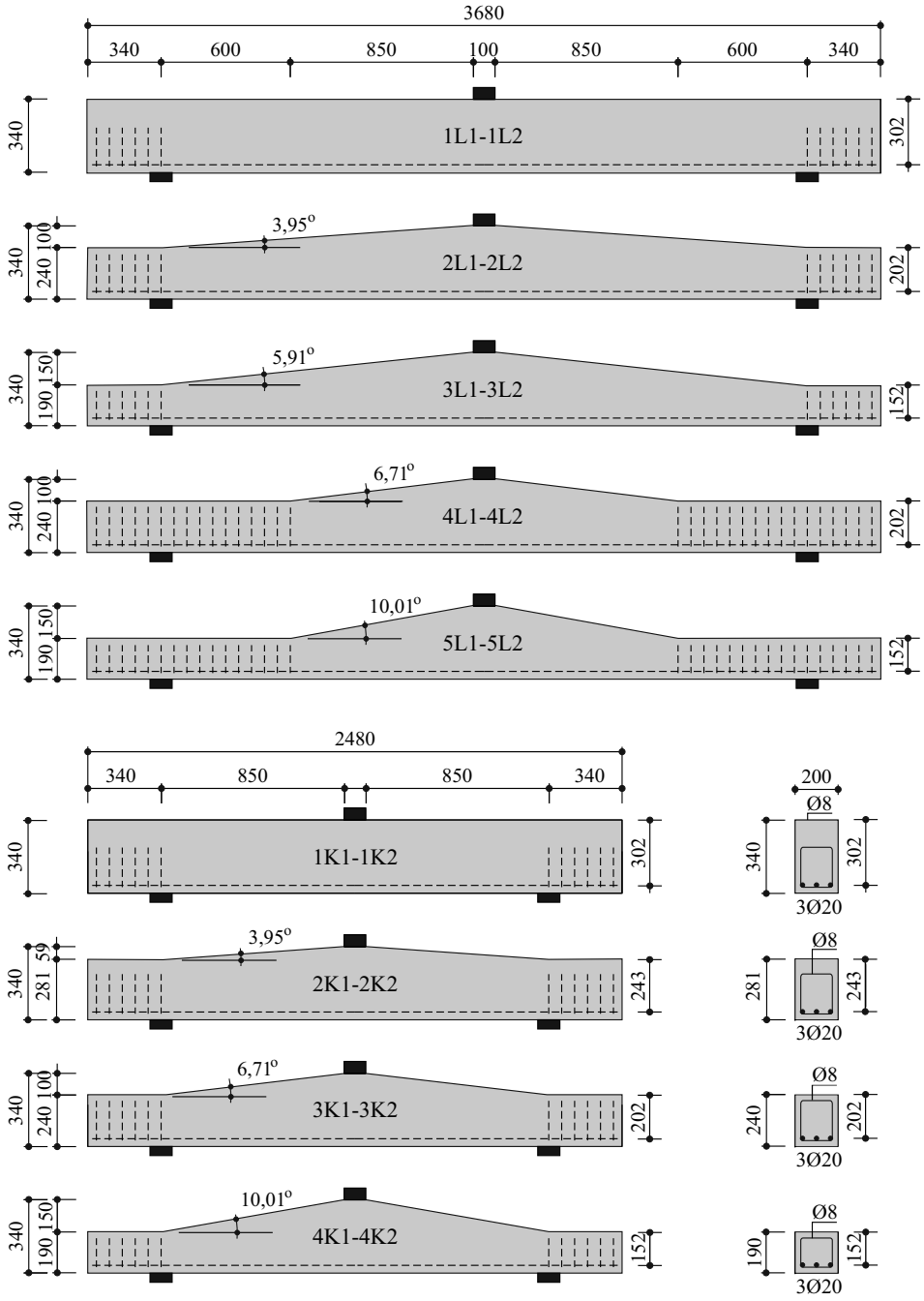

Figure 3.1– Geometrical dimensions of 18 (2x9) test beams

The design for bending of test samples complied with the German code DIN 1045–01. The ordered materials include reinforcement type BSt 500S (design strength f_{yd} = 500 MPa) and ready mixed concrete grade C30/37 (characteristic compressive strength f_{ck} = 30 MPa) with a maximum aggregate size of a_g = 16 mm. The longitudinal reinforcement bars were calculated by considering 2 following conditions: (1) to ensure shear failure to occur in all test beams and (2) to limit the percentage ratio of longitudinal reinforcement within normal ratios of concrete slab structures in practical design. Finally, three longitudinal reinforcement bars ϕ 20 mm were chosen to place in a beam width of 0,2 m. Thus, the percentage ratio of longitudinal reinforcement for effective depths of d = 0,3 m, 0,2 m and 0,15 m are ρ_l = 1,5 %, 2,3 % and 3,1 % respectively. Subsequently the test beams were checked by sectional design method to get some preliminary data about load bearing capacities, displacements and critical sections. The predicted values of the analysis are plotted in figure 3.2 and listed in table 3.1.

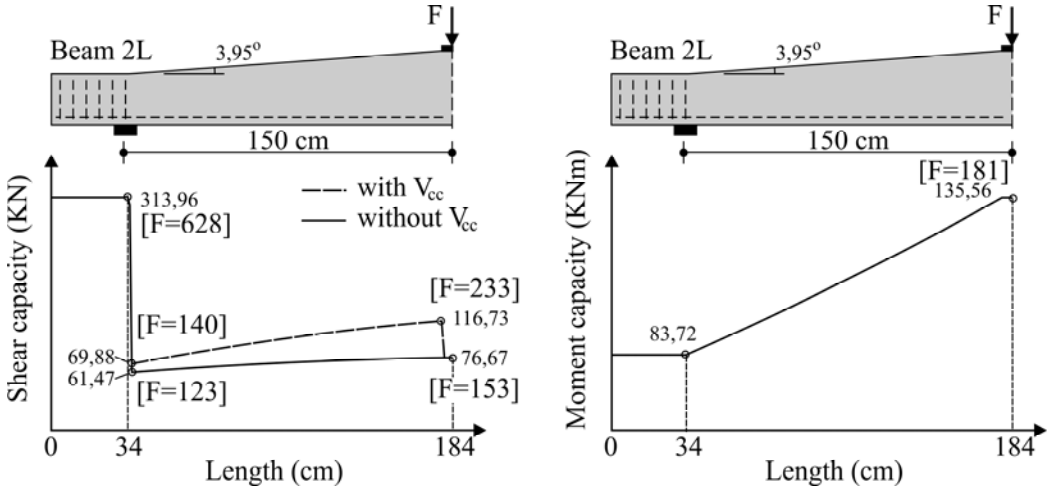

Figure 3.2– Preliminary estimated shear and moment bearing capacity of test beam 2L

Beam	Shear bearing capacity			Moment bearing capacity			Expected failure
	$F_{without}V_{ccd}$ [KN]	$F_{with}V_{ccd}$ [KN]	Critical section	F_M [KN]	Displacement (mm)	Critical section	
1L	153	153	Support	181	10,25	Mid-span	Shear
2L	123	140	Support	181	12,75	Mid-span	Shear
3L	93	119	Support	181	14,75	Mid-span	Shear
4L	123	210	Support	181	15,25	Mid-span	Shear
5L	95	237	Support	181	22,00	Mid-span	Shear
1K	153	153	Support	301	3,60	Mid-span	Shear
2K	140	155	Support	301	4,10	Mid-span	Shear
3K	123	152	Support	301	4,40	Mid-span	Shear
4K	94	139	Support	301	4,50	Mid-span	Shear

Table 3.1– Preliminary estimated load bearing capacity of test beams

3.2.1 Material Properties

(a) Concrete

It was planned to use the concrete class C30/37 according to DIN 1045–01. The composition of used concrete mix is given in table 3.2

Properties	Specification
Cement content	370 kg/m^3
Water content	182 kg/m^3
Water/cement ratio	0,49
Aggregate content: 0 mm – 2 mm 2 mm – 8 mm 8 mm – 16 mm	 748 kg/m^3 368 kg/m^3 700 kg/m^3
Concrete additive (1BV N9)	2,96 kg/m^3
Density of fresh concrete	2.371 kg/m^3

Table 3.2– Used concrete mix

The actual concrete strengths are determined by tests after 28 days, 52 days and 101 days. Since the test samples were tested at different times, characteristic compressive strengths f_{ck} of test beams were estimated according to CEB-FIP MC90 (3.1) and given in table 3.3.

$$f_{ck,t} = f_{cm,28} \cdot e^{s\left[1-\left(\frac{28}{t}\right)^{0,5}\right]} - 4\ MPa \qquad (3.1)$$

Where:

$f_{ck,t}$: Characteristic compressive strength of concrete at time of t (day of test),

$f_{cm,28}$: Mean compressive strength of concrete at 28 days after concreting,

s : Coefficient which depends on the type of cement.

Details of concrete specimens, compressive testing, tensile testing, testing of modulus of elasticity…can be referred to Appendix A or to test reports *[Rombach et al. (2009), (2011)]*.

(b) Reinforcement

It was planned to use the reinforcement class BSt500s according to DIN 1045-01. Three samples of used reinforcement ϕ20 mm were tested. The stress-strain curves are given in figure 3.3. From this figure, it is reasonable to use the value of effective yield strength f_{sd} of 550 MPa for later calculations. Details of geometrical dimensions and material properties of test beams are summarized as in the table 3.3.

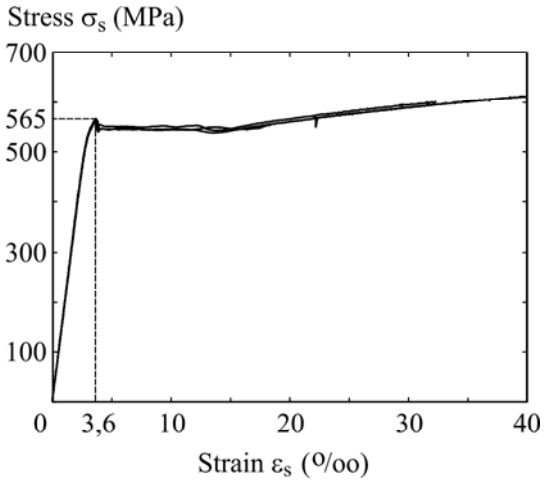

Figure 3.3– Stress–strain graph of main bars ϕ20 mm

No	Beam	*d* (mm)	*b* (mm)	*a*/*d*	f_{ck} [MPa]	f_{sd} [MPa]
1	1L-1	300–300	200	5	48,11	550
2	1L-2	300–300	200	5	49,24	550
3	2L-1	200–300	200	5	49,45	550
4	2L-2	200–300	200	5	49,99	550
5	3L-1	150–300	200	5	50,21	550
6	3L-2	150–300	200	5	50,98	550
7	4L-1	200–300	200	5	52,21	550
8	4L-2	200–300	200	5	52,44	550
9	5L-1	150–300	200	5	53,13	550
10	5L-2	150–300	200	5	53,25	550
11	1K-1	300–300	200	3	53,86	550
12	1K-2	300–300	200	3	53,95	550
13	2K-1	240–300	200	3	54,18	550
14	2K-2	240–300	200	3	54,22	550
15	3K-1	200–300	200	3	54,26	550
16	3K-2	200–300	200	3	54,31	550
17	4K-1	150–300	200	3	54,78	550
18	4K-2	150–300	200	3	54,82	550

Table 3.3– Main parameters of 18 test beams

3.2.2 Fabrication of the Test Specimens

The fabrication of the test beams was done at the Laboratory of the Institute of Concrete Structures, Hamburg University (TUHH). All used materials and the producing procedure including casing, reinforcement, concrete, curing complied with the construction regulations for concrete structures in practice.

(a) Casing

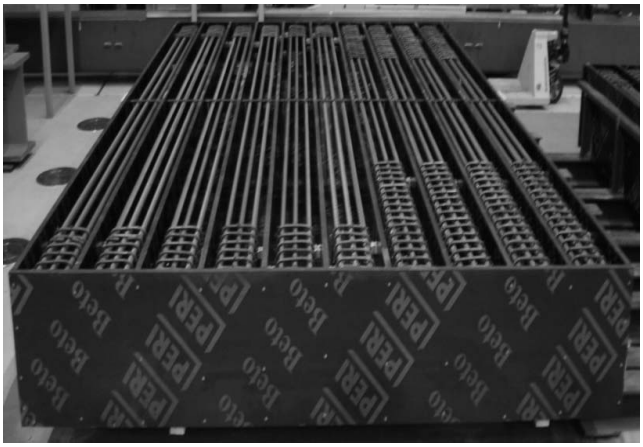

(b) Reinforcing

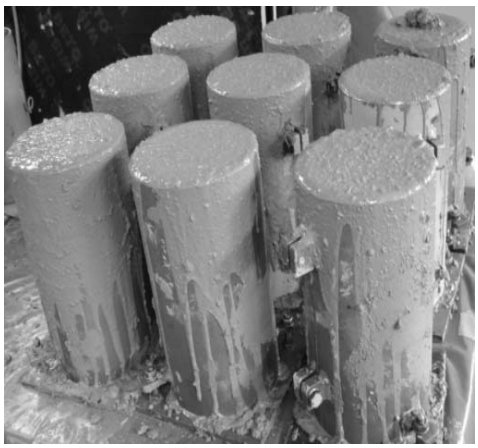

(c) Concrete specimen

(d) Curing

Figure 3.4– Fabrication of the test specimens

3.2.3 Data Acquisition System

To monitor behaviours of the test beams such as strains at the top surface and at the neutral axis of beams, displacements or width opening of critical flexural crack, the used data acquisition devices include:

+ 6 strain gauges ($\varepsilon_{l\,1\text{-}3}$, $\varepsilon_{r\,1\text{-}3}$) located at top surface of beam (3 each left and right side),

+ 2 manual strain meters to measure strain at points 4-12 of both left and right side ($\varepsilon_{l\,4\text{-}12}$, $\varepsilon_{r\,4\text{-}12}$), (see fig. 3.5b)

+ 3 displacement detectors (w_l, w_m, w_r) located at middle, left and right positions of beam,

+ 1 displacement transducer (r_m) measuring the width opening of critical flexural crack at mid-span of beam,

+ 2 cameras and 2 video recorders.

The detailed arrangement of these measuring devices of test beam 2L, for example, is shown in the following figure:

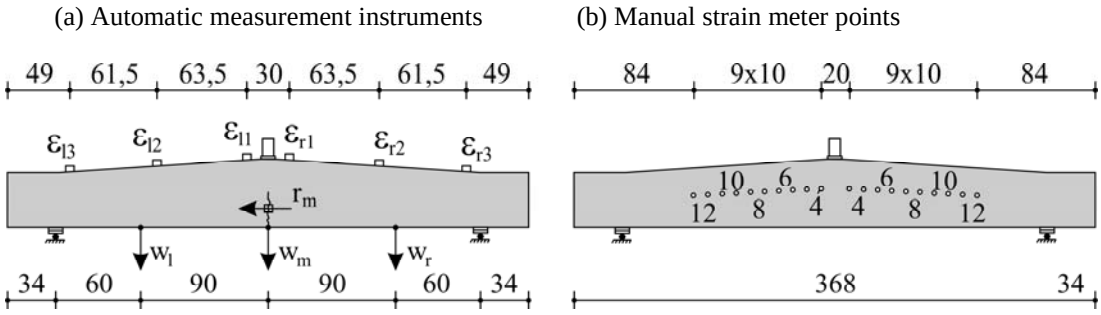

Figure 3.5– Data acquisition system for test beam 2L

3.3 Testing Procedure

3.3.1 Experimental Set–up

A hydraulic jack of 500 KN (max.) attached at a testing steel frame was used to load the test beams at the mid-span through two thick steel plates adhered to the test beams (Fig. 3.6). The contact area between the steel pad and concrete beams is 100 mm × 200 mm. The test beam was supported by two steel-box bearings 100 mm × 200 mm located on steel pins. These two steel-box bearings were later adjusted to be fixed or moveable during the test to ensure the boundary conditions of the system.

3.3.2 Loading Procedure

Loading was gradually increased from 0 kN up to failure with each 10 kN load step. It was decided to stop about 8 minutes after each load step for observation and strain measurement (Fig. 3.7). When the first flexural crack appears, normally at mid-span, a displacement transducer (r_m) was installed to measure the width opening of the critical flexural crack at the

reinforcement layer. All cracks were detected and marked with numerical order and loading value.

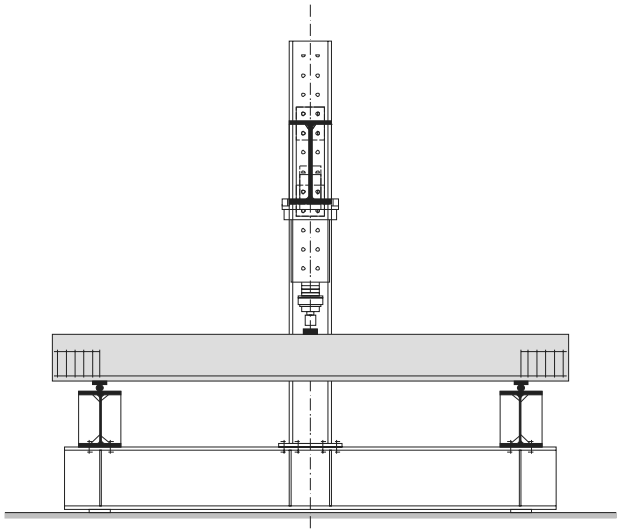

(a) Test Set-Up

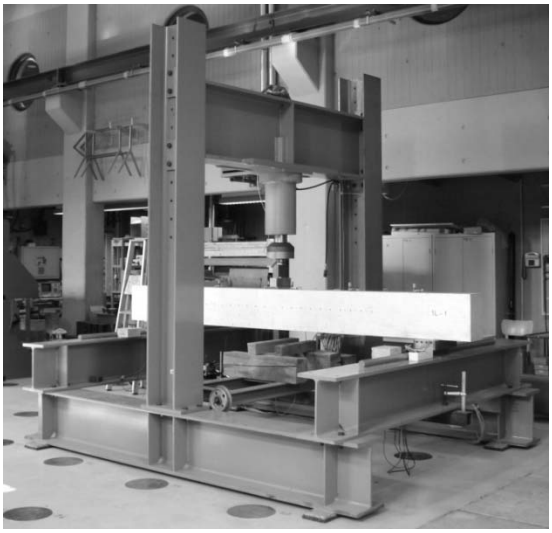

(b) Test Set-Up of beam 1L1

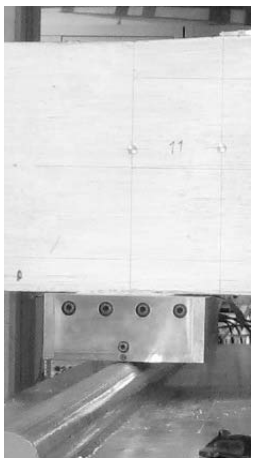

(c) Moveable support

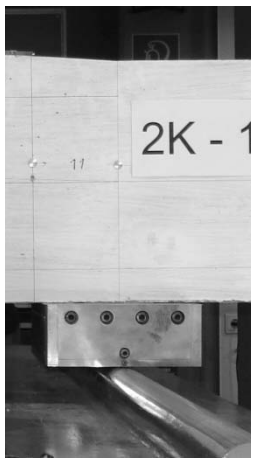

(d) Fixed support

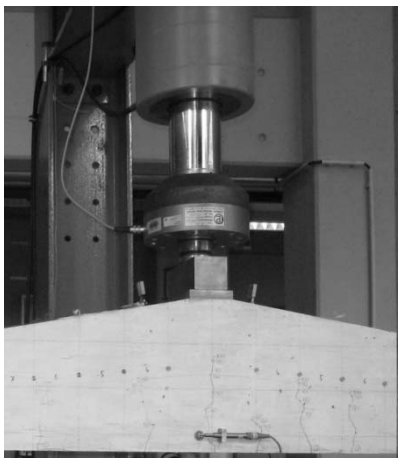

(e) Hydraulic jack

Figure 3.6– Test Set-up

3.4 Experimental Results

3.4.1 Behaviours of Test Beams until Failure

(a) Failure modes: Among the 18 test specimens, 14 beams failed in shear and 4 ones failed in flexure. The test beams failed in shear were pairs of beams 1L, 2L, 3L, 1K, 2K, 3K and 4K whereas the ones failed in flexure were pairs of beams 4L and 5L.

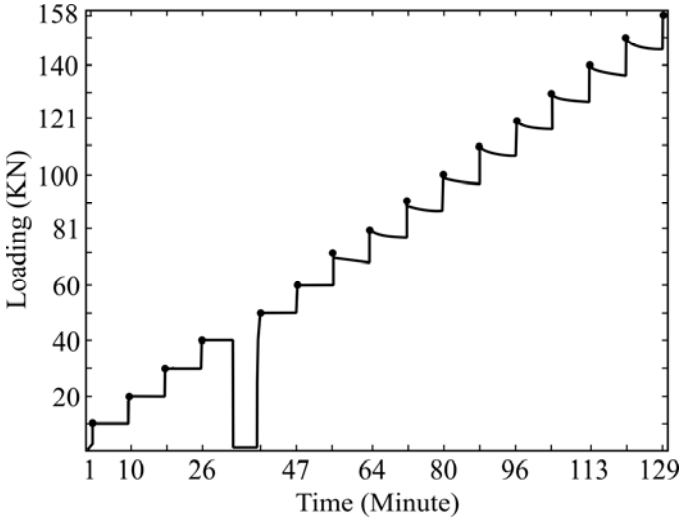

Figure 3.7– Loading procedure of test 1L–2

(b) Phenomena of flexure failure: For beams failed in flexure, ductile failure took place gradually with the widening of the critical flexural crack at the mid-span of beam. The beams still have capability to resist load as long as the longitudinal reinforcements has not exceed the yield strength yet or the compressive strength of concrete is not reached. The deformation of beams failed in flexure is much larger than that of beams failed in shear.

(c) Phenomena of shear failure: For beams failed in shear, in the other hand, brittle failure happened abruptly right after the formation of a critical diagonal shear crack and the beams could not resist any load more. The load at which the test beams collapse is termed as the ultimate load F_u or the load bearing capacity of test beams. The general shear failure process can be divided into three phases as follows:

Phase 1– Pure flexure behaviour with loading $F \approx 0 \div 0{,}5F_u$: the first flexural crack rapidly occurs at the mid–span and then other flexural cracks emerge when loading increases. The direction of these cracks is almost vertical and perpendicular to the bottom of the beams. When the loading achieves $\approx 0{,}5F_u$, the flexural crack at the mid–span reaches or even already exceeds the neutral axis of beam.

Phase 2– Flexure–shear behaviour with loading $F \approx 0{,}5 \div 0{,}9F_u$: the flexural crack at the mid–span almost stay the same while other formerly flexural cracks and new cracks continue to grow up. The direction of these cracks tends to be inclined with the neutral axis of beam. The higher the crack raises, the flatter the direction becomes. These cracks are termed as flexure–shear cracks since they are originated by bending moment and later influenced by both flexure and shear while propagating. At the end of this stage, some of the inclined cracks reach or even exceed the neutral axis of the beam.

Phase 3– Shear failure with loading $F = 0{,}9 - 1{,}0F_u$: in this phase, the flexure–shear cracks seem not to grow up any more. However, there appear cracks with inclined angle of about 45° at the tips of the flexure–shear cracks or there appear pure shear cracks in the web of beam. When the loading reaches the ultimate value F_u, a critical diagonal shear crack forms suddenly to penetrate into the concrete compression zone of beam and go down the position of longitudinal reinforcement. It can be seen at the same time the splitting between longitudinal reinforcements and concrete cover. It is also recognized that the upper end of the critical diagonal shear crack always tends to last to the position of load while the lower end extends to the support.

The further details of the formation and propagation of cracks of all tests can be referred to Appendix B or test reports *[Rombach et al. (2009), (2011)]*.

(d) Test results: The critical failure loads of tests are presented in table 3.4. More details of testing can be referred to Appendix B or test reports *[Rombach et al. (2009), (2011)]*.

Beam	d (mm)	b (mm)	a/d	α (°)	ρ_l (%)	f_{ck} (MPa)	F_{Test} (kN)	Failure
1L-1	300 - 300	200	5	0	1,57 – 1,57	48,11	151	Shear
1L-2	300 - 300	200	5	0	1,57 – 1,57	49,24	158	Shear
2L-1	200 - 300	200	5	3,95	2,36 – 1,57	49,45	150	Shear
2L-2	200 - 300	200	5	3,95	2,36 – 1,57	49,99	149	Shear
3L-1	150 - 300	200	5	5,91	3,14 – 1,57	50,21	133	Shear
3L-2	150 - 300	200	5	5,91	3,14 – 1,57	50,98	139	Shear
4L-1	200 - 300	200	5	6,71	2,36 – 1,57	52,21	207	Flexure
4L-2	200 - 300	200	5	6,71	2,36 – 1,57	52,44	207	Flexure
5L-1	150 - 300	200	5	10,01	3,14 – 1,57	53,13	206	Flexure
5L-2	150 - 300	200	5	10,01	3,14 – 1,57	53,25	207	Flexure
1K-1	300 - 300	200	3	0	1,57 – 1,57	53,86	151	Shear
1K-2	300 - 300	200	3	0	1,57 – 1,57	53,95	139	Shear
2K-1	240 - 300	200	3	3,95	1,96 – 1,57	54,18	167	Shear
2K-2	240 - 300	200	3	3,95	1,96 – 1,57	54,22	170	Shear
3K-1	200 - 300	200	3	6,71	2,36 – 1,57	54,26	159	Shear
3K-2	200 - 300	200	3	6,71	2,36 – 1,57	54,31	160	Shear
4K-1	150 - 300	200	3	10,01	3,14 – 1,57	54,78	170	Shear
4K-2	150 - 300	200	3	10,01	3,14 – 1,57	54,82	168	Shear

Table 3.4– Summary of test results

3.4.2 Results of Measurements

Results measured by the data acquisition system as presented in the section 3.2.3 including loading procedure, load-deflection relations, load-strain relations and opening of critical flexure crack of beams were recorded continuously during testing. The figures 3.8 to 3.12 present results of measurements of the test beam 2L-1. For other test beams refer to Appendix B or test reports *[Rombach et al. (2009), (2011)]*.

These results were used to analyse main behaviours of concrete beams up to failure as well as to find out similarities and differences of all of test beams. Figure 3.13 shows two graphs of load-midspan displacement of two groups of 18 test beams.

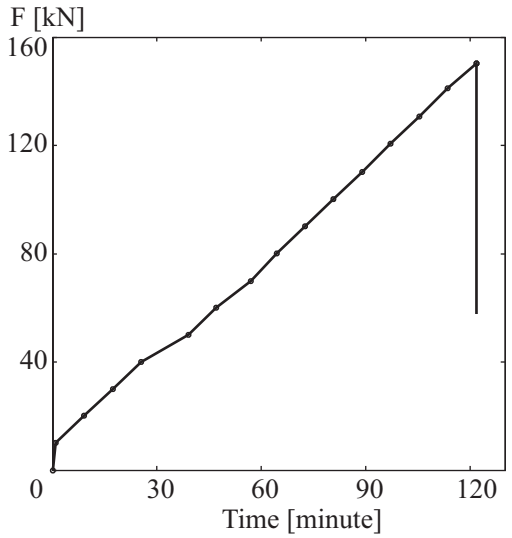

Figure 3.8– Time – Load graph of beam 2L-1

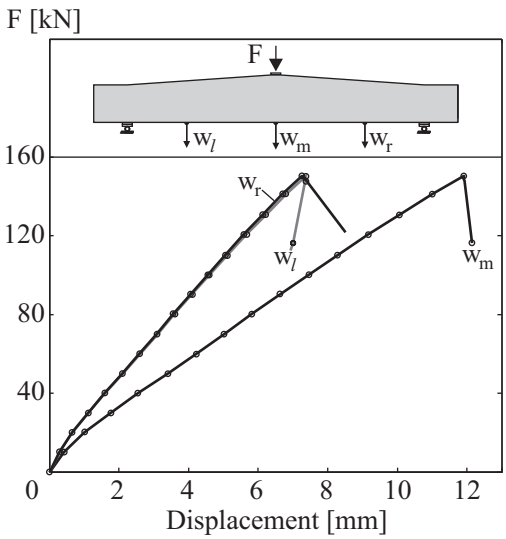

Figure 3.9- Load – Deflection graph of beam 2L-1

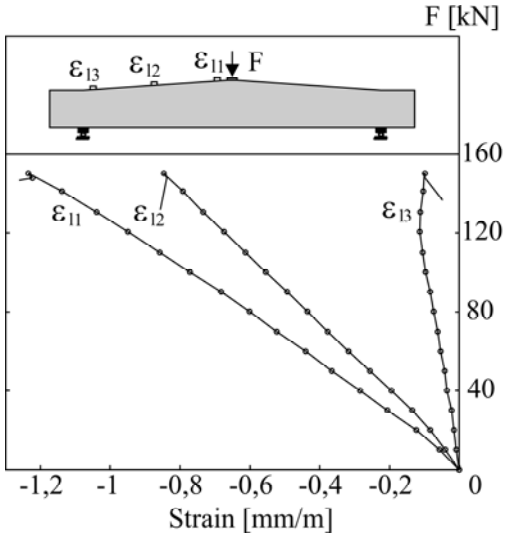

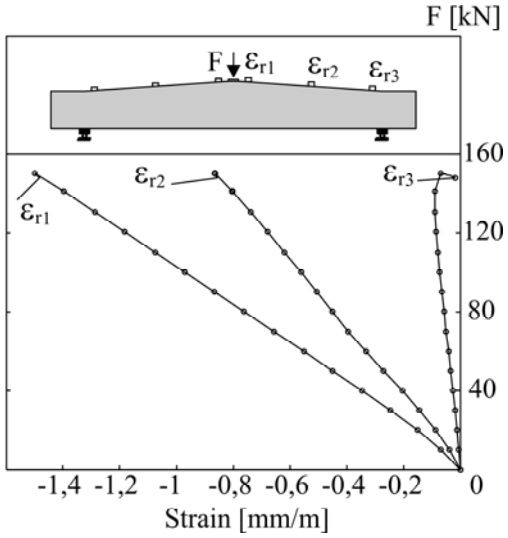

Figure 3.10– Load – concrete strains graph at top surface of beam 2L-1

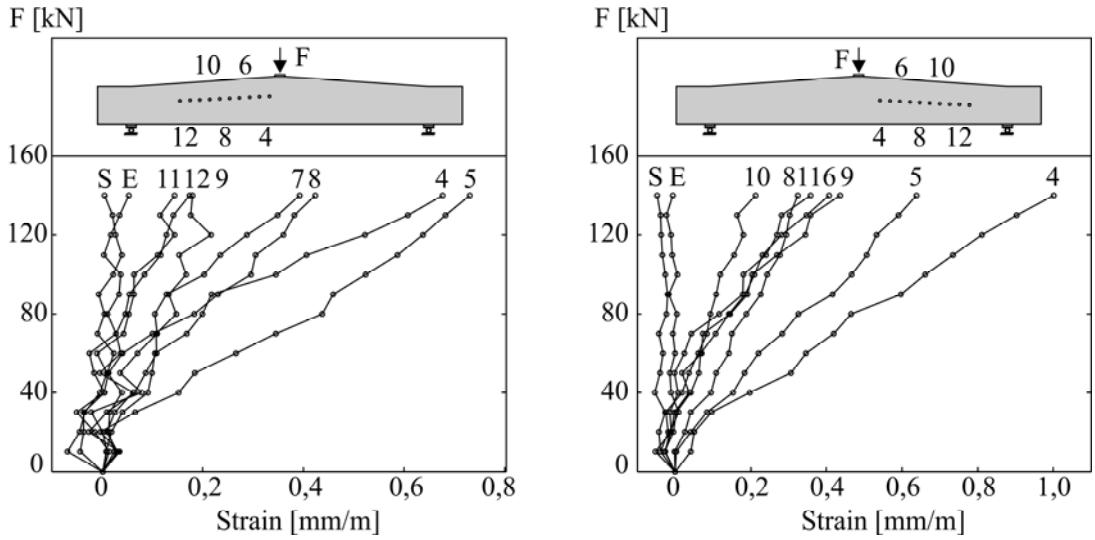

Figure 3.11– Load –Strains graph at mid-depth of beam 2L-1

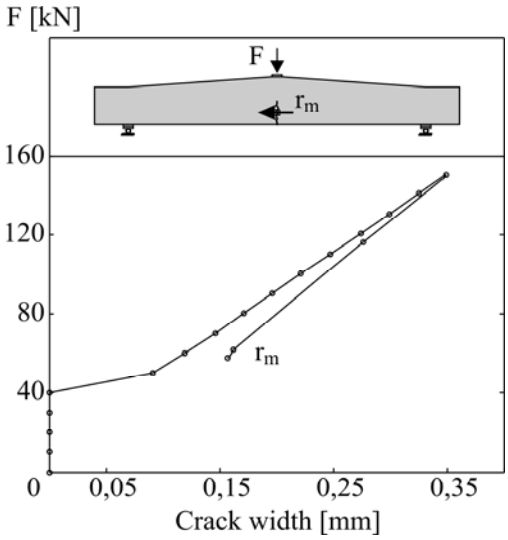

Figure 3.12– Load versus crack width graph of beam 2L-1

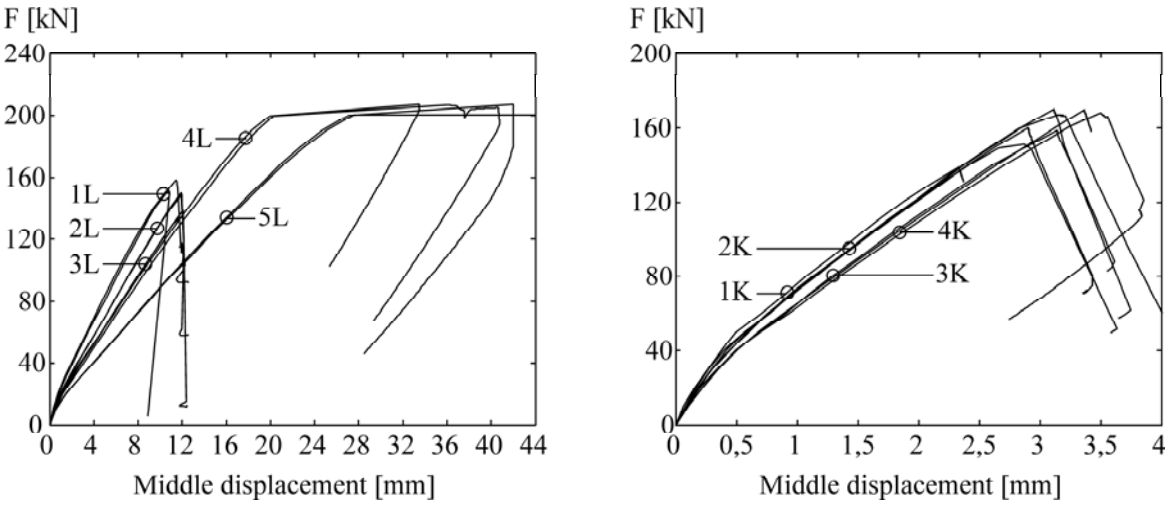

Figure 3.13– Load and displacement curves at mid-span of two groups of 18 test beams

3.4.3 Crack Propagation

Figure 3.14 shows the crack propagation of test beam 2L-1 after each load step until failure. Other tests refer to Appendix B or test reports *[Rombach et al. (2009), (2011)]*. The crack pattern at failure of all test beams is shown in the figure 3.15.

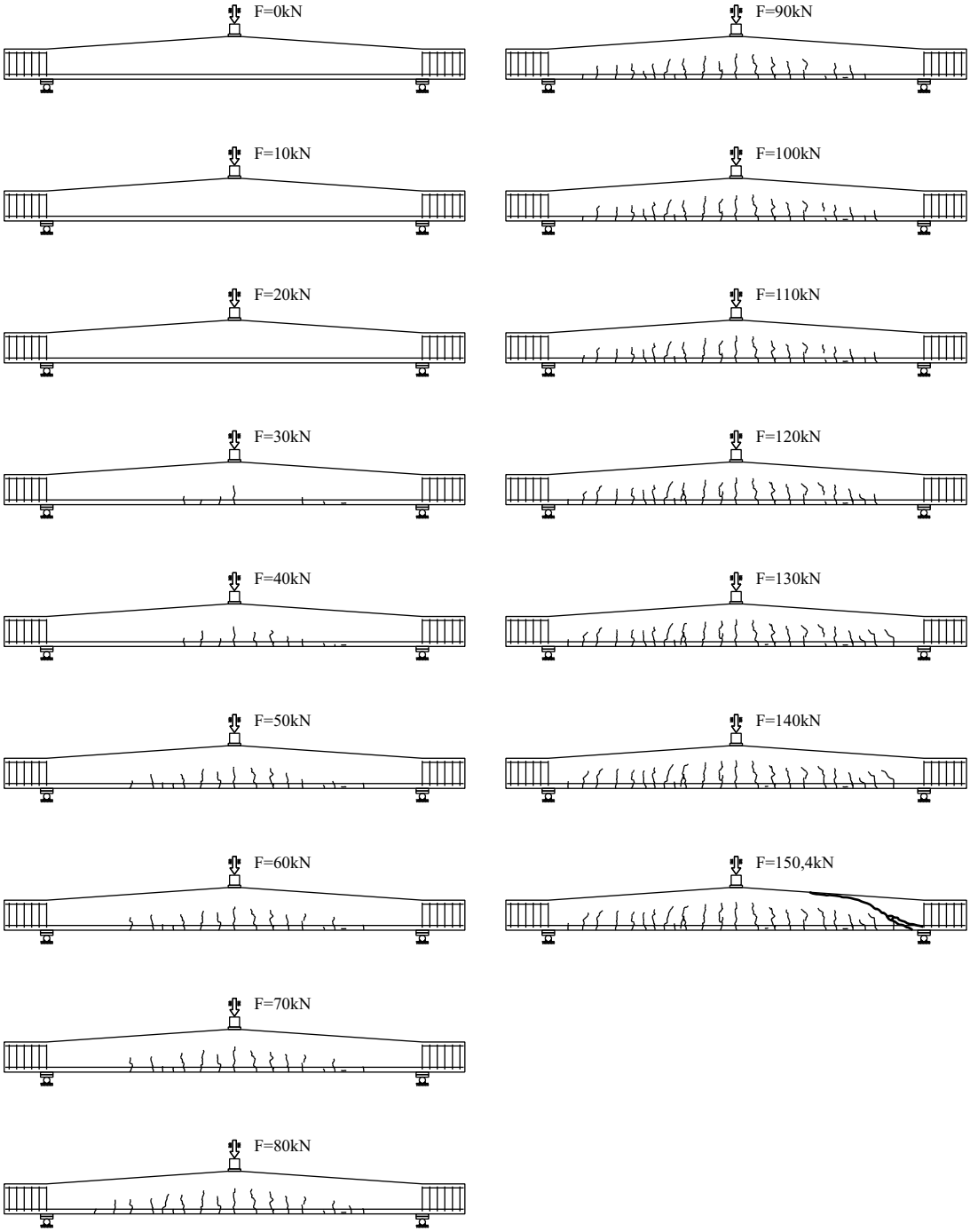

Figure 3.14– Crack propagation of test beam 2L-1

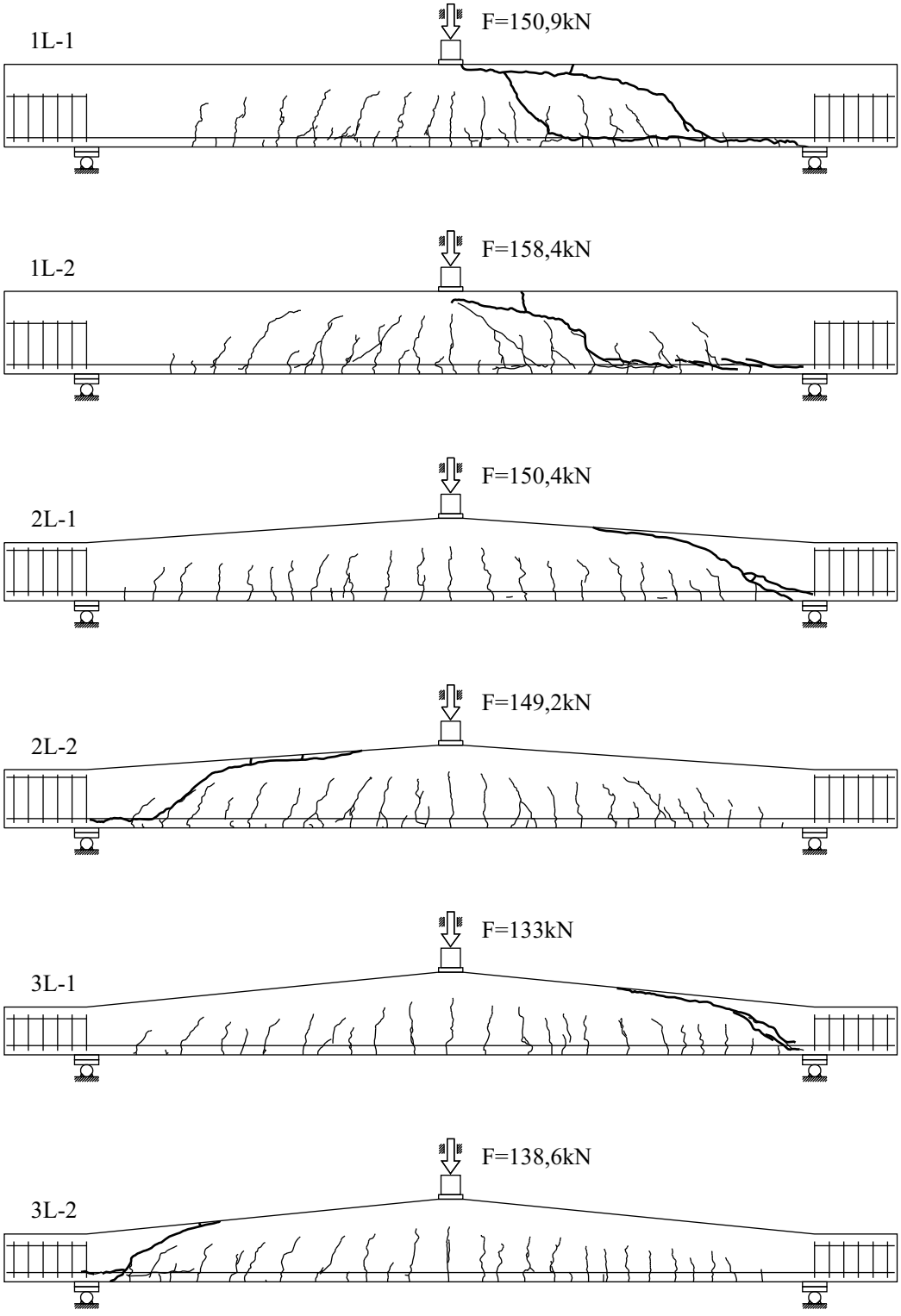

Figure 3.15– Crack pattern at failure of all test beams

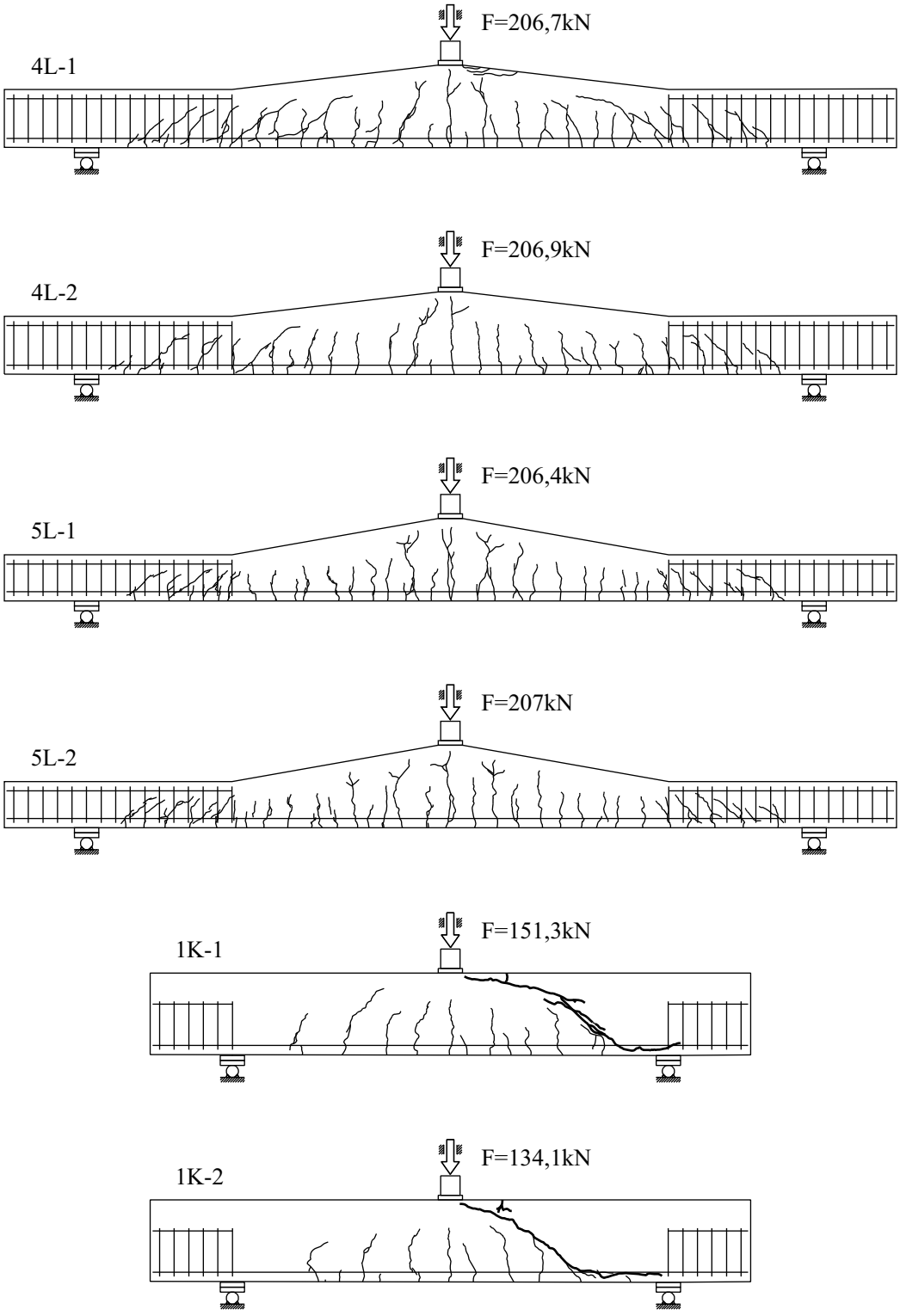

Figure 3.15– Crack pattern at failure of all test beams (cont.)

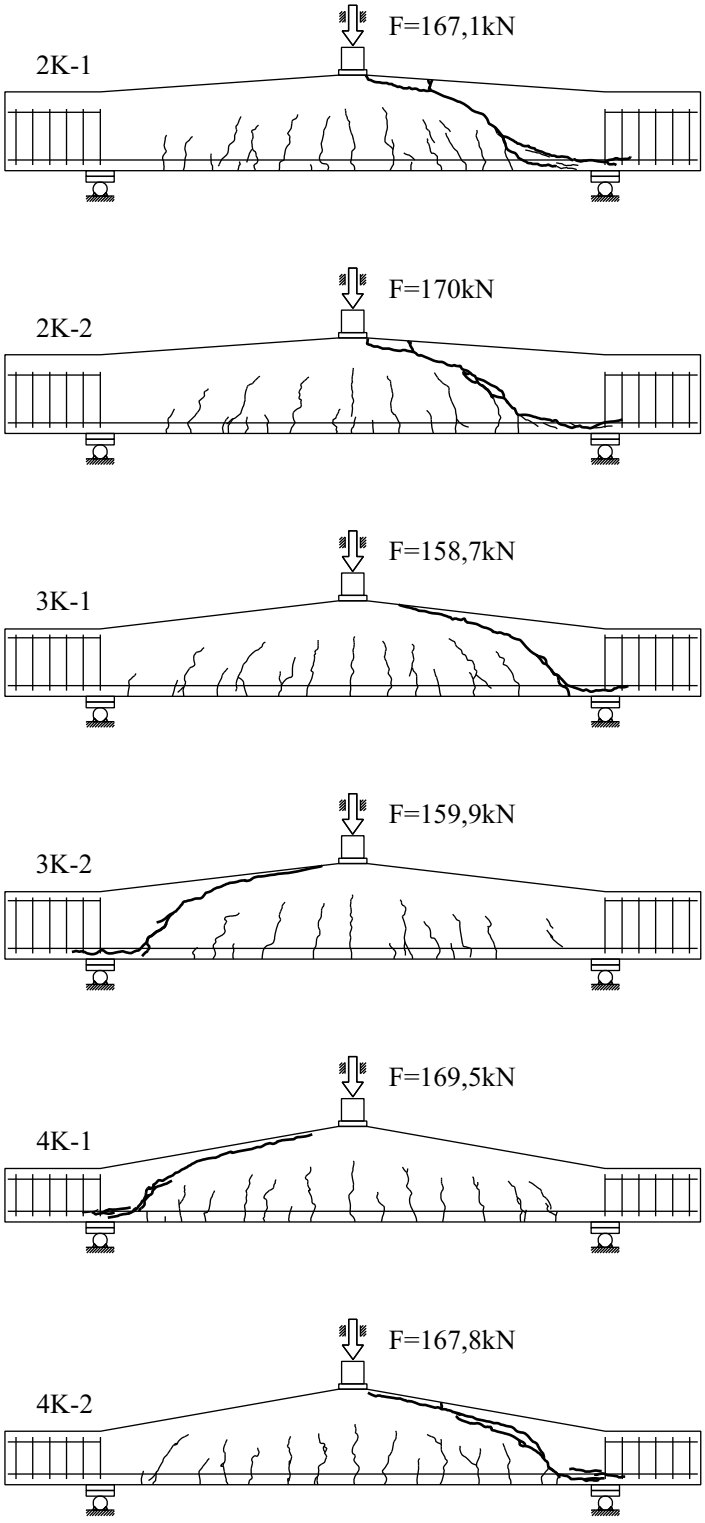

Figure 3.15– Crack pattern at failure of all test beams (cont.)

3.4.4 Shear Strength in Relation with Main Significant Factors

Figure 3.16 shows the relations of the ultimate shear strength of test beams with main significant factors including inclined angle α, effective depth d, a/d ratio, percentage of longitudinal reinforcement ρ_l.

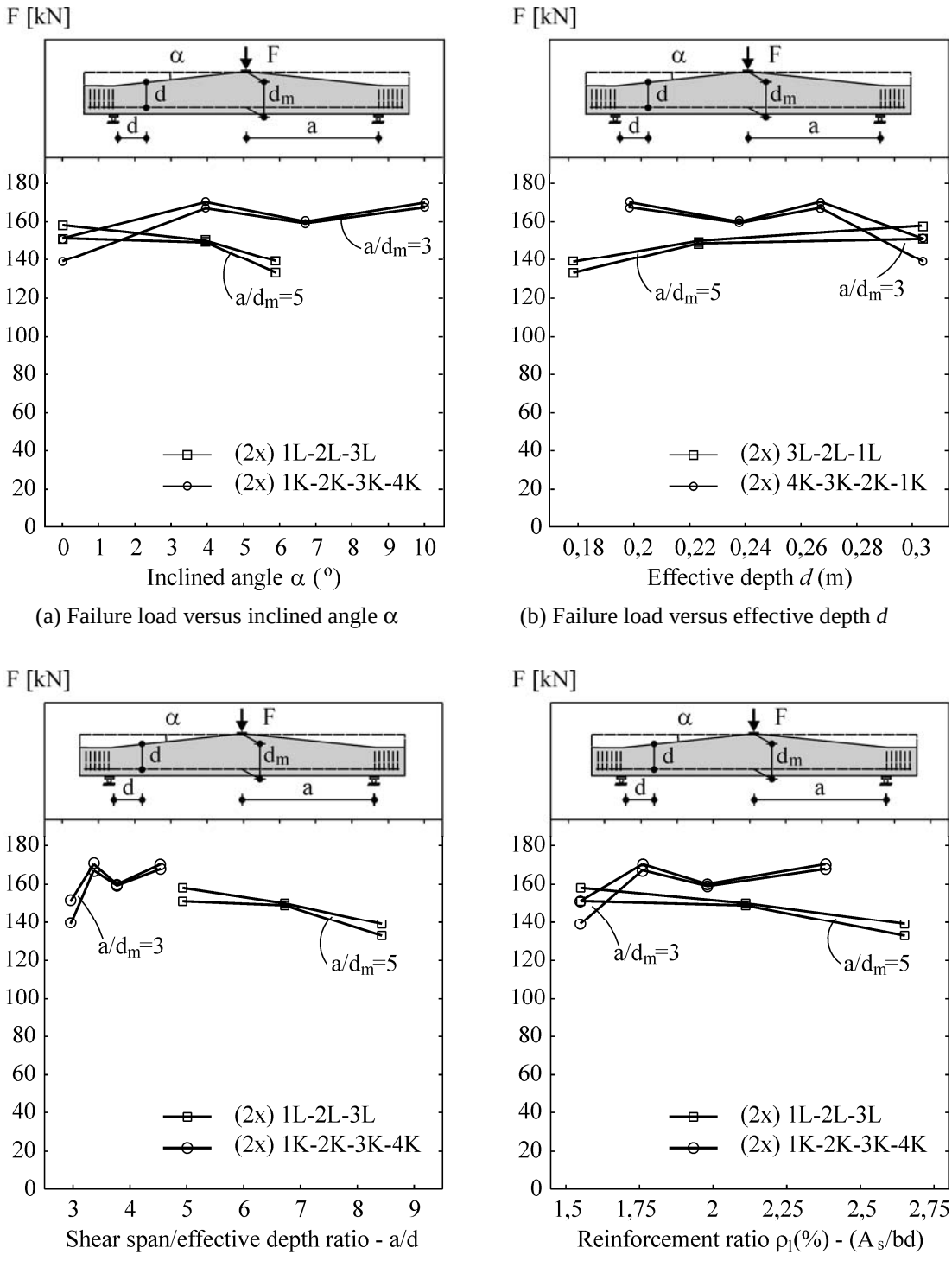

(a) Failure load versus inclined angle α

(b) Failure load versus effective depth *d*

(c) Failure load versus *a/d* ratio

(d) Failure load versus steel ratio ρ_l

Figure 3.16– Relations of failure load to main parameters of test beams

3.4.5 Test Results in Comparison with Shear Design Strength of Codes

Among five codes presented in the Chapter 2, four codes including the German Code (DIN 1045–01), the Swiss Code (SN 262–2003), the ACI Code (ACI 318–05) and the Canadian Standards (CSA A23.3–2004) are chosen to compare the shear strength predicted by these formulae with the test results. The mean values of concrete strength will be used for the evaluation of mean values of shear strength according to these codes. The calculations include (1) evaluating shear strength of test beams by sectional design model, (2) for haunch beams, shear strengths according to DIN 1045–01 and ACI 318–05 will be computed for two cases with and without V_{cc}, (3) presenting the critical sections according to codes and cracks at failure of test beams and (4) estimating the safety limitations of codes from test results.

All formulae of the four codes are referred to the sections 2.5 and 2.6. The critical design sections are referred to figure 3.17. DIN 1045–01 and the ACI 318–05 assumed it at 1,0*d* apart from the support while the CSA A23.3–2004 and the SN 262–2003 assumed it at the positions 0,9*d* and 0,5*d* respectively from the position of load application.

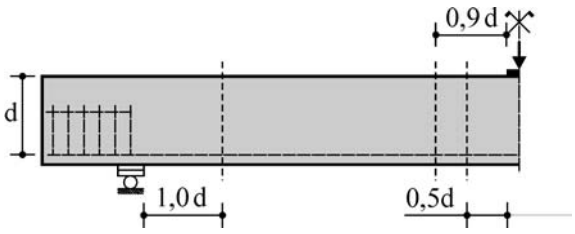

Figure 3.17– The critical sections according to various codes (ACI and DIN 1045-01: *1,0d* from support; CSA: *0,9d* from load application; SN 262-2003: *0,5d* from load application)

Since the tests named 4L and 5L failed in flexure, they will not be considered in the following. The calculated results for test beams 2L-1 are presented in the figures 3.18 and 3.19. The test results and shear strengths according to practical codes are presented in table 3.5 and table 3.6. Further details refer to Appendix C or test reports *[Rombach et al. (2009), (2011)]*.

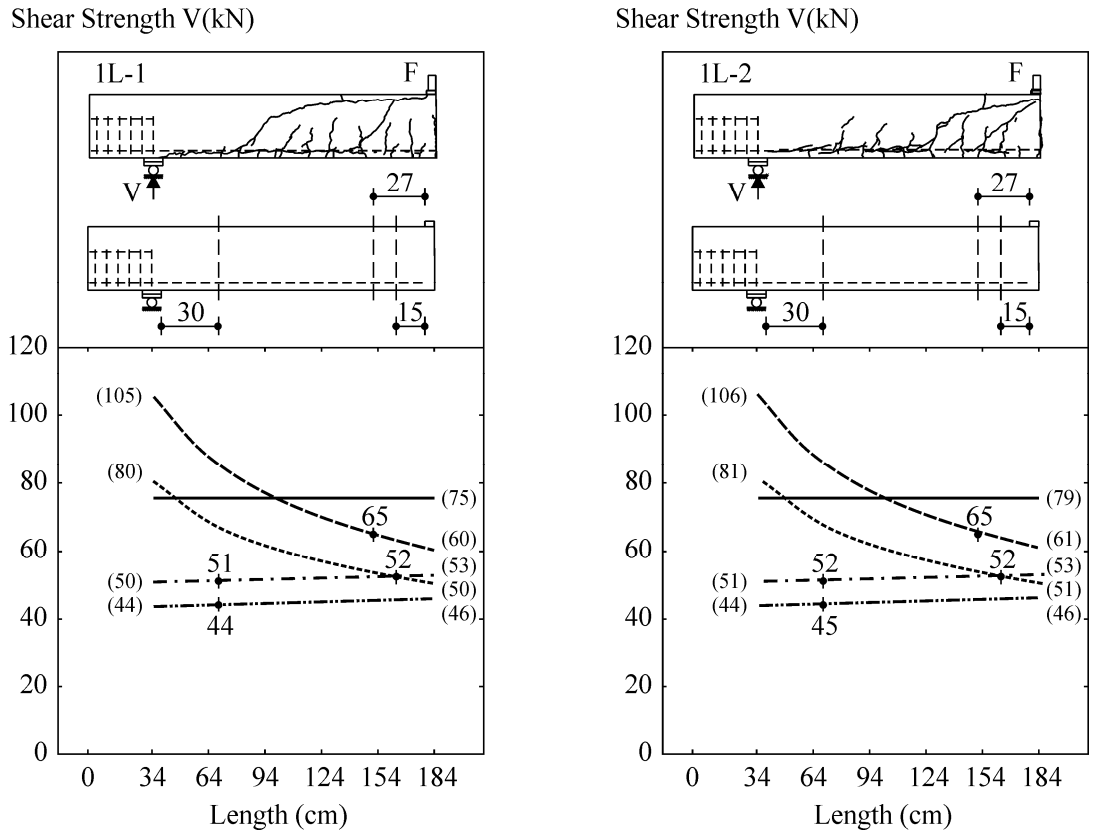

Figure 3.18– Shear strength of test 1L-1 and test 1L-2 according to practical codes compared to test results

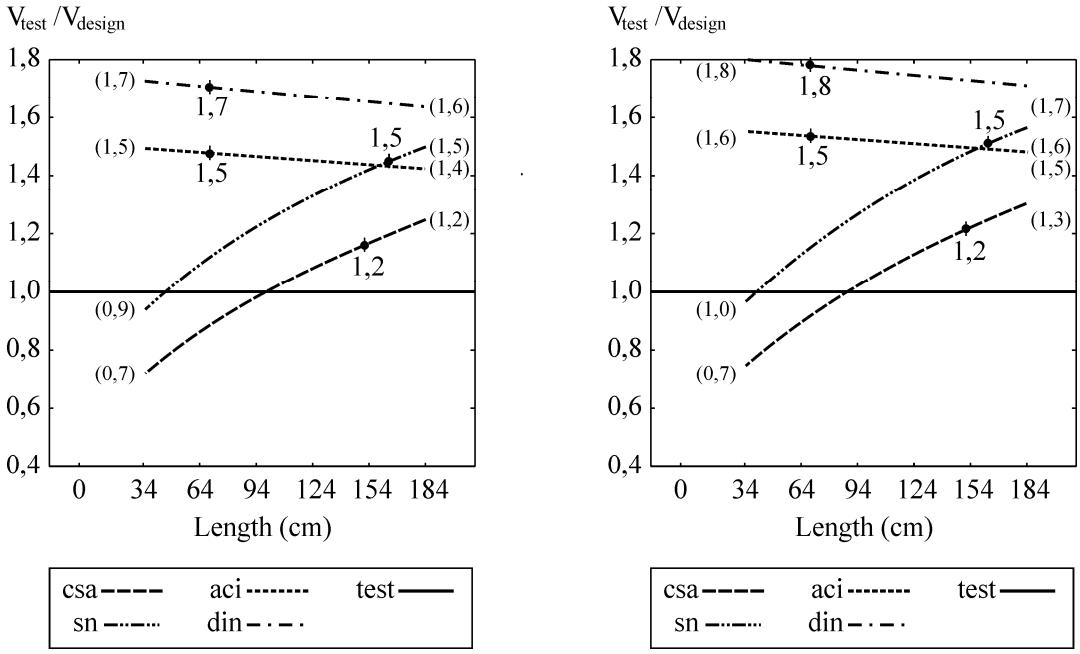

Figure 3.19– Safety level of test 1L-1 and test 1L-2 according to practical codes

Beam	Test		DIN 1045-01					ACI 318-05		
	Failed region	V_{Test} [kN]	Critical section	V_{0DIN} [kN]	V_{1DIN} [kN]	SF_{0DIN}	SF_{1DIN}	Critical section	V_{ACI} [kN]	SF_{ACI}
(1)	*(2)*	*(3)*	*(4)*	*(5)*	*(6)*	*(7)*	*(8)*	*(9)*	*(10)*	*(11)*
1L-1	Load position	75,44	1,0d-S	44,0	44,0	1,7	1,7	1,0d-S	51,0	1,5
1L-2	Load position	79,21	1,0d-S	45,0	45,0	1,8	1,8	1,0d-S	52,0	1,5
2L-1	Support	75,18	1,0d-S	38,0	42,0	2,0	1,8	1,0d-S	38,0	2,0
2L-2	Support	74,60	1,0d-S	38,0	42,0	2,0	1,8	1,0d-S	38,0	2,0
3L-1	Support	66,47	1,0d-S	31,0	36,0	2,1	1,9	1,0d-S	30,0	2,2
3L-2	Support	69,30	1,0d-S	31,0	37,0	2,2	1,9	1,0d-S	30,0	2,3
1K-1	Load position	75,63	1,0d-S	47,0	47,0	1,6	1,6	1,0d-S	55,0	1,4
1K-2	Load position	69,31	1,0d-S	47,0	47,0	1,5	1,5	1,0d-S	55,0	1,3
2K-1	Support	83,53	1,0d-S	44,0	49,0	1,9	1,7	1,0d-S	48,0	1,7
2K-2	Support	85,00	1,0d-S	44,0	49,0	1,9	1,7	1,0d-S	48,0	1,8
3K-1	Support	79,34	1,0d-S	42,0	50,0	1,9	1,6	1,0d-S	43,0	1,9
3K-2	Support	79,93	1,0d-S	42,0	50,0	1,9	1,6	1,0d-S	43,0	1,9
4K-1	Support	84,74	1,0d-S	36,0	49,0	2,4	1,7	1,0d-S	35,0	2,4
4K-2	Support	83,88	1,0d-S	36,0	49,0	2,3	1,7	1,0d-S	35,0	2,4

Table 3.5– Test results compared with shear design models in DIN 1045-01 and ACI 318-05

Beam	Test		CSA-03			SN-262		
	Failed region	V_{Test} [kN]	Critical section	V_{CSA} [kN]	SF_{CSA}	Critical section	V_{SN} [kN]	SF_{SN}
(1)	*(2)*	*(3)*	*(12)*	*(13)*	*(14)*	*(15)*	*(16)*	*(17)*
1L-1	Load position	75,44	0,9d-F	65	1,2	0,5d-F	52	1,5
1L-2	Load position	79,21	0,9d-F	65	1,2	0,5d-F	52	1,5
2L-1	Support	75,18	0,9d-F	62	1,2	0,5d-F	51	1,5
2L-2	Support	74,60	0,9d-F	62	1,2	0,5d-F	51	1,5
3L-1	Support	66,47	0,9d-F	61	1,1	0,5d-F	51	1,3
3L-2	Support	69,30	0,9d-F	61	1,1	0,5d-F	51	1,4
1K-1	Load position	75,63	0,9d-F	81	0,9	0,5d-F	64	1,2
1K-2	Load position	69,31	0,9d-F	81	0,9	0,5d-F	64	1,1
2K-1	Support	83,53	0,9d-F	77	1,1	0,5d-F	62	1,4
2K-2	Support	85,00	0,9d-F	77	1,1	0,5d-F	62	1,4
3K-1	Support	79,34	0,9d-F	75	1,1	0,5d-F	61	1,3
3K-2	Support	79,93	0,9d-F	75	1,1	0,5d-F	61	1,3
4K-1	Support	84,74	0,9d-F	72	1,2	0,5d-F	60	1,4
4K-2	Support	83,88	0,9d-F	72	1,2	0,5d-F	60	1,4

Table 3.6– Test results compared with shear design models in CSA-03 and SN-262

Notes for the Table 3.5 and 3.6:

(1) Test beam
(2) Failed region: region at which critical shear crack appears
(3) V_{Test} [kN]: critical shear strength from tests
(4) Critical section: critical section at 1,0*d* apart from support (1,0*d*-S) according to DIN 1045-01
(5) V_{0DIN} [kN]: calculated shear strength without V_{ccd} according to DIN 1045-01
(6) V_{1DIN} [kN]: calculated shear strength with V_{ccd} according to DIN 1045-01
(7) SF_{0DIN}: safety level of shear strength without V_{ccd} according to DIN 1045-01 (V_{Test}/V_{0DIN})
(8) SF_{1DIN}: safety level of shear strength with V_{ccd} according to DIN 1045-01 (V_{Test}/V_{1DIN})
(9) Critical section: critical section at 1,0*d* apart from support (1,0*d*-S) according to ACI 318-05
(10) V_{ACI} [kN]: calculated shear strength according to ACI 318-05
(11) SF_{ACI}: safeness level of shear strength according to ACI 318-05 (V_{Test}/V_{ACI})
(12) Critical section: critical section at 0,9*d* apart from load application (0,9*d*-F) according to CSA-03
(13) V_{CSA} [kN]: calculated shear strength according to CSA-03
(14) SF_{CSA}: safeness level of shear strength according to CSA-03 (V_{Test}/V_{CSA})
(15) Critical section: critical section at 0,5*d* apart from load application (0,5*d*-F) according to SN-262
(16) V_{SN} [kN]: calculated shear strength according to SN-262
(17) SF_{SN}: safeness level of shear strength according to SN-262 (V_{Test}/V_{SN})

3.4.6 Test Results in Comparison with Shear Strength of 13 Models

13 different shear strength models among which as presented in the Chapter 2 are selected to evaluate the shear bearing capacity of test beams. The analysis includes evaluating shear strength of test beams by sectional design method according to different shear resistance models. The models adopted in codes such as those of the Modified Compression Field Theory (in Canadian Standard and ASSHTO), CEB-FIP model code 1990 (in German code DIN and Eurocode), ACI-ASCE shear committee (in ACI code) and the critical shear crack theory (in Swiss code) are not considered anymore since they were already discussed in the previous section 3.4.5.

In the model group based on the failure mechanism approach, the tooth model with crack friction suggested by Reineck (1990) and those of Zararis et al. (2001), Zink (2000), Tureyen et al. (2003), Park et al. (2006) are selected. The models based on the lower bound theorem of plasticity such as strut–and–tie models or truss models are not used further because they were considered to be inappropriate for slender members without stirrups as discussed in the Chapter 2. The disturbed stress field model by Vecchio (2000) is not employed as well since the shear strength formula is not published yet. It is found among models based on the fracture mechanics approach that the model of Gastebled et al. (2001) seems to be the most appreciable one and therefore this model will be chosen for comparison. Among many empirical models presented in the Chapter 2, it is preferred to calculate the shear strength of latest

ones since 1996 including Bentz (2005), Bažant and Yu (2005), Kim D et al. (1999), Kim JK et al. (1996) and Latte S (2009). The shear strength of haunched beams proposed by Debaiky et al. (1982) as well as that offered by MacLeod I.A et al. (1994) is also included in the analysis. The 13 used shear strength models are presented in the table 3.7.

Because all the above models are for members without shear reinforcements, only the results in regions without stirrups are presented. For test beams owning the same geometrical features such as 1L1 and 1L2 …, shear resistance strength is computed just once with the average value of concrete compressive strengths. All formulae are referred from sections 2.3, 2.4 and 2.6. It is noted that the critical section is assumed at the position $0{,}5d_m$ from load location for model suggested by Latte (2009) and at the position of beam depth of d_r for model proposed by MacLeod et al. (1994) as shown in figure 3.20.

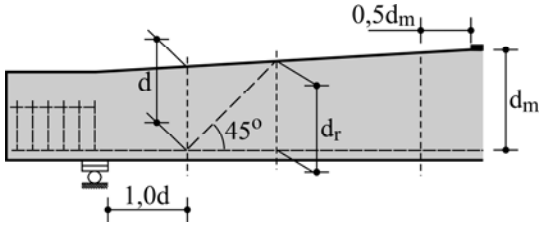

Figure 3.20– Critical section 0,5*d* proposed by Latte (2009) and MacLeod et al. (1994)

No	Author(s) / (Time)	Abbreviation
1	Reineck KH / (1990)	Reineck
2	Zararis PD and Papadakis GC / (2001)	Zararis
3	Zink M / (2000)	Zink
4	Tureyen AK and Frosch RJ V / (2003)	Tureyen
5	Park HG, Choi KK and Wight JK / (2006)	Park
6	Gastebled OJ and May IM / (2001)	Gastebled
7	Bentz EC / (2005)	Bentz
8	Bažant ZP and Yu Q / (2005)	Bažant
9	Kim D, Kim W and White RN / (1999)	Kim D
10	Kim JK and Park YD / (1996)	Kim JK
11	Latte S / (2009)	Latte
12	Debaiky SY and Elniema EI / (1982)	Debaiky
13	MacLeod IA and Houmsi A / (1994)	Macleod

Table 3.7– List of shear strength models used for comparing with test results

Moreover, the tests named 4L and 5L are not consisted further since they failed in flexure and will be analyzed in the next Chapter 4–Nonlinear FEM Analysis. The calculated results for test beams 1L and 2L are presented in figure 3.21.

The test results and shear strengths according to various models are summarized in the table 3.8. Other details can be referred to Appendix D or test reports *[Rombach et al. (2009), (2011)]*.

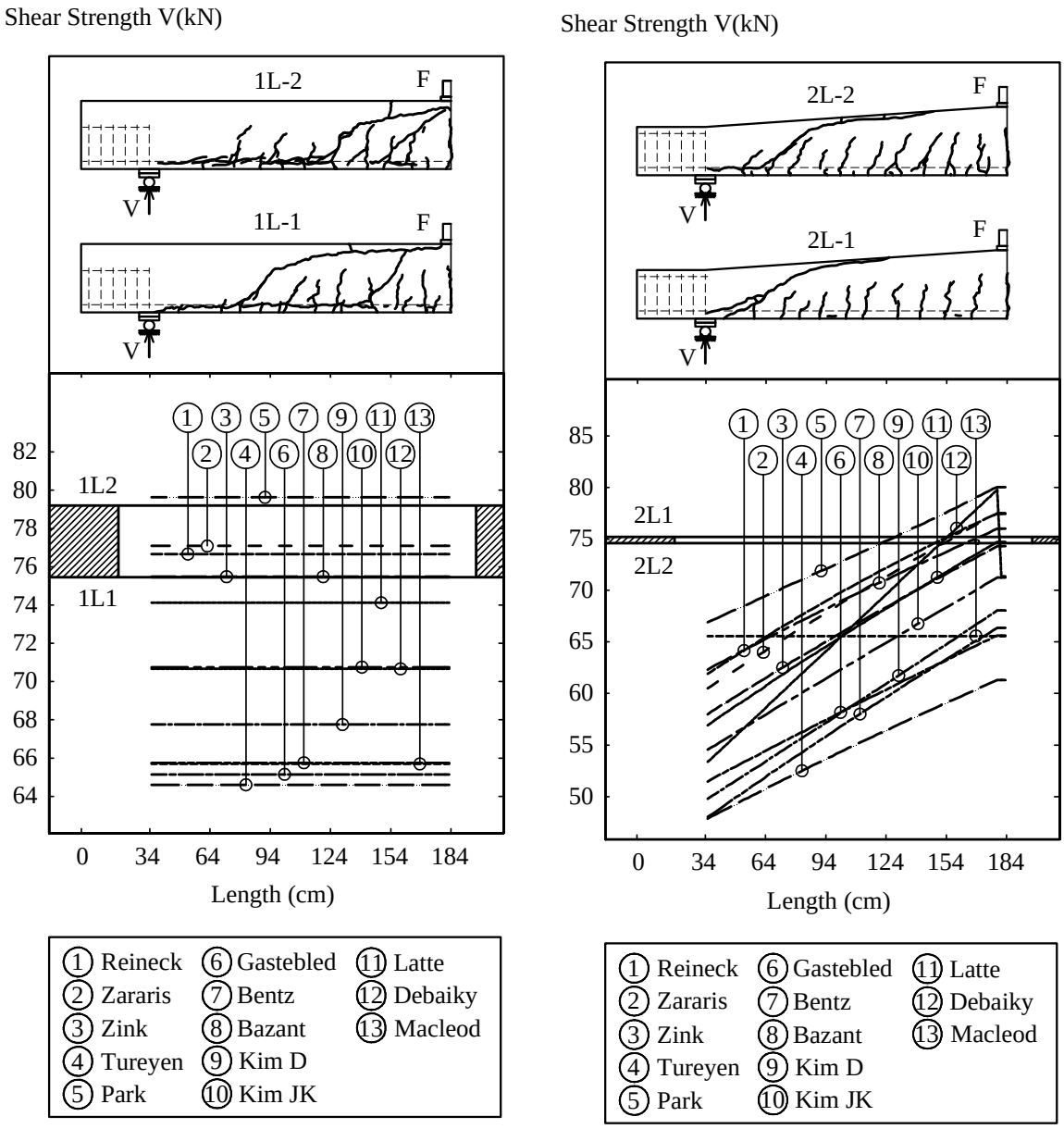

Figure 3.21– Shear strength of Test 1L and Test 2L according to suggested models compared to test results

Beam	Test	Reineck	Zararis	Zink	Tureyen	Park	Gastebled	Bentz
	V [kN] (*)	[kN]	[kN]	[kN]	[kN]	[kN]	[kN]	[kN]
1L	77,32	77	77	75	65	80	65	66
2L	74,89	62-78	61-78	58-74	48-61	67-80	52-66	48-66
3L	67,88	53-78	51-78	49-75	40-62	61-80	44-66	38-67
1K	72,47	81	90	89	68	95	80	69
2K	84,26	72-81	79-90	76-87	56-63	80-95	70-80	58-69
3K	79,63	65-81	70-90	68-87	50-63	71-95	63-80	50-69
4K	84,31	55-81	59-90	57-88	42-64	61-95	54-80	40-70

Table 3.8– Test results compared with suggested shear models

Beam	Test	Bažant	Kim D	Kim JK	Latte	Debaiky	MacLeod
	V [kN] (*)	[kN]	[kN]	[kN]	[kN]	[kN]	[kN]
1L	77,32	75	68	71	74	71	66
2L	74,89	62-76	50-68	55-71	57-75	53-71	66
3L	67,88	55-76	41-68	46-72	47-75	43-72	63
1K	72,47	86	89	89	91	74	68
2K	84,26	77-87	72-89	75-90	79-91	67-75	73
3K	79,63	69-87	61-89	66-90	71-91	60-75	75
4K	84,31	60-87	48-89	54-90	59-91	49-75	75

Table 3.8– Test results compared with suggested shear models (cont.)

Notes for the table 3.8:

(*) V [kN]: Mean value of shear strength from test results.

- The shear capacities of haunched beams according to various models are calculated by sectional method. The values in the table 3.8 are minimum and maximum strengths.

3.5 Discussions and Conclusions

From the experimental program, some discussions and conclusions are given as follows:

The test results showed typical shear failure modes of concrete beams without stirrups that partly described in other shear test reports such as those of Leonhardt et al. (1962), Kani (1966)…In general, these shear failure modes are a combination of diagonal tension failure, shear compression failure, shear tension failure and arch rib failure as presented in the section 2.2. A general phenomenon of these failures is that brittle collapse occurs right after the formation of a critical diagonal shear crack. Then the test beams cannot resist any loading more. For straight test beams (1L-1, 1L-2 with $a/d = 5$ and 1K-1, 1K-2 with $a/d = 3$), the

critical shear crack is originated as a development of a former flexure-shear crack. Thus the failure region is close to the position of load application at mid-span. In contrast for haunched test beams, the critical shear crack is either initiated at the tip of the former flexure-shear crack or newly formed in 'web' of the beam section and particularly locates near supports. This crack has been called as web-shear crack or purely shear crack.

The crack propagation of test beams showed that pure flexure cracks would occur at bottom of beam up to a half of the critical loading. The influences of shear become more obvious at higher loads until approximate 0,9 critical loading because the direction of the former cracks and newly coming cracks tend to be inclined with the neutral axis of beam. These cracks are termed as flexure-shear cracks. At higher loading ranges, the flexure-shear cracks would reach a stable state and not grow up any more but there occur visible inclined cracks at tip of flexure-shear cracks or pure shear cracks in "web" of beam in the region close to supports. When the loading reaches the ultimate value, one of the inclined cracks will further spread on an inclined direction to form the critical shear crack. The upper end goes into the compression zone while the lower end goes down to split concrete along longitudinal reinforcements. For straight depth beams, the upper branch of the critical shear crack lasts to the load application point and the failure region is close to mid-span. For haunched beams, the lower branch of the critical shear crack ends at support and the failure region is close to the support as well.

The test results confirmed the influences of some significant factors as mentioned in the section 2.2.2 and especially the effect of inclined angle on the shear strength of concrete beams without stirrups. It is from the figure (3.16) that inclined angles induces relatively positive effects to increase the shear strength of short concrete beams ($a/d = 3$) without stirrups. Shear strength of beams with an inclination of 10^o (test beam 4K-1) could be 18 % higher than that of straight depth beams (test beam 1K-2). However, effects of inclination become very negative for long concrete beams ($a/d = 5$) when the shear strength of the beam with inclined angle of 6^o (test beam 3L-1) conversely is 16 % lower than that of straight depth beam (1L-2). This finding is totally in contrast to the principle of DIN 1045-01 as described in the equation 2.34 in the term of V_{ccd} that shear strength increases as the inclined angle increases.

The test results also show that the shear design model of DIN 1045-01 is safer and more conservative than that of other practical codes such as ACI 318, CSA-03 or SN-262 (Fig. 3.18 and 3.19, table 3.5 and table 3.6). From the Table 3.5, it is interesting to learn that the safety factor without V_{ccd} (SF_{0DIN}) of DIN 1045-01 is somewhat similar to that of ACI 318 even though both expressions are totally different. Safety factors with V_{ccd} (SF_{1DIN}) for haunched beams apparently make the conservativeness of DIN 1045-01 to become more reasonable (1,6 ÷ 1,9). However, it is from the table 3.6 that the two codes CSA-03 and SN-

262, which do not consider the term V_{ccd}, show a much better safety coefficients of 1,1 ÷ 1,2 for CSA-03 and 1,3 ÷ 1,5 for SN 262. It is noted that the two later codes consider the effects of the slenderness ratio of beam a/d in terms of $(M/d = V{\cdot}a/d)$ while the shear strength formula of DIN 1045-01 do not. Nevertheless, the shear strength formula of DIN 1045-01 for haunched beams takes into account this factor in terms of $M{\cdot}\tan\alpha/z \approx V{\cdot}a{\cdot}\tan\alpha/0{,}9d$. As a result, it leads to a conclusion that (a/d) may be a factor which adjusts the safety factor for haunched beams to become more realistic. The shear resistance component of the compression chord V_{cc} should be more deeply investigated.

The test results in comparison with 13 suggested shear strength formulae shows that some models can predict well the shear capacity of straight beams such as Reineck (1991), Zararis (2001), Zink (2000), Latte (2009)…as in the figure 3.21 and table 3.8. These models will be analyzed in details with the updated shear database in Chapter 5. Among a lot of shear models for straight beams, there is only one for haunched beams suggested by MacLeod et al. (1994). This model predicts quite well the shear strength of haunched test beams (mean of 90 % failure load) and gives details about the critical shear crack. However, this formula can be considered as a modified model of that in DIN 1045-01 in a more complicated way because there are many unnecessarily complex parameters such as F', d_{cr}, C_h requiring to be determined for calculation as presented in the section 2.6.

In conclusions, the experimental program clarifies some aspects of shear behaviours of concrete beams without stirrups. For straight depth beams, it is recognized that their behaviours until failure are similar to those presented by many former authors. However, it is still impossible to identify which shear resistance mechanisms contribute to carry shear and how important they are. As a result, shear design of concrete members without stirrups is still a problem though many models have been suggested. For haunched beams, it is clear that the inclination has a strong influence on the shear behaviour as well as shear capacity of concrete beams without shear reinforcement. Nevertheless, a mechanical model which can explain the effects is not available. The question whether an inclined compression chord improves the shear strength of concrete structures without stirrups has not been solved even though DIN 1045-01 or MacLeod et al. (1994) did suggest a solution. It is believed that the approach based on Nonlinear Finite Element Analysis may give a solution for the problem which will be presented in the next chapter.

4 Nonlinear FEM Analysis

4.1 Introduction

Nonlinear FEM analysis has widely been adopted as a potential numerical method to investigate shear behaviours of concrete structures because of many achieved advances in numerical techniques, material models and computer performance. Especially some various concrete models have been implemented in commercial FEM packages that makes modelling and analysis become much easier. There have been some authors got involved in shear problem of concrete structures by nonlinear FEM analysis such as Malm (2006) or Latte (2009)… The analysis results, for example, the ultimate load bearing capacity, the displacement and crack pattern of these authors show a good and reliable agreement with the results of many typical shear tests by Leonhardt et al. (1962). Therefore, it is expected that nonlinear FEM analysis can give more details on shear behaviours as well as on shear resistance mechanisms until failure of test beams in the above experimental program. The specific purposes of the analysis are: (1) to verify if nonlinear FEM analysis can predict well some typical features of shear failure such as shear strength, maximum displacement, crack pattern…; (2) to reveal changes in stress distribution and crack propagation through each load step until failure of concrete members without stirrups; (3) to study differences in behaviours of haunched beams and straight beams until failure; and finally (4) to clarify the shear resistance actions proposed by many authors as presented in the Chapter 2 and to find out main shear resistance mechanisms used for building up new shear strength models.

The commercial FEM package ABAQUS 6.9 will be used for these investigations. The *'Concrete Damaged Plasticity Model'* based on the theory of plasticity and damage mechanics will be employed for modelling of concrete. Since detailed descriptions and background information of this concrete model can be found in many literatures and in user's documentations of ABAQUS, it will be presented briefly in the section 4.3–Non FEM Analysis with ABAQUS. The analysis outcomes will be described in the section 4.4–Test Verification. Some discussions and conclusions are given in the final section of this chapter.

4.2 Material Behaviour

Reinforced concrete is a composite material consisting of concrete and reinforcement which have different mechanical properties. Reinforcement can be considered on a macro level as homogeneous while concrete, consisting of mortar and aggregates, is a heterogeneous material. The mechanical properties of concrete, as a result, are scattering and difficult to define.

In practice, concrete is usually assumed to be a homogeneous material in the design of a structure for convenience.

The typical behaviour of reinforced concrete structures under bending or uniaxial tension until damage is generalized as in the figure 4.1. The nonlinear response can be divided into three stages including the uncracked elastic stage, the crack propagation stage and finally the damaged stage.

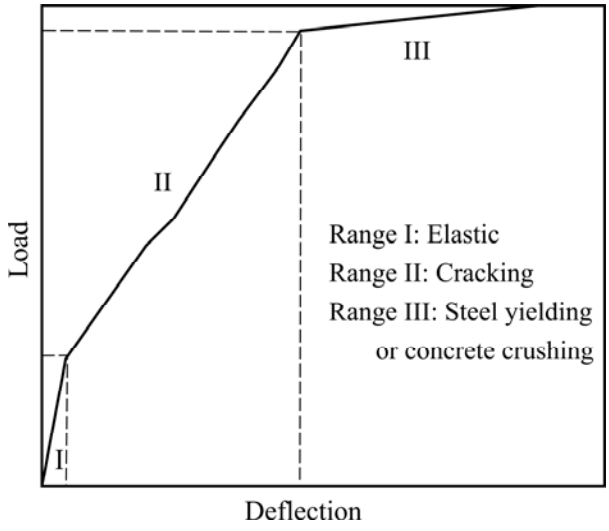

Figure 4.1– Typical load-deflection curve of reinforced concrete members *[CEP-FIB 1990]*

This response is recognized to be caused by three main effects, namely, (1) cracking of concrete in tension, (2) yielding of the reinforcement or crushing of concrete in compression and (3) interaction of the constituents of the reinforced concrete. Interactions include bond–slip between reinforcement and contact concrete, aggregate interlock at cracks and dowel action of reinforcement crossing cracks. In addition, some effects such as creep and shrinkage of concrete, environmental conditions or concrete age at loading can also influence the nonlinear response of RC structures *[Chen (1982), Kwak et al. (1990)]*.

Because of the differences in behaviours of concrete and reinforcement as well as the complex interaction mechanisms between them, a widely accepted way to model the responses of RC structures is to use separate material models for concrete and reinforcement which are then combined with a model of interactions between the two materials. In 1967, it was Ngo and Scordelis to introduce the first publication on the application of the finite element method (FEM) to the analysis of RC structures. In their study of simple beams, concrete and reinforcement were modelled by constant strain triangular elements and a special bond link element was used to describe the interaction between concrete and reinforcement. Many researchers have later made important contributions to both proposing constitute material models and developing reliable algorithms in numerical analysis such as Ottosen (1977),

Chen (1982), Lubliner (1989) or Lee & Fenves (1998). However, modelling the behaviour of concrete and developing consistent analytical models for the response of RC structures are still difficult challenges due to the following reasons:

- Concrete is a heterogeneous material with uncertain mechanical properties under loading.
- Reinforcement and concrete interact in complex mechanisms which are difficult to describe and constitute in a mathematical formulation.

The behaviour of concrete, reinforcing steel and their interactions will be presented in details in the following sections.

4.2.1 Concrete Behaviour

Concrete by itself is a composite material of aggregates and cement paste or mortar that fills in the spaces between aggregate particles and binds them together to form a rock-like solid. Hence, concrete is a non–homogeneous and anisotropic material with high compressive strength and low tensile strength. The two strengths are dependent on effects of creep, shrinkage, environmental conditions or concrete age. They also have different values under different stress states.

In concrete, there are numerous micro–cracks caused by segregation, shrinkage or thermal expansion of the mortar. Some other micro–cracks may appear under low level of loading due to the difference in stiffness of aggregates and mortar. These micro–cracks mostly locate on the contact surface between aggregates and mortar to form an interface which has a significantly lower tensile strength than the other parts. Aggregate size, as a result, plays a large role on the mechanical behaviour of concrete.

Under a microscopic examination, mortar is a non-homogeneous and anisotropic matrix composed of irregularly shaped and unevenly distributed pores attributed to the evaporation of free water and gel pore formation in the calcium silicate hydration. The porosity greatly influences the strength development of the mortar which induces a complex relation between the microstructure and mechanical behaviour of concrete. New strength models are based on the water-cement ratio and the capillary porosity.

Thus, in order to create an appropriate mathematical model it is essential to understand the behaviour of plain concrete under uniaxial and multi-axial stress states. Typical test results are illustrated in the next section and they all refer to normal weight concrete under short term quasi-static loading conditions.

4.2.1.1 Uniaxial Compressive Behaviour

The nonlinear stress-strain behaviour under uniaxial compression of concrete is shown in figure 4.2 *[Chen (1982)]*. This behaviour can be summarized in four stages under different magnitudes of applied load. The first stage is about 30÷60 % of the ultimate strength (shown as 45 % in Fig. 4.2). In this initial stage, localized cracks are initiated but they do not propagate (stationary cracks). Hence, the stress-strain behaviour is linearly elastic and $0{,}3f'_c$ to $0{,}4f'_c$ is usually proposed as the limit of elasticity. In the second stage, the stress-strain curve begins to deviate from a straight line and go up to 70÷90 % of the ultimate strength (shown as 85 % in Fig. 4.2). In this stage, as the applied load increases, cracks multiply and propagate to reduce the material stiffness and cause irrecoverable deformation in unloading. In the third stage, the stress-strain curve continues to extend up to the ultimate strength. In this stage, the progressive failure of concrete is primarily caused by cracks through the mortar. These cracks merge with former bond cracks at the surface of nearby aggregates and form crack zones of internal damage. A fourth stage defines the region beyond the ultimate strength. In this region, the cracks become unstable and self-propagating until complete disruption and failure occurs. In this stage, the major cracks form parallel to the direction of the applied load, causing failure of the concrete.

All the above mentioned stages are for the uniaxial compression case. Stages I, (II and III), and IV could be categorized into the linear elastic, inelastic, and the localized stages respectively.

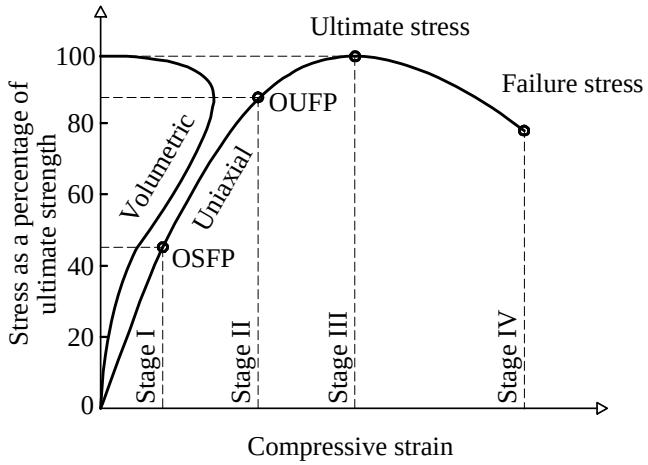

Figure 4.2– Uniaxial compression stress-strain relation of concrete *[Chen (1982)]*

4.2.1.2 Uniaxial Tensile Behaviour

A typical uniaxial tensile behaviour curve of concrete is shown as in figure 4.3. In general, the limit of elastic stage is observed to be about $60 \div 80$ % of the ultimate tensile strength.

Therefore the behaviour of concrete in tension is quite brittle in nature. In addition, the aggregate-matrix interface has a significantly lower tensile strength than the others, which is the primary reason for the low tensile strength of concrete.

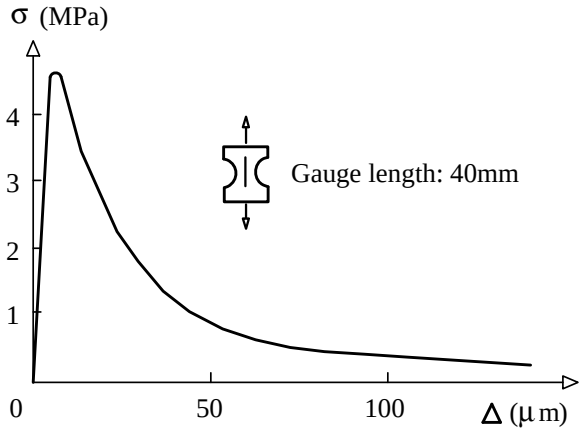

Figure 4.3– Uniaxial tensile stress-strain curve of concrete *[Peterson (1981)]*

The tensile strength f_{ct} is significantly lower than the corresponding strength in compression f'_c, with a ratio of $0{,}05 \div 0{,}1$. This value is difficult to measure experimentally and so, it normally is estimated from the corresponding value of the compression strength for example DIN 1045-1 uses $f_{ct} = 0{,}3\, f_{ck}^{2/3}$.

4.2.1.3 Biaxial Behaviour

Behaviour of concrete under biaxial states was first represented by Kupfer et al. (1969) as in the figure 4.4. It was reported that the strength of concrete subjected to biaxial compression may be up to 27 % higher than the uniaxial strength of concrete. For equal compressive stresses in two principal directions the strength increase in approximately 16 % (Fig. 4.4.b). In the region of combined compression and tension, the compressive stress at failure decreases as the simultaneously acting tensile stress is increased. The strength of concrete under biaxial tension is approximately equal to its uniaxial tensile strength *[Kupfer et al. (1969)]*. In the next few decades, several slightly different yield surfaces have been proposed by Ottosen (1977), Lubliner (1989) or Lee & Fenves (1998) which will be presented in section 4.3.1.

4.2.2 Steel Behaviour

Reinforcement has different types and shapes. The most commonly used style is deformed circular cross-section bars. The properties of reinforcing steel are generally not dependent on environmental conditions or time. A typical stress-strain curve for reinforcing steel bars used in concrete construction is obtained from a tension test as in the figure 4.5. For all practical

purposes steel exhibits the same stress-strain curve in compression as in tension. The steel stress-strain relation exhibits an initial linear elastic portion, a yield plateau, a strain hardening range in which stress again increases with strain and, finally, a range in which the stress drops off until fracture occurs.

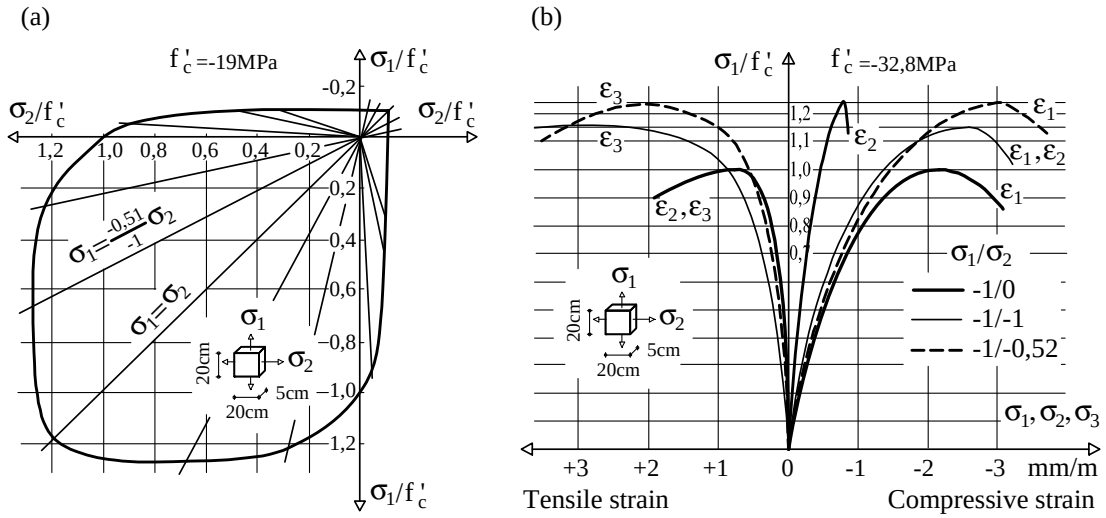

Figure 4.4– (a) Biaxial strength of concrete from experimental investigation; (b) Stress-strain relationships of concrete under biaxial compression *[Kupfer et al. (1969)]*

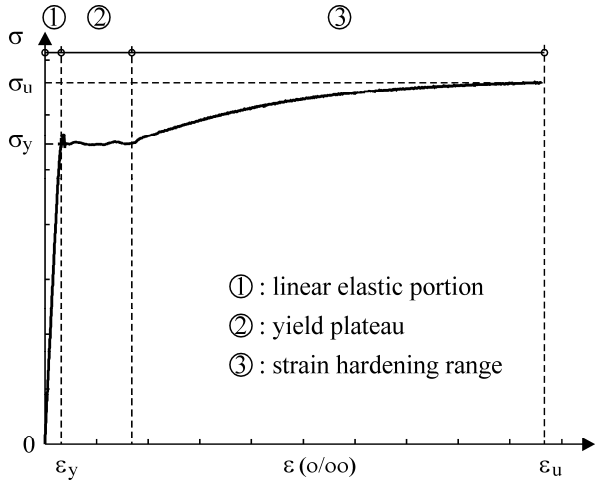

Figure 4.5– Stress-strain relationships of reinforcement *[Figure 3.3 (Chapter 3)]*

4.2.3 Interaction Behaviour between Reinforcing Steel and Concrete

Since plain concrete has very small tensile strength, reinforcing steel will usually be embedded in concrete to create a reinforced concrete composite material which has relatively high strength in both compression and tension. Interaction behaviours refer to load transferring mechanisms as well as failure in the vicinity between reinforcing steel and concrete. The main stress transfer mechanisms or bond between concrete and reinforcement are repre-

sented by (1) chemical adhesion between mortar and bar surface; (2) friction and wedging action of small dislodged sand particles between the bar and the surrounding concrete; and (3) mechanical interaction between concrete and steel.

Bond of plain bars derives primarily from the first two mechanisms while bond of deformed bars is mainly transferred through lugs of bars to concrete. As a result, bond resistance and crack propagation pattern of reinforced concrete members with deformed bars are different from those of reinforced concrete members with plain bars. For reinforced concrete members with deformed bars laid in the tensile zone, cracks tend to be initiated at certain intervals and propagated normal to main bars (Fig. 4.6.a). The bond slip between reinforcement and surrounding concrete will play an important role in the internal force redistribution, overall structural stiffness and load capacity of system (Fig. 4.6.f). It is represented as a means for transfer of tensile stresses from reinforcement to the concrete between two neighbouring cracks (Fig. 4.6.c, d, e). The capacity of the intact concrete between cracks to carry these tensile stresses is termed as tension stiffening effect. In general this effect is quite complicated to consider thoroughly but only partly since it is influenced by many factors such as cracking and crushing of concrete, nonlinearity of concrete, yielding of steel, main bar's spacing, concrete cover…For simplicity, some researchers assumed full bond between the reinforcing steel and concrete.

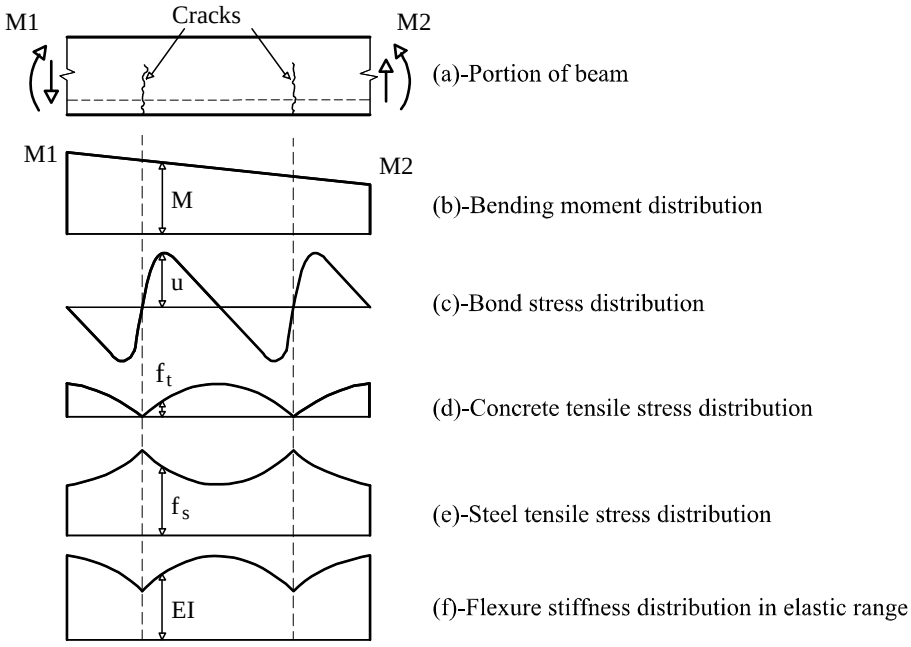

Figure 4.6– Effect of cracking in reinforced concrete beam *[Kwak et al. (1990)]*

Another mechanical interaction between concrete and reinforcement named dowel action has been recognized to be one of shear transfer mechanisms of reinforced concrete members. It is explained that when cracks initiate almost normal to main bars and continue to open, main

bars work as a dowel to carry up to 53% of total shear *[Sarkar et al. (1998)]* as in Fig. 4.7. There have been some researches as well as suggested analysis models for this effect *[Shoroushian et al. (1987), Takahashi et al. (2008)…]*. However, the significance of the dowel action is still under investigation and discussion as presented in the section 2.2.

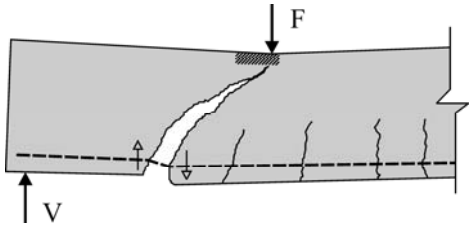

Figure 4.7– Dowel action in resisting shear *[Hwee et al. (1986)]*

4.3 Non FEM Analysis with ABAQUS

4.3.1 Damaged Plasticity Model for Concrete

The concrete damaged plasticity model is based on the models proposed by Lubliner et al. (1989) and by Lee and Fenves (1998). This model employs concepts of isotropic damaged elasticity in combination with isotropic tensile and compressive plasticity to represent the inelastic behaviours of concrete. It assumes that the main two failure mechanisms of concrete are tensile cracking and compressive crushing. The evolution of the yield (or failure) surface is controlled by two hardening variables $\tilde{\varepsilon}_t^{pl}$ and $\tilde{\varepsilon}_c^{pl}$ as tensile and compressive equivalent plastic strains respectively. Since the theoretical background of the model can be found in many literatures *[Lee and Fenves (1998), Malm (2006), Mark (2006), ABAQUS's documentation…]*, some main characteristics of the model defined in ABAQUS will be briefly presented only as in the following.

4.3.1.1 Uniaxial Tension and Compression Behaviour

It is required to define the stress-strain behaviour of plain concrete in uniaxial compression and tension as in figure 4.8. If E_c is the initial (undamaged) elastic stiffness of the material, the stress-strain relations under uniaxial tension and compression loading are, respectively:

$$\sigma_t = (1-d_t)\cdot E_c \cdot (\varepsilon_t - \tilde{\varepsilon}_t^{pl}) \quad (4.1)$$

$$\sigma_c = (1-d_c)\cdot E_c \cdot (\varepsilon_c - \tilde{\varepsilon}_c^{pl}) \quad (4.2)$$

Where: d_t and d_c are two damage variables in tension and compression.

The stress-strain curve under compression (Fig. 4.8.a) can be divided into 3 phases: (1) elastic region $\sigma_c < \sigma_{co}$; (2) pre-failure region $\sigma_{co} < \sigma_c < \sigma_{cu}$; and (3) post-failure region in com-

pression. In ABAQUS the two later relations are specified in the option ‘CONCRETE COMPRESSION HARDENING’.

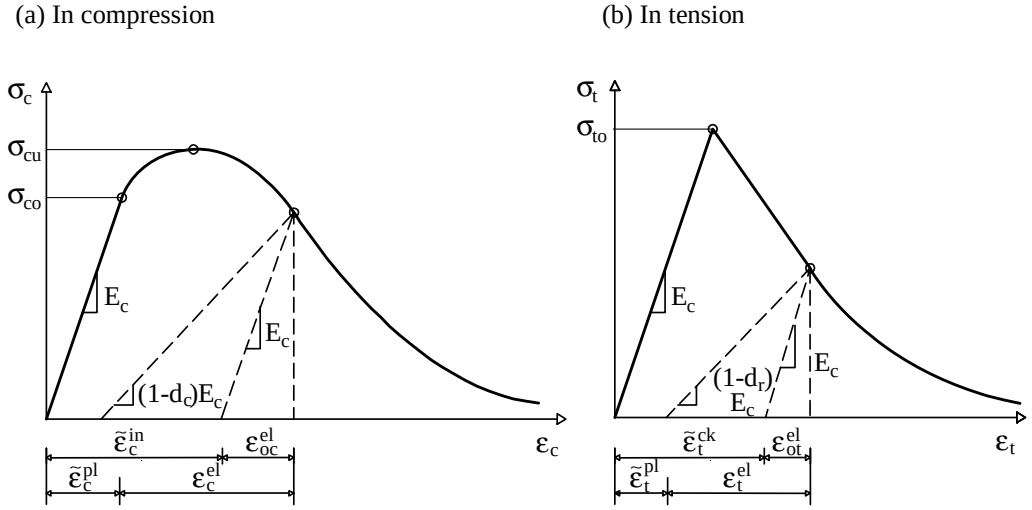

Figure 4.8– Stress-strain graphs of concrete under uniaxial loading [*Abaqus, theory manual*]

The stress-strain response under uniaxial tension follows two stages: (1) a linear elastic relationship until the value of the failure stress σ_{t0}; and (2) post-failure region in tension. The post-failure behaviour is modelled with tension stiffening to define the strain-softening behaviour for cracked concrete. That means interaction effects of the reinforcement and concrete will be simulated in a simple manner. In ABAQUS this relation is specified in the option ‘CONCRETE TENSION STIFFENING’.

In order to define two post-failure regions, the two uniaxial damage variable in compression d_c and uniaxial damage variable in tension d_t are determined as follows:

$$d_c(\varepsilon_c^{in}) = 1 - \frac{\varepsilon_{0c}^{el}}{\varepsilon_c^{in} \cdot (1 - b_c) + \varepsilon_{0c}^{el}} \qquad \text{bzw.} \qquad d_t(\varepsilon_t^{in}) = 1 - \frac{\varepsilon_{0t}^{el}}{\varepsilon_t^{in} \cdot (1 - b_t) + \varepsilon_{0t}^{el}} \tag{4.3}$$

Where: b_c and b_t are damage parameters are as follows:

$$b_c = \varepsilon_c^{pl} / \varepsilon_c^{in} \qquad \text{bzw.} \qquad b_t = \varepsilon_t^{pl} / \varepsilon_t^{in} \tag{4.4}$$

The two damage variables d_c and d_t are specified in the options ‘CONCRETE COMPRESSION DAMAGE’ and ‘CONCRETE TENSION DAMAGE’ respectively.

4.3.1.2 Concrete Plasticity

The plastic-damage concrete model uses a yield condition based on the yield function proposed by Lubliner et al. (1989) and incorporates the modifications proposed by Lee and

Fenves (1998) to account for different evolution of strength under tension and compression as in the figure 4.9.

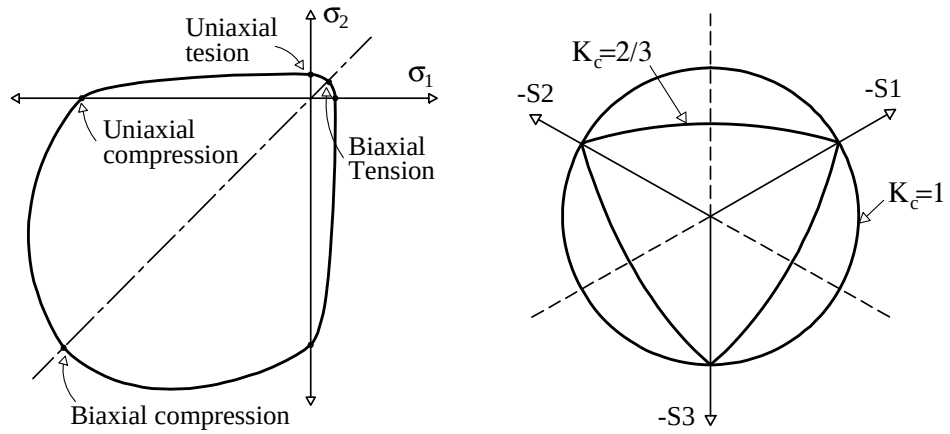

Figure 4.9– Yield surface in plane stress and yield surfaces in the deviatory plane

In addition, the concrete damaged plasticity model assumes a non-associated potential plastic flow. The flow potential *G* used for this model is the Drucker-Prager hyperbolic function:

$$G = \sqrt{(\varepsilon \cdot \sigma_{t0} \cdot \tan\psi)^2 + \overline{q}^2} - \overline{p} \cdot \tan\psi \qquad (4.5)$$

Where: ψ is the dilation angle,

σ_{t0} is the uniaxial tensile stress at failure,

ε is a eccentricity parameter.

For the sake of simplicity, default values as suggested by ABAQUS will be used for these parameters in all the following FE-analysis.

4.3.2 Model for Steel

Usually there have been two different idealizations for reinforcing steel in concrete structures. The first model comprises the first two stages of the stress-strain relation of steel and is named as elastic-perfectly plastic model since it neglects the last hardening stage as in the figure 4.10a. In contrast, the second model ignores a plastic phase to consider only the first phase and the last phase of the stress-strain relation of steel and is named as elastic-hardening model as in the figure 4.10.b. Using of the first model may underestimate the steel stress at high strains and have numerical convergence problems near ultimate strength. The second model which accounts for the strain hardening effect may avoid these two problems to assess more accurately strength of member at large deformations. Another solution which combines the two above models and represents better experimentally obtained stress-strain

relations of steel as in the figure 4.10.c will be used in this research. The analysis process showed numerical stability and solutions in good agreement with test results.

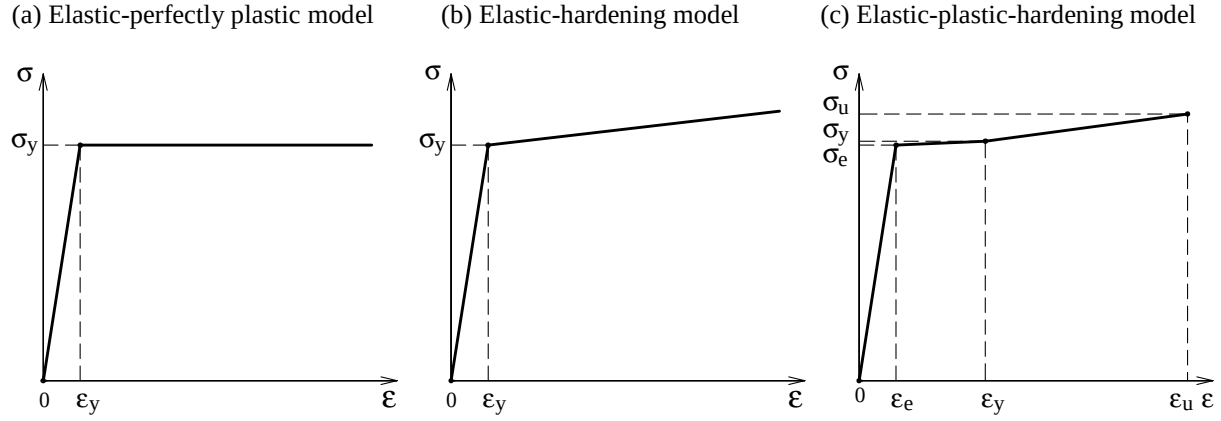

Figure 4.10– Three material models for steel

4.3.3 Explicit Dynamic Analysis

For numerical modelling of unstable problems such as shear tests in which failure occurs very abruptly, dynamic analysis procedures which consider inertia effects will be more suitable than static analysis procedures. The nonlinear dynamic analysis uses direct integration methods to solve equilibrium equations of motion. The direct integration methods can be either implicit direct integration which uses the implicit operator or explicit direct integration which uses central-difference operator. Displacements as well as velocities are calculated in terms of quantities that are known at the beginning of a time increment.

The explicit direct integration is preferred to use for some following important advantages:

- The analysis time increase only linearly with the problem size. As a result, it is suitable for very large FE-models.
- It uses a consistent, large-deformation theory. Therefore models can undergo large rotations and large deformation.
- It is efficient for the analysis of models with short dynamic response times and for the analysis of discontinuous events or processes.

4.4 Test Verification

4.4.1 FEM Model

All of 18 test beams are modelled in ABAQUS 6.9. Because of the symmetric features of the test beams, only a haft of the test beam is modelled to reduce the analysis time. In general, the models in ABAQUS simulate the real working state of test beams as shown in the figures 4.11 and 4.12. In addition to the reinforced concrete beam, the loading plate under the hydraulic jack and the steel-box supports are also modelled. These two parts have the same element type as the concrete beam but have material properties of steel. The tied boundary conditions are assumed at contact surfaces between concrete beam and supports as well as between concrete and loading plate. A typical three dimensional model including FEM mesh, main bars, stirrups, boundary conditions…is presented in figure 4.12.

Figure 4.11– Test set-up of the test beam 2L-1

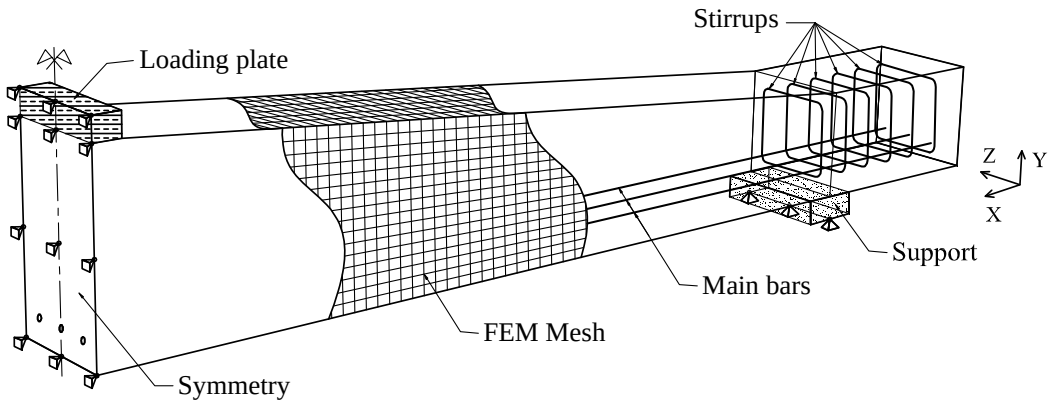

Figure 4.12– Three-dimensional model of test beam 2L-1 in ABAQUS

Elements: The 3D truss elements with 2 nodes (T3D2) are used to model the reinforcing steel bars. The 3D continuum elements with 8 nodes (C3D8R) are utilized for modelling concrete, steel loading plate and supports.

FEM Mesh Size: The size of FEM mesh relates to the calculating results and time consumption. Although the damaged plasticity model for concrete is partly from background of fracture mechanics, it can reduce influence of mesh sensitivity on numerical solution. Nonetheless five different mesh sizes with characteristic element length l_{ch} in the range of 12,5 mm to 30 mm will be modelled to select a most appropriate mesh size to lessen this effect for further investigations. The two tables 4.1 and 4.2 show the number of nodes and elements of concrete, longitudinal reinforcements and stirrups as well as total unknowns of the test beams corresponding to the characteristic element length l_{ch}. It can be seen from these tables that if l_{ch} reduces about 0,67 times (from 30 mm to 20 mm), total unknowns of the system will increase to 3 times. In other case if l_{ch} reduces about 0,41 times (from 30 mm to 12,5 mm), total unknowns of system will increase up to 11 times. However, analysis time consumption may not be significant because all of the numerical analysis can still be performed at the Computer Centre of TUHH where many jobs can be run in parallel. Therefore, the mesh size is chosen mainly from condition of the most reliable analysis results.

l_{ch} (mm)	Concrete		Longitudinal Steel		Stirrups		Total Unknowns
	Element	Node	Element	Node	Element	Node	
30	4.697	5.952	183	186	132	132	18.810
25	8.288	10.125	219	222	156	156	31.509
20	15.640	18.414	273	276	192	192	56.646
15	36.777	41.664	363	366	258	258	126.864
12.5	63.504	70.448	438	441	312	312	213.603

Table 4.1. Mesh size, number of nodes, elements and total unknowns of test beam with a/d=5 (L=3,68m)

l_{ch} (mm)	Concrete		Longitudinal Steel		Stirrups		Total Unknowns
	Element	Node	Element	Node	Element	Node	
30	3.157	4.032	123	126	132	132	12.870
25	5.600	6.885	147	150	156	156	21.573
20	10.540	12.474	183	186	192	192	38.556
15	24.817	28.224	243	246	258	258	86.184
12.5	42.768	47.600	294	297	312	312	144.627

Table 4.2. Mesh size, number of nodes, elements and total unknowns of test beam with a/d = 3 (L = 2,48m)

The preliminary results of the FEM-analysis of all of test beams showed that models with coarse mesh sizes consume very short calculating time and have analysis outcomes such as

relations of force and displacement which are “smoother” than those of models with finer mesh sizes. However, there are no big differences on analysis outcomes among the models with different mesh sizes. It was recognized that the finer the mesh sizes the more comprehensible the crack propagation and stress distribution. For these reasons, the finest mesh size with l_{ch} = 12,5 mm is selected for all further investigations.

Loading Procedure and Analysis Time: For the first test beam 1L1 the load control procedure was applied. At each load step, loading was increased with stable velocity of 1 kN/sec (equivalent to 0,1423 mm/sec) until failure. For other test beams the same load control procedure was applied until the total loading value reached 60 kN. Consequently, the displacement control procedure was utilized with steady velocities until failure as presented in the table 4.3. For simplicity, these values of loading velocities would be used for the whole analysis procedure. In order to make sure that models will experience failure stage, the analysis time needs to be longer than the time of loading in the tests which can be done simply with a certain factor. The detailed values of velocity and analysis time are presented in the table 4.3.

Test Beam	Velocity (mm/sec)	Time of Loading (sec)	Displacement (mm)	Time of Analysis (sec)
1L1	0,1423	151	10,74	175
1L2	0,16	141	11,28	175
2L1	0,18	133	11,93	146
2L2	0,18	132	11,89	145
3L1	0,20	111	11,13	122
3L2	0,20	120	11,98	132
4L1	0,20	202	20,24	223
4L2	0,20	199	19,91	219
5L1	0,28	197	27,60	217
5L2	0,28	193	27,05	213
1K1	0,05	109	2,71	119
1K2	0,05	92	2,31	101
2K1	0,05	124	3,09	136
2K2	0,05	125	3,11	137
3K1	0,05	124	3,11	137
3K2	0,05	116	2,90	127
4K1	0,05	134	3,35	148
4K2	0,05	131	3,26	144

Table 4.3. Velocity of applied loading and analysis time

4.4.2 Results of the FEM-Analysis

This section plans to show main outcomes of the Nonlinear FEM analysis. In general, the program provides full output databases for post processing depending on user's purposes. Since the generation of outputs takes much time for calculating and processing, only main outputs required for comparison with test results or for study of behaviours of beams will be selected to print out such as values of stresses and strains or forces and displacements.

4.4.2.1 Load Bearing Capacity and Displacement

Table 4.4 shows the load bearing capacities and the maximum displacements at mid-span of the test beams predicted by ABAQUS in comparison with those from the experiments. The load bearing capacities are determined as the highest values of applied forces during analysis procedure. The deflections at mid-span, which correspond to these loads, are assumed to be the maximum displacements of the models.

Test Beam	F_{Test} [KN]	F_{ABAQUS} [KN]	$\frac{F_{Test}}{F_{ABAQUS}}$	w_{Test} [mm]	w_{ABAQUS} [mm]	$\frac{w_{Test}}{w_{ABAQUS}}$
1L1	150,9	149,9	1,01	10,7	12,0	0,89
1L2	158,.4	160,0	0,99	11,3	13,9	0,81
2L1	150,4	144,5	1,04	11,9	13,0	0,92
2L2	149,2	147,8	1,01	11,9	13,0	0,92
3L1	133,0	132,9	1,00	11,1	12,1	0,92
3L2	138,6	136,8	1,01	12,0	13,2	0,91
4L1	206,7	204,7	1,01	20,2	22,6	0,89
4L2	206,9	205,4	1,01	19,9	23,6	0,84
5L1	206,4	197,5	1,05	27,6	28,8	0,96
5L2	207,0	197,2	1,05	27,1	28,8	0,94
1K1	151,3	158,2	0,96	2,7	2,9	0,93
1K2	140,0	141,3	0,99	2,3	2,5	0,92
2K1	167,1	173,7	0,96	3,1	3,3	0,94
2K2	170,0	172,1	0,99	3,1	3,2	0,97
3K1	158,7	158,8	1,00	3,1	3,4	0,94
3K2	159,9	148,8	1,07	2,9	3,2	0,91
4K1	169,5	166,2	1,02	3,4	3,7	0,92
4K2	167,8	159,6	1,05	3,3	3,6	0,94

Table 4.4. Load bearing capacity *F* and maximum displacement *w* of test beams from Nonlinear FEM Analysis in comparison with test results

Notes for the table 4.4:

F_{Test} [KN] is the critical load bearing capacity of beam from test results

F_{ABAQUS} [KN] is the critical load bearing capacity of beam from ABAQUS

w_{Test} [mm] is the maximum displacement at midspan of beam from test results.

w_{ABAQUS} [mm] is the maximum displacement at midspan of beam from ABAQUS.

The applied force-displacement relation of all of 18 models in comparison with test result is plotted in the figures 4.13 to 4.30. Again a very good agreement regarding the shape of the load-displacement graph can be observed.

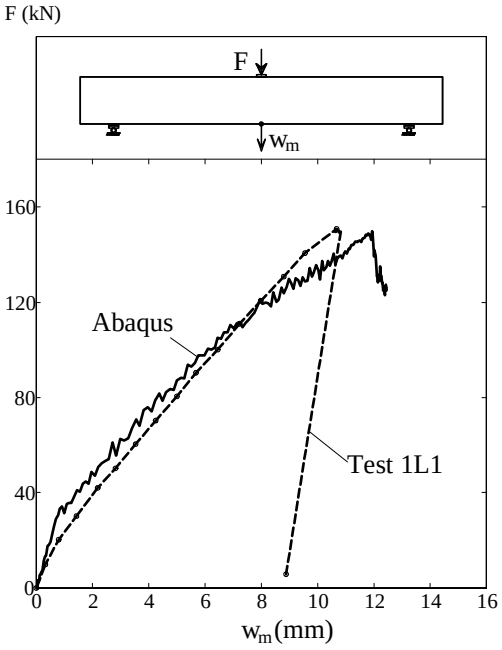

Figure 4.13– Force-displacement relation of test beam 1L1

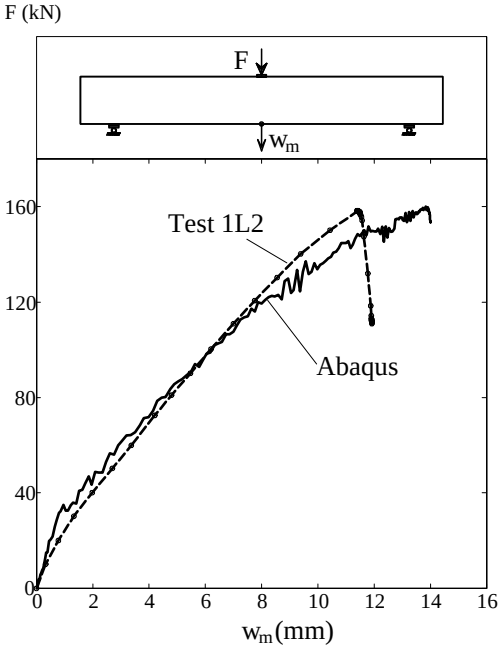

Figure 4.14– Force-displacement relation of test beam 1L2

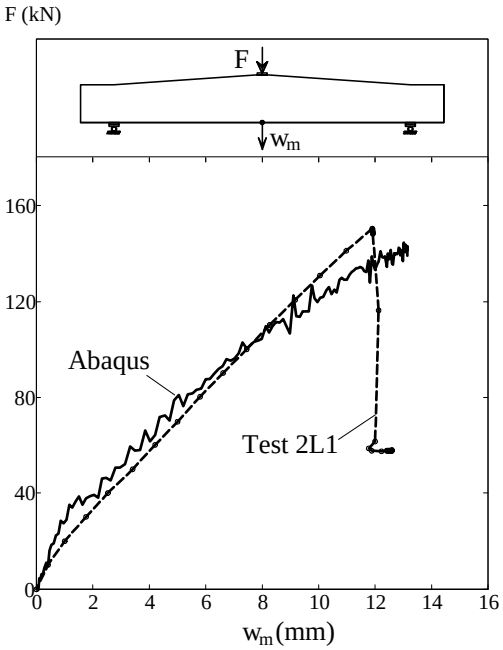

Figure 4.15– Force-displacement relation of test beam 2L1

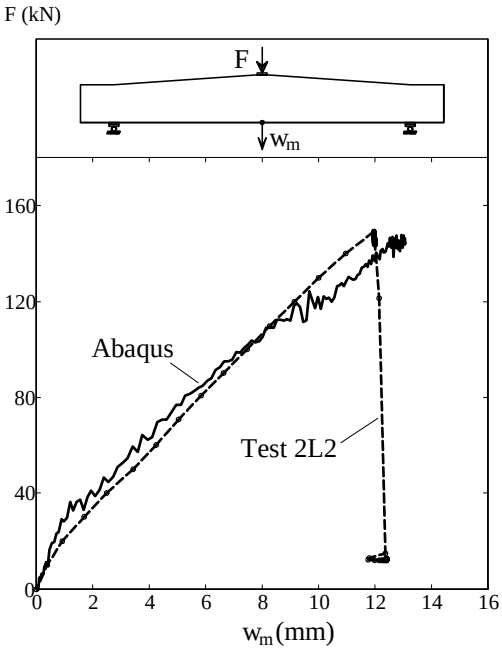

Figure 4.16– Force-displacement relation of test beam 2L2

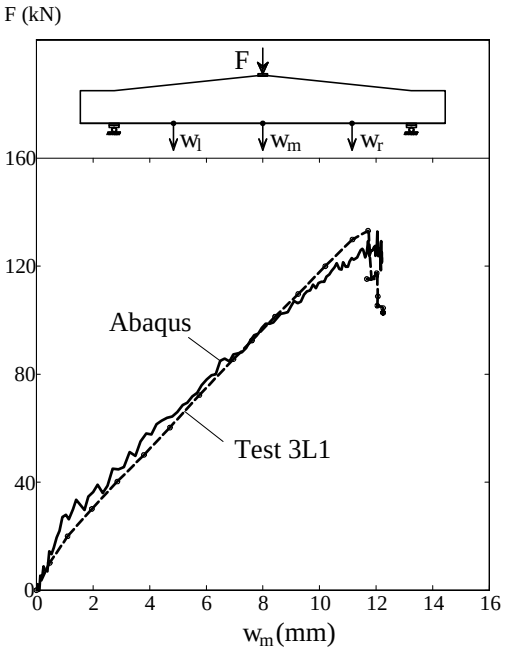

Figure 4.17– Force-displacement relation of test beam 3L1

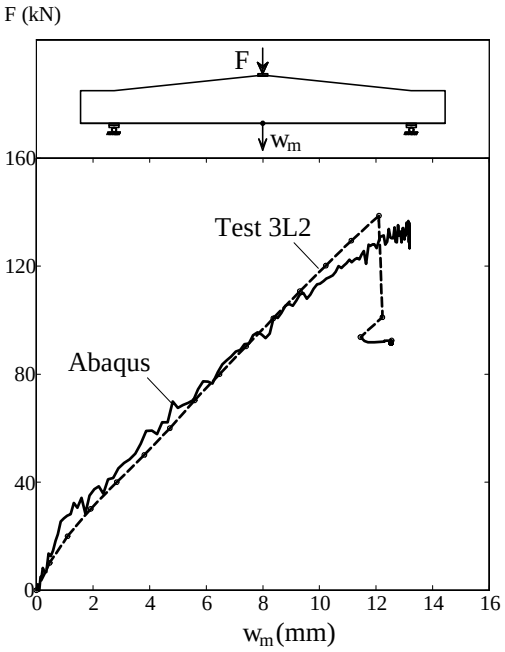

Figure 4.18– Force-displacement relation of test beam 3L2

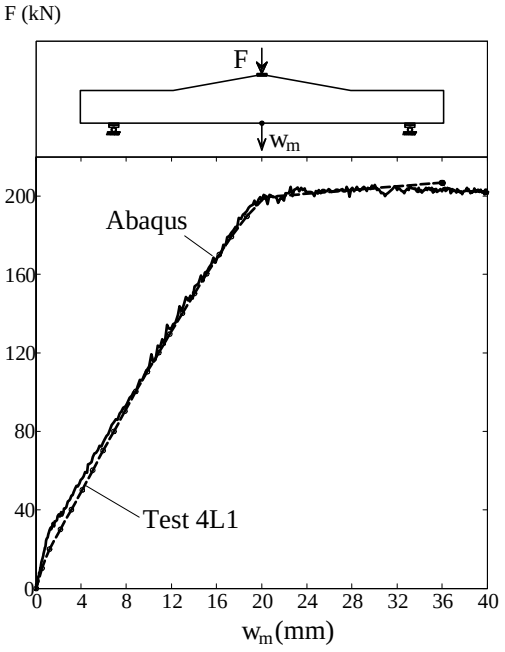

Figure 4.19– Force-displacement relation of test beam 4L1

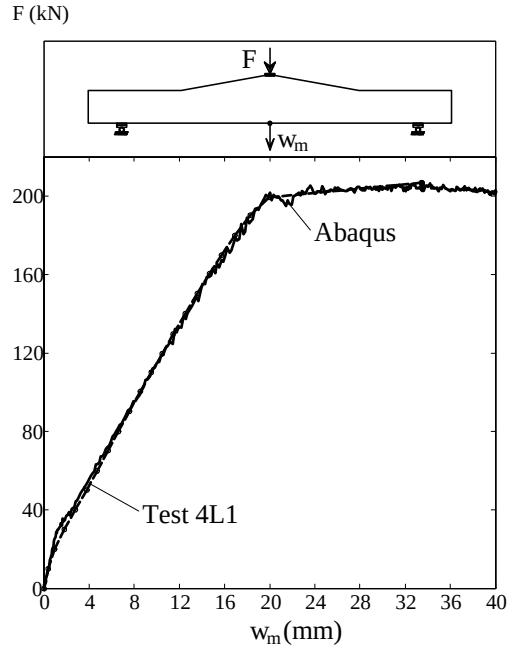

Figure 4.20– Force-displacement relation of test beam 4L2

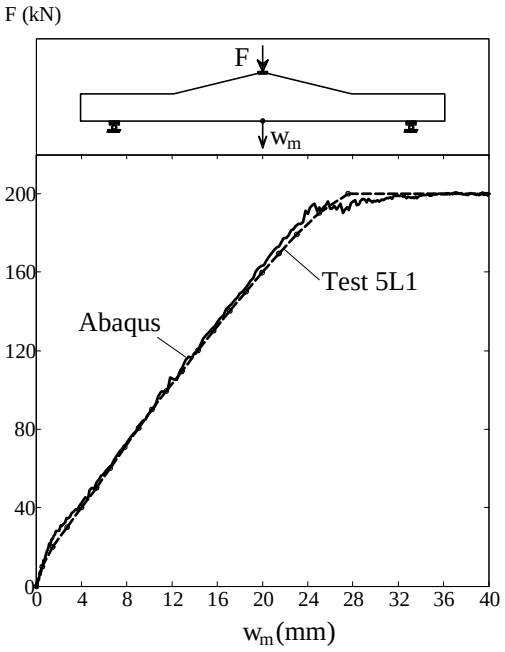

Figure 4.21– Force-displacement relation of test beam 5L1

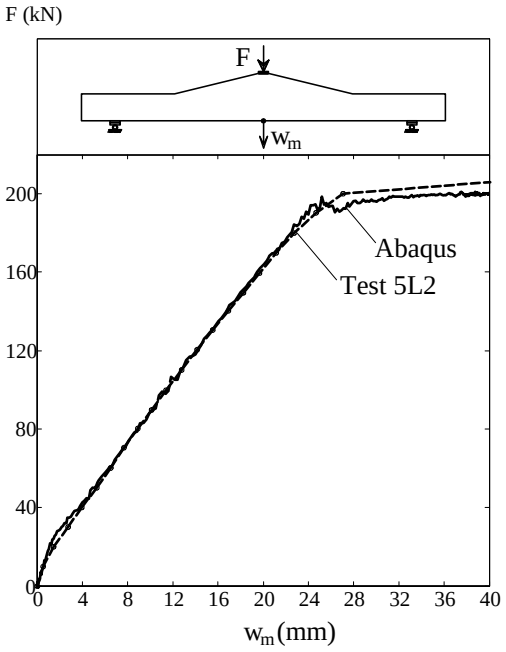

Figure 4.22– Force-displacement relation of test beam 5L2

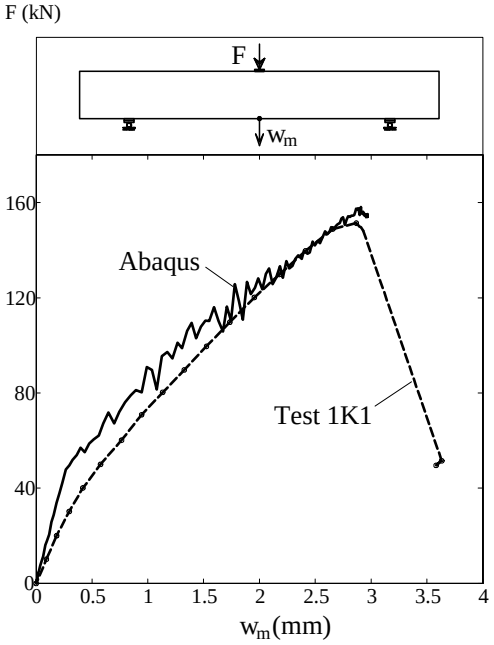

Figure 4.23– Force-displacement relation of test beam 1K1

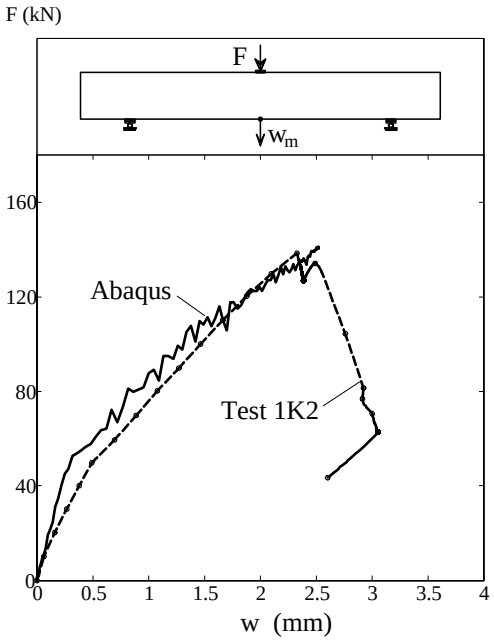

Figure 4.24– Force-displacement relation of test beam 1K2

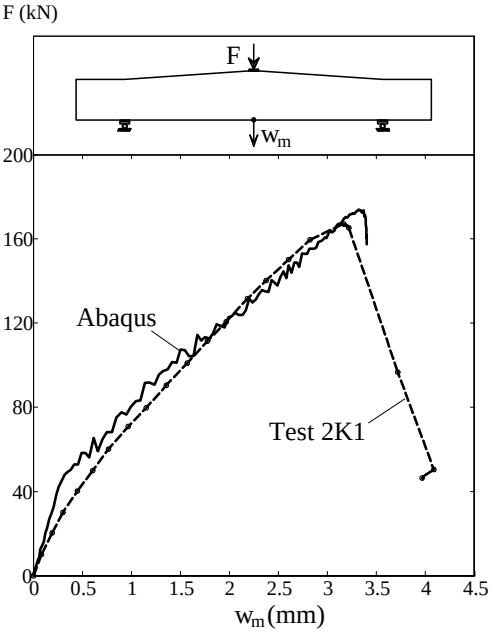

Figure 4.25– Force-displacement relation of test beam 2K1

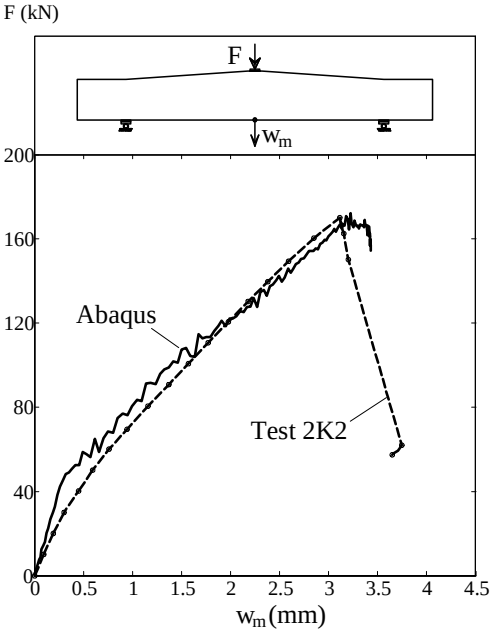

Figure 4.26– Force-displacement relation of test beam 2K2

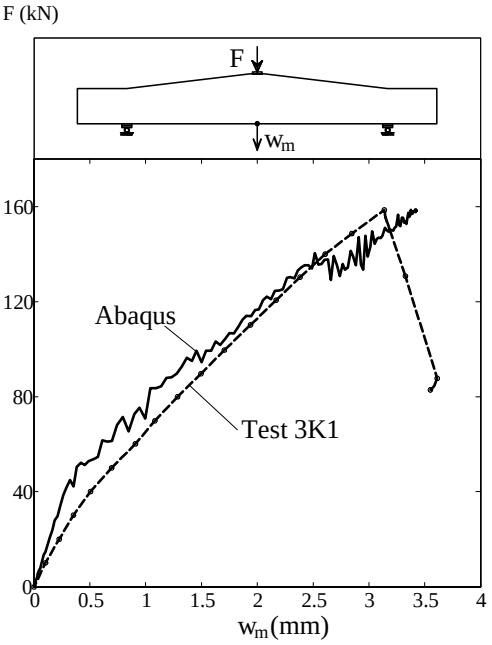

Figure 4.27– Force-displacement relation of test beam 3K1

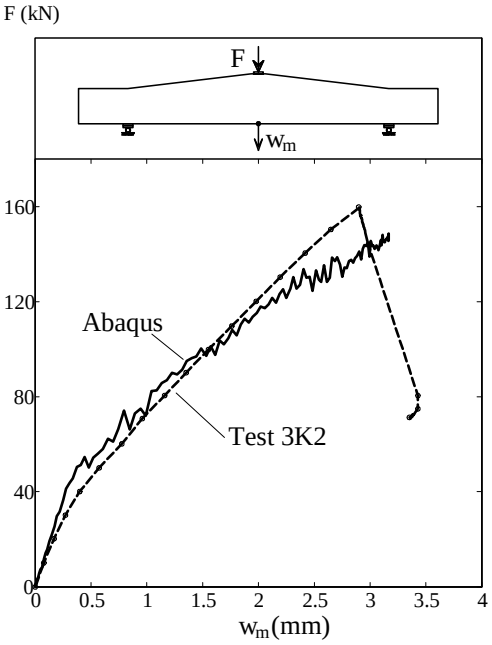

Figure 4.28– Force-displacement relation of test beam 3K2

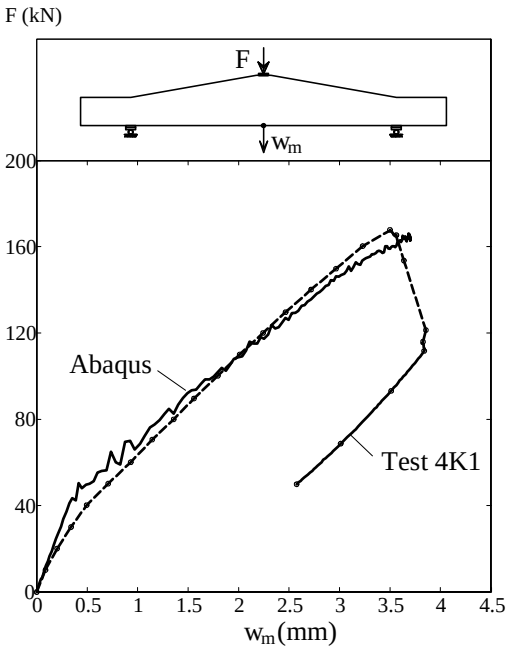

Figure 4.29– Force-displacement relation of test beam 4K1

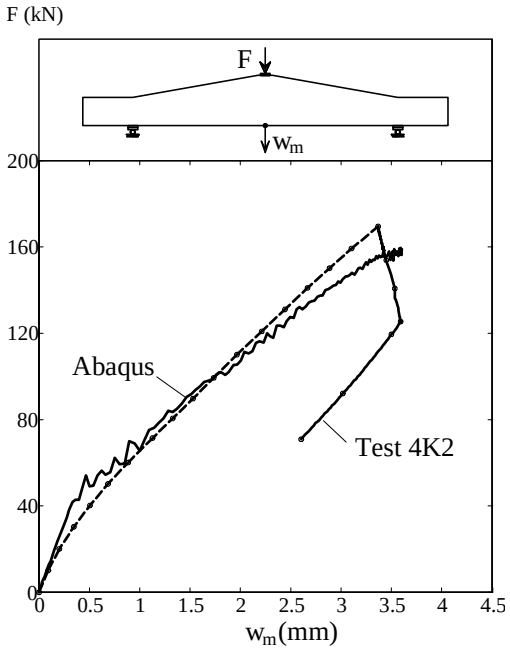

Figure 4.30– Force-displacement relation of test beam 4K2

4.4.2.2 Crack Propagation in Comparison with Test Results

For a better understanding of the progressive failure process, the initiation and propagation of cracks in the FEM-models will also be presented. Figure 4.31 shows the crack pattern from the FE-analysis of test beam 1L2 at a load of F = 60 kN.

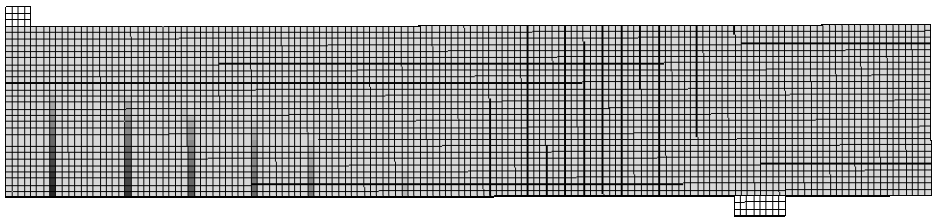

Figure 4.31– Crack pattern of test beam 1L2 at loading of F = 60 kN (FEM-analysis)

For better observation, the crack patterns should be printed in contour mode without FEM mesh. Figure 4.32.b shows the initiation and development of cracks in the FEM-model of test beam 1L2 after each two load steps in comparison with the crack pattern from tests in figure 4.32a as a representative of a straight depth beam. Figure 4.33 shows the same crack propagation for the haunched beam 4K1. For other test beams can be referred to Appendix E. The crack patterns at failure of FEM-models and from testing of all test beams are shown in the figures 4.34 to 4.49.

It can be seen from these figures that there is a good agreement on crack patterns, crack spacing's, location and inclination of relevant shear cracks between the numerical analysis

and the experimental results. These results confirm that the developed nonlinear finite element model can simulate the behaviours of the test beams with reliable accuracy.

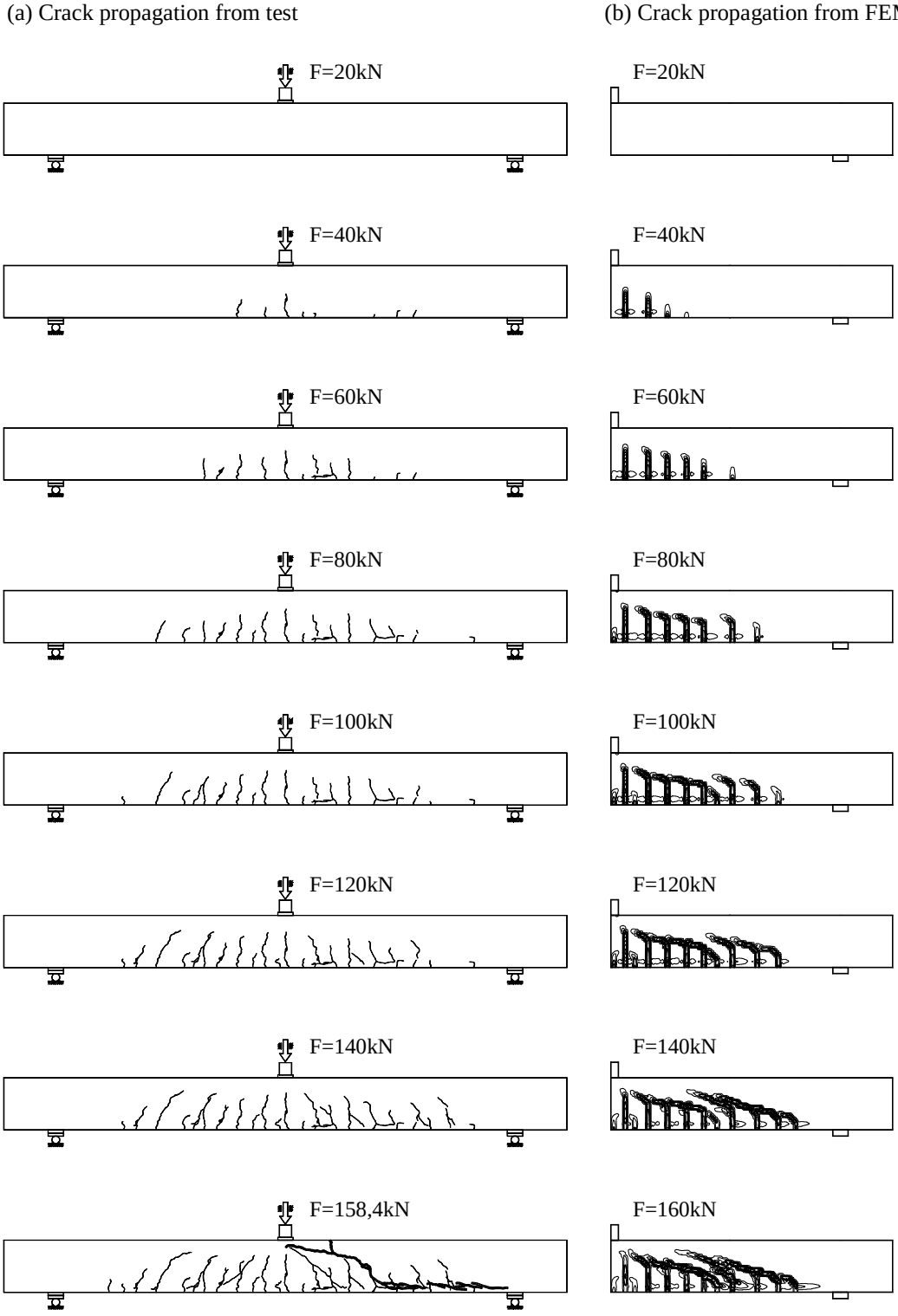

Figure 4.32– Crack propagation of test beam 1L2 from test results and Non-FEM analysis

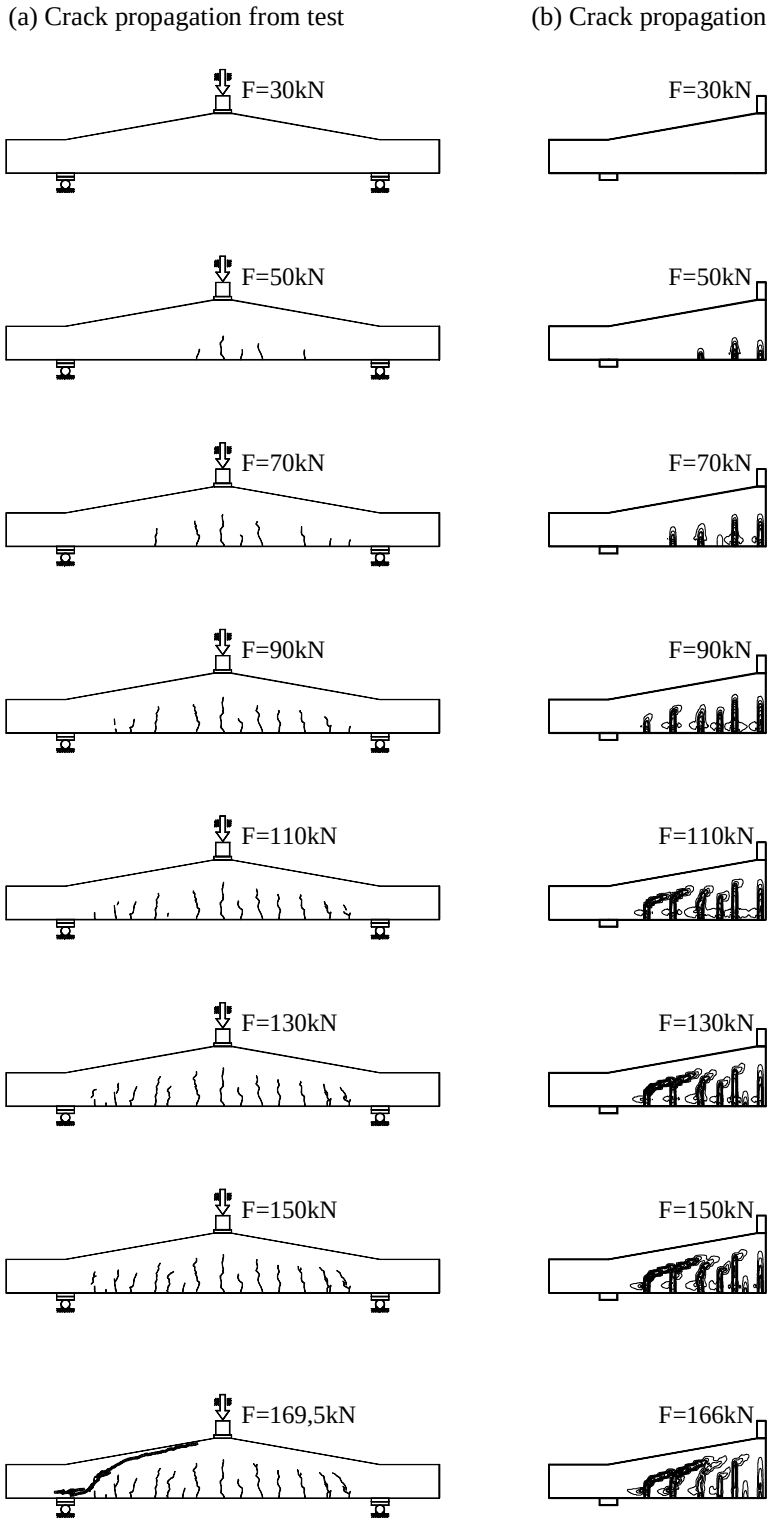

Figure 4.33– Crack propagation of test beam 4K1 from test results and Non-FEM analysis

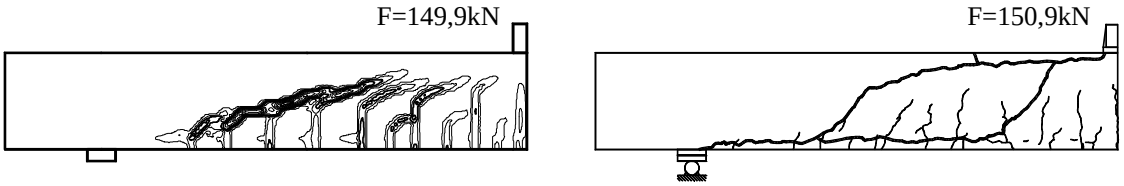

Figure 4.34– Crack propagation at failure of test beam 1L1 from Non-FEM and test

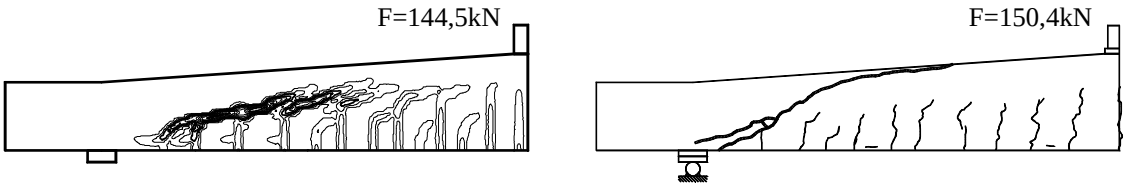

Figure 4.35– Crack propagation at failure of test beam 2L1 from Non-FEM and test

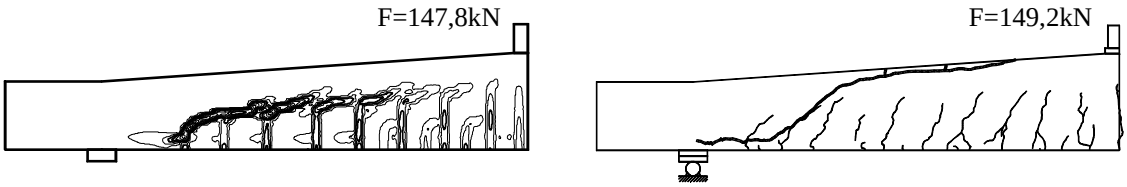

Figure 4.36– Crack propagation at failure of test beam 2L2 from Non-FEM and test

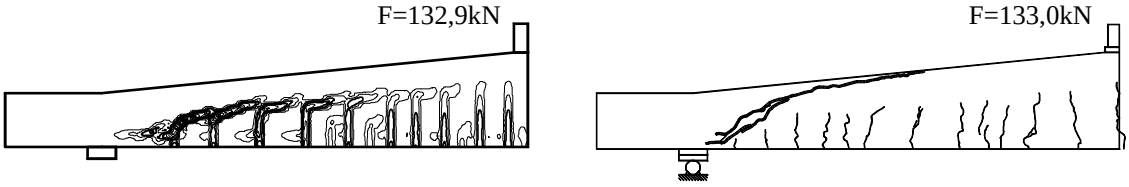

Figure 4.37– Crack propagation at failure of test beam 3L1 from Non-FEM and test

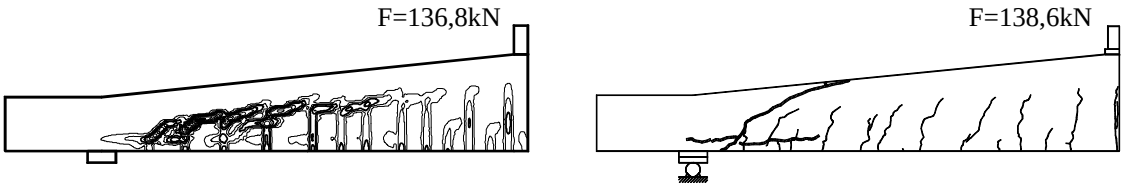

Figure 4.38– Crack propagation at failure of test beam 3L2 from Non-FEM and test

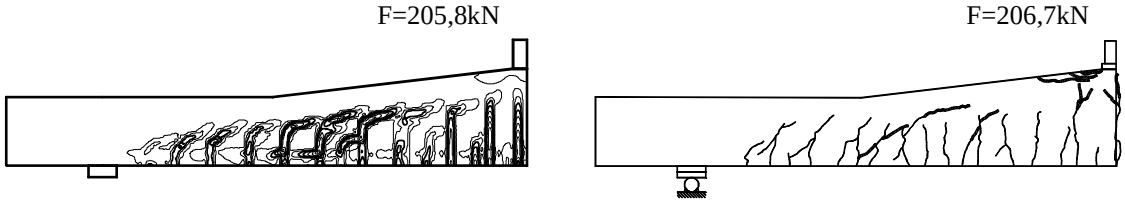

Figure 4.39– Crack propagation at failure of test beam 4L1 from Non-FEM and test

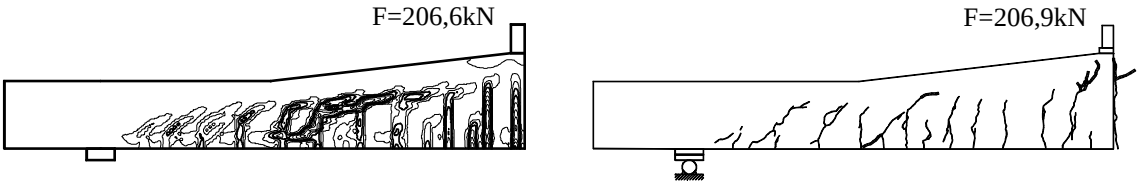

Figure 4.40– Crack propagation at failure of test beam 4L2 from Non-FEM and test

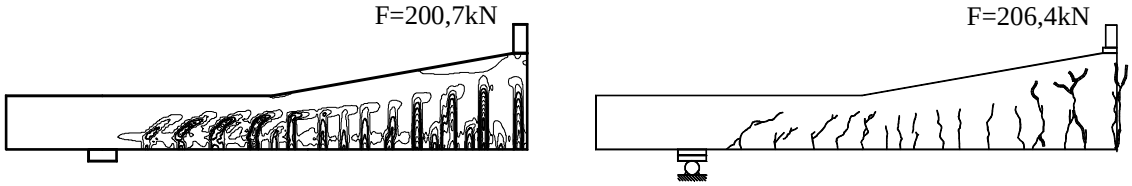

Figure 4.41– Crack propagation at failure of test beam 5L1 from Non-FEM and test

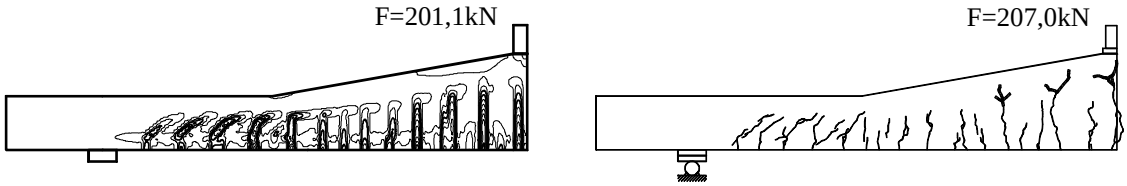

Figure 4.42– Crack propagation at failure of test beam 5L2 from Non-FEM and test

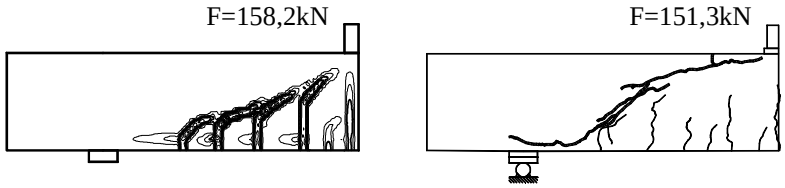

Figure 4.43– Crack propagation at failure of test beam 1K1 from Non-FEM and test

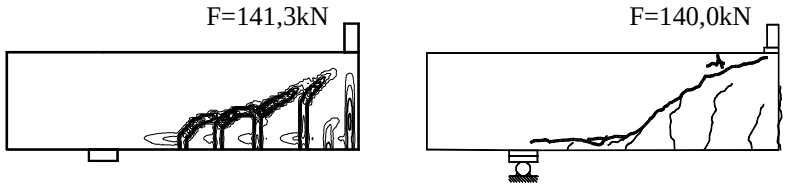

Figure 4.44– Crack propagation at failure of test beam 1K2 from Non-FEM and test

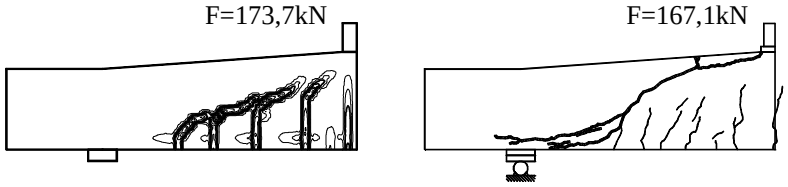

Figure 4.45– Crack propagation at failure of test beam 2K1 from Non-FEM and test

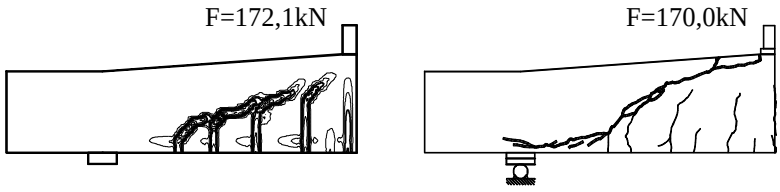

Figure 4.46– Crack propagation at failure of test beam 2K2 from Non-FEM and test

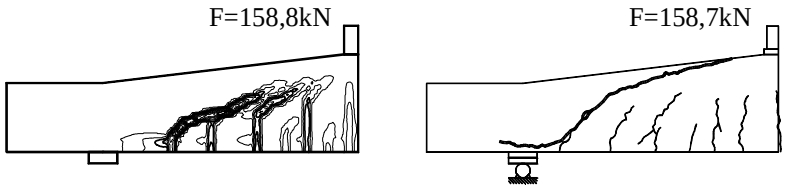

Figure 4.47– Crack propagation at failure of test beam 3K1 from Non-FEM and test

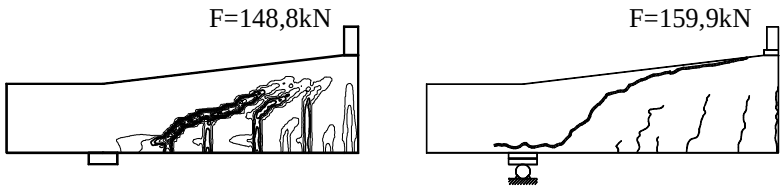

Figure 4.48– Crack propagation at failure of test beam 3K2 from Non-FEM and test

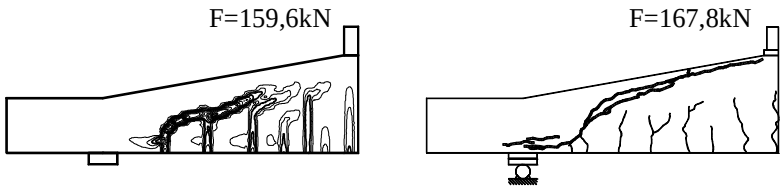

Figure 4.49– Crack propagation at failure of test beam 4K2 from Non-FEM and test

4.4.2.3 Stress Distribution in Models

The stress distribution in stirrups, main bars and concrete is investigated to explain the initiation and propagation of cracks as well as redistribution of stresses when cracks occur up to failure of the beams. For stirrups and longitudinal reinforcements, there exists only normal stress distributed along central axis of element as shown in figure 4.50 for test beam 4L1. Normal stresses and shear stress in the concrete are distributed as in figure 4.51 for straight depth beam 1L2 and in figure 4.52 for haunched beam 4K1.

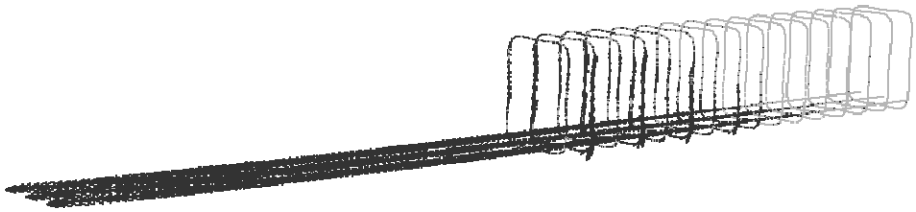

Figure 4.50– Normal stress in stirrups and longitudinal reinforcements of test beam 4L1 (Non-FEM analysis)

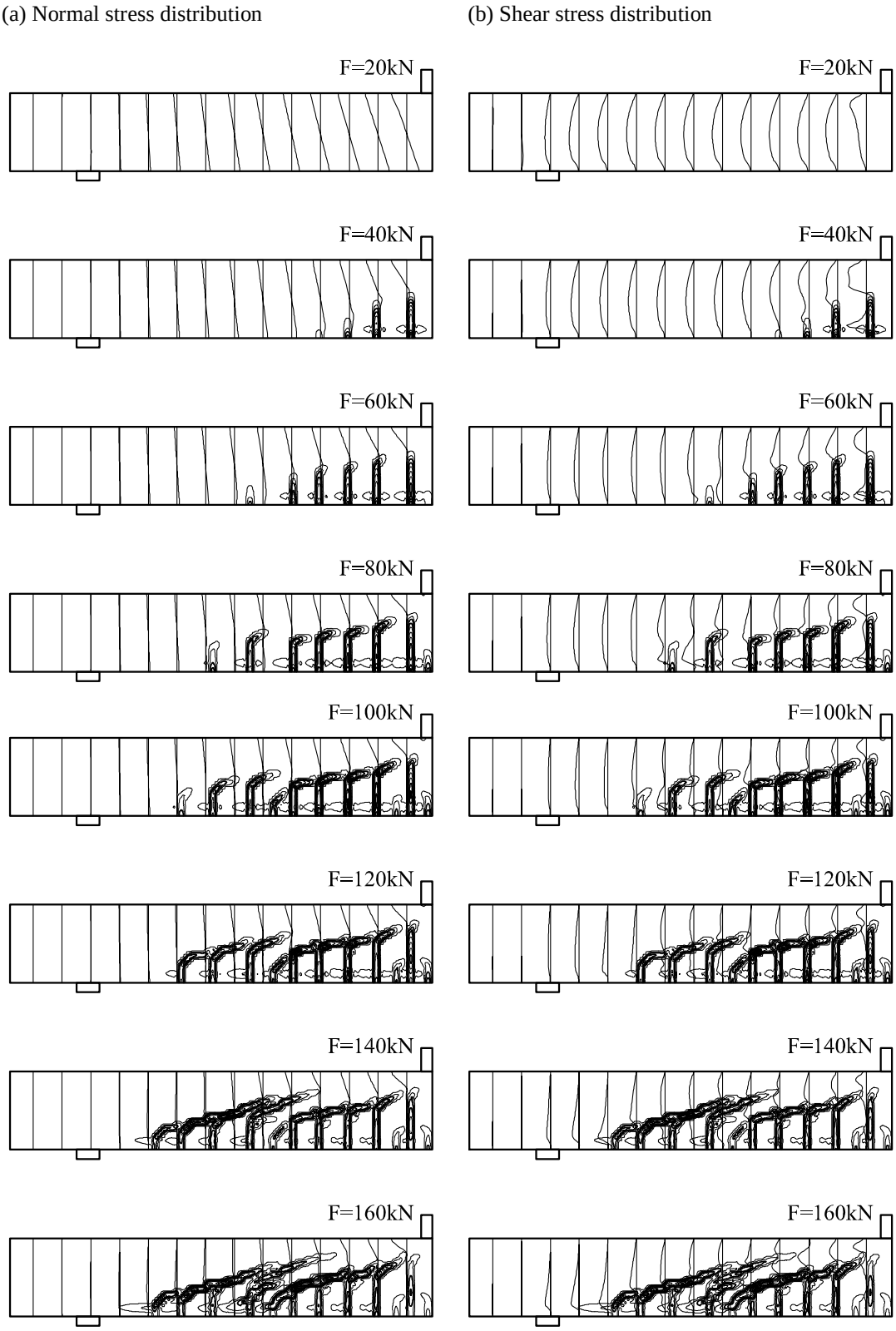

Figure 4.51– Distribution of normal stress and shear stress
in FE-model of test beam 1L2 up to failure

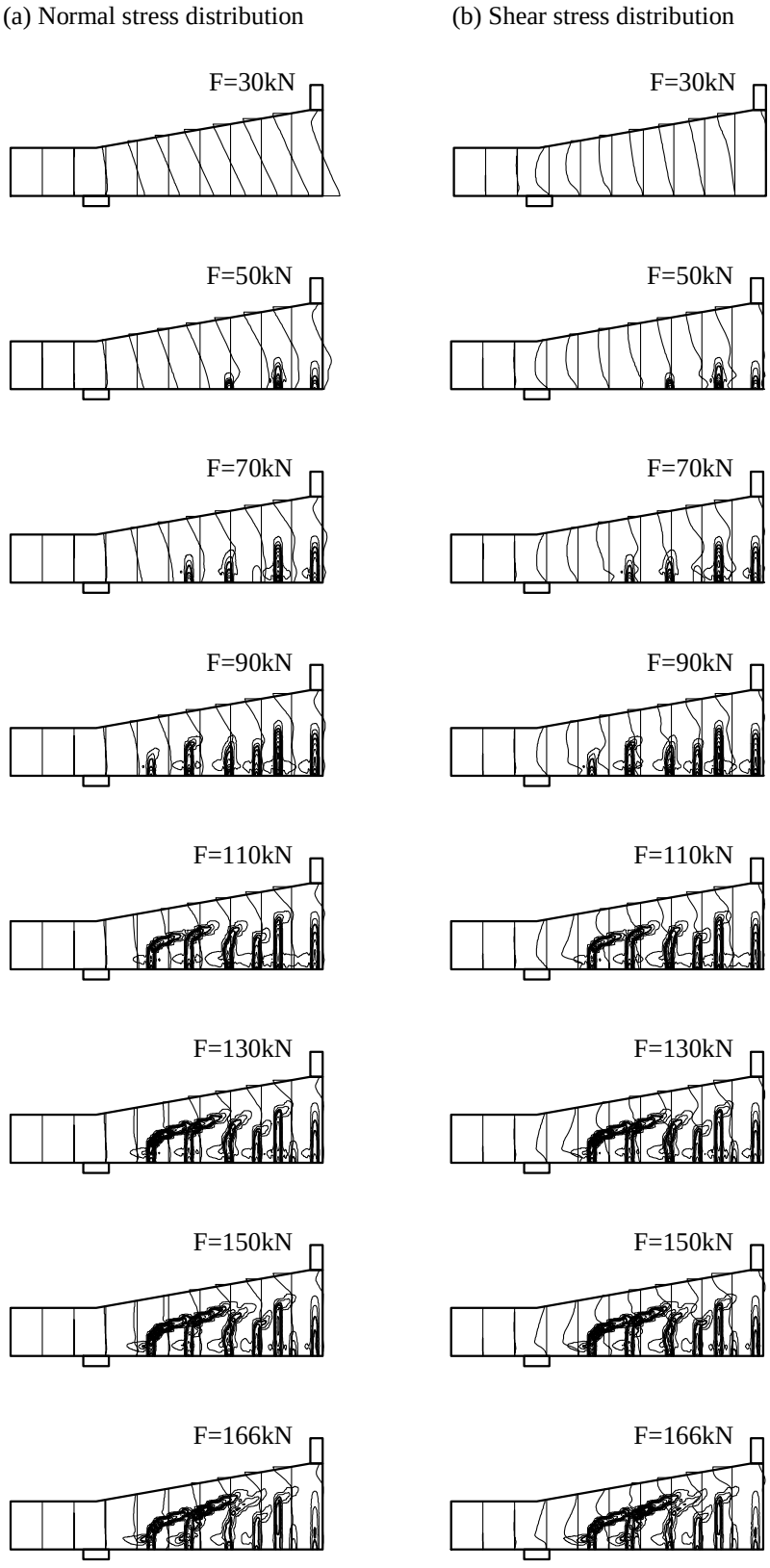

Figure 4.52– Distribution of normal stresses and shear stresses
in FE-model of test beam 4K1 up to failure

4.5 Discussions and Conclusions

Some discussions and conclusions of the chapter 4-Nonlinear Finite Element Analysis are given in the following:

The concrete damaged plasticity model adopted in ABAQUS is a good suggestion for modelling of concrete structures. The results of the numerical analysis of 18 test beams show that some main failure behaviours of concrete members without stirrups such as shear strength, relation of load and displacement or crack propagation predicted by Nonlinear FEM are in very good agreement with test results. These can be briefly described as follows:

Load Bearing Capacity: the table 4.4 and figure 4.53 show that Non-FEM predicted quite exactly the load bearing capacity of all 18 test beams. The largest difference between experiment and numerical analysis is for test beam 3K2 with a tolerance of 6,9 % while the mean value of tolerance of all 18 tests is about 1,3 % only. It is noted in the test program that there are two types of test beams with different a/d ratios (a/d = 3 and a/d = 5) and two types of failure including flexure failure (test beams 4L and 5L) and shear failure (other test beams). Therefore, it can be said that Non-FEM models can be used reliably to predict the load bearing capacity of the test beams or concrete beams in general.

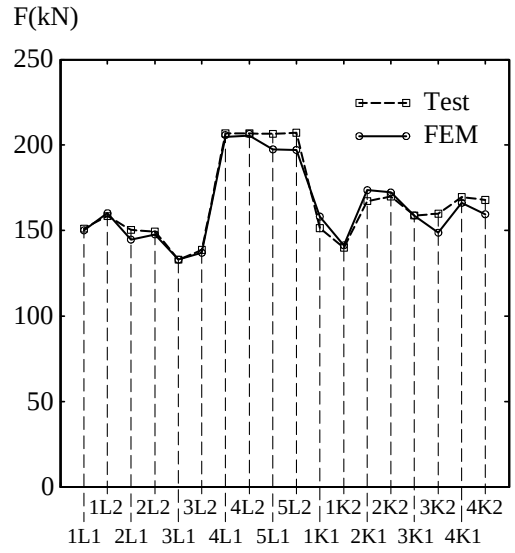

Figure 4.53– Comparison of load bearing capacity between test and Non-FEM

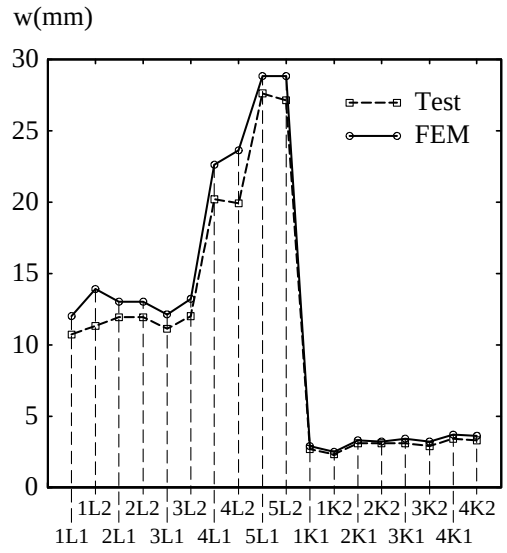

Figure 4.54– Comparison of mid-span deflection between test and Non-FEM

Load/Displacement Curve: Table 4.4 and figure 4.54 show that the maximum mid-span deflections from Non-FEM models always have higher values than those of tests (average of about 9,2 %). For models of test beams failed in shear, the initial inclined angles of the load-displacement curves (or stiffness) from Non-FEM is larger than those of the real tests. When cracks increase in number and in height, the load-displacement curves become flatter and

flatter than those of the tests (Fig. 4.55). That means the preliminary stiffness of Non-FEM model is higher than that of the actual system, but it will rapidly reduce as cracks occur and propagate. Finally, at the critical failure load the stiffness of the Non-FEM model is smaller than that of the actual system. That's why displacements of Non-FEM models will be relatively higher than those of tests. However, there is a very good agreement on the relation of load-deflection between Non-FEM analysis and the test program in general.

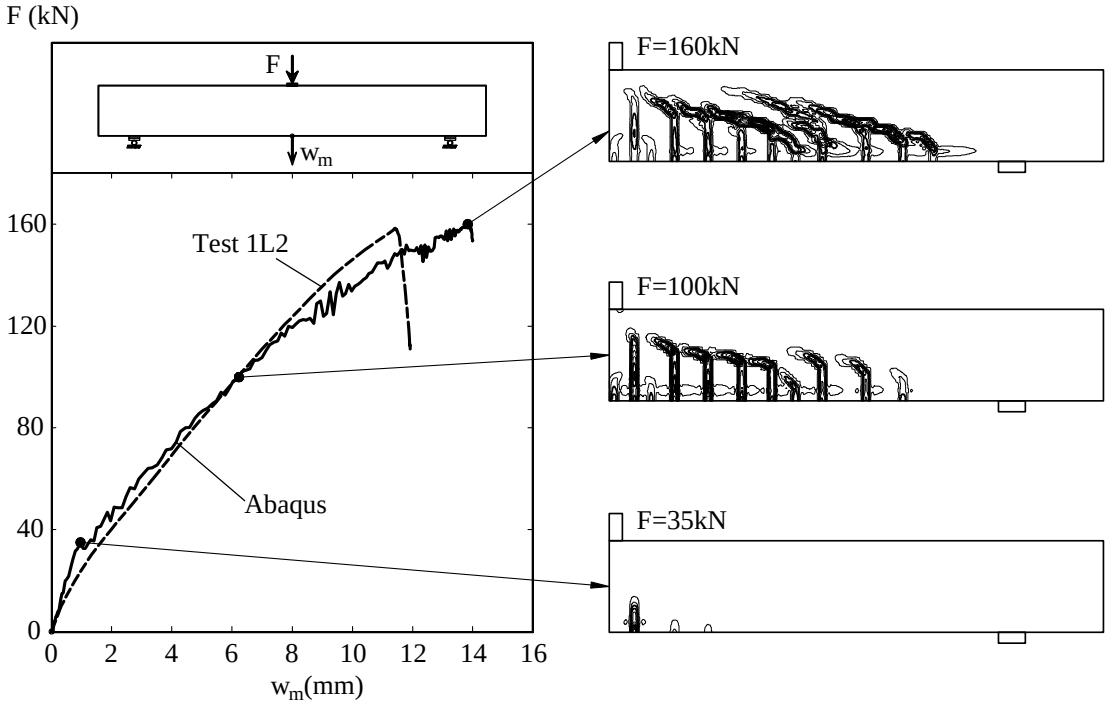

Figure 4.55– Load-deflection curves and crack patterns from FEM of beam 1L2

For models of test beams failed in flexure (4L and 5L), the load-deflection curves are nearly identical with those of test results up to failure (Figs 4.19 to 4.22). This extremely good agreement can be explained that the mechanisms of flexure failure are well-defined in material models where steel undergoes yielding range and failure of concrete is in either tension crack or compressive crushing.

It is also noted from the load-displacement curves of the nonlinear Finite Element models that there exists converge problems during analysis, especially at loadings close to the critical load. However, the program overcame this problem and continued the computation until end of the analysis time. Since it was intended for using ABAQUS to model the test beams as a normal user, this problem is accepted as a matter of course and it is not aimed to solve in this research.

Failure Type and Crack Propagation: The Non-FEM analysis predicts exactly the failure types of all test beams. For shear failure, the load bearing capacity of the model abruptly

drops obviously after reaching critical value which can be recognized from the load-displacement curves. The critical cracks are inclined to the neutral axis of the beams as seen in many shear tests. For flexural failure, the longitudinal reinforcements yield as shown in the figures 4.19 to 4.22 and critical cracks are almost perpendicular to the neutral axis of the beams as shown in the figures 4.39 to 4.42.

Due to the assumptions and simplifications of the used Finite Element approach, it seems impossible to get crack patterns as exactly as in the test. This may be due to differences of the numerical model (half of actual beam…) from testing conditions…But the main reason is due to heterogeneous natures of concrete material. This can be verified from the test program that the load bearing capacity and crack patterns of the two identical test beams are different even though they own the same features of materials, testing conditions…However, it can be seen from the figure 4.32 and figure 4.49 that the Non-FEM models can predict well the initiation and propagation of cracks, the failure region where critical crack occurs, some main characteristics of critical crack such as direction, inclination and crack pattern…which are relatively identical with those from the tests. The figures 4.56 to 4.60 show patterns of critical cracks and failure region predicted by Non-FEM models in comparison with test results of beam 1L2 as a representative of a long straight beam failed in shear and test beam 3L2 as a representative of a long haunched beam failed in shear, test beam 5L1 as a representative of a long beam failed in flexure, test beam 1K2 as a representative of a short straight beam failed in shear and test beam 4K1 as a representative of a short haunched beam failed in shear. For beam failed in shear, it is very interesting to learn from these figures that both Non-FEM models and test results predicted quite accurately that the failure region of straight depth beams is about close to position of load application (Fig. 4.56 and Fig. 4.59) while the failure region of haunched beams is near the support (Fig. 4.57 and Fig. 4.60).

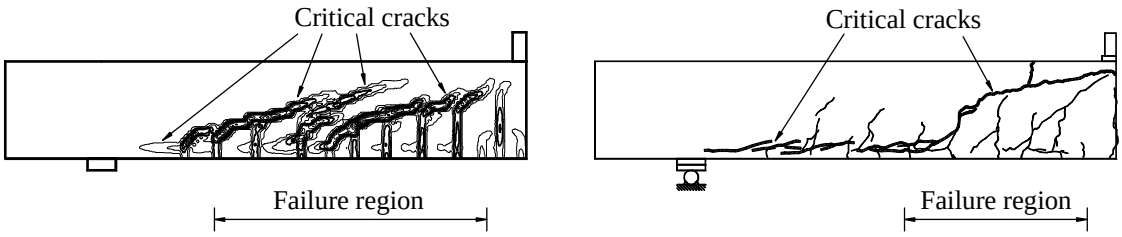

Figure 4.56– Critical crack pattern and failure region of test beam 1L2 from FEM and test results

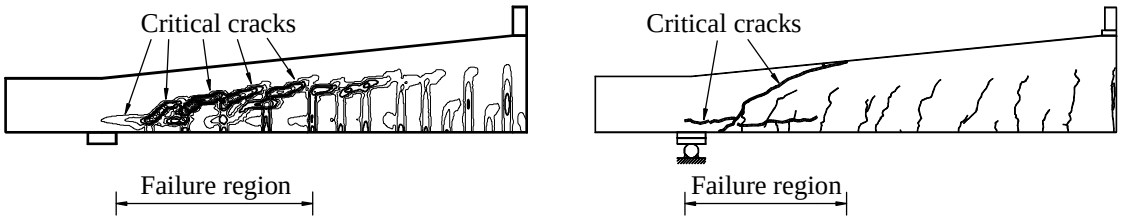

Figure 4.57– Critical crack pattern and failure region of test beam 3L2 from FEM and test results

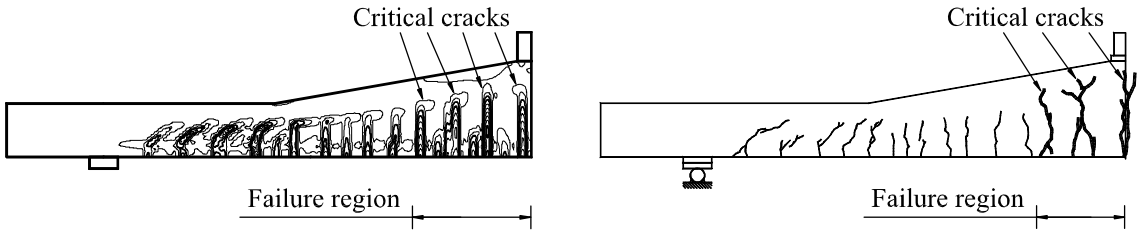

Figure 4.58– Critical crack pattern and failure region of test beam 5L1 from FEM and test results

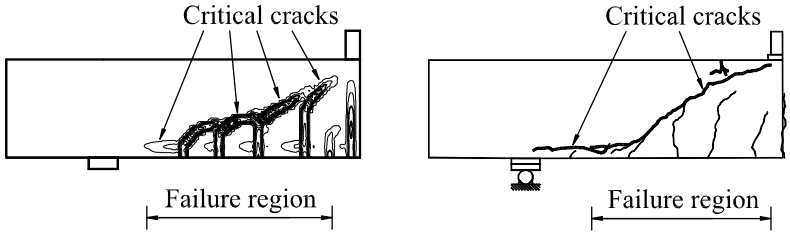

Figure 4.59– Critical crack pattern and failure region of test beam 1K2 from FEM and test results

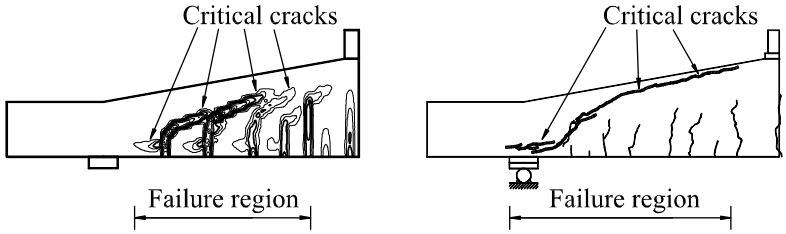

Figure 4.60– Critical crack pattern and failure region of test beam 4K1 from FEM and test results

To get a better understanding of the cracking behaviours of these models, it is required to find out correlations between initiation and propagation of cracks with distribution of stresses in the beams which will be presented in the following.

Stress Distribution: It can be seen from the figure 4.50 that there exists only normal stress in stirrups and longitudinal reinforcements. In contrast, two stress components including normal stresses (in tension and in compression) and shear stress are found distributed on vertical cross-sections in the concrete part of the models as can be seen in figure 4.61 and figure 4.62. For two types of straight and haunched beams, the distribution of normal stresses is absolutely the same at different load stages. At the elastic phase (F = 20 kN for test beam 1L2 and F = 30 kN for test beam 4K1), there exist both compressive normal stress and tensile normal stress in triangle shapes at different side of the neutral axis which locates in the middle of the cross-section (Figure 4.61.a). When cracks occur and increase in number and in height, the region of normal tensile stress becomes smaller and smaller until this type of stress only exists at some local positions such as at the tips of the cracks or at the vicinity of the longitudinal reinforcements. In contrast, compressive normal stress exists at any region where concrete is not cracked yet and the maximum value is still at the top fibre of cross-sections (Fig. 4.61.b and 4.61.c). The shape of the normal compressive stress block is differ-

ent at different cross-sections. However, at sections in mid-span this stress block roughly has the shape of a half-parabola which is assumed in most of the flexure design models (Fig. 4.61.c). The moment diagrams obtained by integration of compressive normal forces multiplied with the inner lever arm to the position of the main reinforcing bars are presented in figure 4.61.d for both test beams 1L2 and 4K1. It can be seen that the shapes and values of these diagrams are in very good agreement with those from common mechanical theory. Except for some sections close to position of load application influenced by the spreading of the force, the average tolerance of moment values between Non-FEM and theory is about smaller 0,5 % for test beam 1L2 and about smaller 1,1 % for test beam 4K1. These results again confirm well the reliability of the Non-FEM in analysis of concrete structures without stirrups.

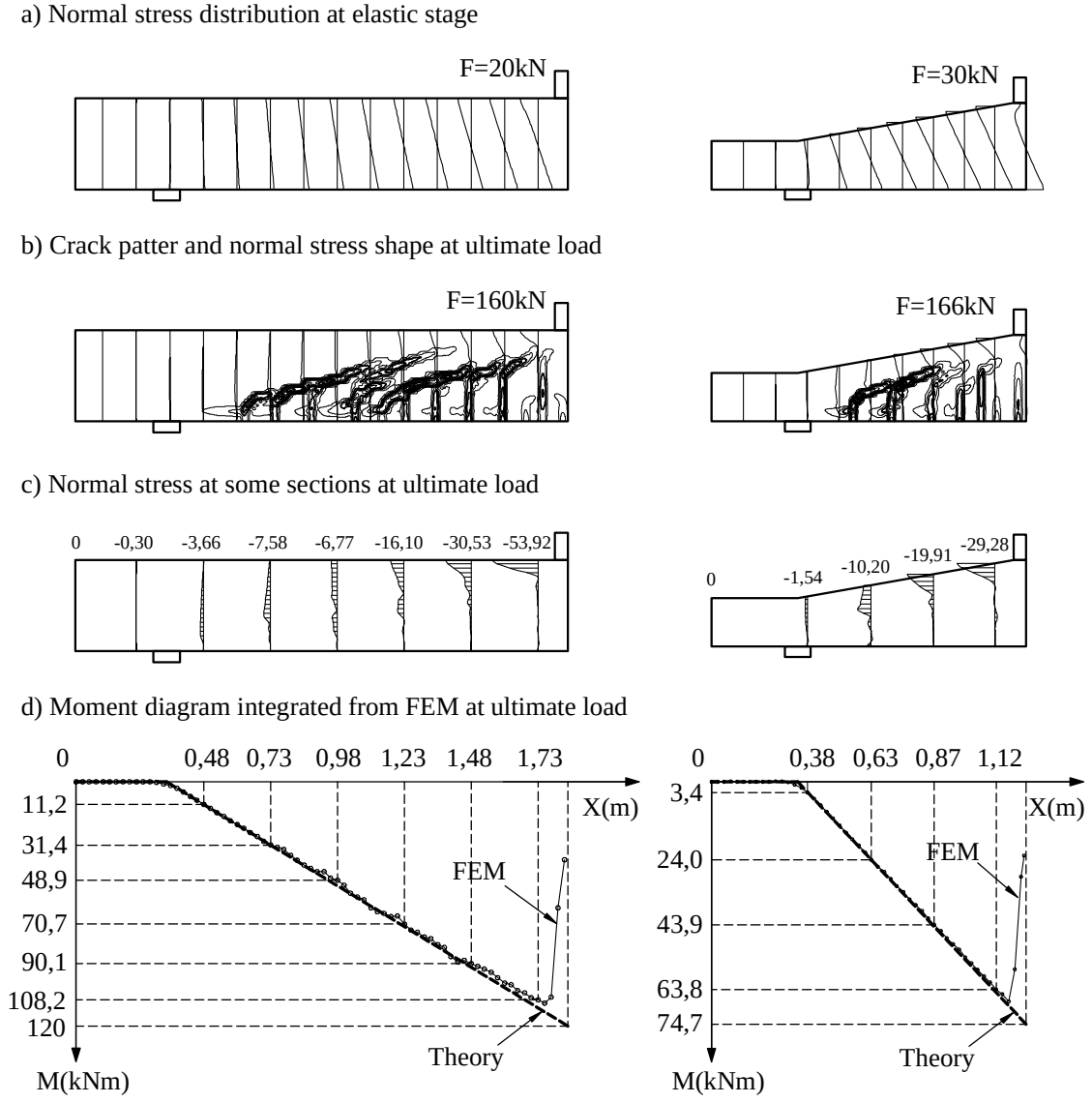

Figure 4.61– Normal stress distribution and moment diagram integrated from Non-FEM models and from theory of test beam 1L2 and 4K1

The distribution of shear stresses of straight depth beams, in the other hand, is totally different from that of haunched beams as presented in the figures 4.51.b, 4.52.b and 4.62. In the elastic stage, the shear stress distribution of straight depth beams has a parabola form with maximum value of the stress in the middle of the cross-sections. This distribution totally complies with classical mechanical theory. In the other hand, the shear stress distribution of haunched beams is diverse at different regions of beam as shown in figure 4.62. At regions close to the position of the load application, this distribution has the form of a half-parabola with maximum value of stress on the top surface of the beam while that close to the support approximately has a parabola form with maximum value of stress in the middle of cross-sections. When cracks occur and increase in number and in height, the distribution of shear stress becomes more complicated as shown in the figures 4.51.b, 4.52.b, 4.62.b and 4.62.c.

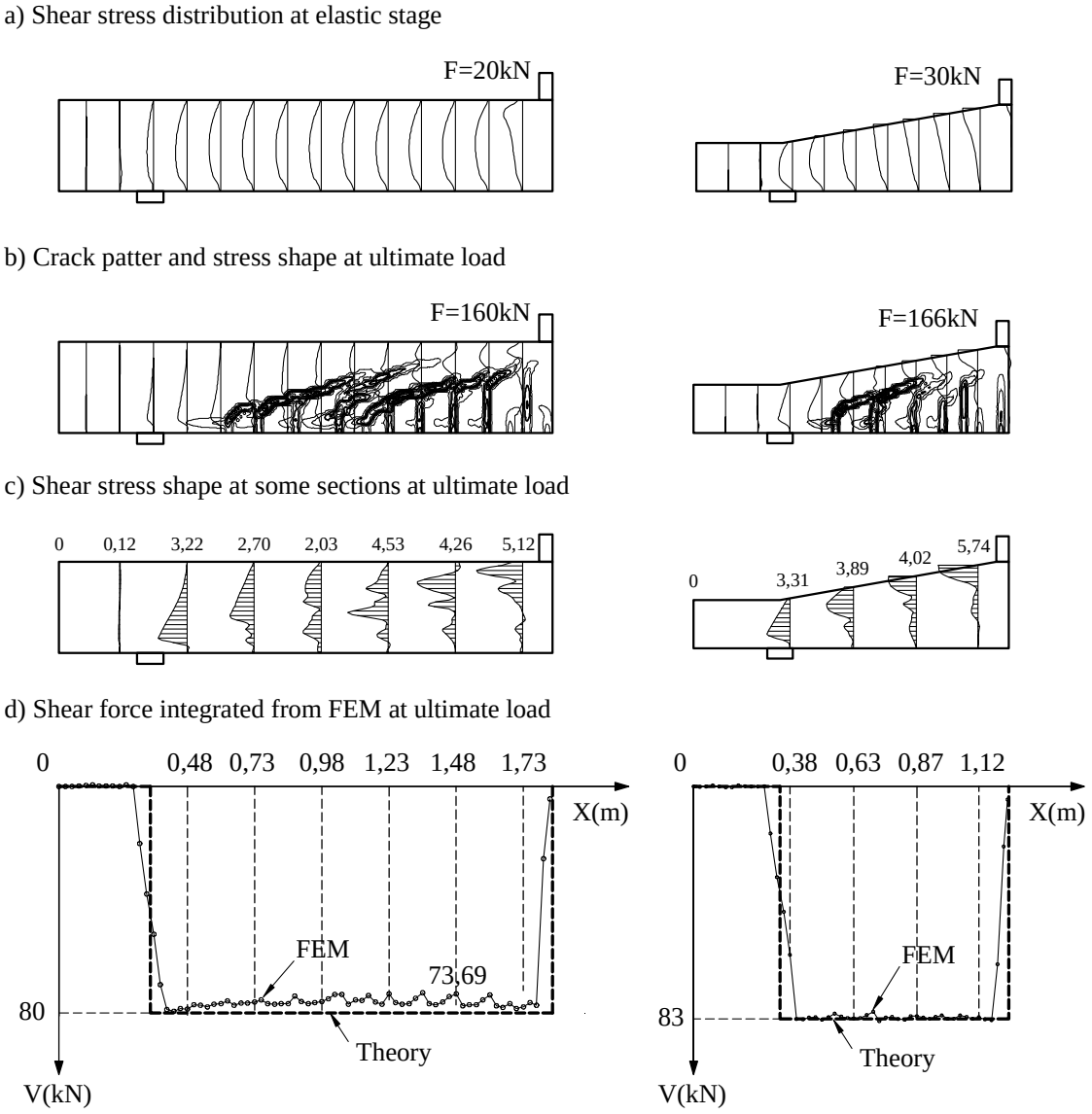

Figure 4.62– Shear stress distribution and shear force diagram integrated from Non-FEM models and from theory of test beam 1L2 and 4K1

However, some features of distribution of shear stresses can be found based on correlations between shear stress redistribution and cracking behaviours in straight depth beams and haunched beams as follows:

(i) There exists very small or no value of shear stress on vertical cracks and inclined cracks.

(ii) There exists mainly shear stress on uncracked concrete parts in both compression zone and tension zone.

(iii) In regions close to the support, large value of shear stress locates on inclined curve (direct strut) going down to the support for both straight depth beams and haunched beams. In region near the position of load application, large value of shear stress normally occurs either at the middle of concrete compression zone or at the middle of uncracked concrete parts in tension zone of straight depth beam. In the other hand, large value of shear stress generally exists on top of concrete compression zone of haunched beams or at the middle of uncracked concrete parts in tension zone (Figure. 4.62).

It is obvious for the first above statement that there is no shear at both surfaces of cracks which have relatively large opening. There perhaps exists shear stress on surfaces of tiny cracks or surfaces next to crack tips due to so-called aggregate interlock. However, it is believed that the shear stress in this region will exist for a short time during crack formation only. When cracks reach a stable state at a certain loading step, the value of shear stress at these cracks becomes smaller or even negligible.

It can be seen from the figure 4.51.b, 4.52.b and figure 4.62 that it is the uncracked concrete parts in both compression zone and tension zone which carry most of the shear force at any vertical cross-section. The shear force integrated from FEM has a similar shape and average value of about 96,9 % of theoretical result for test beam 1L2 and 98,5 % of theoretical result for test beam 4K1 (Fig. 4.62.d). The shear value of FEM V = 73,69 kN (about 92 % of theoretical value V = 80 kN) at section of 1,45m apart from the end of the beam of test beam 1L2 can be considered as an occasional circumstance (Fig. 4.62.d). The remaining small value of shear force can be assumed to be carried by other shear resistance mechanisms such as dowel action, aggregate interlock…

It can be seen from the figures 4.61.b and 4.61.c that there exists mainly compressive stress on any cross-section of the beam at critical state. As a result, it is totally possible to illustrate qualitatively the redistribution of this compressive stress field in a general case for both straight depth beam and haunched beam as in the figure 4.63.a. From this distribution of

stress field, the value of shear stress of any point in the beam can be determined by following formula as in the theory of elasticity:

$$\tau_{xy} = \frac{1}{2}\tan 2\alpha \cdot \left(\sigma_x - \sigma_y\right) \qquad (4.6)$$

Where:

τ_{xy}	is the shear stress at one point (Fig. 4.63.b)
σ_x	is the normal stress (compression) in horizontal direction at one point (Fig. 4.63.b)
σ_y	is the normal stress (tension) in vertical direction at one point (Fig. 4.63.b)
α	is the inclined angle of principal compressive stress to horizontal direction (Fig. 4.63.b)

From the above equation, the value of shear stress at some main points in the beams, for example A1, B1 on the top fibre of the beam; A2, B2 at the middle of the compression zone; A3, B3 at the middle of the uncracked concrete parts in the tension zone and A4, B4 in the vicinity of the support, can be estimated as in the figure 4.63.

a) Compressive stress fields in straight depth beam and haunched beam at critical state

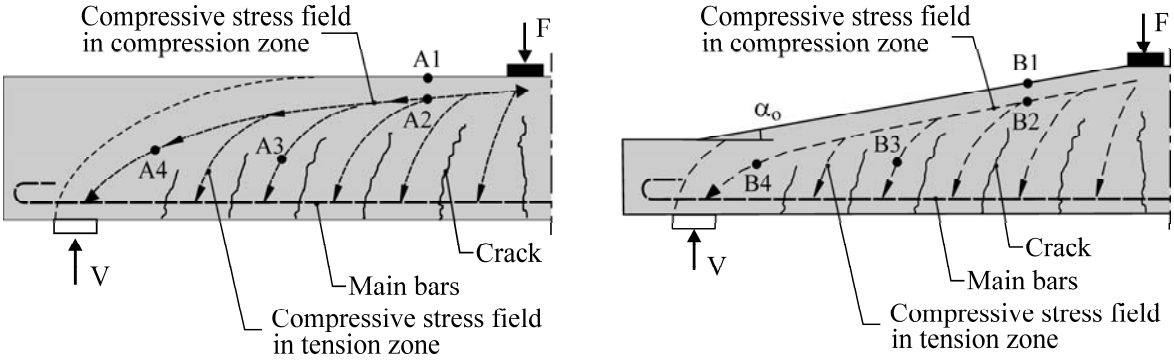

b) Value of shear stress at some main points in straight depth beam and haunched beam

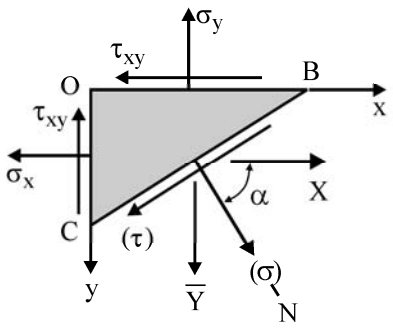

A1	A2	A3	A4
$\sigma_x = max$	$\sigma_x \neq 0$	$\sigma_x \neq 0$	$\sigma_x \neq 0$
$\alpha = 0$	$\alpha \neq 0$	$\alpha \neq 0$	$\alpha \neq 0$
$\tau_{xy} = 0$	$\tau_{xy} = max$	$\tau_{xy} \neq 0$	$\tau_{xy} \neq 0$
B1	**B2**	**B3**	**B4**
$\sigma_x = max$	$\sigma_x \neq 0$	$\sigma_x \neq 0$	$\sigma_x \neq 0$
$\alpha = \alpha_o$	$\alpha \neq 0$	$\alpha \neq 0$	$\alpha \neq 0$
$\tau_{xy} = max$	$\tau_{xy} \neq 0$	$\tau_{xy} \neq 0$	$\tau_{xy} \neq 0$

Figure 4.63– Compressive stress fields and value of shear stress in straight depth beams and haunched beams

The above results obviously showed that large values of shear stress in straight depth beam exist at the middle of the compression zone (point A2), middle of the uncracked concrete parts in the tension zone (Point A3) and on an inclined curve near the support (A4) while those of haunched beams locate at the top of the compression zone (point B1), the middle of the compression zone (point B2), the middle of the uncracked concrete parts in the tension zone (Point B3) and on an inclined curve near the support (B4). These findings are completely suitable with results from Non-FEM analysis as presented in the figures 4.51, 4.52 and 4.62.

If we assume that shear failure would go through regions or points where values of shear stress are large, two types of critical shear crack can be predicted to arise at ultimate loading state. The first type of critical shear crack goes through the concrete compression zone (point A2 or B2) and tends to the support (point A4 or B4) while the second type passes through the concrete compression zone (point A2 or B2), uncracked concrete parts in tension zone (point A3 or B3) and tends to the position of the longitudinal reinforcements as in the figure 4.64. The experimental program showed that straight depth concrete beams were mostly failed by the second critical shear crack while haunched concrete beams were likely damaged by the first critical shear crack. The gradual failure mechanisms of both types of beams were presented in the Chapter 3 (Experimental Program).

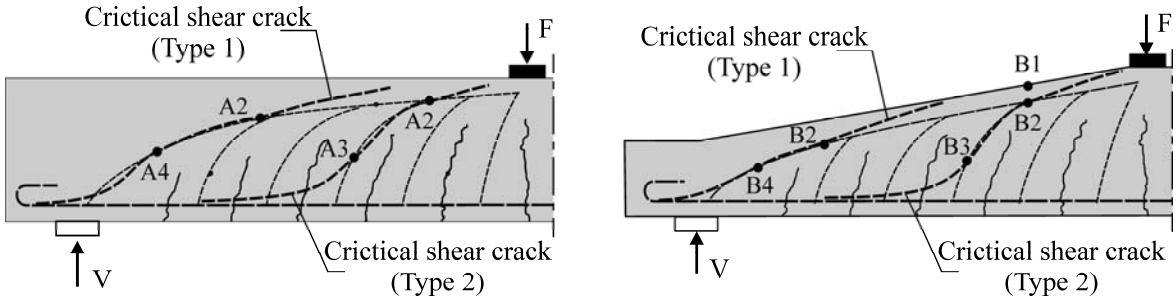

Figure 4.64– Two types of critical shear cracks in straight depth beams and haunched concrete beams.

In summary, some main findings of this chapter can be shortly summarized as follows:

Non-FEM analysis can be used not only to find out failure behaviours of concrete members without stirrups such as shear ultimate strength, load and displacement curve or crack propagation…but also to give rational explanations for shear failure mechanisms by means of stress redistribution and crack propagation.

It is verified that there are many differences in loading behaviours between haunched beams and straight depth beams which can summarized as follows:

(1) Stiffness: System stiffness of haunched beams is smaller than that of straight depth beams. As a result, its displacement is larger than that of straight depth beams. This conclusion totally complies with test results as presented in the figure 3.13 of Chapter 3.

(2) Shear stress distribution: the shear stress distribution of haunched beams is totally different from that of straight beam as presented above. Shear stress in haunched beams concentrates mainly in the compression zone with largest value on top of section while that of straight depth beam has maximum value at the middle of the compression zone.

(3) Failure zone: haunched beams tend to fail at region close to support (min d) by the first type of critical shear crack while straight depth beams fail at region in the mid-span close to position of load application (max M) by the second type of critical shear crack. Therefore, the shear strength of haunched beams should be checked in the region next to support (min d) while that of straight depth beams should be calculated in the vicinity close to mid-span.

It is the uncracked concrete parts in the tension zone accompanied with compression zone which carry most of shear forces in concrete beam without stirrups (at least 90% of total shear force). It is noted that there has never had any statement about the role of uncracked concrete parts in tension zone in carrying shear so far. The other shear resistance mechanisms such as dowel action, aggregate interlock…are not important and can be ignored.

It is possible to find out rational shear strength models of concrete beams without stirrups based on the initiation and propagation of cracks and the redistribution of stress fields in uncracked concrete parts of tension and compression zone at critical state. These proposals will be presented in details in the next Chapter.

5 New Model Proposals

5.1 Introduction

This chapter aims to provide new shear strength models proposed by the author for both straight depth concrete beams and haunched concrete beams without stirrups. The theoretical background of these models is based on the results from the experimental program and the Non-FEM analysis of 18 test beams. The outcomes from the two above mentioned investigations showed that the uncracked concrete parts in the compression zone and in the tension zone carry almost all of the shear force on any vertical cross-section of a concrete beam. In addition, it is also verified that the critical shear crack tends to occur only at a certain region in concrete beams. Therefore, shear resistance mechanisms on the uncracked concrete parts at critical section will be investigated to develop suitable shear strength models for both straight depth and haunched concrete beams without stirrups. Beside the shear behavior mechanisms, the proposed models are also intended to consider some significant factors which control shear strength as formerly presented in the Chapter 2 (State of the Art).

Shear resistance mechanisms on any cross section will be dealt with in the next section in order to provide a general shear resistance formula for concrete beams. The two failure types of straight depth beams and haunched beams will be studied further to find out appropriate shear strength equations for each case. In this research, the term “allowable shear stress” is suggested to use as a characteristic value of shear resistance strength of concrete which will be calibrated from the shear database. This shear database includes almost all of shear test results in the past 60 years and 18 tests in the Chapter 3 (Experimental Program).

The new proposed shear strength formulae will be compared with other typical shear strength models in the Chapter 2 (State of the Art). The design form of the new models will also be suggested and compared with the shear design equations in some practical codes including DIN 1045-01, Swiss code SN 262, ACI 318-05 and Canadian Standard CSA.

5.2 Model Proposals

5.2.1 Shear Resistance Mechanisms Based on Stress Distribution at Critical Sections

The Chapter 4 (Non-FEM Analysis) showed that most of the shear force (minimum of 90%) is carried by concrete part at any cross-section of concrete beam. Therefore, the total shear

force can be calculated approximately by integration of all of shear stresses on the concrete part as the Equation (5.1).

$$V_{Rm} \approx b \cdot \int_0^h \tau_{xy} \cdot dy \qquad (5.1)$$

Where: τ_{xy} is shear stress on concrete part of beam.

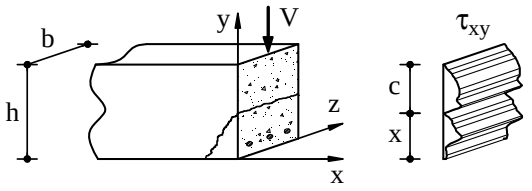

Figure 5.1– Shear stress block on concrete part

As also presented in the Chapter 4 (Non-FEM Analysis), the distribution of shear stress in concrete will change in figure and become very complicated when cracks initiate and propagate. These cracks separate concrete into two parts including an uncracked concrete region above tips of cracks and the other part below tips of cracks which is simply named cracked concrete zone (Fig. 5.2).

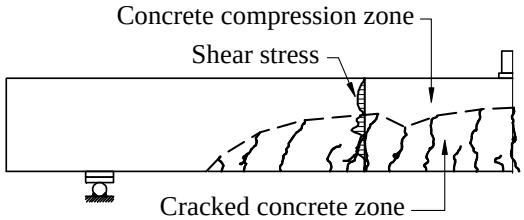

Figure 5.2– Concrete compression region and cracked concrete zone in a beam

Therefore, the equation of shear force can also be a summation of shear resistance components in these two zones as the following form:

$$V_{Rm} \approx b \cdot \int_0^h \tau_{xy} \cdot dy \; = V_t + V_c \; = b \cdot \int_0^x \tau_{xy1} \cdot dy \; + b \cdot \int_x^h \tau_{xy2} \cdot dy \qquad (5.2)$$

Where:

$V_t = b \cdot \int_0^x \tau_{xy1} \cdot dy$ is shear resistance component in cracked concrete zone.

$V_c = b \cdot \int_x^h \tau_{xy2} \cdot dy$ is shear resistance component in concrete compression zone

τ_{xy1}, τ_{xy2} are shear stresses in cracked concrete zone and in concrete compression zone.

From the above Eq. (5.2), we can also find out the shear bearing capacity of a concrete beam if we determine exactly the contributing percentage of shear resistance either in the concrete compression zone or in the cracked concrete zone. As presented in the figure 4.51 and 4.62, the distribution of shear stress in the cracked concrete zone is quite complex while that in the

concrete compression zone is relatively simple. For that reason, it is proposed to find out indirectly the shear bearing capacity of a concrete beam without stirrups by means of the shear capacity of the concrete compression zone.

The experimental program and the Non-FEM analysis also found the rules of failure region and type of critical shear crack for both straight depth beams and haunched beams. Hence, the values of shear stress components in the Eq. (5.2) must be obtained at the most critical section in these failure regions. However, it seems impossible to determine exactly this critical section since the shear failure usually occurs very abruptly and unpredictably. For that reason, the relevant section will be selected in the failure region which satisfies the two following conditions: (1) the shear stress distribution at this section should be simple for calculation and (2) the position of this section should be easy to determine. Because the stress distribution, failure region and the type of the critical shear crack of straight depth beam are different from those of haunched beam, shear design models for these beams are also different and will be separately considered in the next sections.

5.2.2 Shear Strength Model for Straight Depth Concrete Beams

The experimental program and Non-FEM analysis proved that the failure region of straight depth beams is close to position of load application (max *M, d*) (Fig. 5.3). At failure, the lower end of the critical shear crack goes through the uncracked concrete parts in the tension zone downward to the position of the longitudinal reinforcements while the other end passes through the concrete compression zone upward to the position of load application.

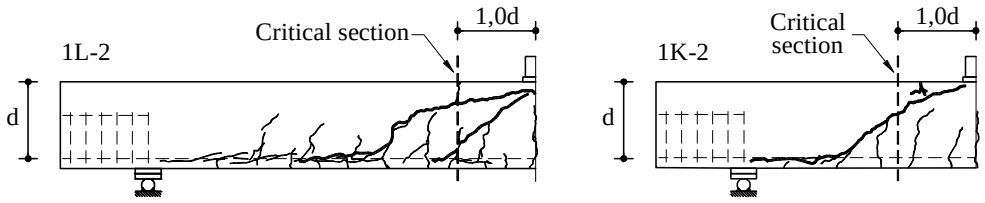

Figure 5.3– Assumed critical section and cracks of straight test beams

It is also noted that the collapse of a beam occurs right after the critical shear crack penetrates the concrete compression zone near loading position and the compression zone fails. Therefore, it is reasonable to assume a critical state at which the critical shear crack has already initiated but it does not break through the compression zone yet. The critical section at distance of *1,0d* apart from loading position will be selected to be the relevant design section. As can be seen from the figure 5.3, this critical section is relatively suitable to represent both failure regions and the critical shear crack for 4 straight test beams in the experimental program. In addition, this selection avoids the disturbed stress region caused by the spread-

ing of the single force. The depth of the compression zone can be approximately determined to be equal to the value at mid-span for a single span under centric point loading.

The FEM analysis showed that the distribution of shear stress in the compression zone at this section has a nearly unchanged parabolic shape after load steps until failure as shown in figure 4.51 for test beam 1L2. The shear stress distribution in the compression zone at failure load for all straight depth beams in the experimental program is presented in the figure 5.4.

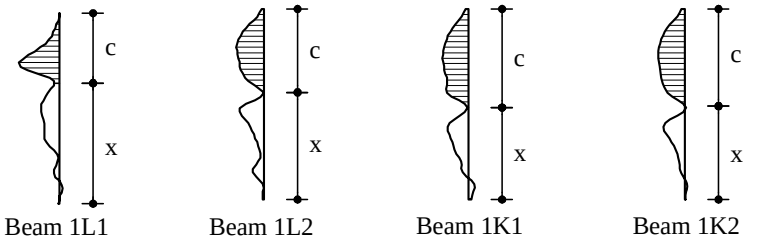

Figure 5.4– Shear stress distribution in the compression zone *x* on relevant section at failure load of test beams from FEM analysis

The shear resistance percentage of the compression zone at the relevant section of all straight test beams after each load step is shown in the figures 5.5 and 5.6. The results revealed that at failure stage the shear resistance component of the concrete compression zone is about 55 % ÷ 70 % of the total shear force at the relevant section (or the shear force V is about 1,8 ÷ 1,4 times V_c in other words as in the figures 5.5 and 5.6).

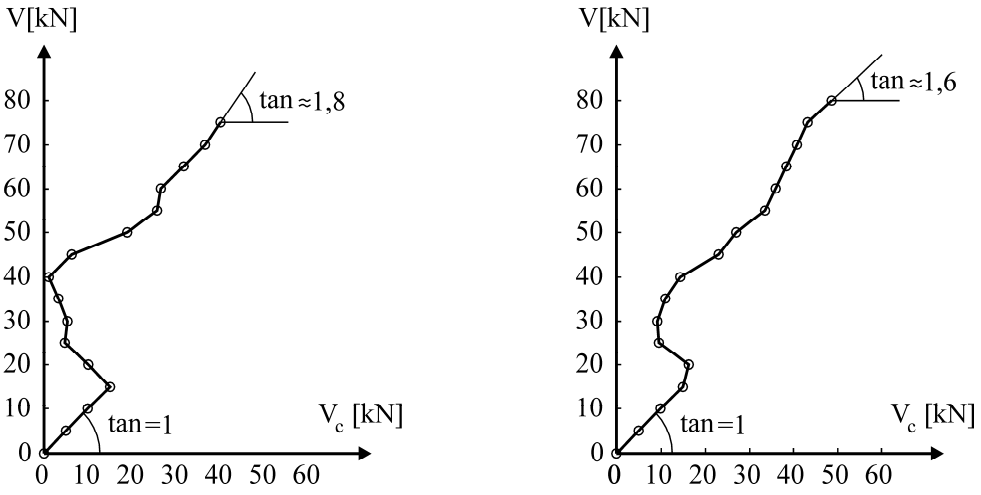

Figure 5.5– Shear resistance component in the concrete compression zone V_c and shear force V from FEM analysis for test beam 1L1 and 1L2

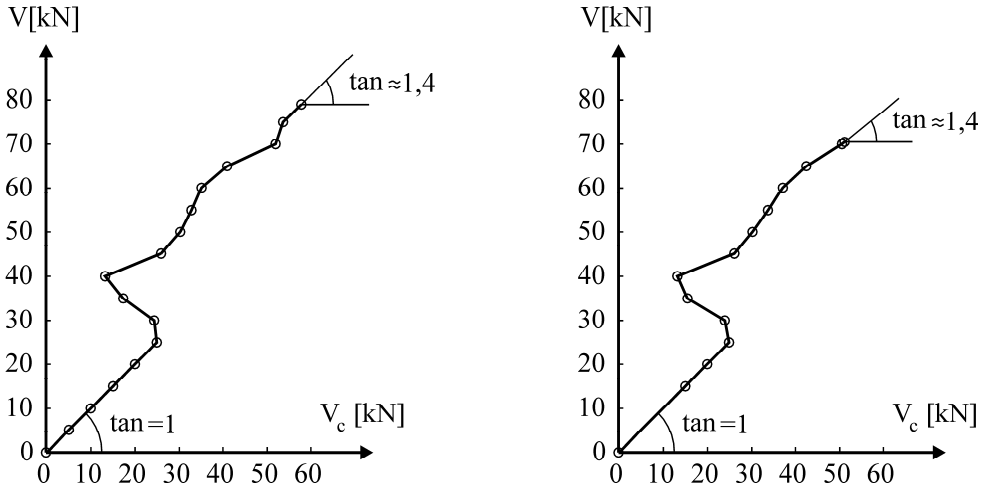

Figure 5.6– Shear resistance component in the concrete compression zone V_c and shear force V from FEM analysis for test beam 1K1 and 1K2

For simplicity, it is assumed that the compression zone in the critical state can carry in average about 60 % the total shear force (or shear force V is about 1,6 times V_c). The remaining 40 % of shear force will be carried by the cracked concrete zone. Therefore, the equation of shear force (5.2) can be written in other form:

$$V_{Rm} \approx V_c + V_t = 0,6V_{Rm} + 0,4V_{Rm} = 1,6V_c \qquad (5.3)$$

The shear stress block in the compression zone has a parabolic shape (Fig. 5.7) and the shear resistance component V_c can be calculated approximately as follows:

$$V_c = b \cdot \int_x^h \tau_{xy2} \cdot dy \approx k_1 \cdot k_2 \cdot \frac{2}{3} \tau_{\max} \cdot c \cdot b \qquad (5.4)$$

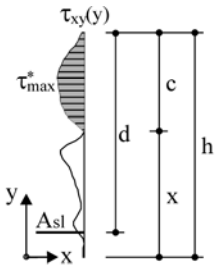

Figure 5.7- Shear stress block at relevant section

where:

τ_{max} is the maximum value of shear stress in the compression zone. As presented in Chapter 4 (Non-FEM Analysis), the shear stress is a function of the normal stresses and the inclined angle α of the principal normal stress. However, at critical state, there exists mainly compressive normal stress and the inclined angle α of the normal principal compressive stress is nearly unchanged at the relevant section (1,0d). Hence, the maximum shear stress in the compression zone can be determined as follows:

$$\tau_{\max} = f(\sigma_x, \alpha) \approx f(f_{ck}) \qquad \text{with } \alpha \approx \text{constant}, \ \sigma_y \approx 0$$

c is the depth of the compression zone which can be determined as follows:

$$c = \left[\sqrt{\left(\rho_l \cdot \frac{E_s}{E_c} \right)^2 + 2\rho_l \cdot \frac{E_s}{E_c}} - \rho_l \cdot \frac{E_s}{E_c} \right] \cdot d \qquad (5.5.a)$$

or another approximation:

$$c = 0,78\left(\rho_l \cdot \frac{E_s}{E_c}\right)^{1/3} \cdot d \qquad \text{(Zink 2000)} \qquad (5.5.b)$$

$\rho_l = \frac{A_{sl}}{b \cdot d}$ is the ratio of longitudinal reinforcements in tension zone to area of cross section.

$E_s \approx 200.000\ MPa$ is the modulus of elasticity of steel

$E_c \approx 9500\ (f_{ck} + 4)^{1/3}$ is the modulus of elasticity of concrete (E_c, f_{ck} in MPa)

The parameter k_1 is used to consider the influence of a/d ratio on the shear strength of a concrete member. The simple form of this factor suggested by Zink (2000) as in the Eq. (5.6) will be used:

$$k_1 = \left(\frac{4d}{a}\right)^{1/4} \qquad (5.6)$$

The factor k_2 is used to consider the size effect on shear strength of concrete structures. The size effect law is proposed to have a similar form of $d^{-1/4}$ as suggested by Kani (1967), Okamura et al. (1980) and Niwa et al. (1986, 1988). In addition, it is believed that the size effect will become irrelevant at a certain depth of beam. Therefore, the simple size effect approach as the Eq. (5.7) is suggested to use in which k_2 = 1,0 with an effective depth of d = 250 mm.

$$k_2 = \left(\frac{250}{d}\right)^{1/4} \qquad (d \text{ in mm}) \qquad (5.7)$$

The final shear strength equation of straight beams without stirrups becomes:

$$V_{Rm} = 1,6\left(\frac{4d}{a}\right)^{1/4} \cdot \left(\frac{250}{d}\right)^{1/4} \cdot \frac{2}{3} \cdot \tau_{\max} \cdot \left[0,78 \cdot \left(\rho_l \cdot \frac{E_s}{E_c}\right)^{1/3} \cdot d\right] \cdot b \qquad (5.8)$$

or in simpler form:

$$V_{Rm} = \frac{2,5}{3} \cdot \left(\frac{4d}{a}\right)^{1/4} \cdot \left(\frac{250}{d}\right)^{1/4} \cdot \tau_{\max} \cdot \left[\left(\rho_l \cdot \frac{E_s}{E_c}\right)^{1/3} \cdot d\right] \cdot b \qquad (5.9)$$

In order to find out the shear capacity of a structure, the maximum value of the shear stress in the compression zone $\tau_{\max}$ is assumed to be equal to the allowable shear stress of concrete used in that structure. However, different from allowable tensile stress and compressive stress, allowable shear stress of concrete is an unknown value. In this research, it is empirically proposed to acquire the allowable shear stress of concrete from the shear database which will be presented in the section 5.2.4 (Shear Database).

5.2.3 Shear Strength Model for Haunched Concrete Beams

The experimental program and the Non-FEM analysis showed that the failure region of haunched beams is close to the support (min *d*). At failure state, the critical shear crack seems to be a further development of a formerly pure shear crack in the disturbed stress region near the support. The lower end of this crack tends downward to the position of the longitudinal reinforcements while the other end passes through the concrete compression zone. The collapse of a beam occurs right after the critical crack penetrates the concrete compression zone. Therefore, a critical state is assumed at which the critical shear crack has already occurred but it does not break through the compression zone yet.

It is noted from the FEM analysis of 10 haunched test beams that there is a region apart about *1,3d* from support at which the shear stress distribution has a very similar shape to that of the relevant section of the straight depth beam as showed in the figure 5.8 for test beam 4K1. This is because the compressive stress field in the compression zone starts to change its direction to concentrate on the support.

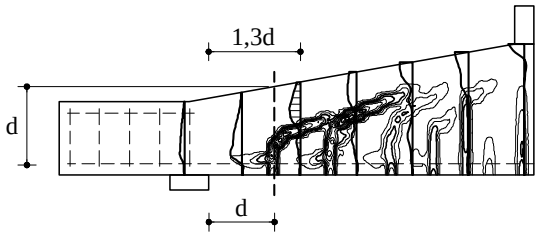

Figure 5.8– Shear stress distribution at some sections along beam length of test beam 4K1 from FEM analysis

Therefore, the section at a distance of *1,3d* apart from support will be selected as relevant section for haunched concrete beams without stirrups. Figures 5.9 to 5.13 show the assumed critical section and cracks at failure state of couple of test beam 2L, 3L, 2K, 3K and 4K.

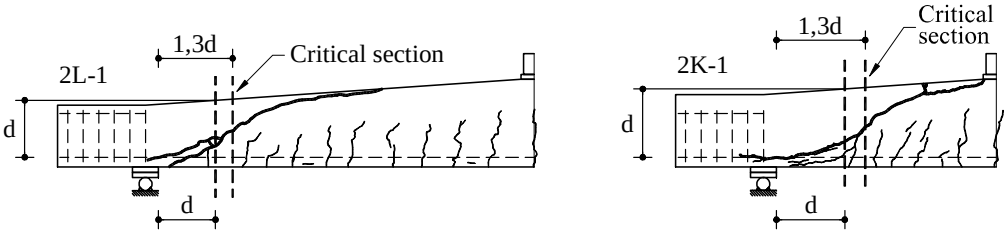

Figure 5.9– Assumed critical section and cracks of test beams 2L-1 and 2K-1

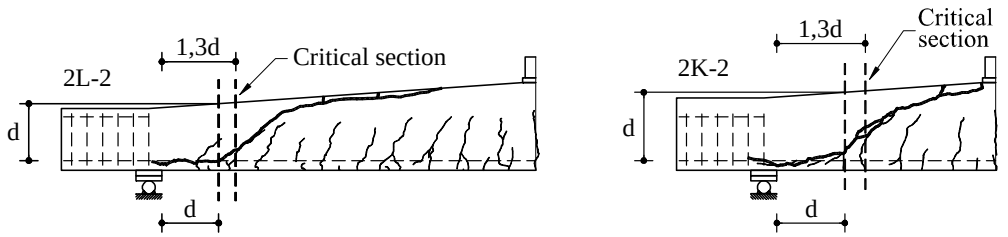

Figure 5.10– Assumed critical section and cracks of test beams 2L-2 and 2K-2

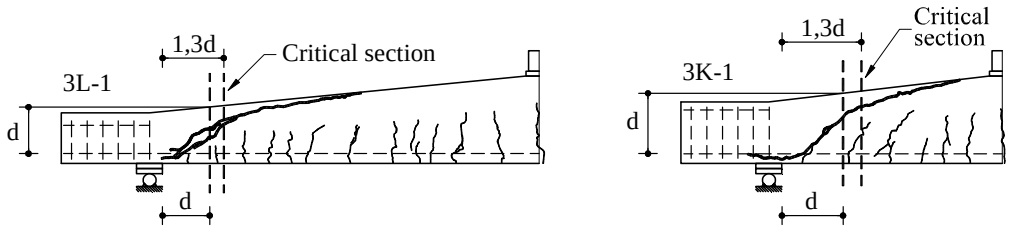

Figure 5.11– Assumed critical section and cracks of test beams 3L-1 and 3K-1

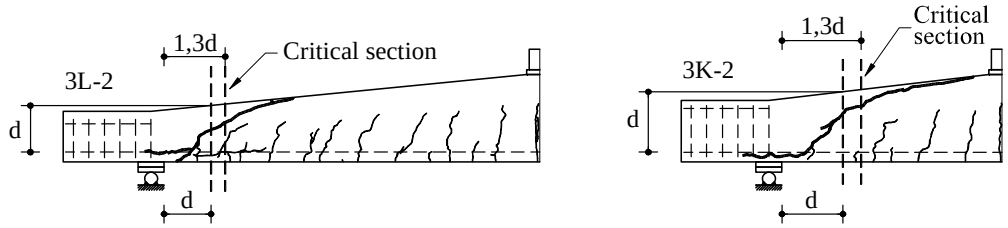

Figure 5.12– Assumed critical section and cracks of test beams 3L-2 and 3K-2

Figure 5.13– Assumed critical section and cracks of test beams 4K-1 and 4K-2

It can be seen from these above figures that the assumed relevant section is relatively suitable to represent both failure region and critical shear crack for haunched test beams in the experimental program. The results also showed that at failure stage the shear resistance component of concrete compression zone V_c has a value of about of 80% the total shear force V at the calculating section (or shear force V is about 1,25 times V_c in other words as in the figures 5.14 to 5.16).

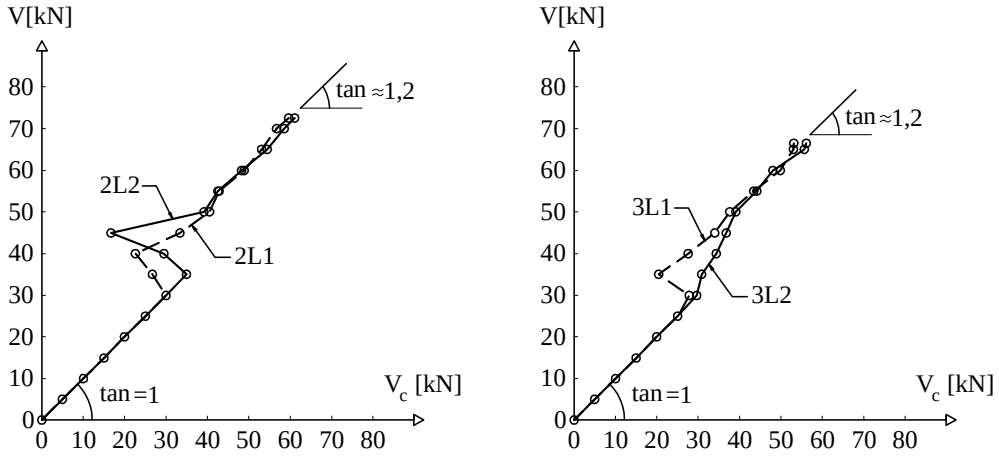

Figure 5.14– Shear resistance component in the concrete compression zone V_c and shear force V from FEM analysis for straight test beams 2L and 3L

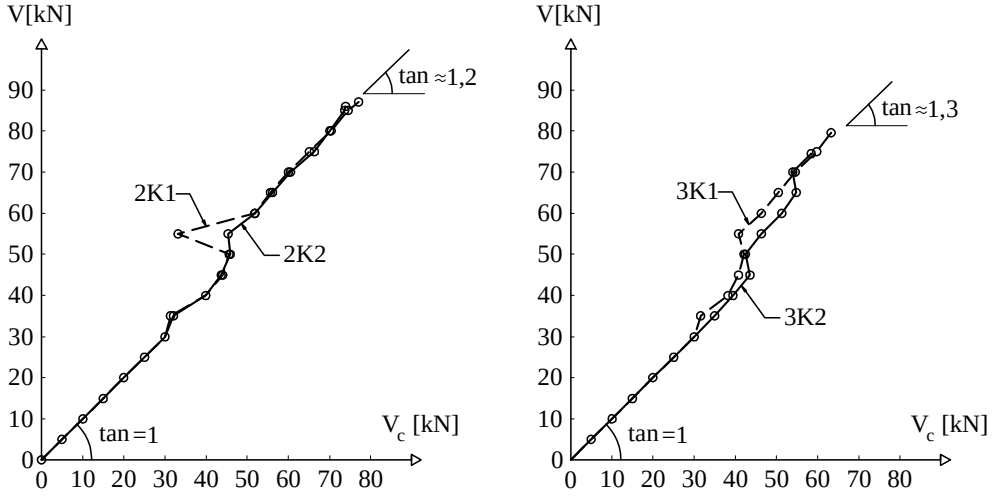

Figure 5.15– Shear resistance component in the concrete compression zone V_c and shear force V from FEM analysis for straight test beams 2K and 3K

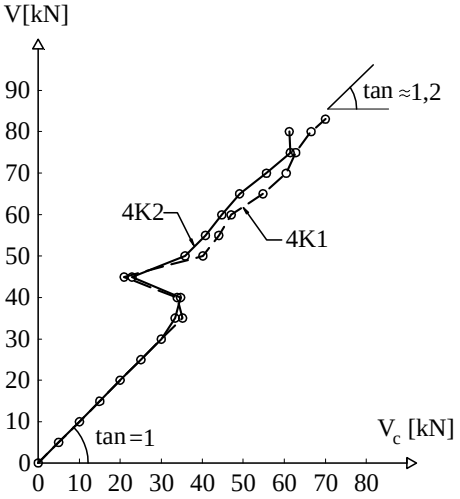

Figure 5.16– Shear resistance component in the concrete compression zone V_c and shear force V from FEM analysis for straight test beams 4K

Therefore, the equation of shear force (5.2) can be written in other form:

$$V_{Rm}^{\alpha} \approx V_c + V_t \approx 0,8V_{Rm}^{\alpha} + 0,2V_{Rm}^{\alpha} = 1,25V_c \tag{5.10}$$

The shear stress block in the compression zone has a parabolic shape (Fig. 5.17) and the shear resistance component V_c can be calculated approximately similar to Eq. (5.4) as follows:

$$V_c = b \cdot \int_C^h \tau_{xy} \cdot dy \approx k_1 \cdot k_2 \cdot \frac{2}{3} \tau_{\max}^* \cdot c^* \cdot b \tag{5.11}$$

Where: $\tau_{\max}^*$ is the maximum shear stress in the compression zone at the relevant section of haunched beams,

c^* is the depth of the compression zone at the relevant section.

As presented in the Chapter 4 Non-FEM analysis, because the principal compressive stress field in the haunched beam tends to be inclined to an angle α of the compression zone, the maximum shear stress in the compression zone of haunched beams should be a function of the normal compressive stress and the inclined angle α_0 as in the following equation:

$$\tau^*_{\max} = f(\sigma_x, \alpha) \approx f(f_{ck}, \alpha) \quad \text{with } \sigma_z \approx 0$$

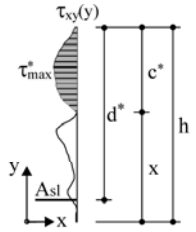

Figure 5.17- Shear stress block at relevant section

It is assumed that the depth of the compression zone at the section of 1,3*d* will be approximately 30 % larger than that of straight beam with the same height *d* at mid-span.

$$c^* = 1,3 \cdot 0,78 \left(\rho_l \cdot \frac{E_s}{E_c} \right)^{1/3} \cdot d^* \tag{5.12}$$

It is noted that the height of beam *d** at the section 1,3*d* is nearly the same as the height *d* at the section 1,0*d* apart from the support. For the sake of simplicity, the effective height of beam *d* at section 1,0*d* apart from support is used for calculation. Other parameters have the same meaning as in the formula for straight depth beams.

The Eq. (5.10) becomes:

$$V^{\alpha}_{Rm} = 1,25 \left(\frac{4d}{a} \right)^{1/4} \cdot \left(\frac{250}{d} \right)^{1/4} \cdot \frac{2}{3} \left[\tau^*_{\max} \cdot 1,3 \cdot 0,78 \left(\frac{\rho_l}{100} \cdot \frac{E_s}{E_c} \right)^{1/3} \right] \cdot b \cdot d \tag{5.13}$$

or in simpler form:

$$V^{\alpha}_{Rm} = \frac{2,5}{3} \left(\frac{4d}{a} \right)^{1/4} \cdot \left(\frac{250}{d} \right)^{1/4} \cdot \left(\rho_l \cdot \frac{E_s}{E_c} \right)^{1/3} \cdot \tau^*_{\max} \cdot b \cdot d \tag{5.14}$$

The shear strength of haunched beams from the Eq. (5.14) has a similar form to that of straight depth beams as presented in the Eq. (5.9). However, it is noted that there are two differences in principle of formulating these equations as follows:

(1) The relevant section for haunched beams is 1,3*d* apart from the support (min *d*) while that of straight depth beams is 1,0*d* apart from the position of the load application (max *M*, *d*) (*d* is the effective depth at the relevant section).

(2) The maximum shear stress of haunched beams is larger than that of straight depth beams because of the influence of haunched side on inclined angle of principal compressive stress to horizontal direction.

The maximum value of shear stress in the compression zone τ_{max}, τ^*_{max} is assumed to be equal to allowable shear stress of concrete used in that member. The value of allowable shear stress of concrete will be studied and calibrated from the shear database in the next section.

5.2.4 Shear Database

Reineck et al. (2003) introduced a shear databank collection including 1007 test results of concrete structures without stirrups. All beams in this database have a rectangular cross section and were subjected to point loads. Collins et al. (2008) provided a more adequate file of 1849 shear tests which consists of the database of Reineck et al. (2003) and others as well. This new shear database includes concrete structures with rectangular or T beam sections, no axial load or no prestressing, no stirrups or no fibers, no limits on concrete strength, no geometrical limits on member size… This shear database includes most of the shear tests from the past 60 years. So, this shear database, accompanied with tests in the experimental program, will be used to find out the allowable shear stress and shear strength models of concrete members without stirrups.

It is noted that the test results of the database are from variety of different researches, institutes or universities…which have, of course, different testing conditions. Therefore, it is quiet normal if test results of specimens owing nearly the same parameters are different from different authors. However, test results of specimens owing nearly the same parameters performed by the same author(s) are too diverse (tolerance about more than 15%) will be considered to be suspect and will be eliminated from the shear database. For that reason, tests performed by 12 authors in the table 5.1 are not considered in the next analysis.

The left database will be filtered to meet these following requirements:

a) Tests beams must have failed in shear.
b) Test type: Point loads P as in the figure 5.18
c) $f_{ck} \geq 10$ MPa
d) $a/d \geq 2{,}35$

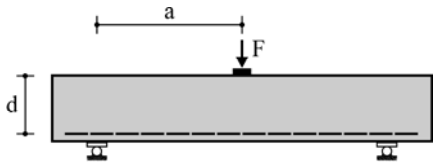

Figure 5.18– Shear test type P

Finally, 878 test results including 874 figures from shear database of Collins et al. (2008) and 4 test results of beams 1L1, 1L2, 4K1 and 4K2 in the experimental program carried out by Rombach & Vu (2009) will be a new shear database for concrete straight depth beam without stirrups.

For haunched beams, the shear database includes 10 tests of couple of beams 2L, 3L, 2K, 3K, 4K in the experimental program carried out by Rombach & Vu (2009) and 4 tests performed by MacLeod et al. (1994). The test results by Rombach & Vu (2009) in the format of

the shear database for straight depth beam and for haunched beams are presented in the Appendix F.

No.	Authors	Year	Beam Name	Amounts
1	Laupa & Siess	1953	T-3 average	1
2	Moody, Viest, Elstner, Hognestad	1954	B-B4	1
3	Bower & Viest	1960	IA-2b, IA-4b, IA-5a, IA-8a	4
4	De Cossio	1962	D29,4-9,8B	1
5	Mphonde & Frantz	1984	AO-15-2a, AO-15-2b	2
6	Ahmad & Lue	1987	A9, B3, B4, B9	4
7	Thorenfeldt & Drangshold	1990	B11-B15, B21-B25, B43-B45, B51-B55, B64	19
8	Hallgren	1994	B90SB13-2-8, B90SB21-2-8	2
9	Matsui, Y. et. al	1995	A1, A2, F1, F2, L1, L2, S1, S2	8
10	Ghannoum	1998	All tests	25
11	Angelakos, Bentz, Collins	2001	DB165, DB180	2
12	Rahal & Al-Shaleh, N	2004	A65-NTR, B65-NTR	2

Table 5.1. Suspect test results in the shear database of Collins et al. (2008)

In the shear database of 878 test results for straight depth beams, it is recognized from many test sets owning the same characteristics except concrete compressive strengths, for example tests conducted by Moody et al. (1954), Chang et al. (1958), Bower et al. (1960), Chana (1981), Mphonde et al. (1984), Muruyama et al. (1986), Walraven et al. (1994), Hallgren (1994), Matsui et al. (1995), Mendis (2000) and Sherwood et al. (2007), that the effect of concrete compressive strength on shear bearing capacity is quite controversy. There are many tests provide almost the same shear capacity even though their concrete strength are visibly different. For that reason, it is believed that the influence of concrete strength on shear bearing capacity of concrete beams without stirrups is not more significant than other main factors such as ratio of longitudinal reinforcement, *a/d* ratio or size effect *d*.

In many literatures, concrete strength exists in shear strength formulae as a form of f_{ck} (or f'_c) to the power of 1, 2/3, 1/2 or 1/3. In this research, the characteristic concrete strength f_{ck} to the power of 1/4 as suggested by Park et al. (2006) will be used to take into account effects of this factor. The maximum value of shear stress or allowable shear stress τ_{max} in the compression zone is subsequently calibrated from the 878 test results as in the following equation:

$$\tau_{\max} \approx 1,3\left(f_{ck}\right)^{1/4} \qquad (5.15)$$

Hence, shear strength model of straight depth beams from Eq. (5.9) is calculated as follows:

$$V_{Rm} = \frac{3,25}{3}\left(\frac{4d}{a}\right)^{1/4} \cdot \left(\frac{250}{d}\right)^{1/4} \cdot \left(f_{ck}\right)^{1/4} \cdot \left[\left(\rho_l \cdot \frac{E_s}{E_c}\right)^{1/3} \cdot d\right] \cdot b \qquad (5.16)$$

For the sake of simplicity, $(E_s/E_c)^{1/3}$ = 1,85 (for E_s = 200.000 MPa and f_{ck} = 33 MPa) can be used as a mean value for other cases. The Eq. (5.16) becomes:

$$V_{Rm} = 2\left(\frac{4d}{a}\right)^{1/4} \cdot \left(\frac{250}{d}\right)^{1/4} \cdot \left(f_{ck}\right)^{1/4} \cdot \rho_l^{1/3} \cdot b \cdot d \qquad \text{(N, MPa, mm)} \qquad (5.17a)$$

or in simpler form:

$$\boxed{V_{Rm} = 11,25\left(\frac{f_{ck}}{a}\right)^{1/4} \cdot \rho_l^{1/3} \cdot b \cdot d} \qquad (5.17b)$$

For haunched beams, the maximum value of shear stress or allowable shear stress $\tau_{\max}^{*}$ in the compression zone has the same form as for straight depth beams but it takes into account the influences of inclined angle α of haunched side as in the following equation:

$$\tau_{\max}^{*} \approx 1,3\left(f_{ck}\right)^{1/4}\left(1+\tan\alpha\right) \qquad (5.18)$$

Thus, shear strength model of haunched beams from Eq. (5.14) is calculated as follows:

$$V_{Rm}^{\alpha} = \frac{3,25}{3}\left(\frac{4d}{a}\right)^{1/4} \cdot \left(\frac{250}{d}\right)^{1/4} \cdot \left(f_{ck}\right)^{1/4} \cdot \left[\left(\rho_l \cdot \frac{E_s}{E_c}\right)^{1/3} \cdot d\right] \cdot \left(1+\tan\alpha\right) \cdot b \qquad (5.19)$$

For the sake of simplicity, $(E_s/E_c)^{1/3}$ = 1,85 (for E_s = 200.000 MPa and f_{ck} = 33 MPa) can be used as a mean value for other cases. The Eq. (5.19) becomes:

$$V_{Rm}^{\alpha} = 2\left(\frac{4d}{a}\right)^{1/4} \cdot \left(\frac{250}{d}\right)^{1/4} \cdot \left(f_{ck}\right)^{1/4} \cdot \rho_l^{1/3} \cdot \left(1+\tan\alpha\right) \cdot b \cdot d \qquad (5.20a)$$

or in simpler form:

$$\boxed{V_{Rm}^{\alpha} = 11,25\left(\frac{f_{ck}}{a}\right)^{1/4} \cdot \rho_l^{1/3} \cdot \left(1+\tan\alpha\right) \cdot b \cdot d} \qquad (5.20b)$$

In summary, shear strength models are determined for concrete straight depth beams as in the Eq. (5.17) and for haunched concrete beams as in the Eq. (5.20). It is noted that *d* in the Eq. (5.17) is the effective height of beam apart 1,0*d* from the position of load location (max

M, *d*) while that in the Eq. (5.20) is the effective height of beam apart 1,3*d* from the support (accuracy) or apart 1,0*d* from the support (min *M*, *d*)(for simplicity). The verification of the two models will be presented in the next section.

5.3 Verification

In order to evaluate the accuracy and safety level of the above proposed shear strength models, a safety factor of the measured ultimate shear capacities and calculated values is defined as follows:

$$X = V_{Test} / V_{cal} \tag{5.21}$$

For the safety evaluation, any test which has $X > 1$ will belong to the safe side while any test which has $X < 1$ will be in unsafe. For the evaluation of accuracy, any test which has $X = 1$ verifies that the proposed shear strength models predict exactly the real shear capacity of the test. Since the shear database exhibits a certain scatter, the following statistical quantities will be used for assessment:

(1) Mean value of safety factor: $$\bar{X} = \frac{1}{n} \cdot \sum_{i=1}^{n} X_i \tag{5.22}$$

(2) Standard deviation: $$s = \left(\frac{1}{n} \cdot \sum_{i=1}^{n} \left(X_i - \bar{X} \right)^2 \right)^{1/2} \tag{5.23}$$

(3) Coefficient of variation: $$c_v = s / \bar{X} \tag{5.24}$$

(4) 5% fractile of safety factor: $\bar{X}_{5\%} \approx \bar{X} - 1,645s$ (Gaussian distribution) (5.25)

(5) 95% fractile of safety factor $\bar{X}_{95\%} \approx \bar{X} + 1,645s$ (Gaussian distribution) (5.26)

Figure 5.19 shows the graph of V_{Test} and V_{cal} of the shear database of straight depth beams including of 878 test results. It can be seen from this figure that the measured shear strength of 878 tests V_{Test} varies in range of 1,9 kN up to 1.295 kN and tends to converge well to the 45^{o} axis ($V_{\text{Test}} = V_{\text{cal}}$). The mean value $\bar{X} = 1,0086$ and standard deviation $s = 0,1379$ show a good agreement between the predicted values of the proposed shear strength model (Eqs. 5.17.a or 5.17.b) and the test results. The distribution of safety factor X is plotted in Fig. 5.20. It follows quite well with the Gaussian distribution function. The relatively high value of 5% fractile $\bar{X}_{5\%} = 0,8103$ and the small value of 95 % fractile of safety factor $\bar{X}_{95\%} = 1,2603$ show a small deviation between calculated values and test results.

It is noted from the shear database of 878 tests that it comprises a diversity of test beams with longitudinal reinforcement ratio ρ_l in range of $0,14\,\% \div 6,64\,\%$; effective depth of beam *d* from 41 mm to 2.000 mm; *a*/*d* ratio of 2,35 to 8,52; and characteristic compressive

strength f_{ck} from 10,6 MPa to 122,9 MPa (see figures 5.21 to 5.24). Therefore, it can be concluded that the shear strength model proposed in Eq. 5.17 predicts very well the shear strength of a broad variety of concrete members without stirrups. The model will be compared with other shear strength models with a variety of shear database in the next sections.

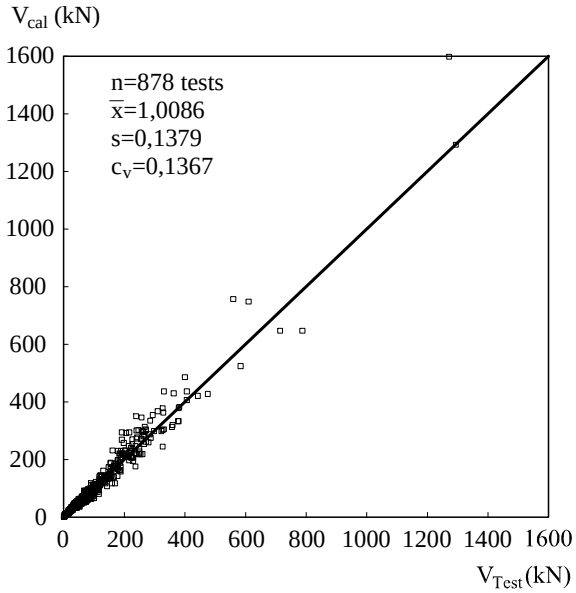

Figure 5.19– Graph of V_{Test} and V_{cal}

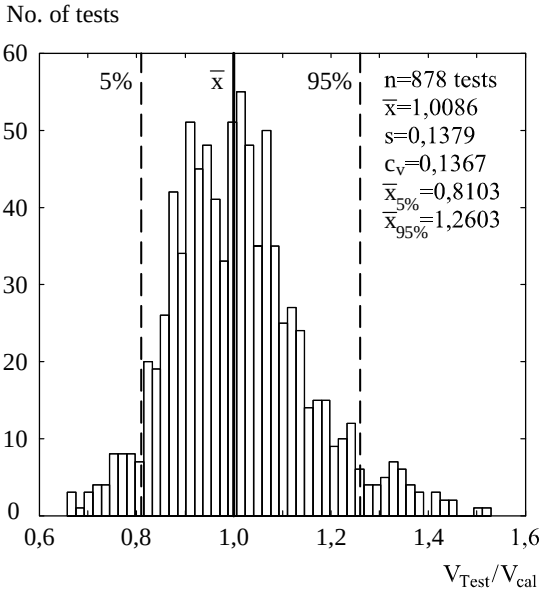

Figure 5.20– The distribution of V_{Test}/V_{cal}

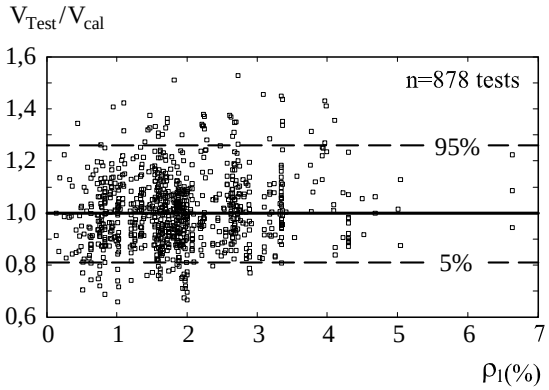

Figure 5.21– Graph of ρ_l (%) versus V_{Test} /V_{cal}

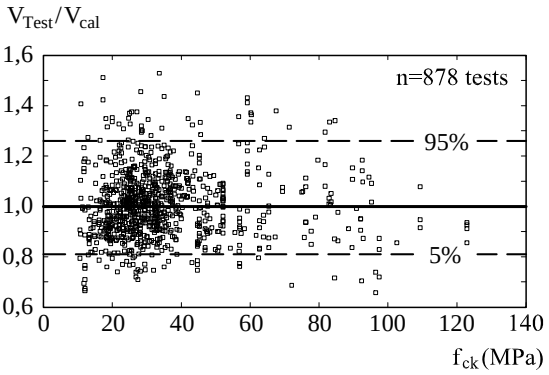

Figure 5.22– Graph of f_{ck} (MPa) versus V_{Test} /V_{cal}

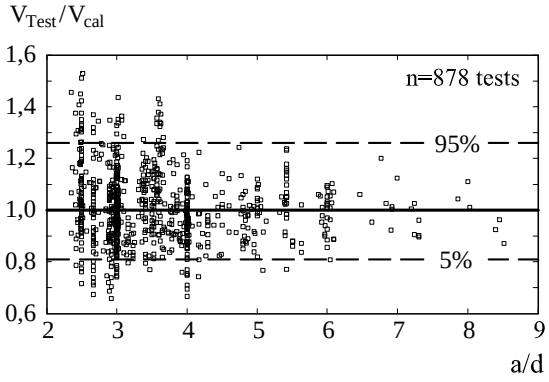

Figure 5.23– Graph of a/d (-) versus V_{Test} /V_{cal}

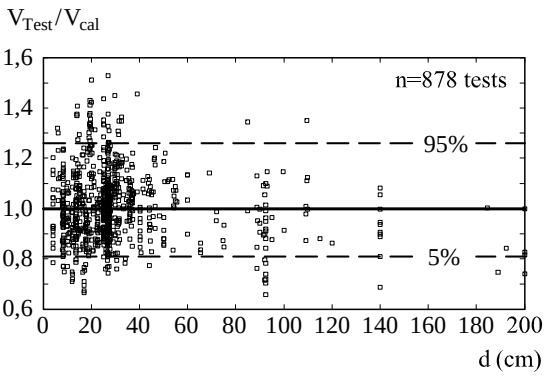

Figure 5.24– Graph of d(cm) versus V_{Test} /V_{cal}

The figures 5.25 to 5.28 show the dependent tendency of test results on the four main parameters including longitudinal reinforcement ratio ρ_l*(%)*, compressive concrete strength f_{ck} (MPa), *a*/*d* ratio and effective depth of beam *d*. It also can be seen from these figures that the suggested functions in the proposed shear strength model (Eq. 5.17) follow quite well these influences. This explains why the shear strength model can predict very well the shear strength of large number of shear tests from the database with different geometrical characteristics and material properties.

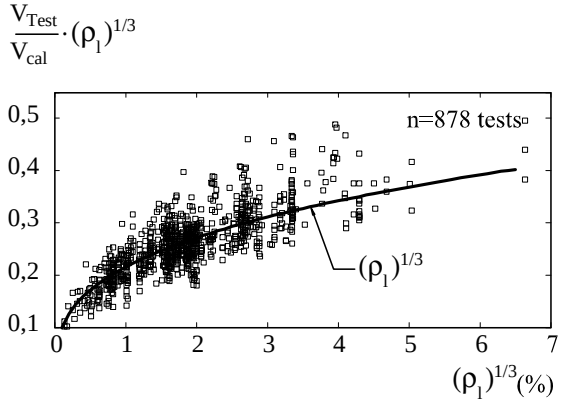

Figure 5.25– Graph of ρ_l (%) and $V_{Test}\cdot(\rho_l)^{1/3}/V_{Cal}$

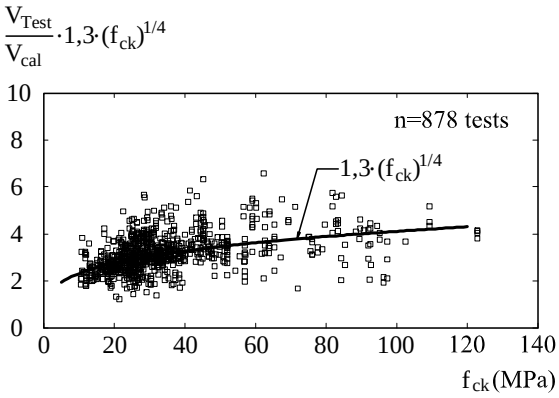

Figure 5.26–Graph of f_{ck}(MPa) and $V_{Test}\cdot1.3(f_{ck})^{1/4}/V_{cal}$

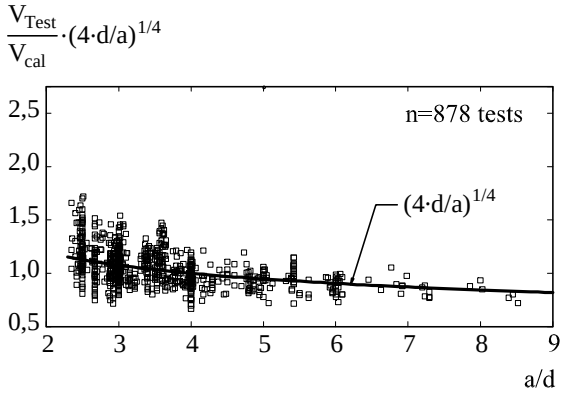

Figure 5.27– Graph of *a*/*d* (-) and $V_{Test}\cdot(4d/a)^{1/4}/V_{cal}$

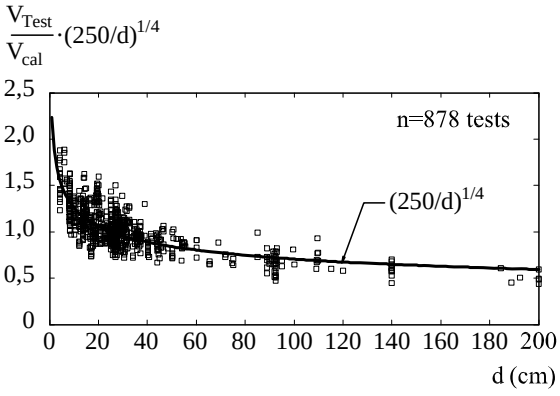

Figure 5.28– Graph of *d* (cm) and $V_{Test}\cdot(250/d)^{1/4}/V_{cal}$

5.3.1 Comparison with other Shear Strength Models

The proposed shear strength models will be compared with the 13 other models presented in the Chapter 2 (State of the Art). Since the shear database comprise a diversity of test beams with different material properties and section geometries, it is necessary to build sets of sub-database which can be considered to be representatives of some certain concrete member groups. These sets of sub-database are created from a selection criterion of 5 main parameters as presented in table 5.2. These selection criteria are established corresponding to some regulations in standards and practical designs.

Parameters	Notation	Selection Criteria				
		1	2	3	4	5
f_{ck} (MPa)	f_{ck}	10,6	25	55	70	123
ρ_l (%)	ρ_l	0,14	0,5	2	3	6,7
a/d (-)	a/d	2,35	2,5	3	5	8,6
d (mm)	d	41	150	500	600	2000
b (mm)	b	21	50	100	500	3000

Table 5.2. Selection criteria of 5 main parameters of materials and geometries.

Explanation for establishing of criteria in the table 5.2:

Criterion $f_{ck}1$ means all tests with 10,6 MPa ≤ f_{ck} will be selected.

Criterion $f_{ck}3$ means all tests with 55 MPa ≤ f_{ck} will be selected.

Criteria $f_{ck}23+\rho_l24$ mean all tests with 25 MPa ≤ f_{ck} ≤ 55 MPa and 0,5% ≤ ρ_l ≤ 3% will be selected.

From the above selection criteria, some typical sets of database are created from the original shear database of 878 test results as presented in table 5.3.

Set	Criteria	Tests	Description
S1	$f_{ck}1$ + ρ_l1 + a/d1 + d1 + b1	878	All concrete members with 10MPa ≤ f_{ck} ; 0,14% ≤ ρ_l ; 2,35 ≤ a/d ; 41mm ≤ d ; 21mm ≤ b.
S2	$f_{ck}2$ + ρ_l2 + a/d2 + d2 + b2	451	Normal concrete members with 25MPa ≤ f_{ck} ; 0,5% ≤ ρ_l ; 2,5 ≤ a/d ; 150mm ≤ d ; 50mm ≤ b.
S3	$f_{ck}13$ + ρ_l13 + a/d13 + d14 + b34	187	Normal concrete short-beams with 10MPa≤ f_{ck} ≤55MPa ; 0,14% ≤ ρ_l ≤2% ; 2,35 ≤ a/d ≤3 ; 41mm≤ d ≤500mm ; 100mm ≤ b ≤500mm.
S4	$f_{ck}14$ + ρ_l14 + a/d14 + d14 + b34	490	Normal concrete beams with 10MPa≤ f_{ck} ≤70MPa ; 0,14% ≤ ρ_l ≤3% ; 2,35≤ a/d ≤5 ; 41mm ≤ d ≤ 600mm ; 100mm ≤ b ≤500mm.
S5	$f_{ck}24$ + ρ_l24 + a/d24 + d24 + b24	243	Normal concrete long-beams with 25MPa ≤ f_{ck} ≤ 70MPa ; 0,5% ≤ ρ_l ≤ 3% ; 2,5 ≤ a/d ≤ 5 ; 150mm ≤ d ≤600mm ; 50mm ≤ b ≤ 500mm.
S6	$f_{ck}24$ + ρ_l14 + a/d2 + d24 + b34	269	Normal concrete members with 25MPa ≤ f_{ck} ≤ 70MPa ; 0,14% ≤ ρ_l ≤ 3% ; 2,5 ≤ a/d ; 150mm ≤ d ≤600mm ; 100mm ≤ b ≤ 500mm.
S7	$f_{ck}24$ + ρ_l14 + a/d1 + d24 + b4	32	Normal concrete slabs with 25MPa ≤ f_{ck} ≤ 70MPa ; 0,14% ≤ ρ_l ≤ 3% ; 2,35 ≤ a/d ; 150mm ≤ d ≤ 600mm ; 500mm ≤ b.
S8	$f_{ck}4$ + ρ14 + a/d1 + d24 + b34	32	High strength concrete beams with 70MPa ≤ f_{ck} ; 0,14% ≤ ρ_l ≤ 3% ; 2,35 ≤ a/d ; 150mm ≤ d ≤ 600mm ; 100mm ≤ b ≤ 500mm.
S9	$f_{ck}1$ + ρ1 + a/d1 + d1 + b1	14	Haunched beams

Table 5.3. Some typical sets of shear database used for comparison

The table 5.4 shows the calculated results of statistical quantities used for assessment of 13 other shear strength models and proposed Eq. (5.17) for the set of database SET 1 of 878 test results. From the sets of database SET 2 to SET 8, only the model suggested by Zink (2000) and the top four models which offer best results will be selected for comparison. The analytical results of these sets of database are presented in tables 5.5 to 5.11. The set of database SET 9 is for haunched beams only. This set includes 4 test results carried out by MacLeod et al. (1994) and 10 test results performed by Rombach et al. (2009). The results will be checked at the two critical sections of 1,3*d* and 1,0*d* apart from support.

SET 1: 878 fulfilled tests: 10MPa $\leq f_{ck}$; 0,14% $\leq \rho_l$; 2,35$\leq a/d$; 41mm $\leq d$; 21mm $\leq b$

Value	Reineck	Zararis	Zink	Tureyen	Park	Gastebled	Bentz	Bazant	KimD	KimJK	Latte	Eq.5.17
$\bar{X}$	1,1564	1,0089	1,043	1,5081	0,9394	1,1096	1,4577	1,0226	0,9672	1,0052	1,3173	1,0086
S	2,2578	0,1523	0,1469	0,3449	0,1489	0,2617	0,3506	0,1443	0,2262	0,1366	0,3475	0,1379
CV	1,9525	0,1509	0,1408	0,2287	0,1585	0,2358	0,2405	0,1411	0,2339	0,1359	0,2638	0,1367
$\bar{X}_{5\%}$	0,7778	0,797	0,8235	1,0121	0,7148	0,7114	0,8893	0,8171	0,6333	0,7908	0,8235	0,8103
$\bar{X}_{95\%}$	1,9647	1,2877	1,3247	2,0988	1,2208	1,5507	2,0633	1,2878	1,3931	1,2573	1,9588	1,2603

Table 5.4. Comparison of all of models for SET 1

SET 2: 451 fulfilled tests
25MPa$\leq f_{ck}$; 0,5% $\leq \rho_l$; 2,5 $\leq a/d$;
150mm $\leq d$; 50mm $\leq b$

Value	Zararis	Zink	Bazant	KimJK	Eq.5.17
$\bar{X}$	0,9830	1,0271	1,0053	0,9914	1,0192
S	0,1271	0,1317	0,1281	0,1308	0,1343
CV	0,1293	0,1282	0,1274	0,1320	0,1318
$\bar{X}_{5\%}$	0,7886	0,8204	0,8119	0,7878	0,8256
$\bar{X}_{95\%}$	1,2356	1,2645	1,2369	1,2241	1,2574

Table 5.5. Selected five models for SET 2

SET 3: 187 fulfilled tests
10MPa $\leq f_{ck} \leq$55MPa ; 0,14%$\leq \rho_l \leq$2%; 2,35 $\leq a/d \leq$3
41mm $\leq d \leq$500mm ; 100mm$\leq b \leq$500mm

Value	Zararis	Zink	KimD	KimJK	Eq.5.17
$\bar{X}$	1,0513	1,1006	0,9960	1,0193	1,0459
S	0,1600	0,1486	0,1760	0,1281	0,1258
CV	0,1522	0,1350	0,1767	0,1257	0,1202
$\bar{X}_{5\%}$	0,8533	0,9004	0,7398	0,8377	0,8723
$\bar{X}_{95\%}$	1,3495	1,3765	1,2610	1,2521	1,3028

Table 5.6. Selected five models for SET 3

SET 4: 490 fulfilled tests
10MPa$\leq f_{ck} \leq$70MPa ; 0,14%$\leq \rho_l \leq$ 3% ; 2,35$\leq a/d \leq$5
41mm$\leq d \leq$600mm ; 100mm $\leq b \leq$500mm

Value	Zararis	Zink	Bazant	KimJK	Eq.5.17
$\bar{X}$	1,0143	1,0708	1,0416	1,0198	1,0263
S	0,1480	0,1415	0,1373	0,1259	0,1305
CV	0,1459	0,1322	0,1318	0,1234	0,1272
$\bar{X}_{5\%}$	0,8137	0,8704	0,8459	0,8320	0,8316
$\bar{X}_{95\%}$	1,2820	1,3345	1,2883	1,2585	1,2731

Table 5.7. Selected five models for SET 4

SET 5: 243 fulfilled tests
25MPa $\leq f_{ck} \leq$ 70MPa ; 0,5% $\leq \rho_l \leq$ 3% ; 2,5 $\leq a/d \leq$ 5
150mm $\leq d \leq$600mm ; 50mm $\leq b \leq$ 500mm

Value	Zararis	Zink	Bazant	KimJK	Eq.5.17
$\bar{X}$	0,9879	1,0472	1,0186	1,0051	1,0330
S	0,1274	0,1304	0,1263	0,1239	0,1280
CV	0,1289	0,1246	0,1240	0,1233	0,1239
$\bar{X}_{5\%}$	0,7967	0,8486	0,8305	0,8134	0,8483
$\bar{X}_{95\%}$	1,2372	1,2851	1,2597	1,2375	1,2662

Table 5.8. Selected five models for SET 5

SET 6: 269 fulfilled tests
25MPa ≤ f_{ck} ≤ 70MPa ; 0,14% ≤ ρ_l ≤ 3% ; 2,5 ≤ a/d
150mm ≤ d ≤600mm ;100mm ≤ b ≤ 500mm

Value	Zararis	Zink	Bazant	KimJK	Eq.5.17
$\bar{X}$	0,9914	1,0520	1,0168	1,0139	1,0329
S	0,1283	0,1328	0,1258	0,1232	0,1246
CV	0,1294	0,1262	0,1238	0,1215	0,1206
$\bar{X}_{5\%}$	0,8002	0,8495	0,8322	0,8279	0,8521
$\bar{X}_{95\%}$	1,2471	1,2943	1,2589	1,2482	1,2515

Table 5.9. Selected five models for SET 6

SET 7: 32 fulfilled tests
25MPa ≤ f_{ck} ≤ 70MPa ; 0,14% ≤ ρ_l ≤ 3% ; 2,35 ≤ a/d
150mm ≤ d ≤ 600mm ; 500mm ≤ b

Value	Zararis	Zink	Bazant	KimJK	Eq.5.17
$\bar{X}$	0,9964	1,0581	1,0167	1,0201	1,0149
S	0,0868	0,1072	0,1141	0,1155	0,1120
CV	0,0871	0,1013	0,1122	0,1132	0,1104
$\bar{X}_{5\%}$	0,8683	0,8922	0,8422	0,8345	0,8391
$\bar{X}_{95\%}$	1,1395	1,2222	1,1948	1,1974	1,1861

Table 5.10. Selected five models for SET 7

SET 8: 32 fulfilled tests
70MPa ≤ f_{ck} ; 0,14% ≤ ρ_l ≤ 3% ; 2,35 ≤ a/d
150mm ≤ d ≤ 600mm ; 100mm ≤ b ≤ 500mm

Value	Zararis	Zink	Gastebled	KimD	Eq.5.17
$\bar{X}$	0,9435	0,9724	0,9556	1,0231	0,9881
S	0,1428	0,1308	0,1859	0,1760	0,1404
CV	0,1514	0,1345	0,1945	0,1720	0,1421
$\bar{X}_{5\%}$	0,7706	0,8119	0,6898	0,7873	0,8375
$\bar{X}_{95\%}$	1,2456	1,2753	1,2755	1,4078	1,3306

Table 5.11. Selected five models for SET 8

SET 9: 14 fulfilled tests
haunched beam

Value	Eq. (5.20) at 1.0d	Eq. (5.20) at 1.3d
$\bar{X}$	1,0274	1,0133
S	0,0643	0,0639
CV	0,0626	0,0630
$\bar{X}_{5\%}$	0,9352	0,9224
$\bar{X}_{95\%}$	1,1281	1,1123

Table 5.12. Models for SET 9 of haunched beams

In order to study the influences of significant factors, figure 5.29 shows the relation of longitudinal reinforcement ratio ρ_l, characteristic concrete strength f_{ck}, a/d ratio and effective depth of beam d with shear strength of some models suggested by Zararis et al. (2001), Zink (2000), Bazant et al. (2005), Kim JK et al. (1996) and proposed model as in Eq. (5.17) for the set of database SET 4 of 490 test results.

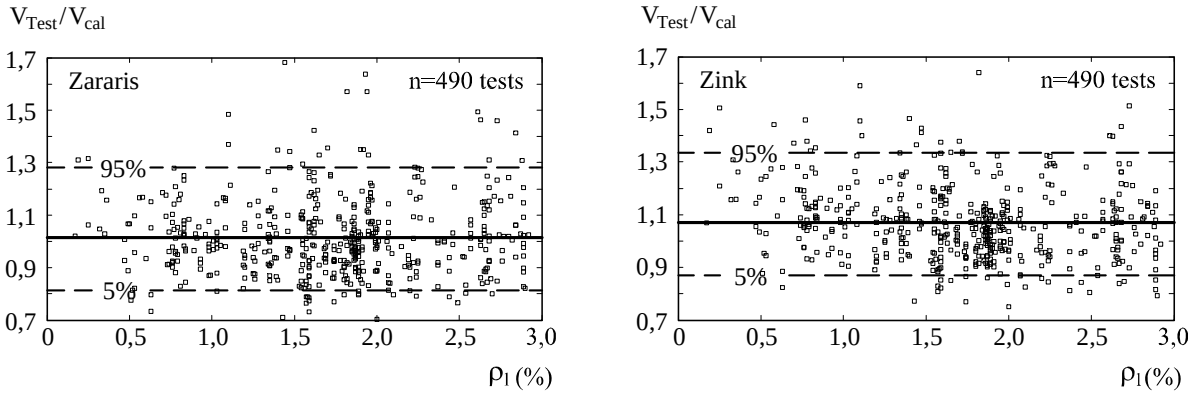

Figure 5.29.a– Graph of ρ_l versus V_{Test}/V_{cal} of 5 shear strength models for the shear data SET 4 (490 tests, 10,6MPa ≤ f_{ck} ≤ 70MPa; 0,14% ≤ ρ_l ≤ 3%; 2,35 ≤ a/d ≤ 5; 41mm ≤ d ≤ 600mm; 100mm ≤ b ≤ 500 mm)

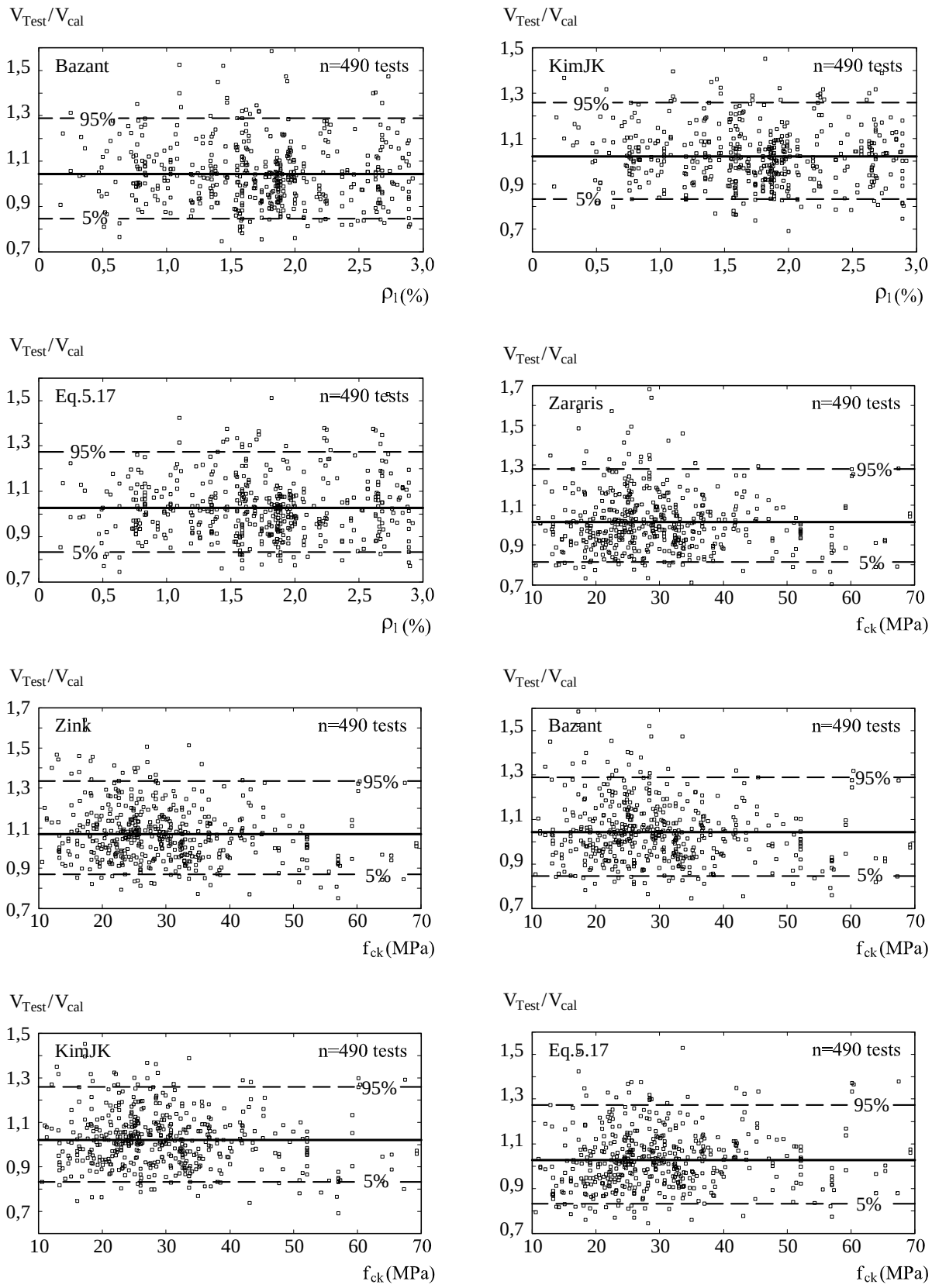

Figure 5.29.b– Graph of ρ_l, f_{ck} versus V_{Test}/V_{cal} of 5 shear strength models for the shear data SET 4 (490 tests, 10,6MPa $\leq f_{ck} \leq$ 70MPa; 0,14% $\leq \rho_l \leq$ 3%; 2,35 $\leq a/d \leq$ 5; 41mm $\leq d \leq$ 600mm; 100mm $\leq$ b $\leq$ 500 mm)

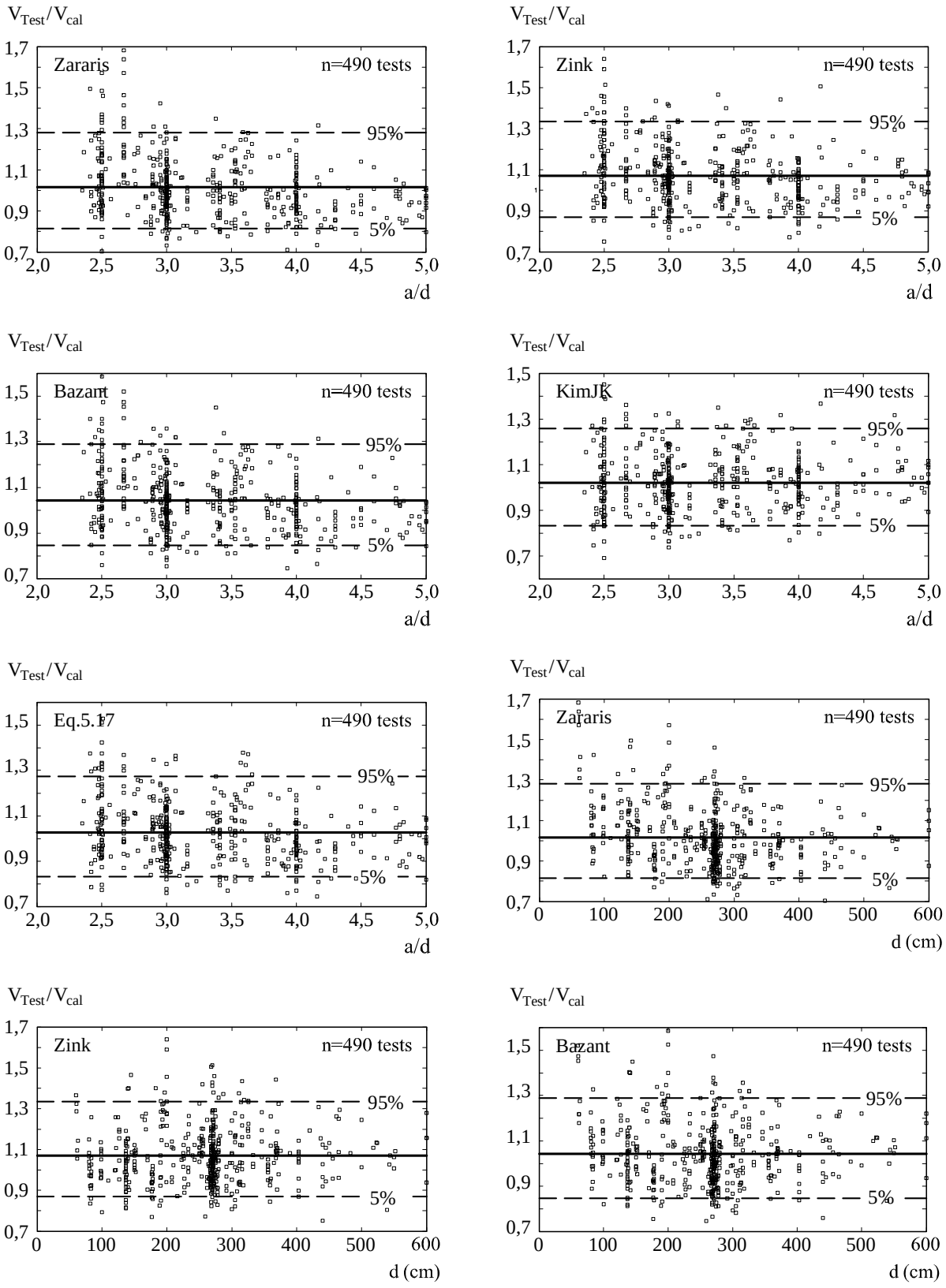

Figure 5.29.c– Graph of a/d, d versus V_{Test}/V_{cal} of 5 shear strength models for the shear data SET 4 (490 tests, 10,6MPa $\leq f_{ck} \leq$ 70MPa; 0,14% $\leq \rho_l \leq$ 3%; 2,35 $\leq a/d \leq$ 5; 41mm $\leq d \leq$ 600mm; 100mm $\leq$ b $\leq$500 mm)

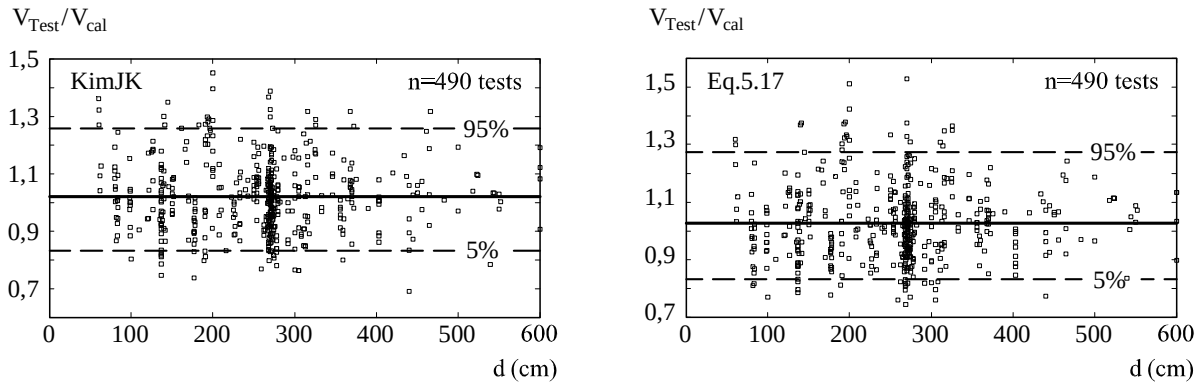

Figure 5.29.d– Graph of d versus V_{Test}/V_{cal} of 5 shear strength models for the shear data SET 4 (490 tests 10,6MPa $\le f_{ck} \le$ 70MPa; 0,14% $\le \rho_l \le$ 3%; 2,35 $\le a/d \le$ 5; 41mm $\le d \le$ 600mm; 100mm $\le$ b $\le$ 500 mm)

5.3.2 Comparison with Practical Codes

In order to provide practical formulas for shear design, a safety factor of $\gamma_{SF} = 1{,}6$ is suggested to use for the Eqs (5.17) and (5.20). This value is selected to make sure that all test results of set of database SET 1 will belong to the safe side ($V_{Test}/V_{cal} > 1$). As a result, design shear strength of straight depth concrete beams without stirrups will be calculated as in the Eq. (5.27a):

$$V_{Rd} = 1{,}25\left(\frac{4d}{a}\right)^{1/4} \cdot \left(\frac{250}{d}\right)^{1/4} \cdot \left(f_{ck}\right)^{1/4} \cdot \rho_l^{1/3} \cdot b \cdot d \qquad (5.27a)$$

or simpler form:

$$\boxed{V_{Rd} = 7\left(\frac{f_{ck}}{a}\right)^{1/4} \cdot \rho_l^{1/3} \cdot b \cdot d} \qquad (5.27b)$$

For haunched beams, design shear capacity will be calculated as in the formula 5.28a:

$$V_{Rd}^{\alpha} = 1{,}25\left(\frac{4d}{a}\right)^{1/4} \cdot \left(\frac{250}{d}\right)^{1/4} \cdot \left(f_{ck}\right)^{1/4} \cdot \rho_l^{1/3} \cdot \left(1+\tan\alpha\right) \cdot b \cdot d \qquad (5.28a)$$

or simpler form:

$$\boxed{V_{Rd}^{\alpha} = 7\left(\frac{f_{ck}}{a}\right)^{1/4} \cdot \rho_l^{1/3} \cdot \left(1+\tan\alpha\right) \cdot b \cdot d} \qquad (5.28b)$$

The four codes including DIN 1045-01, SN262, CSA2003 and ACI 318-05 will be selected to compare with the proposed design shear strength formula. Tables 5.13 to 5.18 show the calculated results of statistical quantities of these codes for sets of database from SET 1 to SET 6. The normal distribution of safety factor V_{Test}/V_{cal} of these codes for sets of database SET 1 and SET 4 are also presented in the figures 5.30 and 5.31.

SET 1: 878 fulfilled tests
10MPa ≤ f_{ck} ; 0,14% ≤ ρ_l ; 2,35≤ a/d ;
41mm ≤ d ; 21mm ≤ b

Value	ACI	SN	CSA	DIN	Eq.5.27
$\bar{X}$	1,8530	1,6432	1,8241	1,9390	1,6210
S	0,5564	0,3028	0,2850	0,3798	0,2216
CV	0,3003	0,1843	0,1562	0,1959	0,1367
$\bar{X}_{5\%}$	0,9503	1,1739	1,4252	1,4498	1,3022
$\bar{X}_{95\%}$	2,8074	2,1783	2,3841	2,6704	2,0256

Table 5.13. Selected five models for SET 1

SET 2: 451 fulfilled tests
25MPa ≤ f_{ck} ; 0,5% ≤ ρ_l ; 2,5 ≤ a/d ;
150mm ≤ d ; 50mm ≤ b

Value	ACI	SN	CSA	DIN	Eq.5.27
$\bar{X}$	1,6744	1,5727	1,7668	1,8600	1,6379
S	0,4916	0,2704	0,2439	0,3426	0,2158
CV	0,2936	0,1720	0,1380	0,1842	0,1318
$\bar{X}_{5\%}$	0,9008	1,1435	1,4126	1,4245	1,3268
$\bar{X}_{95\%}$	2,5779	2,0300	2,2535	2,4966	2,0209

Table 5.14. Selected five models for SET 2

SET 3: 187 fulfilled tests
10MPa ≤ f_{ck} ≤55MPa ; 0,14% ≤ρ_l ≤2%; 2,35 ≤ a/d ≤3
41mm ≤ d ≤500mm ; 100mm≤ b ≤500mm

Value	ACI	SN	CSA	DIN	Eq.5.27
$\bar{X}$	1,8821	1,6642	1,8204	2,0314	1,6809
S	0,5095	0,2917	0,2822	0,3341	0,2021
CV	0,2707	0,1753	0,1550	0,1645	0,1202
$\bar{X}_{5\%}$	1,2335	1,2692	1,4576	1,6358	1,4019
$\bar{X}_{95\%}$	2,8234	2,1909	2,3362	2,6545	2,0937

Table 5.15. Selected five models for SET 3

SET 4: 490 fulfilled tests
10MPa ≤ f_{ck} ≤70MPa ; 0,14%≤ ρ_l ≤3% ;2,35≤ a/d ≤5
41mm≤ d ≤600mm ; 100mm ≤ b ≤500mm

Value	ACI	SN	CSA	DIN	Eq.5.27
$\bar{X}$	1,9032	1,6601	1,8179	1,9636	1,6495
S	0,5053	0,2923	0,2646	0,3410	0,2098
CV	0,2655	0,1761	0,1455	0,1737	0,1272
$\bar{X}_{5\%}$	1,1803	1,2316	1,4539	1,5280	1,3365
$\bar{X}_{95\%}$	2,7838	2,1791	2,3116	2,6072	2,0460

Table 5.16. Selected five models for SET 4

SET 5: 243 fulfilled tests
25MPa ≤ f_{ck} ≤ 70MPa ; 0,5% ≤ ρ_l ≤ 3% ; 2,5 ≤ a/d ≤ 5
150mm ≤ d ≤600mm ; 50mm ≤ b ≤ 500mm

Value	ACI	SN	CSA	DIN	Eq.5.27
$\bar{X}$	1,7511	1,5831	1,7626	1,8839	1,6601
S	0,3883	0,2411	0,2331	0,2807	0,2057
CV	0,2218	0,1523	0,1323	0,1490	0,1239
$\bar{X}_{5\%}$	1,1979	1,2277	1,4330	1,5093	1,3633
$\bar{X}_{95\%}$	2,5085	2,0166	2,2369	2,3767	2,0349

Table 5.17. Selected five models for SET 5

SET 6: 269 fulfilled tests
25MPa ≤ f_{ck} ≤ 70MPa ; 0,14% ≤ ρ_l ≤ 3% ; 2,5 ≤ a/d
150mm ≤ d ≤600mm ;100mm ≤ b ≤ 500mm

Value	ACI	SN	CSA	DIN	Eq.5.27
$\bar{X}$	1,7116	1,5670	1,7728	1,8608	1,6601
S	0,3974	0,2523	0,2300	0,2810	0,2002
CV	0,2322	0,1610	0,1298	0,1510	0,1206
$\bar{X}_{5\%}$	1,1380	1,1705	1,4406	1,4910	1,3694
$\bar{X}_{95\%}$	2,4709	2,0128	2,2287	2,3693	2,0114

Table 5.18. Selected five models for SET 6

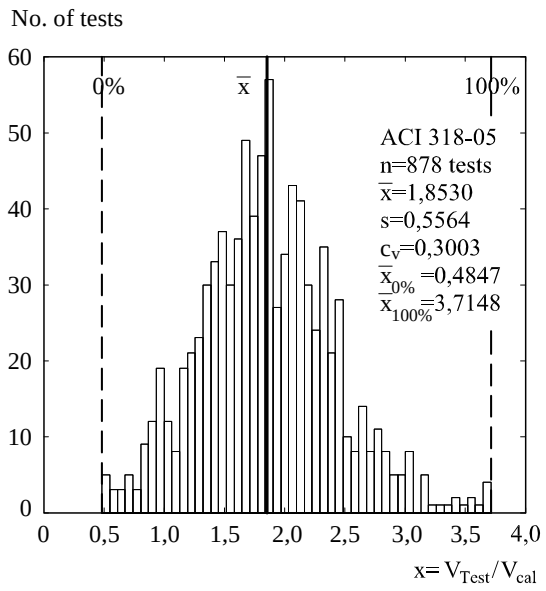

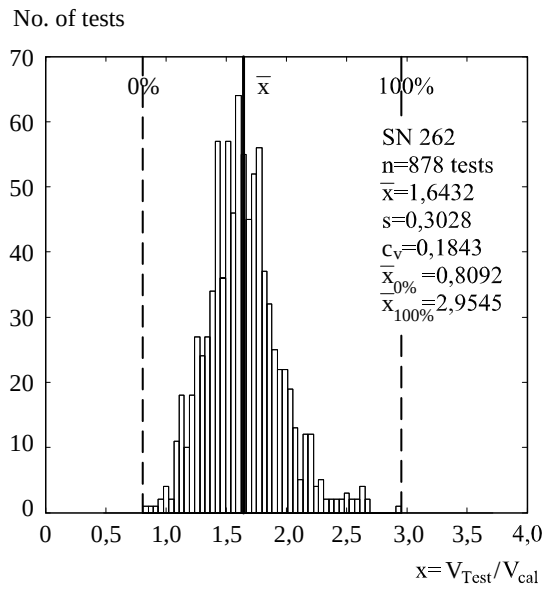

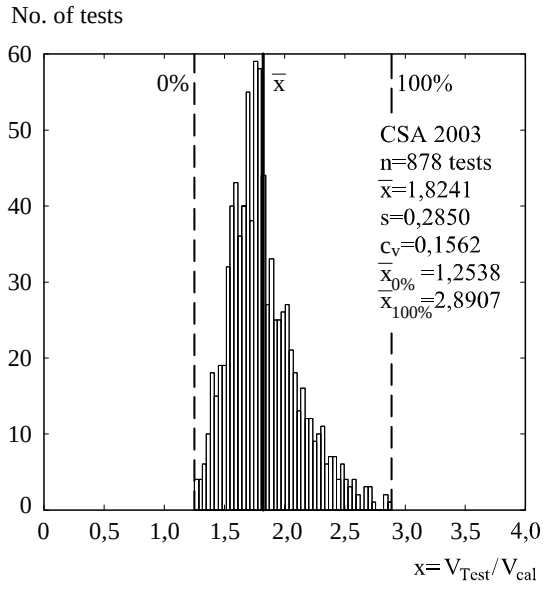

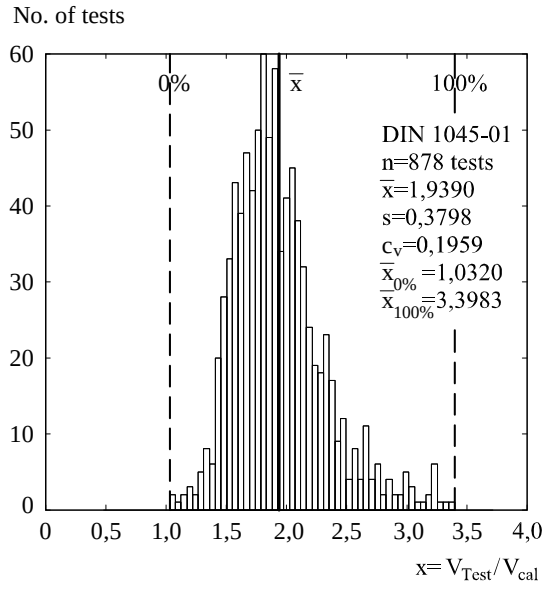

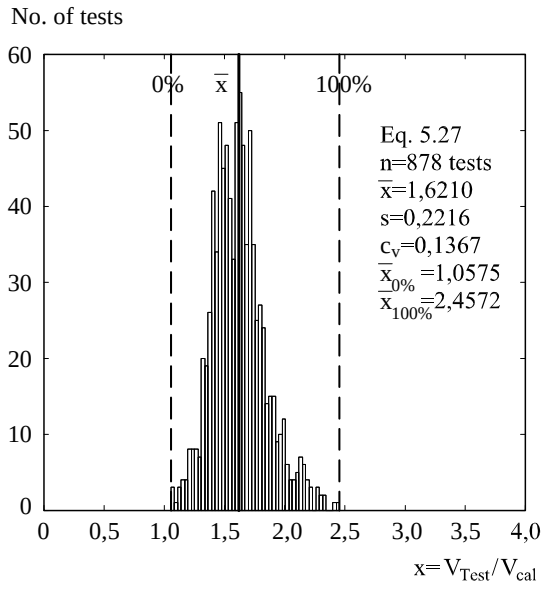

Figure 5.30– Distribution of safety factor V_{Test}/V_{cal} according to four practical codes and proposed design equation (5.27) for set of database S 1 of 878 straight depth concrete beams without stirrups.

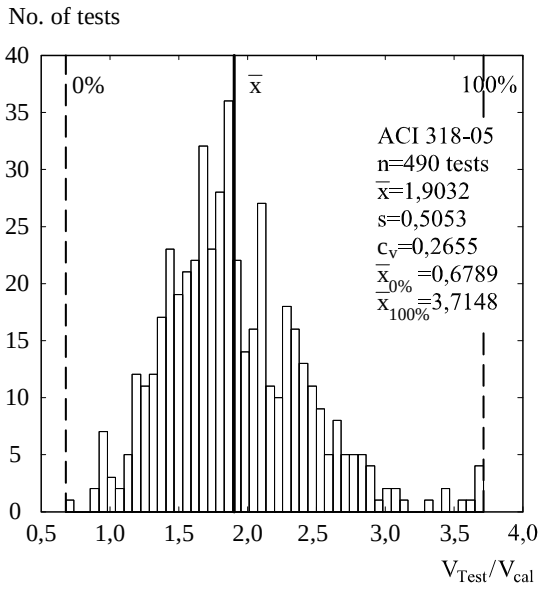

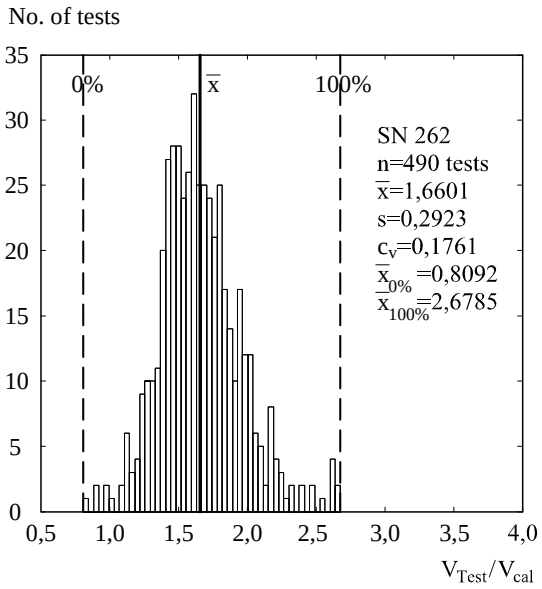

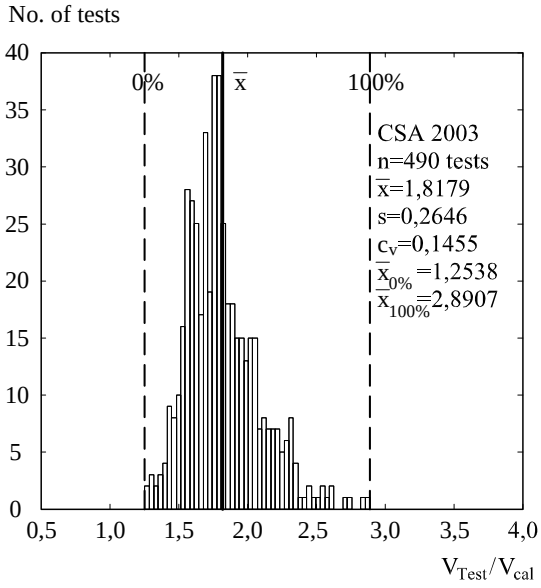

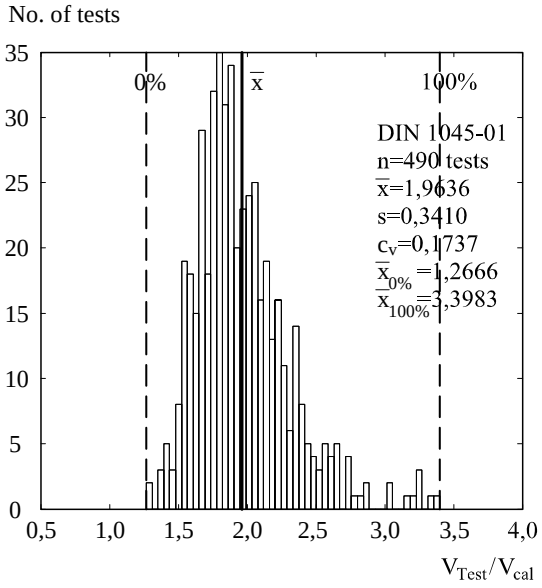

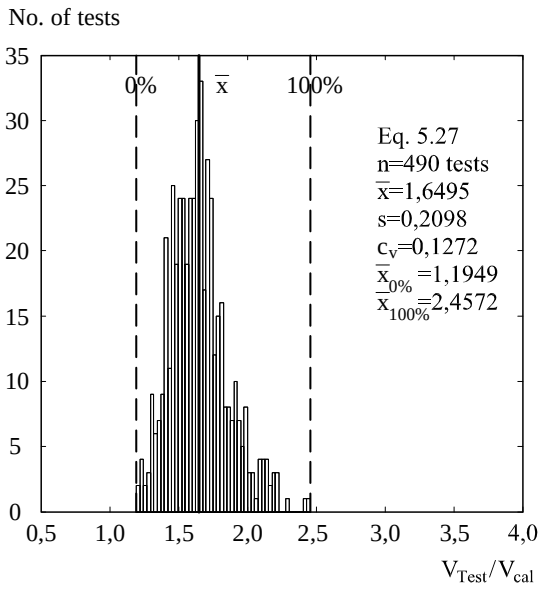

Figure 5.31– Distribution of safety factor V_{Test}/V_{cal} according to four practical codes and proposed design equation (5.27) for set of database S 4 of 490 straight depth concrete beams without stirrups.

For haunched beams, the proposed design shear capacity according to formula 5.28 will be calculated to compare with the design shear value of DIN 1045-01 for the set of database SET 9 of all 14 test results as in the figure 5.32.

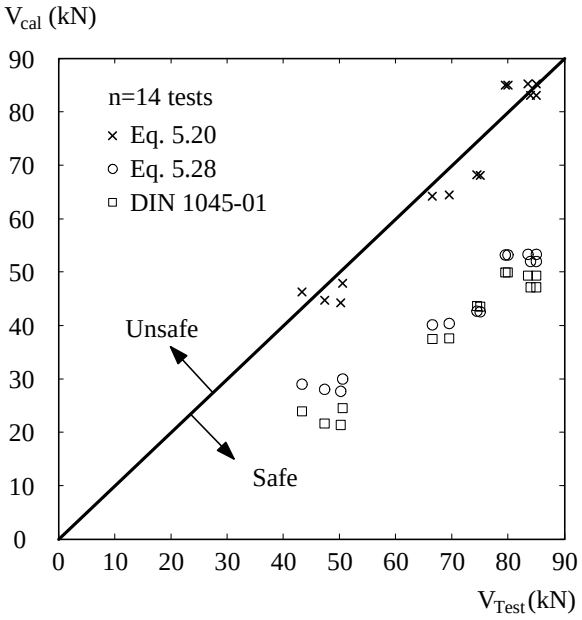

Value	Eq. (5.28)	DIN 1045-01
$\bar{x}$	1,6438	1,8342
S	0,1029	0,2206
CV	0,0626	0,1203
$\bar{x}_{5\%}$	1,4964	1,5953
$\bar{x}_{95\%}$	1,8050	2,3238

Note:

The calculating section is 1,0d apart from support.

Figure 5.32– Graph of V_{Test} and V_{cal} of proposed shear design model and DIN 1045-01 for the shear data SET 9 of 14 test results of haunched beams without stirrups.

5.4 Discussions and Conclusions

This Chapter presented a new approach which combines Non-FEM analysis and test results to find out the shear behaviours of concrete members without stirrups. Based on the recognized shear resistance mechanisms, two new shear strength models were proposed for straight depth concrete beams and haunched concrete beams without stirrups. The two shear design formulae were also suggested for practical purposes. The comparison with other shear strength models and with four practical codes demonstrated that the proposed formulae predict the shear capacity in very good agreement with test results. Some discussions on the models will be presented as follows.

As presented in the Chapter 2 (State of the Art), the shear transferring mechanisms including

(1) Shear resistance of the uncracked compression concrete zone,
(2) Friction of contact surfaces between cracks (aggregate interlock),
(3) Dowel action of longitudinal reinforcements,
(4) Crack–bridging tension forces in closed cracks (residual tensile stress in concrete) and
(5) Arch action

have been thought for a long time to be five main shear resistance actions of concrete members without stirrups.

However, the Non-FEM analysis of cracked concrete beams showed that it is (1) the concrete compression zone and (6) the uncracked concrete parts in tension zone to carry at least 95% of the total shear force at any cross-section in concrete beams without stirrups. It is noted that no literature is known so far which mentions the role of uncracked concrete parts in the tension zone to carry shear. As we know that the value of shear stress τ_{xy} at any point on vertical section can be determined as a function of normal stresses σ_x, σ_y and inclined angle α of principal compressive stress with horizontal axis *x* as the Eq. (5.29):

$$\tau_{xy} = 0,5 \tan 2\alpha \left(\sigma_x - \sigma_y\right) \tag{5.29}$$

At critical state, there exists mainly compressive stresses σ_x in the uncracked concrete parts in both compression zone and tension zone (Fig. 5.33). Though the value of the compressive stress σ_x in the tension zone is much smaller than that of the compressive stress in compression zone, the inclined angle α of principal compressive stresses in the tension zone are much larger than in compression zone. That's why shear stresses τ_{xy} exist and has relatively high value in the uncracked concrete parts of the tension zone. The Non-FEM analysis showed that the uncracked concrete parts of tension zone can carry up to 40% of the total shear force at critical state.

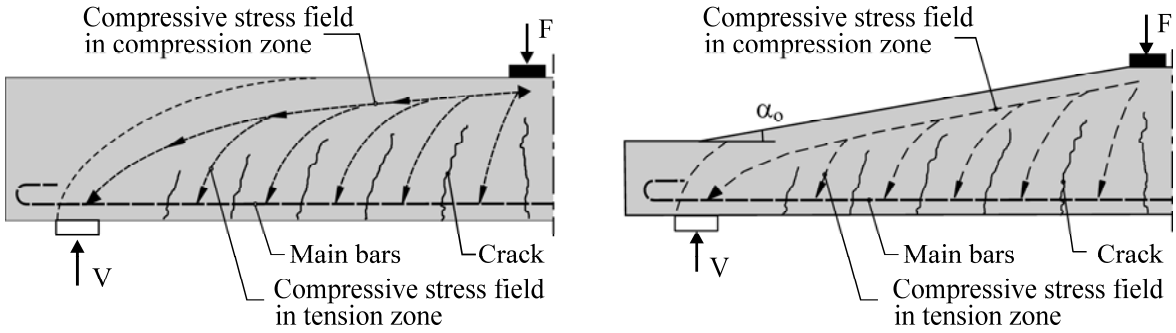

Figure 5.33– Compressive stress fields in uncracked concrete zones

The concrete compression zone carries the remaining (about 60%) of the total shear force at critical state. It is noted that the shear failure only occurs if the critical shear crack completely penetrates through the compression zone. Therefore, it can be said that the concrete compression zone plays the most important role in shear resistance of concrete members without stirrups. In other words, models developed from shear resistance mechanisms of this zone can be considered as an appropriate approach to find out the shear capacity of concrete members without stirrups. Following this principle, many authors such as Zararis et al. (2001), Zink (2000), Tureyen et al. (2003) or Park et al. (2006) suggested equations which predict quite good the shear strength of beams in the shear database (Table 5.4 to 5.11).

Having the same opinion about the key role of concrete compression zone and from Non-FEM analysis as well as from the experimental program in this research, the author proposed a more detailed analytical procedure to study the shear strength of concrete compression zone at a certain critical section. The critical section of straight depth beams is 1,0*d* apart from position of load application (max *M, d*) while that of haunched beams is 1,3*d* apart from support (min *M, d*). The Non-FEM analysis also showed that the shear stress distribution in the concrete compression zone has a parabola shape which is similar to the assumption of Tureyen et al. (2003) but different from the approach of Zink (2000) and Zararis et al. (2001) as shown in the figure 5.34. As presented in the Chapter 4 (Non-FEM analysis), there exist very small or no normal stresses on cracks except in the region in front of the tip of crack where high tensile stresses exist (Fig. 5.34.c). As a result, value of shear stress on cracks is normally very small or negligible.

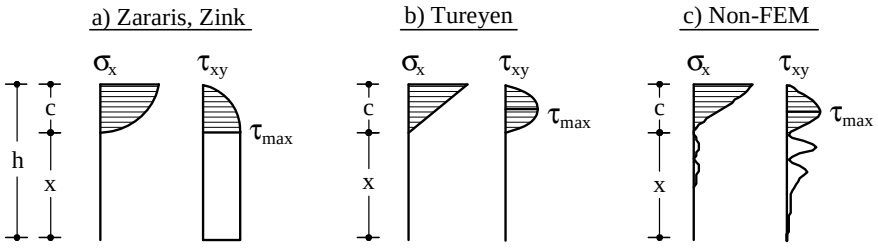

Figure 5.34– Distribution of compressive stress σ_x and shear stress τ_{xz} in concrete

The distribution of the shear stress in the compression zone at critical section as shown in figure 5.34.c makes it relatively easy to propose simple formulae for shear strength of concrete beams as the Eqs (5.4) and (5.11). In these formulae all significant factors which have important effects on the shear strength are taken into account including longitudinal reinforcement ratio ρ_l, shear span to depth ratio a/d, size effect d and concrete strength f_{ck}. The suggested size effect law (Eq. 5.7) shows a very good agreement with test results as presented in the Fig. 5.28. The concrete strength f_{ck} in the shear strength formulae is considered in terms of allowable shear stress τ^*_{max} which had been once proposed by Park et al. (2006). In this research, the value of τ^*_{max} is calibrated from the updated shear database of 878 tests of concrete members without stirrups as Eq. (5.15) for straight depth beams and Eq. (5.18) for haunched beams.

Although the shear strength formulae of straight depth beams and haunched beams have a quite similar form, they were derived from two different failure behaviors. The differences in the two formulae include:

(1) The effective depth of beam d is taken at the relevant section which is 1,0d apart from the position of load application (max *M, d*) for straight depth beams and 1,3d from support (min *M, d*) for haunched beams for single span members. It means that

the shear failure of straight depth beams tends to occur in the region close to position of load application while that of haunched beams is likely to occur in the region near supports (min *M*, *d*).

(2) The shear strength formula of haunched beams additionally includes the inclined angle α of the compression chord of the beam to consider the influence of α on the shear stress distribution of haunched beams.

The proposed shear strength formula for straight depth beams (eq. 5.17), accompanied with 13 models of other authors, were used to predict the critical shear strength of test beams in the updated shear database of 878 shear tests. This shear database covers a quite big range of parameters: ρ_l = 0,14 % ÷ 6,64 %; d = 41 mm ÷ 2000 mm; a/d = 2,35 ÷ 8,52 and f_{ck} = 10,6 MPa ÷ 122,9 MPa. The results showed that all 14 models can predict quiet well the shear capacity of concrete beams without stirrups as presented in the table 5.4. The five models among others which gives the most accurate results of the shear capacity are models suggested by Zararis et al. (2001), Zink (2000), Bazant et al. (2005), Kim JK et al. (1996) and the new proposed one (eq. 5.17) (Table 5.4).

The analysis of all 8 sets of shear database which represent some typical groups of concrete members without stirrups as in the table 5.3 showed that the proposed model (Eq. 5.17) and the model suggested by Kim JK et al. (1996) are the two models which provide the best fit values of statistical quantities including mean value, standard deviation, coefficient of variation, 5 % fractile and 95 % fractile of safety factor as presented from the table 5.4 to table 5.11 and figure 5.29. For example for SET 4 as a group of normal concrete beams with 10 MPa $\leq$ $f_{ck} \leq$ 70 MPa; 0,14 % $\leq \rho_l \leq$ 3 %; 2,35 $\leq a/d \leq$ 5; 41 mm $\leq d \leq$ 600 mm and 100 mm $\leq b \leq$ 500 mm, the new proposed model (Eq. 5.17) and that of Kim JK et al. (1996) show better results than the approaches suggested by Zararis et al. (2001), Zink (2000) and Bazant et al. (2005) as presented in the table 5.7. Besides, the proposed model becomes superior for sets of database of concrete members with large width or high concrete strength as presented in table 5.10 and 5.11 for SET 7 and SET 8. The shear strength model suggested by Kim JK et al. (1996) is a totally empirical equation which is complicated compared with the proposed Eq. (5.17) as re-written in the table 5.19.

Model of Kim JK et al. (1996)	Proposed model (Eq.5.17b)
$V_{Rm} = 3,5 \cdot (f_c')^{1/3} \cdot \rho_l^{3/8} \cdot (0,4 + d/a) \cdot \lambda(d) \cdot b \cdot d$ with $\lambda(d) = \frac{1}{\sqrt{1+0,008d}} + 0,18$ $f'_c = f_{ck} + 1,6$ MPa	$V_{Rm} = 11,25 \left(\frac{f_{ck}}{a} \right)^{1/4} \cdot \rho_l^{1/3} \cdot b \cdot d$

Table 5.19 Mean shear capacity of the model by Kim JK et al. (1996) and the proposed model (Eq. 5.17b)

The proposed shear strength model for haunched beams (Eq. 5.20) also gives values in very good agreement with test results of 14 haunched beams performed by MacLeod et al. (1994) and Rombach et al. (2009) as presented in the table 5.12. The computed results at the section of 1,3*d* apart from support are better than those at the section 1,0*d* apart from support (Table 5.12). However, the value of effective depth *d* of beam at the section 1,0*d* can be used for the sake of simplicity.

The two shear design formulae for straight depth beams and haunched beams are also suggested for practical purposes with a safety factor of $\gamma_{SF} = 1{,}6$ (Eqs 5.27 and 5.28). The proposed shear design equations, accompanied with the shear design equations in 4 practical codes including German Code DIN 1045-01, Swiss Code SN262, Canadian Standard CSA2003 and ACI 318-05, were used to calculate the design shear capacity of test beams as presented in tables 5.13 to 5.18 and figures 5.30 and 5.3 for the shear database of 878 straight depth beams and 14 haunched beams without stirrups.

The computed results of statistical quantities for SET 1 of 878 straight depth test beams as presented in the table 5.13 and figure 5.30 showed that ACI 318-05 is extremely unsafe and also very conservative with a safety factor V_{Test}/V_{cal} in range of 0,49 to 3,71. The Swiss Code SN 262 is also unsafe for some tests and quite conservative with safety factor V_{Test}/V_{cal} from 0,81 to 2,96 while the German Code DIN 1045-01 is safe for all tests but rather conservative with safety factor V_{Test}/V_{cal} in range of 1,03 to 3,40. The Canadian Standard CSA2003, though somewhat conservative, has a very good safety factor varying from 1,25 to 2,89. The proposed shear design equation (Eq. 5.27) gives the best reasonable safety factor which varies from 1,06 to 2,46. The analysis of the first 6 sets of shear database in the table 5.3 also showed that the proposed shear design equation (Eq. 5.27) provides the values of statistical quantities including mean value, standard deviation, coefficient of variation, 5% fractile and 95% fractile of safety factor which are clearly superior to those of the other 4 codes (Tables 5.13-5.18 and Figs 5.30-5.31).

For the set of database SET 9 of 14 tests of haunched beams without stirrups, the proposed shear design equation (Eq. 5.28) also provides the values of statistical quantities which are more reasonable than those of German Code DIN 1045-01 as in the figure 5.32. It can be seen from this figure that the German Code DIN 1045-01 is quite conservative with a safety factor V_{Test}/V_{cal} in the range of 1,60 to 2,32 and a relatively high mean value of safety factor of 1,83 while the safety factor of the proposed shear design equation (Eq. 5.28) varies from 1,50 to 1,81 with mean value of 1,64. It has to be noted, that 14 tests of haunched beams had been conducted so far. Thus the database is very small.

The shear design formulae of the 4 codes and the proposed models (Eq. 5.27 and Eq. 5.28) are re-written as in the table 5.20. Except the shear design formulae of ACI 318-05 which have long been considered to be an unreliable equations for shear design of concrete members without stirrups, the proposed shear design equations (Eq. 5.27) and (Eq. 5.28) are clearly simpler and easier to use than those of the other 3 codes.

<table>
<tr><td>ACI 318-05</td><td>Proposed shear design equations</td></tr>
<tr><td>For straight depth beams:
$V_{Rd} = \frac{0,75}{6}\sqrt{f'_c}\cdot b\cdot d$
or
$V_{Rd} = 0,75\left(0,16\sqrt{f'_c} + 17\rho_l \cdot \frac{V_{Ed}\cdot d}{M_{Ed}}\right)\cdot b\cdot d$
with $f'_c = f_{ck} + 1,6$ MPa</td><td>For straight depth beams (Eq. 5.27):
$V_{Rd} = 7\left(\frac{f_{ck}}{a}\right)^{1/4}\cdot \rho_l^{1/3}\cdot b\cdot d$
For haunched beams (Eq. 5.28):
$V_{Rd}^{\alpha} = 7\left(\frac{f_{ck}}{a}\right)^{1/4}\cdot \rho_l^{1/3}\cdot (1+\tan\alpha)\cdot b\cdot d$</td></tr>
<tr><td>German Code DIN 1045-01</td><td>Swiss Code SN 262</td></tr>
<tr><td>For straight depth beams:
$V_{Rd} = 0,10k\cdot\eta_1\cdot(100\cdot\rho_l\cdot f_{ck})^{1/3}\cdot b\cdot d$
with
$k = 1+\sqrt{\frac{200}{d}} \le 2$ and $\rho_l \le 0,02$
For haunched beams:
$V_{Rd}^{\alpha} = V_{Rd} + \frac{M_{Ed}}{0,9d}\tan\alpha$</td><td>For straight depth beams:
$V_{Rd} = \frac{\tau_{cd}}{1+2,5\varepsilon\cdot d\cdot k_{dg}}\cdot b\cdot d$
$\tau_{cd} = \frac{0,3}{\gamma_c}\cdot\sqrt{f_{ck}} = 0,2\sqrt{f_{ck}}$
$\varepsilon = \varepsilon_s\cdot\frac{0,6d-x}{d-x} \approx 0,41\varepsilon_s = 0,41\frac{f_{sd}}{E_s}\cdot\frac{m_d}{m_{Rd}}$
$f_{sd} = f_s/1,15$ and $k_{dg} = 48/(a_g + 16)$
a_g: size of aggregates (mm)
m_d : the acting design moment
m_{Rd}: the yielding moment.</td></tr>
<tr><td colspan="2">Simlified Shear Design Procedure of Canadian Standard CSA A.23.3-04 [Collins et al. (2008)]</td></tr>
<tr><td colspan="2">For straight depth beams:
$m_{vd} = \frac{a-d}{d}$ and $m = \frac{1,11m_{vd}+1}{\rho_l}$
$a_{eff} = a_g$ if $f'_c < 60$ MPa $a_{eff} = 0$ if $f'_c > 70$ MPa $a_{eff} = a_g\frac{70-f'_c}{10}$
$s_{xe} = \max\left(\frac{31,5d}{16+a_{eff}}; 0,77d\right)$ $\frac{V_{Rd}}{b\cdot d} = 0,65\left[\sqrt{1+\frac{7,02m\cdot\sqrt{f'_c}}{1000+s_{xe}}}-1\right]\cdot\frac{133,3}{m}$</td></tr>
</table>

Table 5.20. Shear design equations of 4 practical codes and proposed models (Eq. 5.27 and Eq. 5.28)

The proposed models have simpler form because they are based on a theoretical background about the stresses distribution of a cracked concrete beams at critical state, they adopted many simplified laws of main factors such as a/d ratio, size effect d, concrete strength f_{ck} while the others are originated from either purely empirical approach or very complicated theories, which anyhow are based on several assumptions. As presented in the experimental program and the Non-FEM analysis, the propagation of cracks in concrete is very random that makes the redistribution of stresses in cracked concrete becomes very complex and unpredictable. Therefore, a model based on mechanics with some simplifications as suggested is believed to be a good solution for the problem.

In conclusion, the main results of Chapter 5 can be summarized as follows:

+ The proposed models are developed from the shear resistance mechanisms of the concrete compression zone and the uncracked concrete parts in the tension zone. The compression zone plays a key role in shear resistance. The action of the uncracked concrete parts in tension zone is an important result of this research work, which formerly has not been mentioned.

+ A logical distribution of shear stress in a cracked concrete region at critical state from Non-FEM analysis is introduced which totally complies with mechanical theory.

+ The research presents two simplified models of size effect d and characteristic compressive concrete strength f_{ck} in terms of allowable shear stress τ^*_{max}.

+ Two simple and accurate shear strength models for straight depth beams and haunched beams are suggested. Compared with many other models, the new proposals were proved to be the most appropriate ones to predict the shear capacity of concrete beams without stirrups.

+ Two shear design equations of straight depth beams and haunched beams are also proposed for practical purposes. These design formulae were proved to be superior to other shear design equations in some practical codes.

+ Finally, the approach which combines theoretical background and simplified effect laws should be used for shear design of concrete beams without stirrups instead of purely empirical formulae.

6 Conclusions and Recommendations

This research has been aimed to improve the understandings of shear behaviours and shear capacity of concrete beams without stirrups. The main tasks of the research as set-up in Chapter 1 (Introduction) include:

(1) Clarifying the main shear resistance mechanisms of concrete beams without stirrups.
(2) Finding the differences of shear behaviours between straight and haunched concrete beams.
(3) Proposing a rational and simple method to calculate the shear carrying capacity of concrete members without stirrups.
(4) Evaluating the level of conservativeness of some practical codes.

have been accomplished and presented in the previous chapters which can shortly summarized as follows:

Chapter 2 (State of the Art) presented a brief overview of shear resistance mechanisms of concrete beams without stirrups suggested by former researchers. These recognized actions were further investigated in the Chapter 3 (Experimental Program) and Chapter 4 (Non-FEM Analysis). The outcomes introduced a new more reasonable shear resistance mechanism of concrete regions in beams which was later used to develop shear strength models of concrete beams without stirrups as in the Chapter 5.

The differences in shear behaviours between straight depth beams and haunched beams were clearly outlined in Chapter 3 (Experimental Program) of 18 test beams with an inclined compression chord in range of 0^o to 10^o. The Non-FEM analysis afterward provided mechanical explanations of the differences in the stresses distribution and the failure region which cause the shear strength model of this type of beams to be different from that of straight depth beams.

The two new proposed shear strength models for haunched concrete beams and straight depth beams without stirrups were presented in the Chapter 5. The evaluation of accuracy and conservativeness of some practical codes was described in this part as well.

Some main results of the research contributing to explain the shear behaviours of concrete beams without stirrups can be summarized as follows:

The research introduced a shear resistance action of uncracked concrete parts in the tension zone in concrete members which combines with that of the uncracked compression concrete region to become the two main shear resistance mechanisms of concrete beams without stir-

rups. The analysis results also confirmed the main role in shear resistance of the uncracked compression zone which has been widely accepted by other authors.

New redistributions of stresses in cracked concrete beams without stirrups were presented, which totally comply with mechanical theories. This helps to give reasonable explanations of different shear behaviours of haunched and straight depth concrete beams. The main differences of the two types of beams include system stiffness, shear stress distribution and failure zone which require a shear strength model for haunched beams different from that of straight depth beams.

The research proposed two new simplified formulae of size effect d and allowable shear stress τ_{max} in terms of characteristic compressive concrete strength f_{ck}. These suggested formulae were proved to be fit well to illustrate the influences of the above mentioned factors on test results.

Based on mainly mechanical background and simplified effect approaches of significant factors, two new simple and accurate shear strength models for straight depth beams and haunched beams were suggested in the Chapter 5. These shear strength equations, formulated as sectional design models, have been proved to be the most appropriate ones to predict the shear capacity of a wide range of concrete test beams without stirrups.

Two shear design models were also suggested for practical purposes. These design formulae were proved to be superior to other shear design equations in some practical codes. The results also showed a too conservative trend of empirical models such as those of ACI 318-05, DIN 1045-01, SN 262 and especially the severe unsafety of ACI 318-05 which has long cautioned by other authors.

Shear behaviours and shear resistance models of concrete members are a very open and promising topic to researchers due to a wide variety of practical concrete members and applications. Based on some above achievements, some recommendations are suggested below for further investigations and practical applications of this research.

Nonlinear Finite Element analysis has been proved to be a powerful tool to study the behaviours of concrete members under elastic and cracked condition, but significant improvements are still required nevertheless. The modeling of the propagation and the behaviour of cracks by means of a smeared approach causes a lot of difficulties and is insufficient. New models such as X-FEM may give good solutions for complex problems in concrete structures. However, material models for concrete and the interactions between concrete and reinforcements are suggested to be further investigated. In addition, some inherent problems of the FEM-analysis such as mesh sensitivity, convergence problem should be reduced or even eliminated.

Though the term shear stress has generally been used to refer to shear strength and shear failure of concrete members, its upper limitation at which shear failure tends to occur is not mentioned in practical codes. In this research, a relatively simple formula of allowable shear stress τ_{max} was suggested in terms of the characteristic compressive concrete strength f_{ck}. It is recommended to conduct further theoretical investigations or specimen tests to determine more evidently values of this parameter.

In general, the shear strength formulae have a common form of $V = \tau \cdot b \cdot d$. It has normally been assumed that the width b of concrete members is constant. However, there exist some special cases in which the effective width is lessened. It is believed that the stress flow in this type of beams is different from those of constant width beams. Therefore, it is recommended to have further investigations for this kind of members.

More than 2000 shear tests have been conducted so far. Nevertheless, further experimental investigations seem to be required to get a better understanding of the shear behaviours of concrete beams.

This research was performed with single span concrete beams without stirrups under concentrated loads. Its extended applications for concrete members under constant loading, axial force, prestressing or other types of loading are recommended to have more data for verifying the models.

The experimental data for haunched concrete beams is still insufficient. There have been only 14 reliable tests conducted at TUHH so far. In consequence, further tests on this member should be conducted.

In practice, concrete slabs are the most typical and popular concrete members without stirrups. In these members the crack is generally not perpendicular to the longitudinal reinforcement. Therefore, shear behaviours and shear strength of these structural elements should be studied more in detail.

Since the shear failure of the roof beams in warehouses of the US Air Force in 1955, there have been many researches on the shear behaviours of concrete beams and many shear strength models for concrete members without stirrups have been suggested. In order to have timely adjustments for safe design principles, it is recommended to replace unreliably empirical shear design formulae in practical codes with simply and effectively theoretical background ones.